ACTIVE WAVE ATTENUATION BY A SUBMERGED HEAVING AND PITCHING FLAT PLATE

by

Andrea Mueller

Dipl.-Ing., Civil Engineering, TU Dresden, 1989

Submitted to the Institute for Graduate Studies in
Science and Engineering in partial fulfillment of
the requirements for the degree of
Doctor of Philosophy

Graduate Program in Civil Engineering

Boğaziçi University

2016

ACTIVE WAVE ATTENUATION BY A SUBMERGED HEAVING AND PITCHING FLAT PLATE

APPROVED BY:

Assoc. Prof. Emre N. Otay (Thesis Supervisor)	.....
Prof. Hilmi Luş	.....
Assoc. Prof. Osman S. Börekçi	.....
Prof. Sedat Kabdaşlı	.....
Prof. Serdar Beji	.....

DATE OF APPROVAL: 13.07.2016

ACKNOWLEDGEMENTS

I would like to express my special appreciation and gratitude to my advisor, Dr Emre Otay, for his guidance, motivation and immense knowledge, especially for having faith in me when I had lost it. The tunnel was long and dark...

My sincere thanks go to my thesis committee members, Dr Osman Börekçi and Dr Serdar Beji, for their insightful comments and encouragement. Dr Osman Börekçi showed me the potential of modelling with RBF and always asked the right questions to let me find a solution to the problem at hand. Dr Serdar Beji got never tired of my questions and always shared his immense knowledge about hydrodynamics of floating and submerged bodies. When in doubt I could always ask him.

I am especially grateful to Dr Richard Porter from the University of Bristol who provided me with analytical data to calibrate my RBF model and gave me permission to display them in my thesis. Without these data, I would not have been able to finish my thesis.

This thesis is the culmination of years of research which would not have been possible without solid knowledge foundation laid by all the professors whose courses I was fortunate to attend. My thanks to all of them for their support and input!

I also want to say thank you to my fellow PhD and master students, especially Mohammadsadegh Aslani, for their support, inspiring discussions, laughter: A problem shared is a problem halved! You guys kept me going.

Very special thanks go to my family who always believed in me, supported me, funded me and encouraged me to continue. This was a rollercoaster experience and I am very grateful that I had you by my side.

ABSTRACT

ACTIVE WAVE ATTENUATION BY A SUBMERGED HEAVING AND PITCHING FLAT PLATE

Protecting the coastline and structures in its vicinity are main tasks of coastal engineering. Here an environmental-friendly and cost-efficient active submerged flat plate (SFP) breakwater is proposed. It is investigated whether through introduction, phase and amplitude control of two motion modes, heaving and pitching, and in-situ adaptations of submergence depth and plate inclination in dependence on the incidence wave, wave attenuation can be improved and the bandwidth of appreciable performance can be widened. It is examined whether maximum wave attenuation results in energy loss of the system so that the energy can be harvested and used for motion control and structural adaptations. The wave/structure boundary value problem (BVP) is formulated in two dimensions (vertical) and covers monochromatic waves only, linear wave theory is applied; non-linearities are introduced by applying the body-nonlinear method. Motion amplitude and incidence wave height restrictions are enforced to ensure that the assumptions for linear wave theory are not violated. Plate motion is introduced through prescribed forcing with incident wave frequency. The BVP is solved numerically using the radial basis function (RBF) collocation method. A novel lateral boundary condition is developed that allows wave incidence and radiation simultaneous. The RBF method proved to be able to model wave/structure interaction and plate motion; model calibration is required. Through the applied body-nonlinear method higher harmonics are introduced. Research results suggest that wave attenuation of the SFP is improved through above-stated measures and performance bandwidth widened. Motion phase angle control is paramount to ensure destructive interference between scattered and radiated wave on the lee side of the plate. Configurations with minimum wave transmission allow for energy harvesting.

TABLE OF CONTENTS

LIST OF FIGURES

LIST OF TABLES

LIST OF SYMBOLS

a	half-width of plate
$\mathbf{a}$	added mass coefficient vector
$a_{diffracted}$	amplitude of diffracted wave
a_{inc}	amplitude of incident wave
$a_{radiated}$	amplitude of radiated wave
a_{heave}	amplitude of plate motion
a^{nm}	added mass coefficient in direction m due to structure oscillation in mode n
b^{nm}	radiation damping coefficient in direction m due to structure oscillation in mode n
c	water wave celerity
$c_c^{(mn)}$	damper coefficients of the motion control
d	plate submergence depth
ef	energy flux per mass
EF	energy flux of system
$F_{exc}^{(m)}$	exciting force due to wave motion in m^{th} DoF
$F_s^{(m)}$	supporting force to balance wave motion in m^{th} DoF
g	gravitational acceleration
h	water depth
H	wave height
i	imaginary number
k	wave number
k_{Motion}	motion coefficient
k_R	reflection coefficient
k_{Rad}	radiation coefficient
k_T	transmission coefficient
k	wave number
K	deep water wave number
$k_c^{(mn)}$	spring coefficients of the motion control

L	wave length
n	normal direction
p	pressure
R_{total}	complex total reflection coefficient
S_B	surface of submerged structure
t	time
T	wave period
T_{total}	complex total transmission coefficient
u	velocity in x-direction
v	velocity in y-direction
V_n	structural velocity component normal to structure surface
$\vec{v}$	velocity vector
w	velocity in z-direction
$\mathbf{x}$	coordinates of the six DoF
α_i	source weights
$\beta, \beta(t)$	instantaneous pitching angle
β_0	plate inclination angle
β_{pitch}	pitching amplitude
ε	phase lag between incidence wave and motion response
η	free surface displacement
$\hat{\eta}^{(m)}$	complex wave amplitude due to plate radiation in motion mode (m)
ω	angular frequency
φ	(unit amplitude) velocity potential as function of space
ϕ	complex velocity potential as function of space
Φ	velocity potential as function of space and time
Ψ	coordinate for yaw motion
ρ	density
τ	separation constant
θ	angle between incident wave and x-axis

θ_{heave}	phase lag between incident wave and plate heave motion
θ_{motion}	phase lag between incident wave and plate motion
θ_{pitch}	phase lag between incident wave and plate pitch motion
Υ	coordinate for pitch motion
$\xi^{(m)}$	motion amplitude for motion mode (m)
$\hat{\xi}^{(m)}$	complex motion amplitude for motion mode (m)
Ξ	coordinate for roll motion

LIST OF ACRONYMS/ABBREVIATIONS

2D	Two Dimensional Vertical
3D	Three Dimensional
2wABC	Two way Artificial Boundary Condition
BBC	Bottom Boundary Condition
BC	Boundary Condition
BVP	Boundary Value Problem
CFSBC	Combined Free Surface Boundary Condition
DFSBC	Dynamic Free Surface Boundary Condition
DoF	Degree of Freedom
FBW	Floating Breakwater
KFSBC	Kinematic Free Surface Boundary Condition
LBC	Lateral Boundary Condition
MAC	Marker And Cell
MFS	Method of Fundamental Solution
MME	Matched Eigenfunction Expansion
NRBC	Non-Reflecting Boundary Condition
PDE	Partial Differential Equation
PTO	Power Take-Off
RBF	Radial Basis Function
SFP	Submerged Flat Plate

1. INTRODUCTION AND CRITICAL LITERATURE REVIEW

1.1. Introduction

Protecting harbours and coastlines from excessive wave action and sheltering coastal structures permanently and/or during their erection are important assignments in coastal engineering. In addition to the conventional bottom-mounted breakwaters, engineers started focussing on floating breakwaters (FBW) and submerged FBW because they are structures that combine the capability of considerable wave attenuation with the advantages of fast installation and mobility.

In addition to their short installation time, ease of removal and possibility of prefabrication, FBWs and submerged FBWs exhibit a number of other advantages - they allow for water circulation, fish migration, and sediment transport and are therefore an environment-friendly coastal protection; installation in deep water, on unstable sea bottoms or steep slopes is possible as they are in general moored which also allows adaptation to tidal ranges and changing sea levels; their installation, maintenance, and removal costs are lower than for bottom-connected fixed breakwaters. Submerged FBWs offer the additional advantage of less visual impact and being exposed to smaller wave forces.

Between 1950 and 1990 the problem of wave scattering by submerged obstacles had been investigated by a number of researchers (Heins, 1950; Burke, 1964; Levine, 1965; Mei and Black, 1969; Siew and Hurley, 1977; Bird and Sheperd, 1984; Patarapanich, 1984b; McIver, 1985; Patarapanich and Cheong, 1989 and Liu and Iskandarani, 1991) and results suggested that submerged flat plates (SFP) are a potential configuration for a submerged FBW.

Wave attenuation is based on the same mechanisms as for surface and submerged FBWs: SFPs do not terminate the incoming waves but attenuate them by reflection, wave transformation (diffraction and radiation) and energy dissipation (through the generation of turbulences or inducing wave breaking). As SFPs do not extend over the whole water depth, waves are transmitted above and under the plate, and through the plate via its motions (radiated waves).

Unlike reflecting the waves from the structure as fixed bottom-mounted breakwaters or tightly-moored FBWs do, according to Shankar *et al.* (1996) and Yu (2002) for horizontal SFPs the reflection relies mainly on fluid-fluid interaction meaning that the flat plate alters the fluid flow and causes backflow underneath the plate.

As long waves penetrate deep into the water, a considerable part of the wave energy is transmitted underneath the SFP. This leads to almost no wave attenuation for long waves and poses one of the shortcomings of SFPs as for all FBWs.

Further shortcomings of submerged horizontal flat plate breakwaters are the narrow frequency bandwidth of appreciable wave attenuation and the occurrence of zero wave reflection as function of the frequency as presented in Patarapanich (1984), Parsons and Martin (1992), Liu *et al.* (2008), Porter (2002) and Porter (2015).

A remedy to the latter disadvantage is the application of inclined flat plates; according to Parsons and Martin (1992), Murakami *et al.* (1994), Rao *et al.* (2009) and Porter (2002), application of submerged plates with a positive slope in the wave propagation direction lower the transmission coefficient and diminish the periodicity of the reflection coefficient.

Studies of Yu and Chwang (1994), Neves *et al.* (2000) and Cho and Kim (2013) showed that applying porous plates widens the range of wave frequencies with acceptable wave attenuation due to increased wave energy dissipation by flow through the plate pores. The performance of horizontal porous plates as wave attenuator depends highly on the plate width, the submergence depth and the porosity of the plate mate-

rial according to research by Cho and Kim (2008); that's why the applicability to the real wave environment is questionable as a decrease in the porosity can be expected due to suspended particles and minuscule organisms in sea water and will alter the performance of the submerged porous plate.

Cho and Kim (2008) combined plate inclination and porosity and stated that an inclined porous plate can pose an effective wave absorber if optimally designed; they included plate width, porosity, submergence depth, and inclination angle as design parameters and determined the optimum parameters in a comprehensive numerical parametric study.

The use of flexible membranes as submerged wave attenuators widens the performance bandwidth according to a study by Cho and Kim (1998). As the efficiency of the elastic membrane depends on its tension, a framework has to maintain the optimum tension in the membrane; this and the maintenance of the design elasticity might prove a challenge under real sea conditions.

Wang and Shen (1999), Usha and Gayathri (2005), Neelamani and Gayathri (2006), Liu *et al.* (2008), and Liu *et al.* (2009) investigated the performance of twin plates and groups of flat plate breakwaters and achieved in general only a slightly improved wave attenuation.

The wave attenuating performance of a submerged horizontal flat plate is governed by its structural dimensions, the submergence depths, and the incident wave characteristics. In order to improve the performance of submerged plates with their predefined structural dimensions in real sea conditions for the varying incident waves and widen their bandwidth of satisfactory performance, Yip (1997) and Yip and Chwang (1997) suggested the implementation of active control as introduced by Milgram (1970).

By allowing the submerged plate to pitch, two new parameters, that influence the performance and can be used to control it, are introduced: pitching amplitude and phase. The research results suggest that performance modification by pitching control

and adaptation to specific requirements is possible. This outcome encourages the use of active motion-control to overcome the disadvantages of submerged flat plate FBWs and opens up the link to wave energy harvesting.

1.2. Critical Literature Review Motion-enabled Submerged Flat Plate and Motion Control

To achieve the required wave attenuating performance, designer of floating breakwaters mainly focus on structural parameters like width, draft, mass and moment of inertia. These FBWs are designed as passive systems and work like barriers against the incoming waves; good performance requires high stiffness and sufficient draft of the system to reflect as much wave energy as possible. This results in large structural and mooring forces.

Although moored FBWs always radiate waves and therefore out-of-phase damping can occur, only few authors (Evans and Linton, 1989; Evans and Linton, 1991; Loeffler-Lenz, 1994; Evans and Porter, 1996; Yip, 1997; Yip and Chwang, 1997; Yip and Chwang, 1998; Hall and Fischer, 1998; Takaki and Lee, 2003; Zheng *et al.*, 2007; An and Faltinsen, 2013 and Porter, 2015b) have considered motion and researched FBWs that are intentionally allowed to move or actively forced to move and therefore hold the potential of active and controllable out-of-phase damping to improve their wave-attenuating performance.

Most of the above-cited researchers focus on the hydrodynamic characteristics (radiation damping, added mass/inertia) of moving bodies without incidence wave present. Only Evans and Linton (1991) solve the combined diffraction and radiation problem for a hinged vertical plate and a submerged tethered horizontal circular cylinder analytically and Yip (1997), Yip and Chwang (1997) and Yip and Chwang (1998) focus on submerged impermeable and porous horizontal plates and introduce pitching as the controllable motion of the FBW.

Yip (1997) and Yip and Chwang (1997 and 1998) use the method of matched eigenfunction expansion and apply linear wave theory with the assumption of inviscid and incompressible fluid and irrotational flow; the plate boundary condition is applied on the zero-position of the plate. They show that the wave-generating ability of a submerged pitching plate varies little over a wide range of relative water depths h/L (Yip, 1997; Figure 2.4).

Yip (1997) concludes that wave attenuation with an SFP is significantly influenced by the submergence depth of the plate d/h and the relative plate width $2a/L$. The performance of the SFP fluctuates in dependence on the relative plate width $2a/L$, but has an appreciable value for the range $0.5 \leq 2a/L \leq 1.0$ (Figure 2.3. in Yip (1997). As the plate width has to be defined in the preliminary design and cannot be adapted during FBW employment, it is crucial to choose the optimum width in dependence on the local wave climate.

Yip (1997) confirms that smaller submergence depths result in higher radiated wave heights for equal pitching amplitude and states that the maximum wave-making ability was achieved at a relative plate submergence of d/h=0.175 (Yip, 1997; Figures 2.19.-2.22.).

Numerous other studies of submerged bodies as wave attenuators also show that the submergence is one of the most influential parameters (Patarapanich, 1984b; Patarapanich and Cheong, 1989; Cheong and Patarapanich, 1992; Neelamani and Reddy, 1992; Yu *et al.*, 1995; Wang and Shen, 1999; Yu, 2002; Zheng *et al.*, 2007; Cho and Kim, 2008; Rao *et al.*, 2009; Rao *et al.*, 2009; Cho and Kim, 2013).

Yip (1997) and Yip and Chwang (1997) further investigated the influence of the pitching amplitude, phase difference between pitching and incident wave and plate permeability on transmission and reflection coefficient and energy state of the system and their research results show that minimum transmission is achieved when the radiated wave towards the lee side of the plate is 180° out-of-phase with the resultant of incident and diffracted wave towards transmission side. The phase angle between the incident

wave and pitching motion needs adjustments in dependence on plate width in order to yield minimum transmission (Yip, 1997; Figures 2.12. and 2.14.).

Yip (1997) states that it is not possible to minimize transmission and reflection coefficient simultaneously with an impermeable pitching plate and that depending on the phase shift between plate motion and incident wave, energy has to be put into the system or can be taken out of the system.

Further research results were that the wave height of the radiated wave is linearly proportional to the pitching amplitude and that the pitching amplitude has no influence on the phase angle between incident and radiated wave required to yield minimum transmission.

The research results of Yip (1997) and Yip and Chwang (1997) for the variation of the transmission coefficient with the relative water depth h/L (Figures 2.15 to 2.18 in Yip, 1997) require critical examination. Firstly, the continuously decreasing transmission coefficient of the zero-pitching (stationary) flat plate for h/L$\rightarrow$ 0 does not display the behaviour of a floating structure. A moored flat plate, which is able to make small motions, displays a narrow-bandwidth of good performance (Cho and Kim, 1998; Figure 4.), (Abul-Azm and Gesraha, 2000; Figure 6.b), (Cho and Kim, 2013; Figure 7.a).

Secondly it has to be noted that the transmission coefficient for long waves (h/L=0) has to be one (and the reflection coefficient has to be zero) as due to their deep penetration, long waves get transmitted unattenuated as described by a number of researchers (Parsons and Martin, 1992 ; Cho and Kim, 1998; Abul-Azm and Gesraha, 2000; Usha and Gayathri, 2005; Cho and Kim, 2013). Additionally the asymptotic behaviour of transmission and reflection coefficients for a pitching plate (k_t,$k_r\rightarrow\infty$) as h/L$\rightarrow$0 is physically not explicable.

The agreement between theoretical and experimental results in the study of Yip (1997) is in general not good but becomes poor for great relative plate widths $2a/L$

even for the fixed plate. The author attributes the discrepancies to the non-linear effects in the experiments due to the steepening of waves over the plate, an effect that is confirmed by Shankar *et al.* (1996).

For the pitching plate, the discrepancies between theoretical and experimental results become more pronounced with decreasing relative submergence depth due to increasing non-linear effects. Additionally, Yip (1997) states that the wave/plate interaction amplifies the higher harmonics generated by the wavemaker and that this leads to further discrepancy between experimental data and theoretical results.

Overall Yip (1997) and Yip and Chwang (1997) concluded that the relationship between plate width, wavelength, submergence depth and the pitching parameter is very complex but by careful pitching control the performance of a submerged pitching plate as breakwater can be modified and adapted according to the local wave climate.

Takaki and Lee (2003) investigated the non-linear effects of a submerged plate oscillating in heave near the free surface. They used the composite grid method to numerically determine the radiated waves and compared the numerical results (added mass, radiation damping, radiation wave amplitude, and heave radiation force) with experimental and LWT results. They concluded that differences between LWT results and experimental/numerical results increase for large heaving amplitudes; the numerical and experimental results increasingly deviate from the LWT results when the submergence decreases. These research results confirm that the submergence depth has to be large enough and that the plate motion amplitudes have to be kept small to avoid non-linearity effects.

Theoretical analysis by McCormick (1981) and Falnes (2002) has established that ideally 100% wave energy attenuation through body oscillation in two degrees of freedom (DoF) is possible (see Figure 1.1). Here a motion that radiates symmetric waves (heave) is combined with a motion that radiates anti-symmetric waves (pitch) and for the case that the natural frequency of heave and pitch coincide, the transmitted waves of both motions can cancel each other totally (destructive interference).

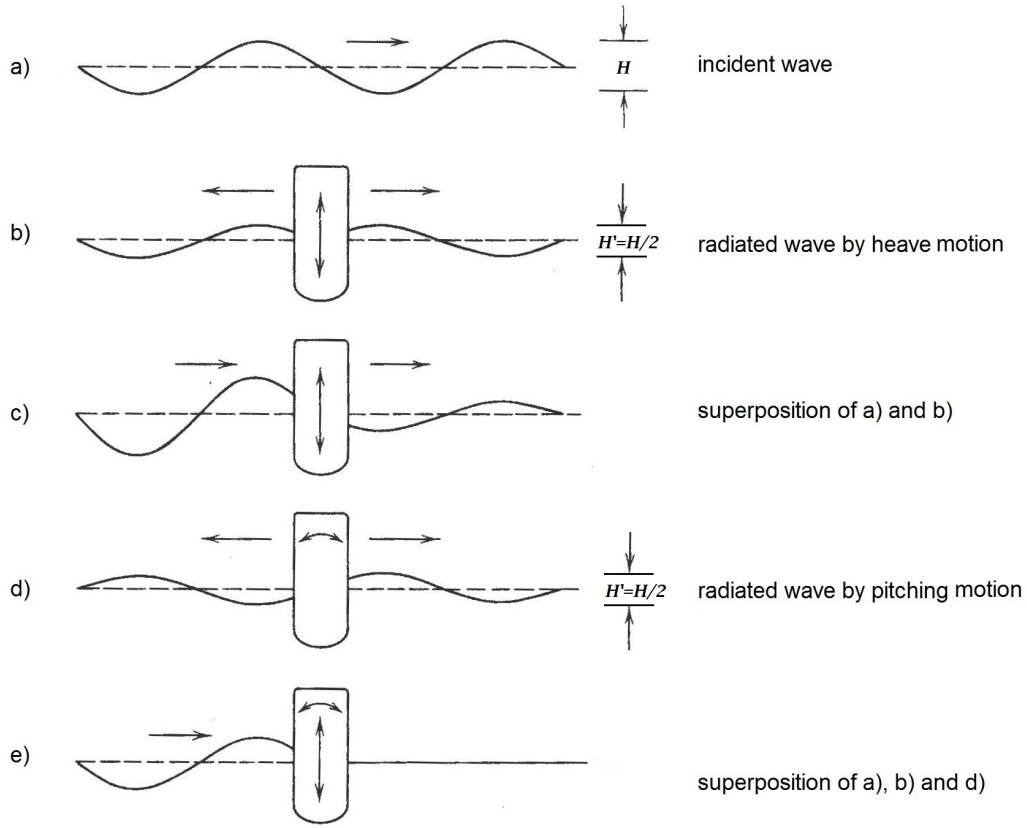

Figure 1.1. Wave cancellation by interference of incident and radiated waves (adapted from (McCormick, 1981)).

As already mentioned in 1.1, positioning the flat plate with a positive inclination in wave propagation direction reduces the frequency-dependent periodicity of the reflection coefficient. This has been investigated and confirmed with different approaches: Rao *et al.* (2009) tested the influence of inclination experimentally; Cho and Kim (2008) placed the inclined submerged flat plate in front of a vertical wall and applied a multi-domain boundary-element method (BEM) to solve the boundary value problem (BVP). Parsons and Martin (1992) solved the BVP analytically for infinite water depth using hypersingular integral equations; Porter (2002) extended this approach to finite water depth.

1.3. Objectives

After analysis and consideration of the available results from former research regarding the performance of an SFP and radiation by structure motion summarised in Section 1.2, the following features are implemented in the here proposed active wave attenuator:

In this thesis, the introduction of heave as second DoF is proposed. The submerged flat plate will be forced to heave and/or pitch with the incident wave frequency and it will be investigated whether wave attenuation can be increased and/or a wider bandwidth of appreciable performance can be achieved.

The wave radiated by pure heave, pure pitch and combined motion and the parameters that affect the magnitude and phase angle of the radiated wave are explored. By implementing motion phase control, the generated radiated wave will be tuned to destructively interfere with the resultant of incident and diffracted wave on the lee side of the plate in order to achieve appreciable wave attenuation.

As motion amplitude and amplitude of radiated surface wave are linearly dependent as stated by Falnes (2002) and Yip (1997), amplitude control can then, in addition, be used to lower the transmitted wave height to the required value.

Additionally, it will be investigated whether combined heave and pitch motion in connection with individual amplitude control makes the radiated wave manipulable.

In this thesis, horizontal and inclined SFP will be investigated in order to compare their performance as wave attenuator. It will be explored whether inclination not only reduces the frequency-dependency of the performance of a stationary plate but also positively affects the radiated wave, e.g. increases the radiated wave towards transmission side.

The critical literature review in Section 1.2 revealed that the submergence depth is one of the most important parameters affecting the wave attenuation performance of the flat plate. In this thesis, adaptable submergence depth is proposed. This allows to adjust the plate submergence in dependence on the incidence wave height to avoid surface piercing and according to plate performance criteria, e.g. to achieve the plate submergence with maximum radiated wave.

Being aware that the discrepancies between theoretical and experimental results in Yip (1997) became more pronounced with decreasing relative submergence depth due to growing non-linear effects that are not covered by linear wave theory, plate-submergence will be kept here sufficiently deep.

By allowing for motion, the SFP becomes an active device similar to wave energy converters. Although the primary aim of the proposed SFP breakwater is to ensure low wave transmission by phase and amplitude control of the heaving and pitching motion, it will be also investigated whether it is possible to exploit the permitted motion of the flat plate to extract wave energy.

If achieving minimum transmission and low reflection with the same system configuration is possible and therefore energy harvesting is feasible, this energy could be stored e.g. in gas accumulators as suggested by Falcão (2007) and used to force the optimum plate motion through motion damping and autonomously power required structural adaptation like submergence depth and inclination angle, or directly converted to electrical energy by different generator types as suggested by Polinder *et al.* (2007).

The plate motion in this study will be modelled by prescribed forcing but it is shown how the power-take-off (PTO) has to be implemented as additional forcing terms in the equation of motions. Following the approach of Evans (1976), Falcão (2008), Falcão (2010), the PTO is modelled as linear spring and linear damper.

Figure 1.2 shows a schematic representation of the proposed SFP breakwater and summarizes the main points of the critical literature review. Note that combined heave and pitch motion with phase angles of θ=0 or θ=π between the two motions is equivalent to shifting the pitching axis and therefore controlling the directional pitching amplitude; its influence on the transmission of waves over the SFP breakwater will also be investigated.

1.4. Summary

In this thesis it is attempted to improve the wave attenuation of an SFP by:

- Allowing for two DoF - heaving and pitching and combined heaving and pitching motion
- Investigating the influence of plate inclination on performance of heaving and/or pitching plate
- In-situ structural adaptations (submergence depth, initial plate inclination)
- Providing the possibility for directional pitching amplitude control through changing the pitching axis position
- Introducing and optimizing motion control to lower the transmission coefficient and/or widen the bandwidth of satisfactory performance
- Extracting energy and using it for forcing the plate motion, performing structural adaptations or converting it to usable electric energy.

The research will cover monochromatic waves; in order to avoid violation of the assumptions of linear wave theory, the motion amplitude will be kept small and sufficient submergence depth is allowed for.

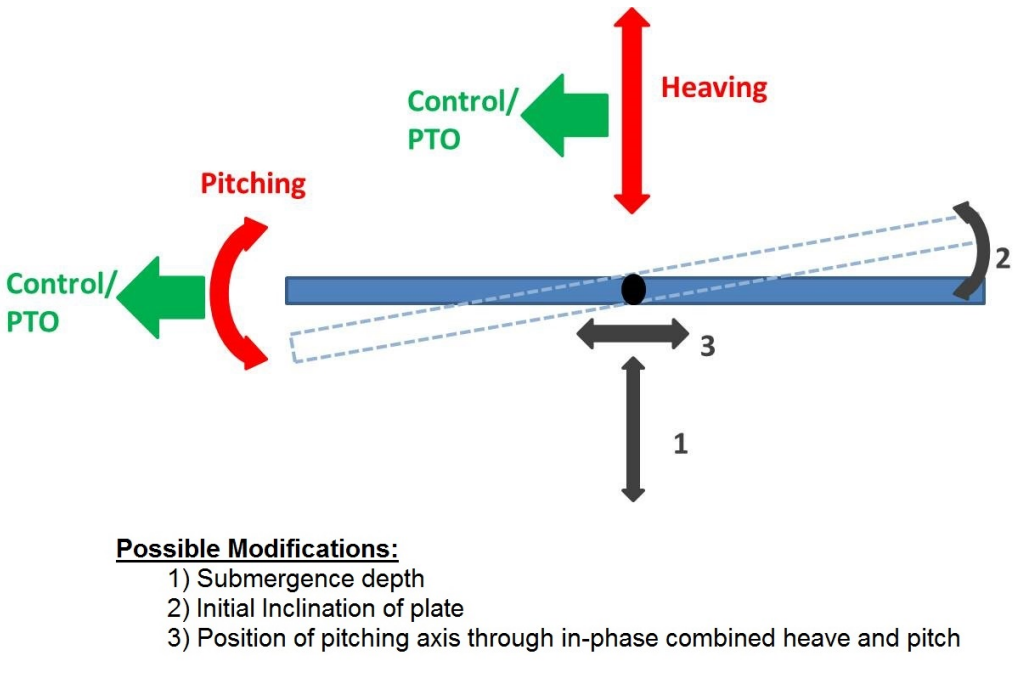

Figure 1.2. Schematic presentation of proposed submerged heaving and pitching flat plate.

2. DERIVATION OF WAVE/STRUCTURE BOUNDARY VALUE PROBLEM

Water-wave/structure interactions constitute boundary-value problems and are described by the governing equation of the fluid motion and the boundary conditions on the free surface, on the sea bottom, on the lateral boundaries and on the flat plate boundaries; the BVP is derived in the following sections. Throughout the thesis linear water wave theory is applied under the assumption of small amplitude waves and small structure motions.

2.1. Water-wave Boundary Value Problem

To describe the water-wave BVP, a Cartesian coordinate system is selected so that the origin is placed on the mean free surface of the water, the positive x-axis points into the wave propagation direction; the y-direction is parallel to the wave crest and the z-axis points vertically upwards (see Figure 2.1).

2.1.1. Inviscid Water-wave Theory

Conservation of mass in a fluid requires that

$$\frac{\partial \rho}{\partial t} + \nabla \rho \vec{v} = 0 \qquad \text{where} \quad \vec{v} = \begin{pmatrix} u \\ v \\ w \end{pmatrix}$$

with ρ being the fluid density and $\vec{v}$ representing the fluid particle velocity vector with its components u, v and w.

In this thesis, for the modelling of all water-wave/structure interactions it is assumed that:

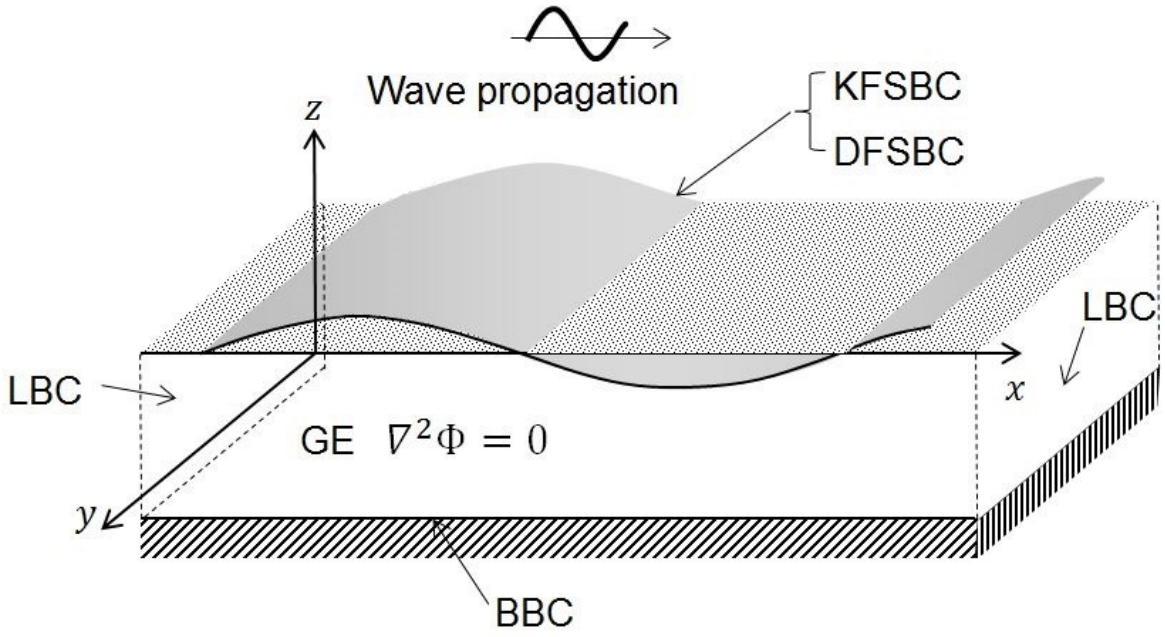

Figure 2.1. Schematic 3D water-wave boundary value problem.

(i) Water is inviscid and incompressible.

(ii) Water motion is irrotational.

Because of the incompressibility assumption, $\frac{\partial \rho}{\partial t} = 0$ and density ρ does not change in space. Then the conservation of mass becomes $\nabla \vec{v} = 0$. As the fluid motion is irrotational, the fluid velocity $\vec{v}$ can be described by the gradient of a scalar velocity potential $\Phi = \Phi(x, y, z, t)$; that is $\vec{v} = \nabla\Phi$. Then the velocity potential Φ satisfies the Laplace equation (Governing Equation GE):

$$\nabla^2\Phi = 0 \tag{2.1}$$

The vertical position of an arbitrary point on the free surface is defined as:

$$z = \eta(x, y, t) \tag{2.2}$$

The kinematic free surface boundary condition (KFSBC), that fluid particles on the free surface move only tangentially to the surface (see Dingemans (1997)), is obtained by equating the vertical velocity of the free surface to the surface particle velocity:

$$\frac{\partial \Phi}{\partial z} = \frac{\partial \eta}{\partial t} + \frac{\partial \eta}{\partial x}\frac{\partial \Phi}{\partial x} + \frac{\partial \eta}{\partial y}\frac{\partial \Phi}{\partial y} \qquad \text{on} \quad z = \eta(x, y, t) \tag{2.3}$$

The Dynamic Free Surface Boundary Condition (DFSBC) ensures that the pressure at the interface between the two fluids air and water matches. Neglecting surface tension (as the waves considered here are not capillary waves), the Bernoulli equation for unsteady potential flow has to hold:

$$\frac{\partial \Phi}{\partial t} + \frac{1}{2}\Big[\Big(\frac{\partial \Phi}{\partial x}\Big)^2 + \Big(\frac{\partial \Phi}{\partial y}\Big)^2\Big] + gz + \frac{p}{\rho} = C\big(t\big) \tag{2.4}$$

Here ρ is the water density, g is the gravitational acceleration and p is the water pressure at the free surface relative to the air pressure. Referencing the water pressure to the air pressure (zero gauge pressure) and absorbing the Bernoulli constant $C(t)$ in a new defined velocity potential yields:

$$\frac{\partial \Phi}{\partial t} + \frac{1}{2}|\nabla \Phi|^2 + g\eta = 0 \qquad \text{on} \quad z = \eta(x, y, t) \tag{2.5}$$

Assuming an impermeable sea bottom of variable height $h = h(x, y)$, the following no-flow Bottom Boundary Condition (BBC) applies:

$$\frac{\partial \Phi}{\partial n} = 0 \qquad \text{on} \quad z = -h(x, y) \tag{2.6}$$

where n represents the direction normal to the sea bottom.

The Lateral Boundary Conditions (LBC) for waves periodic in space and time express this periodicity as follows:

$$\Phi(x, y, z, t) = \Phi\Big(x + L\cos(\theta), y + L\sin(\theta), z, t\Big) \tag{2.7a}$$

$$\Phi(x, y, z, t) = \Phi\Big(x, y, z, t + T\Big) \tag{2.7b}$$

where L represents the wave length, T the wave period and θ the angle between x-axis and wave incidence direction.

2.1.2. Linearized Equations

Under the assumption of small amplitude waves ($H/L \ll 1$), the non-linear free surface boundary conditions (2.3) and (2.5) can be linearized about and applied to the still water line $z = 0$. Here H represents the wave height of the incidence wave. For the small amplitude wave assumption to be valid, the motions of structures or bodies in the water have to be small too.

Then the KFSBC (2.3) becomes

$$\frac{\partial \Phi}{\partial z} = \frac{\partial \eta}{\partial t} \qquad \text{on} \quad z = 0 \tag{2.8}$$

and the DFSBC (2.5) becomes

$$\frac{\partial \Phi}{\partial t} + g\eta = 0 \qquad \text{on} \quad z = 0 \tag{2.9}$$

By combining (2.8) and (2.9) through differentiating (2.9) with respect to time and then substituting $\frac{\partial \eta}{\partial t}$ by $\frac{\partial \Phi}{\partial z}$ according to (2.8) gives the following Combined Free Surface

Boundary Condition CFSBC:

$$\frac{\partial^2 \Phi}{\partial t^2} + g\frac{\partial \Phi}{\partial z} = 0 \qquad \text{on} \quad z = 0 \tag{2.10}$$

For time-periodic waves of frequency $\omega = 2\pi/L$ the time dependency can be separated from the spatial problem by using the complex velocity potential ϕ:

$$\Phi(x, y, z, t) = Re\Big\{\phi(x, y, z)e^{-i\omega t}\Big\} \qquad \text{with} \quad \phi(x, y, z) = \frac{-iga_{inc}}{\omega}\varphi(x, y, z) \tag{2.11}$$

Here g is the acceleration due to gravity and a_{inc} is the amplitude of the incident wave. Using this spatial velocity potential $\phi(x, y, z)$ in equations (2.1), (2.8), (2.9), (2.10), (2.6) and (2.7a) leads to the following expressions for the 3D linearized water-wave BVP:

GE $$\nabla^2 \phi = 0 \tag{2.12}$$

KFSBC $$\frac{\partial \phi}{\partial z} = \frac{\partial \eta}{\partial t} \qquad \text{on} \quad z = 0 \tag{2.13}$$

DFSBC $$\frac{\partial \phi}{\partial t} + g\eta = 0 \qquad \text{on} \quad z = 0 \tag{2.14}$$

CFSBC $$\frac{\partial^2 \phi}{\partial t^2} - \frac{\omega^2}{g}\frac{\partial \phi}{\partial z} = 0 \qquad \text{on} \quad z = 0 \tag{2.15}$$

BBC $$\frac{\partial \phi}{\partial n} = 0 \qquad \text{on} \quad z = -h(x, y) \tag{2.16}$$

LBC $$\phi(x, y, z) = \phi\Big(x + L\cos(\theta), y + L\sin(\theta), z\Big) \tag{2.17}$$

2.1.3. Further Simplifications

Taking the submerged flat plate geometry and performance into account, further simplifications are adopted without extensively restricting the applicability of the model.

(i) Normal wave incidence: Cho and Kim (2013) stated that the performance of a submerged horizontal plate for long waves improves with oblique wave incidence. This is primarily due to the decrease of effective wavelength in the direction normal to the breakwater or increase of effective plate width in the (oblique) wave incidence direction.

In this thesis only normal wave incidence on the SFP breakwater is assumed; this will cover the low performance cases of the proposed breakwater. All oblique wave incidence cases will exhibit better performance of the submerged flat plate as wave attenuator.

(ii) Two-dimensional vertical case: Since the flat plate's width (dimension in x-direction) is small compared to its length (dimension in y-direction) and the plate geometry along the y-axis is assumed to be constant, it is sufficient to consider the reduced potential $\phi(x, z)$ for the two-dimensional vertical (2DV) case.

With these two simplifications the LBC (2.17) becomes:

$$\text{LBC} \qquad \phi(x, z) = \phi(x + L, z) \tag{2.18}$$

(iii) Horizontal Bottom: As in the following paper the focus lies on wave scattering by a submerged plate breakwater, the horizontal dimension (in x-direction) of a real application is of order $O(10^1)$ (e.g. plate width of 20m). With an average slope of $1 : 500$ in the continental shelf, the height difference between the plate edges would be in the order of $O(10^{-2})$.

Due to this fact and the reasoning that a floating breakwater will be installed in water of finite depth, in the following derivation only the case of uniform finite water depth is considered. (In Chapter 8 the extension to piecewise horizontal bottom is discussed.)

Therefore the BBC (2.16) becomes:

$$\text{BBC} \qquad \frac{\partial \phi}{\partial z} = 0 \qquad \text{on} \quad z = -h \tag{2.19}$$

Figure 2.2 displays the water wave problem schematically including the governing equation in the fluid and the boundary conditions. Both free surface boundary conditions are applied on the still water level $z = 0$ due the linearization of the BVP.

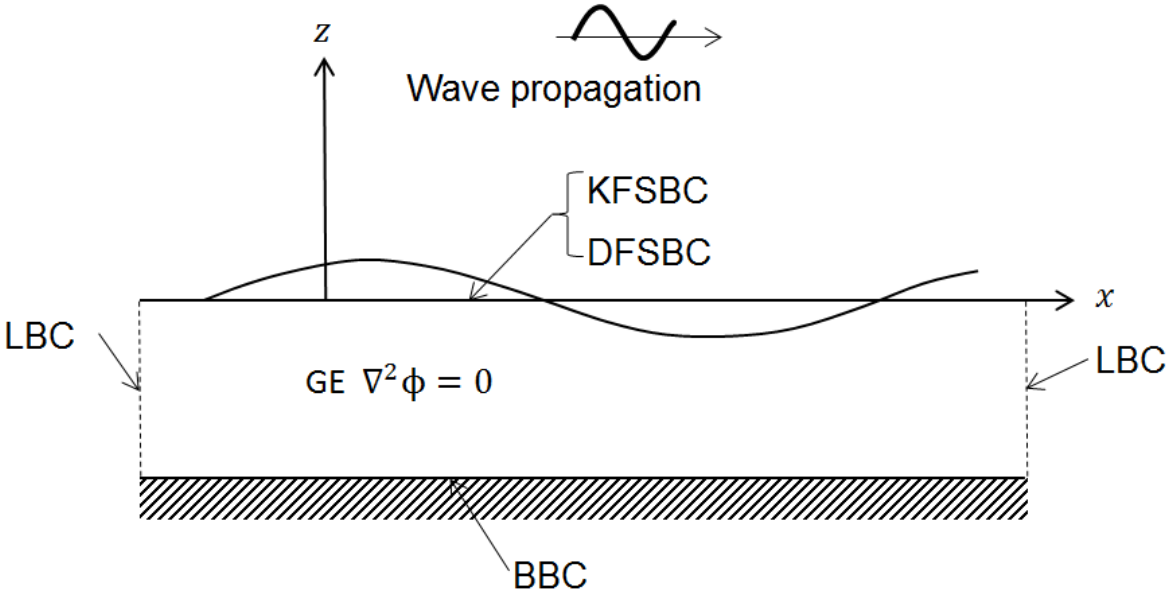

Figure 2.2. Schematic 2DV water-wave boundary value problem.

By employing separation of variables to construct vertical eigenfunctions for the BVP, a solution for the GE (2.12) can be built in the form of:

$$\phi(x, z) = X(x)Z(z). \tag{2.20}$$

Using this form of the velocity potential ϕ in the Laplace equation, gives the following relationship:

$$\frac{1}{X}\left(\frac{\partial^2 X}{\partial x^2}\right) = \frac{1}{Z}\left(\frac{\partial^2 Z}{\partial z^2}\right) = \tau^2 \tag{2.21}$$

The separation constant (or eigenvalue) τ has to be determined using the boundary conditions. A possible solution for $Z(z)$ can be found with

$$Z(z) = C\cos\tau(z+h) + D\sin\tau(z+h) \tag{2.22}$$

To satisfy the BBC (2.19), it is required that $D = 0$. The CFSBC (2.15) is satisfied if the eigenvalue τ is a root of

$$0 = K + \tau\tan\tau h \qquad \text{where} \qquad K = \frac{\omega^2}{g} \tag{2.23}$$

Equation (2.23) has an infinite sequence of real roots (evanescent waves) and a pair of imaginary roots (progressive waves) denoted by $\tau = \pm k_0$ with $k_0 = ik$ and k being the positive root (wave number) of the dispersion relation

$$K = \frac{\omega^2}{g} = k\tanh kh \tag{2.24}$$

Equations (2.12) - (2.15), (2.18), (2.19) and (2.24) describe the 2DV water-wave BVP that is utilized and built upon for the description of water-wave / structure interaction.

2.2. Water-wave / Structure Interaction and Plate Motion Implementation

The surfaces of obstacles or structures in the fluid represent additional boundaries on which the following boundary conditions apply:

(i) For the case of a fixed structure, the velocity component of a fluid particle normal to the structural boundary has to be zero;

$$\frac{\partial\phi}{\partial n} = 0 \qquad \text{on} \quad S_B \tag{2.25}$$

with S_B representing the submerged structure surface.

(ii) For the case of a moving structure (either floating or submerged), the velocity component of a fluid particle normal to the submerged structural boundary has to equal the velocity of the structure in this direction;

$$\frac{\partial \phi}{\partial n} = V_n \qquad \text{on} \quad S_B \tag{2.26}$$

Here V_n is the structural velocity component in the direction of the coordinate normal to the structure surface directed out of the fluid.

In the latter case, further distinction is possible:

(i) Submerged or floating structure is set into motion by the resultant buoyancy force and moves freely.
(ii) The motion of the submerged or floating structure is forced and does not depend on wave or buoyancy forces.

In accordance with linear wave theory, S_B denotes the equilibrium surface of the moving structure. This is the approach Isaacson and Nwogu (1987), Sannasiraj *et al.* (1995), Yip (1997), Yip and Chwang (1997), Yip and Chwang (1998), Cho and Kim (1998), Sannasiraj *et al.* (1998), Mousavizadegan and Rahman (2005), Lee and Newman (2005), An and Faltinsen (2013), Porter (2015) applied (see Table B.1).

Parallel to applying the plate velocity on the equilibrium position of the plate, another approach has been taken by a number of researchers (Danmeier (1998), Hamilton and Yeung (2000), Qiu and Peng (2007), Zhou *et al.* (2014)): the body-non-linear method. Here the free surface is linearized but the body boundary condition is applied on the instantaneous body position. An in-detail description is executed in Section 2.4.

2.2.1. Stationary Plate - Diffraction Problem

When waves encounter a fixed rigid structure, wave diffraction occurs and the superposition of incident and diffracted wave generates a scattered wave field. Please

note that the definition of diffracted and scattered field follows Linton and McIver (2001).

Since linear wave theory is assumed, the principle of superposition is applicable and the total velocity potential can be decomposed into incident potential (Φ_I) and diffracted potential (Φ_D):

$$\Phi_{Sc} = \Phi_I + \Phi_D \tag{2.27}$$

Separating the time dependency of the harmonic motion yields as in equation (2.11)

$$\Phi_{Sc}(x, z, t) = Re\Big\{\Big(\phi_I(x, z) + \phi_D(x, z)\Big)e^{-i\omega t}\Big\} \tag{2.28}$$

The velocity potential of the diffracted wave, ϕ_D, as well as the velocity potential of the incident wave, ϕ_I, have to satisfy the GE in the fluid domain Eq.(2.12), the CFSBC Eq.(2.15), the BBC Eq.(2.19) and the additional boundary condition on the surface of the structure:

$$\frac{\partial \phi_D}{\partial n} = -\frac{\partial \phi_I}{\partial n} \qquad \text{on} \quad S_B \tag{2.29}$$

To acquire a unique solution, the diffracted waves Φ_D have to satisfy a radiation condition that ensures the outwards direction of the diffracted waves. Additionally it is assumed that no localised oscillations (trapped modes) exist. The radiation condition for the diffracted wave in 2D is formulated as

$$\lim_{kx \to \pm\infty} \Big(\frac{\partial \phi_D}{\partial x} \mp ik\omega\Big) = 0 \tag{2.30}$$

with k being the wave number defined in Eq.(2.24).

2.2.2. Moving Plate - Diffraction and Radiation Problem

When waves run over a freely moving structure, wave diffraction occurs and in addition the structure itself is set into motion by the incident wave and radiates waves. Since linear wave theory is assumed, the principle of superposition is applicable and the total velocity potential can be separated into scattered and radiated potential.

$$\Phi = \Phi_{Sc} + \Phi_R \tag{2.31}$$

If the body surface boundary condition is applied on the equilibrium surface of the moving structure, Φ_{Sc} represents the velocity potential due to wave scattering by a fixed structure; Φ_R denotes the solution of the radiation problem assuming forced structure oscillations in otherwise calm water. Separating the time dependency of the harmonic motion yields as in (2.28)

$$\Phi(x,z,t) = Re\Big\{\Big(\phi_{Sc}(x,z) + \phi_R(x,z)\Big)e^{-i\omega t}\Big\} \tag{2.32}$$

with ϕ being the complex-valued spatial velocity potential.

Assuming a rigid body, every structure has six degrees of freedom (DoF) - three lateral motions - surge, sway and heave along the x, y and z axis respectively and three rotational motions - roll, pitch and yaw about the x, y and z axis respectively, a 3D radiation problem is described by six equations of motion and can be decomposed into six velocity potentials due to linearity assumption:

$$\Phi_R = \sum_{m=1}^{6} \Phi_R^{(m)} = Re\Bigg\{\sum_{m=1}^{6}\Big(\phi_R^{(m)} e^{-i\omega t}\Big)\Bigg\} \tag{2.33}$$

Here m represents the radiation due to body oscillation in mode m with: $m = 1$ surge, $m = 2$ sway, $m = 3$ heave, $m = 4$ roll, $m = 5$ pitch and $m = 6$ yaw.

When structural oscillations are forced by an incident wave, incident wave and oscillation are of the same frequency but not necessarily in phase. Thus a phase lag $\varepsilon^{(m)}$ for each of the six DoFs is introduced; leading to a complex oscillation amplitude $\hat{\xi}^{(m)}$ in the form:

$$\hat{\xi}^{(m)} = \xi^{(m)} e^{i\varepsilon^{(m)}} \tag{2.34}$$

Amplitude $\xi^{(m)}$ and phase lag $\varepsilon^{(m)}$ of the plate oscillation are unknown and depend on structural and wave parameters; they are thus part of the solution of the BVP.

The radiation potential due to a structure oscillating in mode m ($m = 1, 2, \ldots, 6$) with complex amplitude $\hat{\xi}^{(m)}$ can then be described with the following expression:

$$\phi_R^{(m)} = -i\omega \hat{\xi}^{(m)} \varphi_R^{(m)} \tag{2.35}$$

As the radiated waves are generated by a submerged structure, the depth dependency of $\varphi_R^{(m)}$ is different from surface wave potentials.

The velocity potentials of the radiated waves, $\phi_R^{(m)}$ ($\varphi_R^{(m)}$) have to satisfy the Laplace equation in the fluid domain, the CFSBC, the BBC and the additional boundary condition on the surface of the structure:

$$\frac{\partial \phi_R^{(m)}}{\partial n} = n^{(m)} \qquad \text{on} \quad S_B \tag{2.36}$$

where $n^{(m)}$ with $m = 1, 2, 3$ are the x, y, z components of the inward unit normal to the body defined by the directional cosines

$$n^{(1)} = \cos(n, x) \qquad n^{(2)} = \cos(n, y) \qquad n^{(3)} = \cos(n, z) \tag{2.37}$$

and $n^{(m)}$ with $m = 4, 5, 6$ represent the components due to rotation about the x, y and z axis. For a point (x, y, z) on S_B rotating about the equilibrium position of the centre of rotation (x', y', z'), $n^{(4)}$, $n^{(5)}$ and $n^{(6)}$ are defined as:

$$\begin{aligned} n^{(4)} &= (y - y')n^{(3)} - (z - z')n^{(2)} \\ n^{(5)} &= (z - z')n^{(1)} - (x - x')n^{(3)} \\ n^{(6)} &= (x - x')n^{(2)} - (y - y')n^{(1)} \end{aligned} \tag{2.38}$$

For a 2D BVP the degrees of freedom reduce to three. Hence the radiation motion of a submerged rigid flat plate can be decomposed into three radiation potentials. For the 2DV case they are: heave - the vertical motion along the z-axis ($m = 3$), surge - the horizontal motion parallel to the x-axis ($m = 1$), and pitch - the rotation about the y-axis ($m = 5$). Then the total velocity potential can be decomposed into potentials of the scattered wave (incident wave and diffracted wave), and the radiated waves due to surging, heaving and pitching of the structure:

$$\Phi(x, z, t) = Re\big\{\big(\phi_{Sc} + \phi_R^{(1)} + \phi_R^{(3)} + \phi_R^{(5)}\big)e^{-i\omega t}\big\} \tag{2.39}$$

In this thesis it is assumed that the flat rigid plate is restrained in the horizontal direction (surge) and therefore it has only two degrees of freedom: heave and pitch (see Figure 2.3). Here d represents the submergence depth of the plate, β_0 is the initial plate inclination and $2a$ indicates the plate width.

With the assumption of surge restraint Equation (2.39) reduces to

$$\Phi(x, z, t) = Re\big\{\big(\phi_{Sc} + \phi_R^{(3)} + \phi_R^{(5)}\big)e^{-i\omega t}\big\} \tag{2.40}$$

where

$$\phi_{Sc}(x, z) = -i\frac{ag}{\omega}\varphi_{Sc}(x, z) \tag{2.41}$$

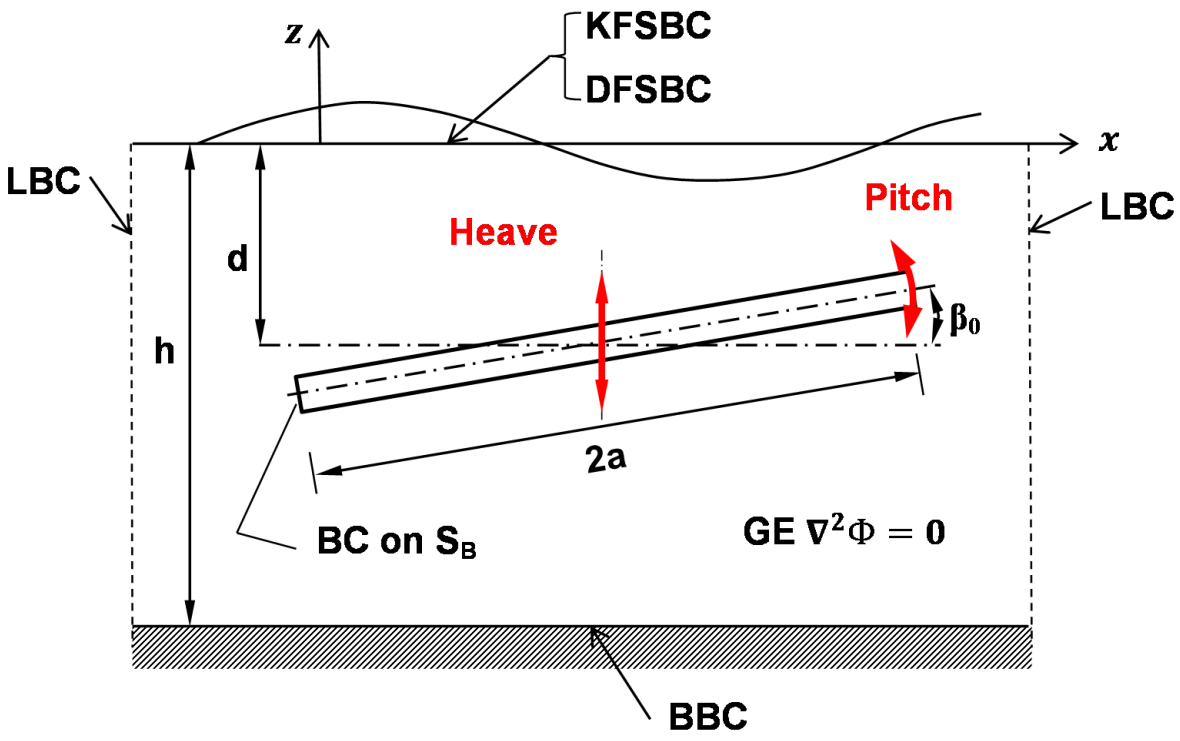

Figure 2.3. Schematic 2DV water-wave/submerged inclined heaving and pitching plate boundary value problem.

$$\phi_R^{(3)}(x,z) = -i\omega\hat{\xi}^{(3)}\varphi_R^{(3)}(x,z) \tag{2.42}$$

$$\phi_R^{(5)}(x,z) = -i\omega\hat{\xi}^{(5)}\varphi_R^{(5)}(x,z) \tag{2.43}$$

As mentioned earlier in the text, the plate motion (amplitude $\xi^{(m)}$ and phase angle $\varepsilon^{(m)}$) caused by excitation through the incident wave is part of the solution of the BVP and depends on structural parameters of the plate (e.g. mass, geometry and submergence) as well as on wave parameters (wave period, water depth and wave height).

Figure 2.4 shows the incidence wave conditions for pure heave and pure pitch. The pressure difference between plate top and bottom are bigger under the wave trough;

under the assumption of uniform mass distribution in the plate, the buoyancy force acting on the plate is bigger under the trough than under the crest and forces the plate to tilt up under the trough (see Figure 2.4b). All other incidence wave positions

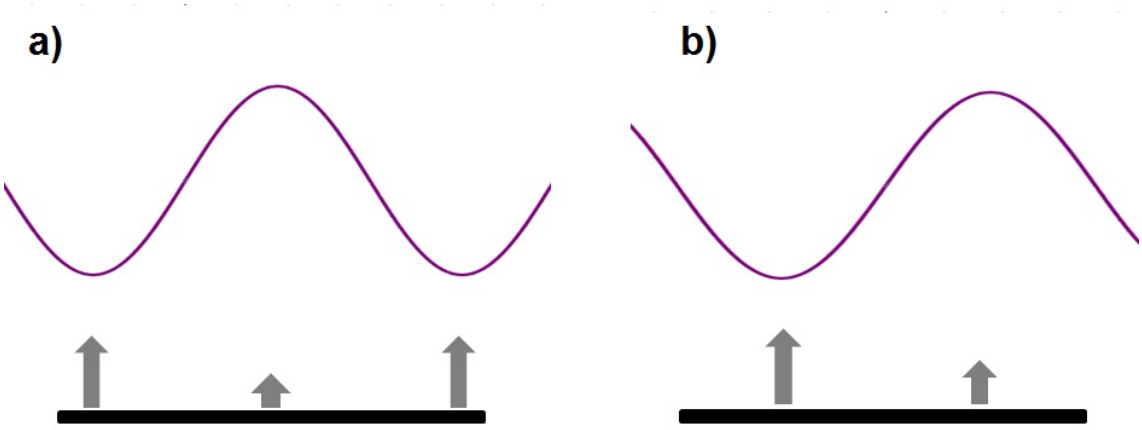

Figure 2.4. Wave incidence conditions for a) pure heave and b) pure pitch.

over the plate will generate combined heaving and pitching; the ratio of the motions depends on structural plate parameters and the plate submergence.

In order to determine the motion response of the structure and implement control via damping, forces and moments induced onto the structure by the incidence wave have to be determined, added mass and radiation damping coefficient of the system for each of the motion modes have to be determined and the equations of motion have to be solved at every time step. This is a complex process and is separately described in APPENDIX A.

A method to avoid this complexity is to prescribe the motion of the submerged or floating body (forced motion). This approach has been used by a number of researchers to either solve pure radiation problems or combined diffraction and radiation setups (Yip, 1997; Yip and Chwang, 1997; Yip and Chwang, 1998; Mousavizadegan and Rahman, 2005; Holmes *et al.*, 2001; Zhou *et al.*, 2014 and Porter, 2015b) and is also applied in this thesis; the implementation of the forced plate motion is described in the following section.

2.2.3. Implementation of Forced Plate Motion

The proposed submerged rigid flat plate breakwater is restrained in surge and allowed to heave and pitch. Heave and pitch amplitudes and the phase shifts between heaving (pitching) and the incident wave are prescribed and do not depend on the incidence wave. However, the motion frequency equals the frequency of the incident wave as this approach albeit simplifying the process still intends to mirror the actual wave-excited radiation.

To distinguish the forced plate motion from the wave-excited plate motion, here a_{heave} and β_{pitch} represent the prescribed plate motion amplitudes as shown in Figure 2.5.

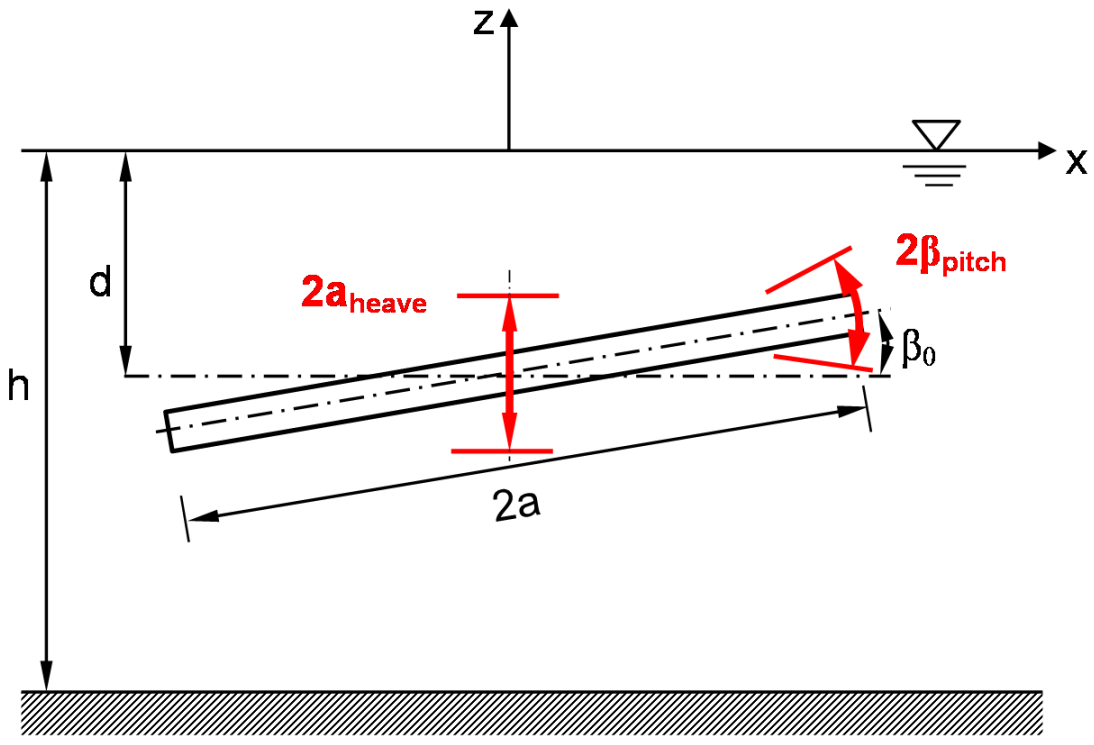

Figure 2.5. Schematic presentation of submerged inclined plate with forced heaving and pitching motion.

Following the approach of McCormick (1981) the forced heaving motion of a flat plate can be described by

$$z(t) = d(x) + a_{heave}\sin(\omega t + \theta_{heave}) \quad \text{for} \quad x \leq \pm a. \tag{2.44}$$

Here $d(x)$ is the initial submergence of the flat plate, a_{heave} represents the prescribed heave amplitude of the plate, ω is the circular wave frequency of the incident wave, and θ_{heave} represents the prescribed phase angle between incident wave and plate heave motion. The distance that the plate moves in one wave period is four times the heave amplitude a_{heave}. The translational velocity of the plate and the acceleration due to heaving are defined as:

$$v_{heave} = \frac{dz}{dt} = \omega a_{heave}\cos(\omega t + \theta_{heave}) \tag{2.45}$$

and

$$\frac{d^2z}{dt^2} = -\omega^2 a_{heave}\sin(\omega t + \theta_{heave}) = -\omega^2 z(t) \tag{2.46}$$

The pitching motion of a flat plate can be described by

$$\beta(t) = \beta_0 + \beta_{pitch}\sin(\omega t + \theta_{pitch}) \tag{2.47}$$

Here β_0 is the design inclination of the flat plate, β_{pitch} represents the prescribed pitching amplitude of the plate in Radian, ω is the circular wave frequency of the incident wave, and θ_{pitch} represents the prescribed phase angle between incident wave and plate pitching motion.

The angular velocity of the plate and the angular acceleration due to pitching are defined as:

$$v_{pitch} = \frac{d\beta}{dt} = \omega\beta_{pitch}\cos(\omega t + \theta_{pitch}) \tag{2.48}$$

and

$$\frac{d^2\beta}{dt^2} = -\omega^2\beta_{pitch}\sin(\omega t + \theta_{pitch}) = -\omega^2\beta(t) \tag{2.49}$$

As the plate is free to move in heave and pitch, combination of both motions are possible and will be investigated. Plate velocity and acceleration are then a combination of Equations (2.45) and (2.48) (velocity) and Equations (2.46) and (2.49) (acceleration).

Velocity and acceleration are equal for all points on a heaving plate; velocity and acceleration of points on a pitching plate however depend on its distance from the pitching axis; this means that water particles near the edges of a pitching plate experience maximum acceleration whereas water particles on the pitching axis are not accelerated in pure pitching motion.

The instantaneous plate position $\big(x(t),\, z(t)\big)$ due to combined forced heaving and pitching can be represented as

$$\begin{aligned} x(t) =& (x_0 - x_p)\cos\big(\beta_{pitch}\sin(\omega t + \theta_{pitch})\big) - \\ & (z_0 - z_p)\sin\big(\beta_{pitch}\sin(\omega t + \theta_{pitch})\big) + x_p \end{aligned} \tag{2.50}$$

for

$$-a\cos\big(\beta_{pitch}\sin(\omega t + \theta_{pitch})\big) \leq x - x_p \leq a\cos\big(\beta_{pitch}\sin(\omega t + \theta_{pitch})\big)$$

and

$$z(t) = z_p + a_{heave}\sin(\omega t + \theta_{heave}) + (x_0 - x_p)\sin\left(\beta_{pitch}\sin(\omega t + \theta_{pitch})\right) + (z_0 - z_p)\cos\left(\beta_{pitch}\sin(\omega t + \theta_{pitch})\right) \tag{2.51}$$

for

$$-a\sin\left(\beta_{pitch}\sin(\omega t + \theta_{pitch})\right) \leq z - z_p \leq a\sin\left(\beta_{pitch}\sin(\omega t + \theta_{pitch})\right)$$

Here (x_p, z_p) is the location of the pitching axis, a is the half-width of the plate, (x_0, z_0) is the initial location and $\beta_{pitch}\sin(\omega t + \theta_{pitch})$ is the instantaneous pitching angle.

Water particle acceleration by plate motion happens on the instantaneous surface of the plate; when modelling with linear wave theory however, the body boundary condition (Eq: 2.36) is also linearized about its equilibrium position $d(x)$ (see Figure 2.5).

As mentioned before, Danmeier (1998), Hamilton and Yeung (2000), Qiu and Peng (2007), Zhou *et al.* (2014) although working with the linearized KFSBC (2.13) and DFSBC (2.14), applied the body boundary condition on the instantaneous body surface under the assumption of small structure motion and thus introduced non-linearity into their otherwise linear models. This approach is called Body-Nonlinear Method and investigated in Section 2.4.

Additionally, by introducing the plate motion with prescribed forcing, energy is put into the system (domain) or taken out of it. This subject is discussed in the following section.

2.3. Discussion of Energy Flux Conservation

In order to analyse the energy flux of a system, Reynold's Transport Theorem can be applied. It provides a general relationship to convert conservation laws from

control mass to control volumes and is given as:

$$\left.\frac{D(F)}{Dt}\right|_{CM} = \frac{d}{dt}\int_{CV} \rho f dV + \int_{CS} \rho f\Big(\vec{v}_{rel}\hat{n}\Big) dA \tag{2.52}$$

Here F is represents any scalar extensive property that obeys conservation laws and f represents its intensive counterpart. The left-hand side represents the material derivative of the property F of the control mass; the first term of the right-hand side describes the time-rate of change inside the control volume corresponding to the control mass (local or internal changes); the second right-hand term represents the net flux of the property leaving the control volume through the available control system surfaces.

Applying Reynold's Transport Theorem to the energy flux of the BVP yields:

$$\left.\frac{D(EF)}{Dt}\right|_{CM} = \frac{d}{dt}\int_{CV} \rho(ef) dV + \int_{CS} \rho(ef)\Big(\vec{v}_{rel}\hat{n}\Big) dA \tag{2.53}$$

Here (EF) represents the total energy flux of the domain and (ef) represents the energy flux per mass. Due to the assumption made in the model setup, the incident wave energy is not converted to thermal energy as fluid is inviscid and irrotational and wave breaking is not permitted. Additionally, the no-flow condition on the bottom avoids energy losses through the bottom boundary. The system does not do any work; plate motion (if present) is due to prescribed forcing and not caused by fluid motion. Only the lateral boundaries allow for energy flux in and out of the domain (system) as can be seen in Figures 2.3 and 2.6.

In Figure 2.6, $EF_{incidence}$ represents the energy flux into the system by the incident wave. $EF_{reflected}$ shows the energy flux out of the system due to wave diffraction towards the wave incidence side and $EF_{transmitted}$ represents the superposition of incidence and diffracted energy flux towards transmission side. These terms are present for a stationary plate in the domain.

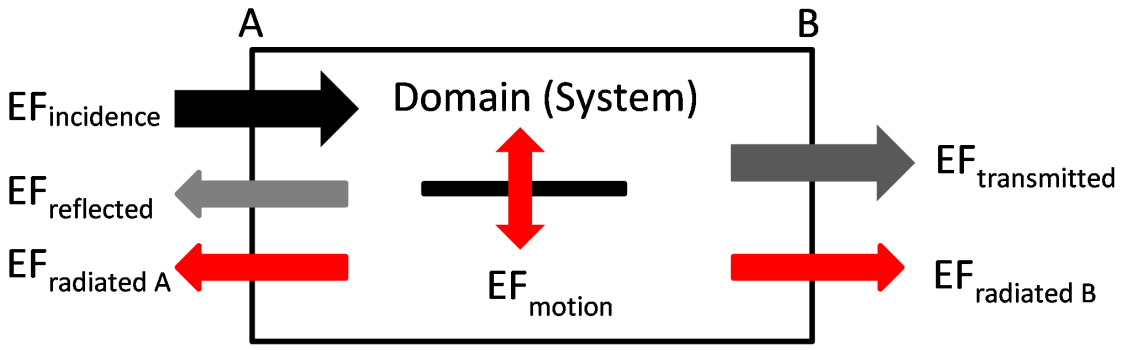

Figure 2.6. Energy flux of domain.

When the plate is forced to move by an external energy source, three additional energy flux terms enter the equation: the flux into the system for forcing the plate to move (EF_{motion}) and the energy flux radiated outwards ($EF_{radiatedA}$ and $EF_{radiatedB}$).

When modelling the stationary plate case under above described assumptions, Equation (2.53) can be simplified to yield the following expression:

$$0 = -EF_{incidence} + EF_{reflected} + EF_{transmitted} \tag{2.54}$$

The energy flux in a progressing wave is described with the following equation:

$$EF = \frac{\rho g H^2}{8} c_g \quad \text{with} \quad c_g = \frac{c}{2}\left\{1 + \frac{2kh}{\sinh 2kh}\right\} \tag{2.55}$$

Here H represents the wave height and c_g the group velocity.

Applying Equation (2.55) in (2.54) and simplifying the expressions, yields:

$$H^2_{incidence} = H^2_{reflected} + H^2_{transmitted} \tag{2.56}$$

Normalising Equation (2.56) with the incidence wave height results in the following expression:

$$1 = \frac{H_{reflected}^2}{H_{incidence}^2} + \frac{H_{transmitted}^2}{H_{incidence}^2} \tag{2.57}$$

Defining the transmission coefficient k_T and the reflection coefficient k_R as

$$k_T = \frac{H_{transmitted}}{H_{incidence}} \tag{2.58}$$

$$k_R = \frac{H_{reflected}}{H_{incidence}} \tag{2.59}$$

and implementing these expressions in Equation (2.56) yields:

$$k_T^2 + k_R^2 = 1 \tag{2.60}$$

Equation (2.60) therefore expresses that the sum of the ratios of reflected and transmitted energy to the incident energy is 100%; no energy is lost or added. In the following chapters the sum of k_T^2 and k_R^2 is referred to as relative energy flux. Relative energy flux is conserved for all stationary plate test runs.

When modelling a moving plate with prescribed plate forcing under above described assumptions, additional terms have to be added to account for the forced plate motion and the radiated waves and Equation (2.53) leads to the following expression:

$$0 = -EF_{incidence} - EF_{motion} + EF_{reflected} + EF_{transmitted} + EF_{radiated} \tag{2.61}$$

where

$$EF_{radiated} = EF_{radiatedA} + EF_{radiatedB} \tag{2.62}$$

Following the steps done for the stationary plate and defining

$$k_{Motion} = \frac{2a_{motion}}{H_{incidence}} \tag{2.63}$$

$$k_{Rad} = \frac{H_{radiated}}{H_{incidence}} \tag{2.64}$$

as motion and radiation coefficient respectively, Equation (2.61) yields:

$$k_T^2 + k_R^2 = 1 + k_{Motion}^2 - k_{Rad}^2 \tag{2.65}$$

When

$$k_{Rad}^2 > k_{Motion}^2$$

the system shows an energy deficit and when

$$k_{Rad}^2 < k_{Motion}^2$$

the systems gains energy.

2.4. Body-Nonlinear Method

In their research Zhou *et al.* (2014) compared linear, body-nonlinear and fully nonlinear models for the radiation problem of submerged spheres and cylinders. Their investigations show that the results based on body-nonlinear and fully non-linear model agree well for small oscillation frequency whereas the linear model results differ strongly. The differences between results yielded with body-nonlinear and fully nonlinear method increase with increasing wave number but outperform the linear model. Zhou *et al.* (2014) state that when the surface non-linearity is kept small, the body-nonlinear method is a promising alternative to the fully nonlinear method as it avoids the prob-

lems of dealing with the instantaneous free surface and related possible numerical instabilities.

2.4.1. Introduction of Nonlinearity through Body-Nonlinear Method

By prescribing the instantaneous plate velocity and plate position using Equations (2.45), (2.48), (2.50) and (2.51), an additional dependency between plate velocity and plate position is introduced.

For simplicity here the analytical proof of the introduction of nonlinearity is done for heave only but can be extended to pitch and combined heaving and pitching. For further simplification, the coordinate system origin is placed on $(0, -d)$ so that the plate position for heaving motion is now prescribed by

$$z(t) = a_{heave} \sin(\omega t + \theta_{heave}) \tag{2.66}$$

Velocity and acceleration are defined by Equations (2.45) and (2.46). The heaving plate accelerates the water particles on its surface while moving in the water. The particle velocity due to the heaving plate is a function of plate location and time:

$$w = w(z, t) \tag{2.67}$$

The acceleration of the water particles ($a_{particle}$) is the time rate of change of their velocity. As the velocity is a function of position and time (see Figure 2.7), the acceleration is affected by the change in time as well as the change in particle position:

$$a_{particle} = \frac{\partial w}{\partial t} + w\frac{\partial w}{\partial z} \tag{2.68}$$

With the known plate velocity (2.45) and acceleration (2.46), the spatial rate of change in particle velocity is described by:

$$\frac{\partial w}{\partial z} = \frac{\partial w}{\partial t}\frac{\partial t}{\partial z} = \frac{-\omega^2 a_{heave}\sin(\omega t + \theta_{heave})}{\omega a_{heave}\cos(\omega t + \theta_{heave})}$$

$$\frac{\partial w}{\partial z} = \omega\frac{\sin(\omega t + \theta_{heave})}{\cos(\omega t + \theta_{heave})} = \omega\tan(\omega t + \theta_{heave}) \tag{2.69}$$

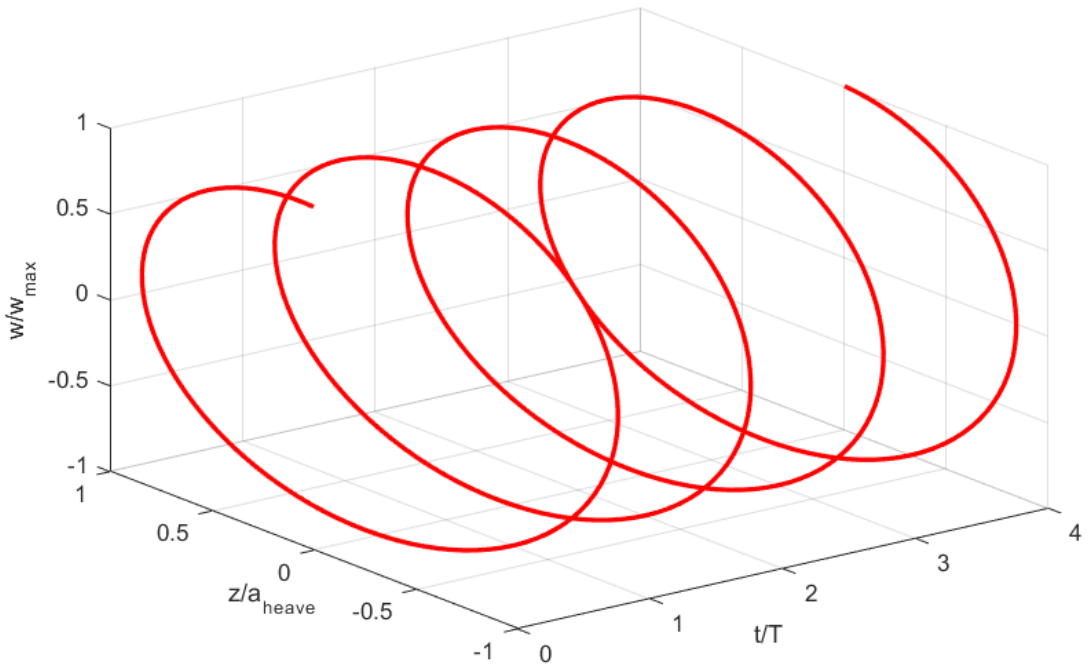

Figure 2.7. Heaving plate velocity in space and time.

The tangent function has singularities at $\pm\frac{N\pi}{2}$ with $N = 1, 3, 5\ldots$. This means that these singularities occur harmonically with a period of $\frac{1}{2}T$ of the plate motion period. Every time when the plate velocity passes through zero, the spatial derivative becomes singular (see Figure 2.5).

Equation (2.69) shows that the plate motion now introduces nonlinearity into the model. The generation of higher harmonics is due to the application of the body boundary condition on the instantaneous body surface.

This effect has been described by Isichenko and Yan'kov (1984) for laser radiation and by Försterling and Wüster (1951) for electromagnetic waves and was utilized by Danmeier (1998), Hamilton and Yeung (2000), Qiu and Peng (2007), Zhou *et al.* (2014) to include generated higher harmonics in linear modelling.

2.4.2. Necessary Conditions for Applicability of Linear Approximation of Body-Nonlinear Wave Problem

For ensuring the applicability of linear wave theory and the superposition principle, the nonlinearities introduced by the body-nonlinear method have to be small. Following the approach of Hammack (1973) to determine the necessary conditions for applicability of the linear solution, the following governing equations have to be examined to determine the magnitude of the introduced nonlinear effects by the plate motion:

(i) Equation of motion in x-direction (inviscid fluid):

$$u^*_{t^*} + u^* u^*_{x^*} + w^* u^*_{z^*} + \frac{1}{\rho} P^*_{x^*} = 0 \tag{2.70}$$

(ii) Equation of motion in z-direction (inviscid fluid):

$$w^*_{t^*} + u^* w^*_{x^*} + w^* w^*_{z^*} + \frac{1}{\rho} P^*_{z^*} + g = 0 \tag{2.71}$$

(iii) Two-dimensional conservation-of-mass equation for an incompressible fluid:

$$u^*_{x^*} + w^*_{z^*} = 0 \tag{2.72}$$

Here ρ and P^* are the fluid density and pressure; the asterisk marks dimensional variables. The surface and plate boundary conditions are (for a heaving plate):

$$w^* = \begin{cases} \eta^*_{t^*} + u^* \eta^*_{x^*} & \text{on} \quad z^* = \eta^* \\ \xi^*_{t^*} + u^* \xi^*_{x^*} & \text{on} \quad z^* = -d + \xi^* \end{cases} \tag{2.73}$$

The magnitude of the nonlinear terms neglected in the linear treatment of the problem has to be determined for continuous plate movement for which is assumed that the water surface elevations due to diffraction and radiation have sufficient time to travel from the plate centre into $+x$ and $-x$ direction during one plate motion cycle. At the end of one cycle, the water displaced by presence and motion of the heaving plate will be distributed over a length proportional to

$$L = \frac{gT^2}{2\pi} \tanh\left(\frac{2\pi}{L} h\right)$$

This is used as appropriate length scale for the generated wave.

The characteristic amplitude for the displaced water is determined by assuming that the water volume displaced by the heaving plate is equal to the water volume of the radiated surface wave; additionally the incident wave amplitude has to be implemented.

This gives

$$\frac{a_{heave} a + a_{inc} L}{L}$$

with a being the half-width of the plate, a_{heave} the heaving amplitude and a_{inc} the amplitude of the incident wave.

An appropriate time scale will be the time, the variations of the generated wave need to travel across half of the plate; which is (aT/L).

In heaving motion, the horizontal velocity u^* arises from the motion of the radiated and the incident waves only (plate motion has no direct influence) and is of order

$$\frac{a_{heave}a + a_{inc}L}{Td}$$

with d being the submergence depth of the plate.

The vertical motion of a fluid particle above the plate is influenced by the wave as well as the plate motion. Here the diffracted and incident waves have opposite signs and the resultant vertical velocity due to scattering on the horizontal plate boundary is zero. This leaves the plate velocity on the instantaneous plate boundary as the dominant vertical motion of the fluid particle in the vicinity of the plate. The appropriate vertical velocity is therefore

$$\frac{4a_{heave}}{T}$$

The pressure is scaled by $\rho g d$. This gives the following scaling equations:

$$\begin{gathered} x^* = L \cdot x, \qquad z^* = d \cdot z, \qquad t^* = a\frac{T}{L}t, \qquad u^* = \frac{a_{heave}a + a_{inc}L}{Td}u \\ w^* = \frac{4a_{heave}}{T}w, \qquad \eta^* = \frac{a_{heave}a + a_{inc}L}{L}\eta, \qquad \xi^* = \frac{a_{heave}a}{L}\xi, \qquad P^* = \rho g d P \end{gathered} \tag{2.74}$$

Using Equations (2.74) to write Equations (2.70) - (2.73) in non-dimensional variables yields:

$$\begin{aligned} u_t + \Big(\frac{a_{heave}a + a_{inc}L}{Ld}\Big)\frac{a}{L}uu_x + \frac{a}{L}\frac{4a_{heave}}{d}wu_z \\ + \frac{gT^2}{L}\frac{a}{L}\Big(\frac{a_{heave}a + a_{inc}L}{d^2}\Big)^{-1}P_x = 0 \end{aligned} \tag{2.75}$$

$$w_t + \Big(\frac{a_{heave}a + a_{inc}L}{Ld}\Big)\frac{a}{L}uw_x + \frac{a}{L}\frac{4a_{heave}}{d}ww_z + \frac{gT^2}{L}\Big(\frac{4a_{heave}}{a}\Big)^{-1}(P_z + 1) = 0 \tag{2.76}$$

$$u_x + \frac{4a_{heave}L}{a_{heave}a + a_{inc}L}w_z = 0 \tag{2.77}$$

$$w = \begin{cases} \dfrac{a_{heave}a + a_{inc}L}{4a_{heave}a}\eta_t + \dfrac{(a_{heave}a + a_{inc}L)^2}{4a_{heave}d \cdot L^2}u\eta_x & \text{on} \\ & z = \dfrac{a_{heave}a + a_{inc}L}{d \cdot L}\eta \\ \dfrac{1}{4}\xi_t + \dfrac{1}{4}\dfrac{a_{heave}a + a_{inc}L}{Ld}\dfrac{a}{L}u\xi_x & \text{on} \\ & z = 1 - \dfrac{a_{heave}a}{d \cdot L}\xi \end{cases} \tag{2.78}$$

Equations (2.75) - (2.78) show that linear wave theory is applicable when the following two conditions are satisfied:

$$\frac{a_{heave}a + a_{inc}L}{Ld}\frac{a}{L} \ll 1 \tag{2.79}$$

$$\frac{a}{L}\frac{4a_{heave}}{d} \ll 1 \tag{2.80}$$

$$\frac{(a_{heave}a + a_{inc}L)^2}{4a_{heave}L^2d} \ll 1 \tag{2.81}$$

The above derived conditions are pre-requisites for the application of linear wave theory and restrict the magnitude of the heaving amplitude (pitching amplitude) and

the wave height of the incidence wave. For the configuration of the model parameters in Section 5.1, Equations (2.79), (2.80) and (2.81) will be utilized.

3. REVIEW OF AVAILABLE METHODS TO SOLVE THE WAVE / STRUCTURE BOUNDARY VALUE PROBLEM

Difficulties in solving the linearized water wave equations are mainly due to the mixed boundary conditions on the mean free surface. For harmonic waves, the FSBCs involve the velocity potential and its directional derivative. Due to this only few explicit solutions for wave scattering by fixed bodies with simple geometries are available (see Porter, 2002) and therefore according to Evans and Porter (1997) often numerical methods have to be applied.

In APPENDIX B an overview of the theoretical approaches to solve the boundary value problem of wave and structure interactions in the context of linear wave theory is given. Table B.1 covers solution approaches of the last 68 years.

In the following sections, the different available solution methods are described, their advantages and restrictions of applicability are summarised in Table C.1 in APPENDIX C.

3.1. Eigenfunction Expansion Technique and Matched Eigenfunction Expansion (MEE)

Scattering Problem: If separation of variables is possible, the velocity potential can be written in terms of an infinite series of separated eigenfunctions (eigenfunction expansion).

Separation of variables for Laplace's equation is possible in different coordinate systems. But the separation of variables of the boundary conditions is restricted to simple geometries. For these cases, the boundary value problem can be solved accurately with a single eigenfunction expansion (e.g. vertical circular cylinder).

For more realistic obstacle or body geometries, the scattering BVP can be divided into a number of regions where then different suitable eigenfunction expansions represent the solution in the respective region and have to be matched across the boundaries of the adjacent regions (matched eigenfunction expansions).

If other techniques like finite-element technique (as in Bai, 1975 and Patarapanich, 1984a) or boundary integral equation method (as by Liu and Abbaspour, 1982a; Liu and Abbaspour, 1982b; Cho and Kim, 1998; Cho and Kim, 2008 and An and Faltinsen, 2013) are applied to the regions that contain obstacles, the inner numerical representation has to be matched to the outer analytical solutions achieved by eigenfunction expansions. This solution form represents a hybrid element technique.

Radiation Problem: Assuming rigid body motions, dynamic responses of the moored structure in 2D are determined through three equations of motion (for heave, roll and sway). The BVP is decomposed into four different velocity potentials: wave scattering by a fixed structure and wave radiation by each mode of motion; this approach has been used by Abul-Azm and Gesraha (2000) and McIver (1996).

For each mode of motion, the coefficients of the series of separated eigenfunctions have to be determined and matched across the boundaries of adjacent regions. Prescribing the motion of the submerged obstacle (forced motion) instead of determining the response to the incident wave is another possible approach and has been used by Yip (1997), Yip and Chwang (1997) and Yip and Chwang (1998) with constriction to pitch only.

3.2. Multipole Expansion Method

In the multipole expansion method, the velocity potential in the fluid is composed of a linear combination of multipoles (singularities) appropriately distributed in the bodies present in the fluid. In addition to the governing equation, the individual singularities satisfy the free surface and bottom conditions, and a radiation condition that ensures that the constructed waves are outgoing waves in the far-field.

The complete set of multipoles satisfies the boundary condition on the body; depending on the number and type of multipoles, different body geometries can be represented. The singularities are represented by integral equations and the velocity potential (sum of singularities) can be obtained by power series or eigenfunction series expansion as described in Linton and McIver (2001). The thus obtained infinite system of linear algebraic equations for the unknown coefficients in the multipole sum can be solved numerically. In general only a few equations are required to achieve satisfactory accuracy as the simultaneous equations converge quickly.

3.3. Wiener-Hopf Technique

The Wiener-Hopf technique is an effective method to solve a range of linear partial differential equations with boundary conditions in semi-infinite domains explicitly. In the Wiener-Hopf technique, the governing differential equation is reduced to a functional equation by means of Fourier transform:

$$A(\lambda)\Psi_+(\lambda) + B(\lambda)\Psi_-(\lambda) + C(\lambda) = 0$$

where A, B and C are known functions of the complex variable $\lambda = \sigma + i\tau$ in a strip $\tau_- < \mathrm{Im}\,\lambda < \tau_+$ and A and B are nonzero; $\Psi_+(\lambda)$ and $\Psi_-(\lambda)$ are to-be-determined functions with the following properties: $\Psi_+(\lambda)$ is analytic for $\mathrm{Im}\,\lambda > \tau_-$ and $\Psi_-(\lambda)$ is analytic for $\mathrm{Im}\,\lambda < \tau_+$.

Assuming that a representation $A(\lambda)/B(\lambda) = L_+(\lambda)/L_-(\lambda)$ is possible and substituting $L_-(\lambda)C(\lambda)/B(\lambda) = D_+(\lambda) + D_-(\lambda)$, the functional equation becomes:

$$L_+(\lambda)\Psi_+(\lambda) + D_+(\lambda) = -L_-(\lambda)\Psi_-(\lambda) - D_-(\lambda)$$

As the left and right hand side of this equation have a common strip of analyticity, a unique function $P(\lambda)$ exists in the entire domain of analyticity and equals both, the left and the right hand side. Using this function $P(\lambda)$ the unknown functions $\Psi_+(\lambda)$

and $\Psi_{-}(\lambda)$ can be determined.

Further information about the method can be found in Dmitriev (2011) and Noble (1958).

3.4. Combination of Matched Eigenfunction Expansions and Residue Calculus Theory

In this method the matched eigenfunction expansions (as described in Section 3.1) are solved exactly by establishing a meromorphic function that exhibits a distribution of poles and zeros such that the residues of the meromorphic function correspond to the unknown coefficients of the eigenfunction expansion.

This method is described by Linton and McIver (2001) and Evans (2004) and is applicable to problems where one of the boundary conditions is only valid in a finite interval e.g. finite obstacle.

3.5. Hypersingular Integral Equation

Linton and McIver (2001) and Porter (2002) describe two main approaches for this method:

(i) Solution is built by distributing wave sources over the surface of the floating or submerged body that satisfy the governing equation and the boundary conditions. An integral equation is formed for the to-be-determined source strengths.
(ii) Application of Green's Theorem and a suitable fundamental solution to obtain a second-kind integral equation of Fredholm type for the velocity potential on the submerged obstacle.

The so obtained integral equations can then be transformed into standard boundary integral equations and solved numerically.

For the case of thin plates the cross-sectional area shrinks to zero; then the integral equation declines to a hypersingular integral equation (see Martin and Farina (1997)) and the above approaches need adaptations as the kernel of the integrals become singular and numerical treatment is problematic as stated in Porter (2002).

Parsons and Martin (1992) and Parsons and Martin (1994) developed a method for wave scattering by thin plates (horizontal, inclined, vertical) with formulating a hypersingular integral equation for the unknown jump of the velocity potential across the plate; their approach was limited to infinite water depth.

Porter (2002) formulated the wave scattering problem as integral equation for a function related to the tangential fluid velocity around the submerged obstacle; the kernel of the integral operator is only weakly singular. This and the introduction of special test functions for correctly modelling the singular behaviour at the plate edges allow for results in finite and infinite water depths. This approach is extended to the radiation problem of forced oscillation in Porter (2015b).

3.6. Numerical Methods

In addition to analytical and hybrid approaches described above, a number of researchers applied pure numerical methods to solve the wave scattering and/or radiation problem.

The marker and cell (MAC) method has been applied by Takaki (2001) and Takaki *et al.* (2002) to determine the forces and moments on and transmission coefficients of stationary submerged horizontal and inclined plates.

In essence, the MAC method is a finite difference solution technique based on an Eulerian staggered grid system and employs the variables' pressure and velocity (see McKee *et al.* (2008)). For solving free surface flow problems, the codes are very complex. As they are not available to the author, this method is albeit its potential not further considered.

Finite Element Method (FEM) has been applied by Bettess and Zienkiewicz (1977) for parabolic shoals, by Sannasiraj *et al.* (1998) for floating rigid pontoons and by Wu *et al.* (2013) for a submerged cylinder in viscous fluid.

The Boundary Element Method (BEM) has been used by Isaacson and Nwogu (1987) for a semi-immersed floating cylinder, by Yu and Chwang (1994) for a submerged horizontal porous plate, by Hsu and Wu (1999) for a stationary submerged horizontal plate, by Mousavizadegan and Rahman (2005) for submerged spheres and ellipsoids, by Qiu *et al.* (2006) for floating hemispheres and cylinders, by Lee and Newman (2005) for a submerged spar and by Wang *et al.* (2012) for a submerged horizontal plate.

3.7. Summary

Table B.1 shows, that a large selection of methods has been used to solve wave/ structure interaction BVPs, very often with geometrical restriction to ensure solvability. Table C.1 summarises the benefits and disadvantages of the methods described in Sections 3.1 - 3.6.

Taking this information into account and considering the finite width, the implemented option of inclination and motion of the submerged rigid flat plate utilized in this thesis, the following conclusion regarding the applicability of the above-described methods can be made:

Eigenfunction Expansion technique and Multipole Expansion Method require that boundaries have to coincide with coordinate lines or surfaces; as plate inclination is proposed, these methods are not applicable.

The Combination of Matched Eigenfunction Expansion and Residue Calculus Theory can only be applied to the finite plate case if the plate width is big enough compared to the wavelength; this would restrict the design parameter choice and is therefore discarded.

The Wiener-Hopf technique is limited to semi-infinite plate width and can therefore not be used here.

The Hypersingular Integral Equation method has been employed to stationary plates by Parsons and Martin (1992), Parsons and Martin (1994), Kanoria and Mandal (2001) and Porter (2002); Porter (2015b) extended this method to the pure radiation case but stated that there is no analytically established relation between motion amplitude and surface wave Porter (2015a). This prohibits the application of this analytical method to the combined diffraction/ radiation problem.

To avoid the disadvantages of the FEM and BEM methods described in Table C.1, this research is conducted numerically using the meshless, boundary-only radial-basis-function collocation method following the approach of Wu *et al.* (2006), Wu *et al.* (2008) and Börekçi (2014) and extending it to accommodate the presence and motion of the SFP.

4. NUMERICAL SOLUTION OF WAVE-STRUCTURE BVP USING RBF COLLOCATION METHOD

4.1. Introduction

The propagation of gravity driven waves occurs in a horizontally unbounded (computationally infinite) domain. To be able to model water wave propagation numerically, the initially unbounded setup has to be truncated and a finite BVP has to be established. Suitable and feasible boundary conditions (BCs) have to be applied on physical and artificially defined boundaries so that the numerical solution yielded in the finite domain matches the solution in the original, unbounded domain.

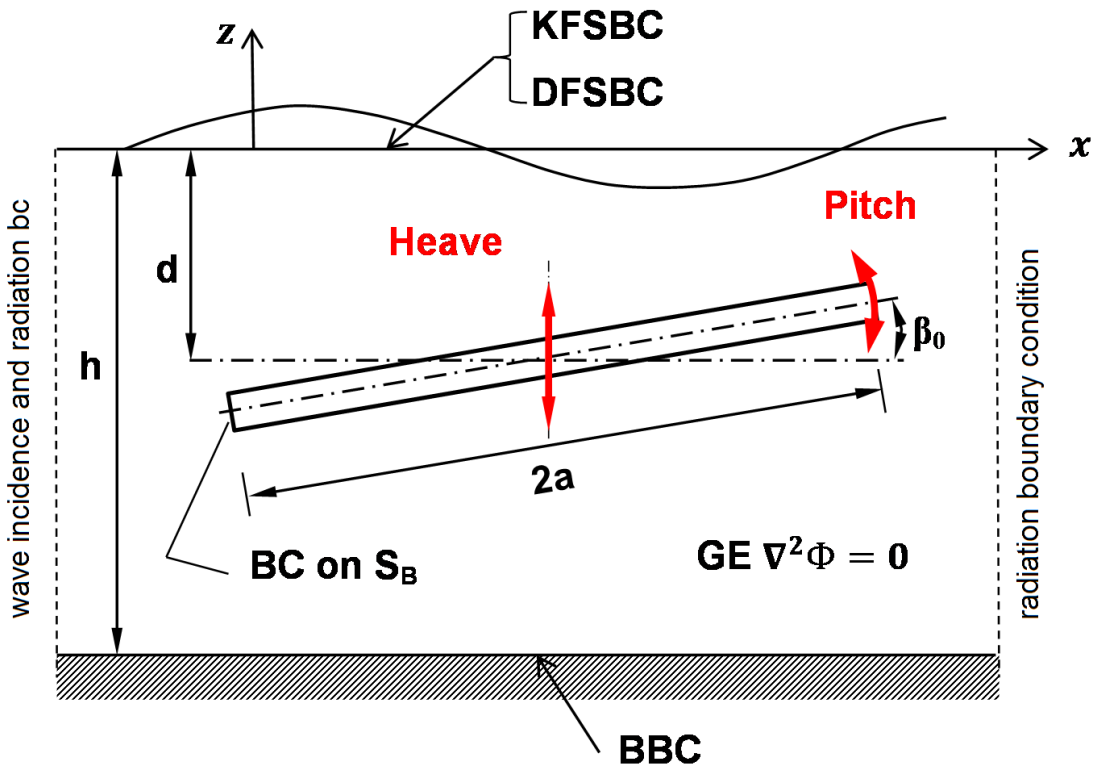

Figure 4.1. Numerical domain for 2DV water-wave/structure boundary value problem.

In a two-dimensional vertical (2DV) domain (see Figure 4.1) the water surface and the sea bottom comprise two physical boundaries of the computational domain

and the appropriate BCs (KFSBC, DFSBC and BBC) have been derived in Chapter 2 (Equations 2.13, 2.14 and 2.19 respectively).

The wave propagation direction is truncated by two artificial boundaries: a wave incidence boundary (either in form of a moving wave paddle as done by Dean and Dalrymple (1991), Wu *et al.* (2006), Wu *et al.* (2008), or a fixed boundary on which the wave input is given in form of the analytical velocity potential as in Haas (1997) and Börekçi (2014)), and the radiation boundary. Due to the presence of the submerged obstacle, waves are diffracted and/or radiated towards the wave incidence boundary so that it becomes a combined incidence and radiation boundary. This poses an additional problem and is investigated in Section 4.4.

For pure radiation boundaries, the Sommerfeld radiation condition is often used in linear wave theory to guarantee that only outgoing waves are present and thus ensure the uniqueness of the solution (Schot, 1992; Cao *et al.*, 1993; Dean and Dalrymple, 1991 and Linton and McIver, 2001). The Sommerfeld radiation condition is defined as

$$\frac{\partial \Phi}{\partial t} = -c\frac{\partial \Phi}{\partial x} \qquad \text{on} \qquad x = x_R \tag{4.1}$$

with x_R being the x-coordinate of the radiation boundary. As (4.1) is only a relation between time derivative and spatial derivative of the velocity potential normal to boundaries far away from sources, according to Espinoza *et al.* (2014) it is not exact when the wave incidence is non-perpendicular or the radiation boundary is located close to sources (e.g. scatterers). Further investigation will be carried out in Section 4.4.

4.2. RBF Collocation Method and Method of Fundamental Solution

The water-wave/structure 2DV BVP derived in Chapter 2 is solved numerically using the RBF collocation method introduced by Kansa (1990).

In the RBF collocation method only the Euclidean distance between collocation points (or collocation points and RBF centres) is used to approximate the unknown function that satisfies the partial differential equation (PDE); no mesh has to be generated, thus it is independent of the geometric complexity of the problem at hand. With this numerical technique it is possible to satisfy boundary conditions at the boundary (if necessary even more than one) and also the governing equation inside the domain of interest.

The GE of the water-wave/structure BVP is the Laplace equation (2.12). Using the fundamental solution (or Green's function) of the Laplace equation $f(r) = \ln r$ as radial basis function allows for a boundary-only solution because the governing equation inside the domain is automatically satisfied. This approach is known as Method of Fundamental Solution (MFS) and has been used by Wu *et al.* (2006), Wu *et al.* (2008) and Börekçi (2014) to model water-wave BVPs.

As no internal collocation points are necessary, computation time and storage requirements are kept small compared to the full solution.

Green's function RBF for the GE is defined as:

$$f(r_{ij}) = \ln r_{ij} \qquad \text{with} \qquad r_{ij} = \sqrt{(xc_i - xrbf_j)^2 + (zc_i - zrbf_j)^2} \tag{4.2}$$

with (xc,zc) representing the x- and z-coordinates of the collocation points and the variables ($xrbf$,$zrbf$) representing the x- and z-coordinates of the RBF centres.

The spatial derivatives of Green's function are:

$$f^x_{ij}(r_{ij}) = \frac{xc_i - xrbf_j}{r^2_{ij}} \qquad f^z_{ij}(r_{ij}) = \frac{zc_i - zrbf_j}{r^2_{ij}} \tag{4.3}$$

Here the superscript defines the derivative direction; xc, zc, $xrbf$ and $zrbf$ are the x and z coordinates of the collocation points and RBF centres respectively.

As the natural logarithm has a singularity at zero, the distance between RBF centres and collocation points has to be non-zero. Thus two different sets of nodes have to be selected: the collocation points (xc, zc) are located on the actual boundary of the domain and the RBF centres $(xrbf, zrbf)$ are placed outside the domain. The number and placement of collocation points and the RBF centre location affect the accuracy of the solution and an optimization procedure is required.

Figure 4.2 displays an example for the positioning of collocation points and RBF centres for the linear BVP with a stationary horizontal submerged flat plate.

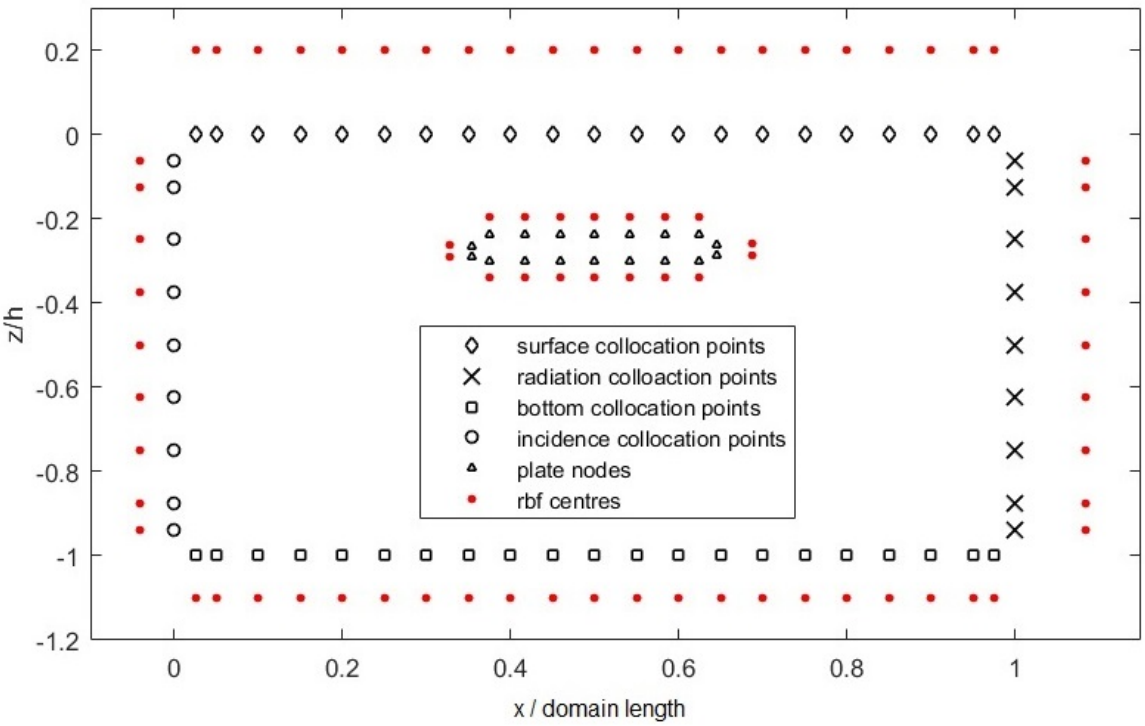

Figure 4.2. Alignment of boundary collocation points and RBF centres in setup of numerical model.

The unknown velocity potential Φ of the water-wave/structure BVP for a fixed structure is approximated by a linear combination of N radial basis functions f with N being the number of collocation points (RBF centres):

$$\Phi_i(x, z, t) \cong \sum_{j=1}^{N} \alpha_j(t) f_{ij}(x, z) \tag{4.4}$$

where the factors $\alpha_j(t)$ are time-dependent and represent the weights of the RBF centres (or sources) at each time step.

Using the superscript (n) to denote the n^{th} time step, the spatial derivatives of the velocity potential are defined as:

$$\left(\frac{\partial \Phi_i}{\partial x}\right)^{(n)} \cong \sum_{j=1}^{N} \alpha_j^{(n)} \frac{\partial f_{ij}}{\partial x} = \sum_{j=1}^{N} \alpha_j^{(n)} f_{ij}^x(r_{ij}) \tag{4.5}$$

$$\left(\frac{\partial \Phi_i}{\partial z}\right)^{(n)} \cong \sum_{j=1}^{N} \alpha_j^{(n)} \frac{\partial f_{ij}}{\partial z} = \sum_{j=1}^{N} \alpha_j^{(n)} f_{ij}^z(r_{ij}) \tag{4.6}$$

with $f_{ij}^x(r_{ij})$ and $f_{ij}^z(r_{ij})$ defined in Equation (4.3). The fundamental-solution-RBF has to satisfy the boundary conditions on all boundaries of the BVP.

In the following sections the applied numerical method is described for a water-wave BVP only, then as mentioned before, the numerical treatment of combined incidence and radiation boundary, as well as the pure radiation boundary, are investigated and consecutively the numerical method extended to the water-wave/structure BVP.

4.3. Setup of the Water - wave Boundary Value Problem with the RBF Collocation Method

The numerical configuration of the BVP follows the approach of (Börekçi, 2014); the schematic numerical BVP domain with GE and applicable boundary conditions is represented in Figure 4.3; here the boundaries 1 - 4 represent:

- 1 Free surface with KFSBC (Eq.(2.13)) and DFSBC (Eq.(2.14))
- 2 Radiation side with Sommerfeld radiation condition (Eq.(4.1))
- 3 Sea bottom with BBC (Eq.(2.19))
- 4 Wave incidence side with input from analytical solution

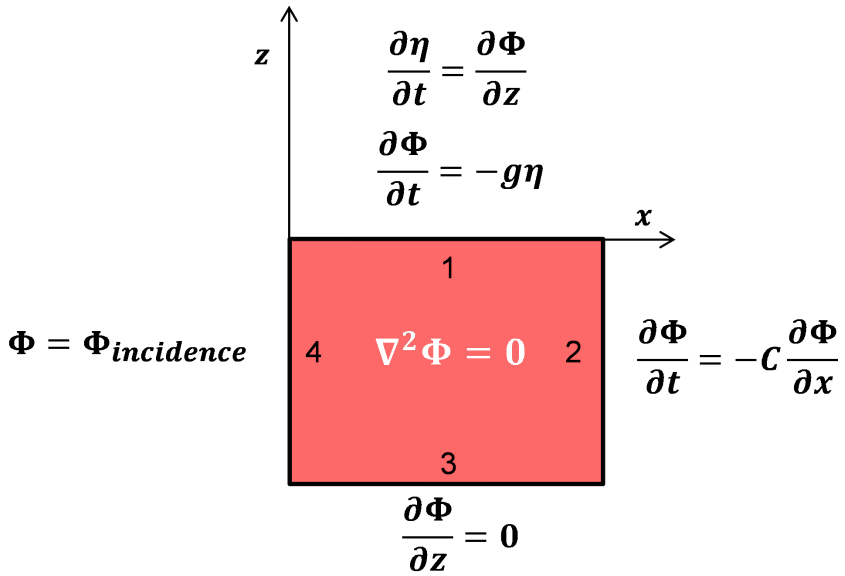

Figure 4.3. Numerical setup of BVP with original boundary conditions.

As all BCs but the BBC hold a time dependency, these equations will be employed for the time integration and only the velocity potential on the sea bottom boundary is computed with the RBF collocation method. As in Börekçi (2014), for every time step the velocity potential on the wave incidence boundary (4) is determined using the analytical solution of the LWT. The KFSBC is time-integrated to compute the surface displacement $\eta^{(n+1)}$ at the new time step $(n+1)$ and the DFSBC is time-integrated to determine the velocity potential $\Phi^{(n+1)}$ on the surface. On the radiation boundary, the RBC is time-integrated to determine the velocity potential $\Phi^{(n+1)}$ on the radiation boundary.

After establishing the configuration of collocation points and RBF centres, the elements of the RBF matrix ($f(r_{ij})$) and the elements of the derivative matrices (f^x_{ij} and f^z_{ij}) are computed using Eq.(4.2) and Eq.(4.3) respectively. Then the system matrix $\boldsymbol{A}$ in Eq.(4.18) is generated and the time marching scheme as follows is applied:

(i) Compute the velocity potential $\Phi^{(n+1)}_{4\_analyt}$ of the incident wave using the analytical solution - Eq.(4.11).

(ii) Integrate the KFSBC to determine $\eta^{(n+1)}$ using Eq.(4.7).

(iii) Integrate the DFSBC to determine $\Phi_{1\_AB4}^{(n+1)}$ using Eq.(4.8).

(iv) Integrate the RBC to determine $\Phi_{2\_AB4}^{(n+1)}$ using Eq.(4.9).

(v) Set up the RBF system with Dirichlet BCs $\Phi_{1\_AB4}^{(n+1)}$ on surface, $\Phi_{2\_AB4}^{(n+1)}$ on radiation and $\Phi_{4\_analyt}^{(n+1)}$ on incidence boundaries and determine $\Phi_{3_RBF}^{(n+1)}$ on bottom boundary ($z = -h$) solving Eq.(4.19).

(vi) Determine the partial derivatives of the velocity potential utilizing Eq.(4.21) and Eq.(4.22).

(vii) Downshift the solutions and repeat steps 1-7 until the final time has been reached.

The time integration of KFSBC, DFSBC and RBC is done using the Adam-Bashforth (AB) Integrator of order O(4) as proposed in Börekçi (2014), hence subscript $AB4$. This yields the following formulae:

$$\eta^{(n+1)} = \eta^{(n)} + \frac{\Delta t}{24}\left[55 \cdot \frac{\partial \Phi_1}{\partial z}^{(n)} - 59 \cdot \frac{\partial \Phi_1}{\partial z}^{(n-1)} + 37 \cdot \frac{\partial \Phi_1}{\partial z}^{(n-2)} - 9 \cdot \frac{\partial \Phi_1}{\partial z}^{(n-3)}\right] \tag{4.7}$$

$$\Phi_{1\_AB4}^{(n+1)} = \Phi_{1\_AB4}^{(n)} - g\frac{\Delta t}{24}\left[55 \cdot \eta^{(n)} - 59 \cdot \eta^{(n-1)} + 37 \cdot \eta^{(n-2)} - 9 \cdot \eta^{(n-3)}\right] \tag{4.8}$$

$$\begin{aligned}\Phi_{2\_AB4}^{(n+1)} = \Phi_{2\_AB4}^{(n)} \\ - c\frac{\Delta t}{24}\left[55 \cdot \frac{\partial \Phi_2}{\partial z}^{(n)} - 59 \cdot \frac{\partial \Phi_2}{\partial z}^{(n-1)} + 37 \cdot \frac{\partial \Phi_2}{\partial z}^{(n-2)} - 9 \cdot \frac{\partial \Phi_2}{\partial z}^{(n-3)}\right]\end{aligned} \tag{4.9}$$

Here the numbered subscript defines the boundary (e.g. 1 - surface, 2 - radiation boundary as displayed in Figure 4.3).

This time integration scheme requires data of four time levels; the data of time levels $n = 0, -1, -2, -3$ (η, Φ and the derivatives of Φ) are supplied by the analytical

solution on all collocation points. For subsequent time steps, analytical Φ are supplied on the wave incidence boundary collocation points only.

The following analytical solutions for the surface displacement η, the velocity potential Φ and its derivatives $\frac{\partial \Phi}{\partial x}$ and $\frac{\partial \Phi}{\partial z}$ are utilized:

$$\eta = \frac{H}{2} \sin\left(kx - \omega t\right) \tag{4.10}$$

$$\Phi = -\frac{H}{2}\frac{g}{\omega}\frac{\cosh k(h+z)}{\cosh kh} \cos\left(kx - \omega t\right) \tag{4.11}$$

$$\frac{\partial \Phi}{\partial x} = \frac{H\omega}{2}\frac{\cosh k(h+z)}{\sinh kh} \sin\left(kx - \omega t\right) \tag{4.12}$$

$$\frac{\partial \Phi}{\partial z} = -\frac{H\omega}{2}\frac{\sinh k(h+z)}{\sinh kh} \cos\left(kx - \omega t\right) \tag{4.13}$$

where H represents the wave height, ω the angular frequency, k the wave number and

$$t = t_0 + n\Delta t \tag{4.14}$$

with t_0 being the initial time, Δt the time increment and n the number of time steps.

The Neumann-type BBC (Equation (2.19)) is expressed as the sum of N radial basis function derivatives $\frac{\partial f}{\partial z}$ as defined in Equation (4.6) and here adapted for convenience:

$$\left(\frac{\partial \Phi_i}{\partial z}\right)^{(n+1)} = \frac{\partial f_{ij}}{\partial z}\alpha_j^{(n+1)} = 0 \tag{4.15}$$

Using Equation (4.4) and solving it for α yields:

$$\alpha_j^{(n+1)} = f_{ij}^{-1} \Phi_i^{(n+1)} \tag{4.16}$$

Using (4.16) in (4.15) results in the following expression:

$$\underbrace{\frac{\partial f_{ij}}{\partial z} f_{jk}^{-1}}_{m_{ik}^*} \Phi_k^{(n+1)} = 0 \tag{4.17}$$

As in linear wave theory, the free surface boundary conditions are applied on the still water level $z = 0$, the nodes on the free surface are stationary and do not change in time. Thus the Euclidian distances between collocation points and RBF centres are fixed and the system matrix elements m_{ik}^* are not time-dependent.

The manipulation in Equation (4.17) permits the formulation of the BVP in terms of the velocity potential Φ only:

$$\underbrace{\begin{bmatrix} 1 & 0 & 0 & 0 \\ 0 & 1 & 0 & 0 \\ m_{31}^* & m_{32}^* & m_{33}^* & m_{34}^* \\ 0 & 0 & 0 & 1 \end{bmatrix}}_{\boldsymbol{A}} \underbrace{\begin{Bmatrix} \Phi_{1\_RBF}^{(n+1)} \\ \Phi_{2\_RBF}^{(n+1)} \\ \Phi_{3\_RBF}^{(n+1)} \\ \Phi_{4\_RBF}^{(n+1)} \end{Bmatrix}}_{\boldsymbol{\Phi}_{RBF}^{(n+1)}} = \underbrace{\begin{Bmatrix} \Phi_{1\_AB4}^{(n+1)} \\ \Phi_{2\_AB4}^{(n+1)} \\ 0 \\ \Phi_{4\_analyt}^{(n+1)} \end{Bmatrix}}_{\boldsymbol{b}^{(n+1)}} \tag{4.18}$$

$$\boldsymbol{A}\ \boldsymbol{\Phi}_{RBF}^{(n+1)} = \boldsymbol{b}^{(n+1)}$$

Solving Equation (4.18) for $\Phi_{RBF}^{(n+1)}$ yields the following equation system:

$$\boldsymbol{\Phi}_{RBF}^{(n+1)} = \boldsymbol{A}^{-1} \boldsymbol{b}^{(n+1)} \tag{4.19}$$

To avoid additional computational errors, the velocity potential values for the free surface, radiation boundary and wave incidence are replaced by the time-integrated values $\Phi_1^{(n+1)}$ and $\Phi_2^{(n+1)}$ and analytical values $\Phi_4^{(n+1)}$ respectively. Then the velocity potential vector at time step $(n+1)$ becomes:

$$\boldsymbol{\Phi}^{(n+1)} = \begin{Bmatrix} \Phi_{1\_AB4}^{(n+1)} \\ \Phi_{2\_AB4}^{(n+1)} \\ \Phi_{3\_RBF}^{(n+1)} \\ \Phi_{4\_analyt}^{(n+1)} \end{Bmatrix} \tag{4.20}$$

and as described above, the derivatives of the velocity potential for the new time step can be computed using the following formulae:

$$\boldsymbol{F}^x \boldsymbol{F}^{-1} \boldsymbol{\Phi}^{(n+1)} = \left(\frac{\partial \boldsymbol{\Phi}}{\partial \boldsymbol{x}} \right)^{(n+1)} \tag{4.21}$$

$$\boldsymbol{F}^z \boldsymbol{F}^{-1} \boldsymbol{\Phi}^{(n+1)} = \left(\frac{\partial \boldsymbol{\Phi}}{\partial \boldsymbol{z}} \right)^{(n+1)} \tag{4.22}$$

This completes the algorithm with all utilized equations for each time step as presented in the time marching scheme above.

Here a pure wave incidence BC and the Sommerfeld radiation BC is applied; this is feasible as only a progressing wave from left to right is present. Börekçi (2014) achieves excellent results with this setup of the BVP for progressing waves.

When implementing a submerged flat plate (stationary or moving), wave radiation and/or diffraction will occur; thus an additional wave will travel towards the wave incidence side. This requires the wave incidence boundary in addition to the generation of the incidence wave to be transparent for the outgoing wave to avoid back-reflections into the numerical domain.

To achieve the transparency for the diffracted and radiated wave, different approaches have been used. They are briefly described in the next section before a novel 2 way Artificial Boundary Condition (2wABC) is derived. Furthermore, additional non-reflecting boundary conditions (NRBC) are investigated to ensure that only outgoing waves are present.

4.4. Novel 2 way Artificial Boundary Condition (2wABC)

4.4.1. Introduction to non-reflecting boundary conditions

As stated in Section 4.1, the Sommerfeld BC is not exact when the radiation boundary is close to sources (here the submerged flat plate). More sophisticated NRBCs have been developed by following three basic approaches as described in Tsynkov (1998), Arnold (2007), Nataf (2013) and Givoli (2004): exact (transparent or global) ABCs (i.a. Ting and Miksis, 1986; Dgaygui and Joly, 1994; Givoli and Cohen, 1995; Engquist and Majda, 1977), approximated (or local) ABCs (i.a. Engquist and Majda, 1977; Keller and Givoli, 1989; Romate, 1992; Broeze and Romate, 1992) and absorbing (sponge or damping and perfectly matched) layers (i.a. Berenger, 1994; Hesthaven, 1997; Abarbanel and Gottlieb, 1997; Vay, 2002; Hu *et al.*, 2008; Arbabanel *et al.*, 2009 and Nataf, 2013).

Tsynkov (1998) states that the exact NRBCs are non-local operators in space (for steady-state problems) and additionally in time (for time-dependent problems); they achieve generally high accuracy, are numerically robust but can be laborious and computationally expensive and are often only available for simple geometries.

The approximate NRBCs usually consist of simple algorithms and therefore allow easy implementation; they are applicable to complex geometries but yield only low accuracy. In order to achieve the necessary accuracy with non-local NRBCs, often the computational domains have to be very large leading to long computation time for time-domain modelling.

Absorbing layers are material based; the domain is artificially enclosed by a dissipative layer that either retards or attenuates all waves exiting the computational domain. The parameters and thickness of the layer have to be selected in dependence on the particular problem; large domain sizes can be required especially when absorbing layers have to be applied on both incidence and radiation side due to existing scatterers; additionally the boundary between the model domain and absorbing layer has to be designed to permit minimal (sponge or damping layer) or zero reflection (perfectly matched layer) as described in Tsynkov (1998) and Abarbanel *et al.* (2009). It becomes clear that the best choice in terms of accuracy, robustness and size of computational domain are the transparent (exact) NRBCs.

For the case of scatterers excited by impinging plane waves e.g. an obstacle in the wave train, the boundary on which the incident wave is defined should simultaneously transmit this wave and let waves travelling in the opposite direction pass through it with no or little back-reflection into the domain. Fibich and Tsynkov (2001) call these BCs two-way artificial boundary conditions (2wABC) and derive such 2wABC for the nonlinear Helmholtz equation.

The situation when 2wABCs are needed is common in water wave propagation: obstacles in the domain, bottom changes, and existing wall boundaries reflect the incoming wave partially or completely and the wave incidence boundary has to be transparent to these reflected waves.

In the following section the exact NRBCs for the propagation of gravity driven linear waves in 2DV are derived and applied to the numerical boundary-only RBFCM model; this approach allows for combining the non-reflecting properties of the boundary with a wave input and therefore represents a 2wABC but can also be applied as pure radiation boundary. (The derived 2waBC has been adapted to non-linear waves and performed well for a calibrated setup.)

Similar approaches to determine exact NRBCs (radiation only) have been presented by Ting and Miksis (1986) for scattering problems in acoustics and Givoli and

Cohen (1995) for elastic waves (geophysics).

4.4.2. Derivation for Radiation Boundary

For simplicity, the novel 2wABC is here derived for pure radiation only (boundary 2 - see Figure 4.3) and in the next section extended to simultaneously accommodate an additional incidence wave input on the same set of collocation points.

Instead of determining the velocity potential Φ on the radiation boundary by means of time integration using the AB O(4) integrator on the Sommerfeld BC as described in step 4 of the time marching scheme in Section 4.3, now a different approach is used.

An additional inner lateral boundary is introduced. It is located at a distance $\Delta l = c\Delta t$ away from the radiation boundary; Δl represents the distance that the wave travels during the applied time step size Δt and c represents the wave celerity. The nodes on the inner boundary (xi_k, zi_k) are located at the same z positions as the radiation boundary nodes. For the initial time t_0 the velocity potential Φ on the inner and outer nodes is determined with the analytical solution using Equation (4.11). For subsequent time steps the velocity potential on the inner nodes is computed by RBF interpolation. For this purpose the source weights $\alpha_j^{(n)}$ are determined using Equation (4.16) applied to the boundary collocation points and RBF centres:

$$\boldsymbol{\alpha^{(n)}} = \boldsymbol{F}^{-1}\boldsymbol{\Phi}^{(n)} \tag{4.23}$$

Using these source weights the velocity potentials on the inner nodes are interpolated with the following formulae:

$$\boldsymbol{\Phi}^{(n)}_{\boldsymbol{inner}}\Big|_{x=x_R-\Delta l} = \boldsymbol{F}_{\boldsymbol{inner(2)}}\boldsymbol{\alpha}^{(n)} \tag{4.24}$$

where

$$f_{inner(2)\_ij} = \ln r_{ij} \tag{4.25}$$

and

$$r_{ij} = \sqrt{(xi_i - xrbf_j)^2 + (zi_i - zrbf_j)^2} \tag{4.26}$$

The velocity potentials on the radiation boundary nodes at time step $(n+1)$ are now computed using the following formulae:

$$\boldsymbol{\Phi}^{(n+1)}_{2\_2wABC}\Big|_{x=x_R} = \boldsymbol{\Phi}^{(n)}_{inner}\Big|_{x=x_R-\Delta l} \tag{4.27}$$

they equal the velocity potentials on the inner-boundary nodes at time step (n). The velocity potential vector (Eq.(4.20)) becomes:

$$\boldsymbol{\Phi}^{(n+1)} = \begin{Bmatrix} \Phi^{(n+1)}_{1\_AB4} \\ \Phi^{(n+1)}_{2\_2wABC} \\ \Phi^{(n+1)}_{3\_RBF} \\ \Phi^{(n+1)}_{4\_analyt} \end{Bmatrix} \tag{4.28}$$

It has not been tested whether the 2wABC applied as pure radiation condition performs better than the Sommerfeld radiation condition for linear waves; a successful setup with second order non-linear waves demonstrated that this novel 2wABC worked efficiently and accurately as pure radiation condition: no sponge layer or perfectly matched layer are required.

4.4.3. Application as 2wABC

If now in addition to an outgoing wave an incidence wave has to be prescribed on boundary 4 (see Figure 4.3), step 1 of the time marching scheme described in Section 4.3 has to be adapted. In order to make the boundary transparent for left-going waves,

the following approach is introduced.

As for the pure radiation boundary, inner nodes (xi_k^*, zi_k^*) $\Delta l = c\Delta t$ away from the incidence boundary are established. The source weights, determined with Equation (4.23) are used to interpolate the numerical velocity potentials on the inner nodes close to the incidence boundary:

$$\boldsymbol{\Phi}^{(n)}_{\boldsymbol{inner\_numerical}}\Big|_{x=\Delta l} = \boldsymbol{F}_{\boldsymbol{inner(4)}}\boldsymbol{\alpha}^{(n)} \tag{4.29}$$

where

$$f_{inner(4)\_ij} = \ln r_{ij} \tag{4.30}$$

and

$$r_{ij} = \sqrt{(xi_i^* - xrbf_j)^2 + (zi_i^* - zrbf_j)^2} \tag{4.31}$$

Now the analytical values $\boldsymbol{\Phi}^{(n)}_{\boldsymbol{inner\_analytical}}\big|_{x=\Delta l}$ of the incidence wave on the inner nodes are computed utilizing Equation (4.11).

Then the difference between the numerically determined $\boldsymbol{\Phi}^{(n)}_{\boldsymbol{inner\_numerical}}\big|_{x=\Delta l}$ and the analytical $\boldsymbol{\Phi}^{(n)}_{\boldsymbol{inner\_analytical}}\big|_{x=\Delta l}$ values is computed:

$$\boldsymbol{\Delta\Phi}^{(n)}_{\boldsymbol{inner}}\Big|_{x=\Delta l} = \boldsymbol{\Phi}^{(n)}_{\boldsymbol{inner\_numerical}}\Big|_{x=\Delta l} - \boldsymbol{\Phi}^{(n)}_{\boldsymbol{inner\_analytical}}\Big|_{x=\Delta l} \tag{4.32}$$

This difference $\boldsymbol{\Delta\Phi}^{(n)}_{\boldsymbol{inner}}\Big|_{x=\Delta l}$ represents the left-going wave and is now used to adapt the analytical velocity potential on the incidence nodes for time step $(n+1)$ (make the boundary transparent for the left-going wave):

$$\boldsymbol{\Phi}^{(n+1)}_{\boldsymbol{4\_2wABC}}\Big|_{x=0} = \boldsymbol{\Phi}^{(n+1)}_{\boldsymbol{incidence\_analytical}}\Big|_{x=0} + \boldsymbol{\Delta\Phi}^{(n)}_{\boldsymbol{inner}}\Big|_{x=\Delta l} \tag{4.33}$$

When using the 2wABC on radiation and incidence boundary, the velocity potential vector (Equation (4.20)) becomes:

$$\mathbf{\Phi}^{(n+1)} = \begin{Bmatrix} \Phi_{1\_AB4}^{(n+1)} \\ \Phi_{2\_2wABC}^{(n+1)} \\ \Phi_{3\_RBF}^{(n+1)} \\ \Phi_{4\_2wABC}^{(n+1)} \end{Bmatrix} \tag{4.34}$$

To determine the accuracy of the proposed 2wABC, a wave interference model has been set up and the numerical results have been compared with the available analytical solution. This is described in the next section.

4.4.4. Error Evaluation for 2wABC

In order to evaluate the performance of the 2wABC, a numerical BVP model for wave propagation and interference over a horizontal bottom has been set up and tested against the available analytical solution. The schematic numerical wave interference model is displayed in Figure 4.4. The domain length is $3L$; relative water depths from shallow to deep water have been covered.

In order to achieve smooth surface displacement graphs, 51 horizontal nodes per wavelength have been used; per metre water depth five vertical nodes (but at least five per lateral boundary) have been placed. Depending on the actual water depth, between 316 and 506 collocation points were required.

To establish the accuracy of the model, the numerical results for η, Φ, $\frac{\partial \Phi}{\partial x}$ and $\frac{\partial \Phi}{\partial z}$ are compared with the analytical solution as given in Equations (4.10) - (4.13) and the maximum RMS error during the last 50% of the model time of 100T is determined using the formula:

$$RMS(f) = \sqrt{\frac{\sum_{i=1}^{n}(f_{i\_analytical} - f_{i\_numerical})^2}{n}} \tag{4.35}$$

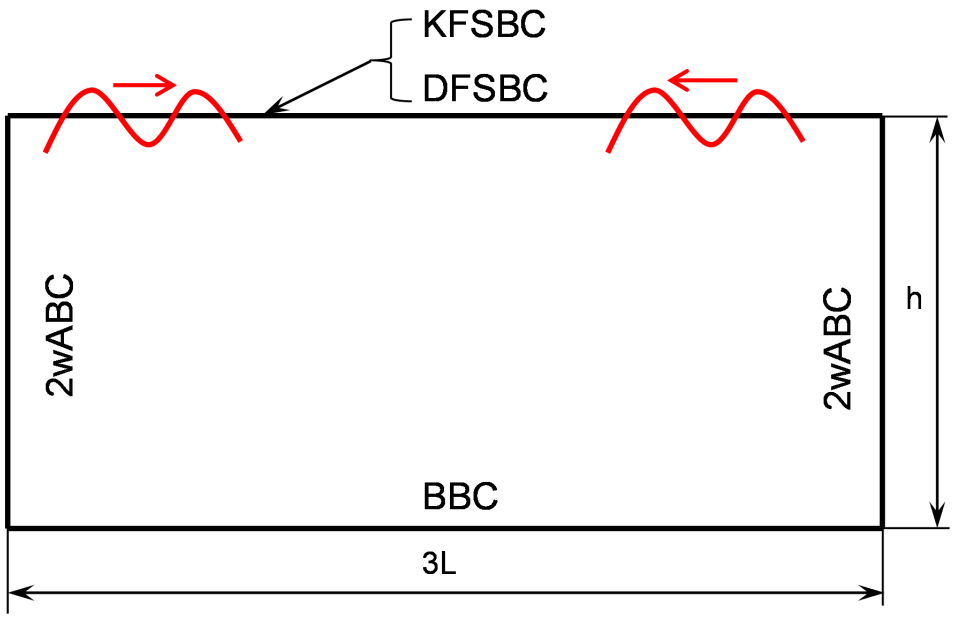

Figure 4.4. Numerical BVP setup: wave interference.

where f represents η, Φ, $\frac{\partial \Phi}{\partial x}$ and $\frac{\partial \Phi}{\partial z}$.

Wave propagation of left- and right-going waves as well as partially standing and standing wave setups have been tested and the results are summarized in Tables 4.1 - 4.3.

For propagating waves (left- or right-going) the maximum RMS errors in the surface displacement are 0.0012m for deep and intermediate water and 0.0003m for shallow water; maximum errors always occur on the surface nodes and are for the velocity potential $0.0067\text{m}^2/\text{s}$, $0.0073\text{m}^2/\text{s}$ and $0.002\text{m}^2/\text{s}$ in deep, intermediate water and in shallow water respectively; for $u = \frac{\partial \Phi}{\partial x}$ and $w = \frac{\partial \Phi}{\partial z}$ they are 0.0013m/s, 0.0014m/s and 0.0007m/s in deep, intermediate and shallow water respectively. Results are summarised in Table 4.1. Note that the wave steepness for shallow water waves had to be lowered to avoid wave breaking. For wave interference standing and partially standing waves have been tested. With left- and right-going waves simultaneously present, both lateral sides of the domain worked as 2wABC. The maximum RMS errors are summarised in Tables 4.2 and 4.3:

Table 4.1. RMS errors for BVP: wave propagation over horizontal bottom with Δt/T=0.00025.

Relative water depth		Relative wave steepness	Maximum RMS errors			
	h/L	H/L	η [m]	Φ_{surface} [m^2/s]	u_{surface} [m/s]	w_{surface} [m/s]
deep water	0.801	0.06	0.0011	0.0067	0.0013	0.0013
		0.04	0.0007	0.0045	0.0009	0.0009
		0.02	0.0004	0.0022	0.0004	0.0004
intermediate water	0.225	0.06	0.0012	0.0073	0.0014	0.0012
		0.06	0.0008	0.0049	0.0009	0.0008
		0.04	0.0004	0.0024	0.0005	0.0004
shallow water	0.044	0.03	0.0003	0.0020	0.0007	0.0002
		0.02	0.0002	0.0014	0.0004	0.0001
		0.01	0.0001	0.0007	0.0002	0.0001

Different time step lengths have been tested; the smaller time step yields better results in u and w whereas the bigger time step achieves better results in η and Φ. Note that the maximum RMS error in η occurs when zero-line (η_0) or η_{min} is present in the standing-wave and partially standing-wave setup respectively; here the maximum value is 0.018m. The RMS error in η_{max}-values is never above 0.0006m. The maximum RMS error in Φ is 0.0028m^2/s.

The maximum RMS error in u and w is 0.001m/s for the smaller time step size and 0.0485m/s for the bigger step size. This maximum RMS error occurs for wave steepness $H/L = 0.06$; due to the nonlinearity restrictions (see Section 2.4.2), the wave steepness in the numerical wave/structure model will be 0.01 for intermediate water and 0.02 in deep water and thus the maximum error in u and w will be below 0.02m/s for the $\Delta t/T = 0.0125$.

Table 4.2. RMS errors for BVP: partially standing wave over horizontal bottom.

Relative water depth		Relative wave steepness		Time step	Maximum RMS Errors				
	h/L	HR/L	HL/L	Δt/T	η_{max} [m]	η_{min} [m]	Φ [m²/s]	u [m/s]	w [m/s]
deep water	0.801	0.03	0.021	0.00025	0.0005	0.0114	0.0114	0.0006	0.0007
				0.01250	0.0001	0.0038	0.0003	0.0304	0.0345
		0.03	0.015	0.00025	0.0005	0.0101	0.0015	0.0005	0.0006
				0.01250	0.0001	0.0034	0.0003	0.0269	0.0304
		0.03	0.003	0.00025	0.0006	0.0074	0.0018	0.0004	0.0004
				0.01250	0.0002	0.0025	0.0005	0.0197	0.0223
intermediate water	0.225	0.03	0.022	0.00025	0.0004	0.0110	0.0014	0.0008	0.0007
				0.01250	0.0001	0.0042	0.0003	0.0413	0.0364
		0.03	0.016	0.00025	0.0004	0.0097	0.0016	0.0007	0.0006
				0.01250	0.0001	0.0037	0.0004	0.0364	0.0321
		0.03	0.003	0.00025	0.0005	0.0071	0.0024	0.0005	0.0005
				0.01250	0.0002	0.0027	0.0007	0.0267	0.0236
shallow water	0.044	0.02	0.011	0.00025	0.0000	0.0004	0.0000	0.0005	0.0001
				0.00250	0.0000	0.0002	0.0000	0.0054	0.0011
		0.02	0.008	0.00025	0.0000	0.0006	0.0001	0.0005	0.0001
				0.00250	0.0000	0.0005	0.0000	0.0048	0.0010
		0.02	0.002	0.00025	0.0000	0.0008	0.0001	0.0004	0.0001
				0.00250	0.0000	0.0006	0.0001	0.0035	0.0007

In the error evaluation done so far, only waves of fundamental frequency have been present. In Section 2.4.1 the introduction of nonlinearity in the form of higher frequency was described. In order to be an efficient 2wABC, the lateral boundary conditions have to be transparent not only for the fundamental wave but also for the generated higher harmonics. Additional tests covering this issue are evaluated in the next section.

Table 4.3. RMS errors for BVP: standing wave over horizontal bottom.

Relative water depth		Relative wave steepness	Time step	Maximum RMS Errors				
	h/L	$H_{standing}/L$	$\Delta t/T$	η_{max} [m]	η_0 [m]	Φ [m^2/s]	u [m/s]	w [m/s]
deep water	0.801	0.06	0.00025	0.0005	0.0134	0.0016	0.0007	0.0008
			0.01250	0.0001	0.0044	0.0003	0.0358	0.0406
		0.04	0.00025	0.0004	0.0089	0.0015	0.0005	0.0005
			0.01250	0.0001	0.0030	0.0002	0.0239	0.0270
		0.02	0.00025	0.0002	0.0045	0.0005	0.0002	0.0003
			0.01250	0.0000	0.0015	0.0001	0.0119	0.0135
intermediate water	0.225	0.06	0.00025	0.0006	0.0180	0.0028	0.0010	0.0009
			0.01250	0.0002	0.0068	0.0010	0.0485	0.0428
		0.04	0.00025	0.0004	0.0120	0.0018	0.0006	0.0006
			0.01250	0.0001	0.0046	0.0007	0.0324	0.0285
		0.02	0.00025	0.0002	0.0060	0.0009	0.0003	0.0003
			0.01250	0.0001	0.0023	0.0003	0.0162	0.0143
shallow water	0.044	0.03	0.00025	0.0000	0.0031	0.0003	0.0006	0.0001
			0.00250	0.0000	0.0024	0.0002	0.0064	0.0013
		0.04	0.00025	0.0000	0.0021	0.0002	0.0004	0.0001
			0.00250	0.0000	0.0016	0.0002	0.0043	0.0009
		0.02	0.00025	0.0000	0.0010	0.0001	0.0002	0.0000
			0.00250	0.0000	0.0008	0.0001	0.0021	0.0004

4.4.5. Error Evaluation for Presence of Higher Harmonics

In order to be able to evaluate the performance of the 2wABC in the presence of higher harmonics, the model for testing the accuracy of the 2wABC (see Figure 4.4) was adapted as follows: In addition to left- and right-going waves of fundamental frequency, a left-going wave of second harmonics was introduced. The schematic setup

is displayed in Figure 4.5.

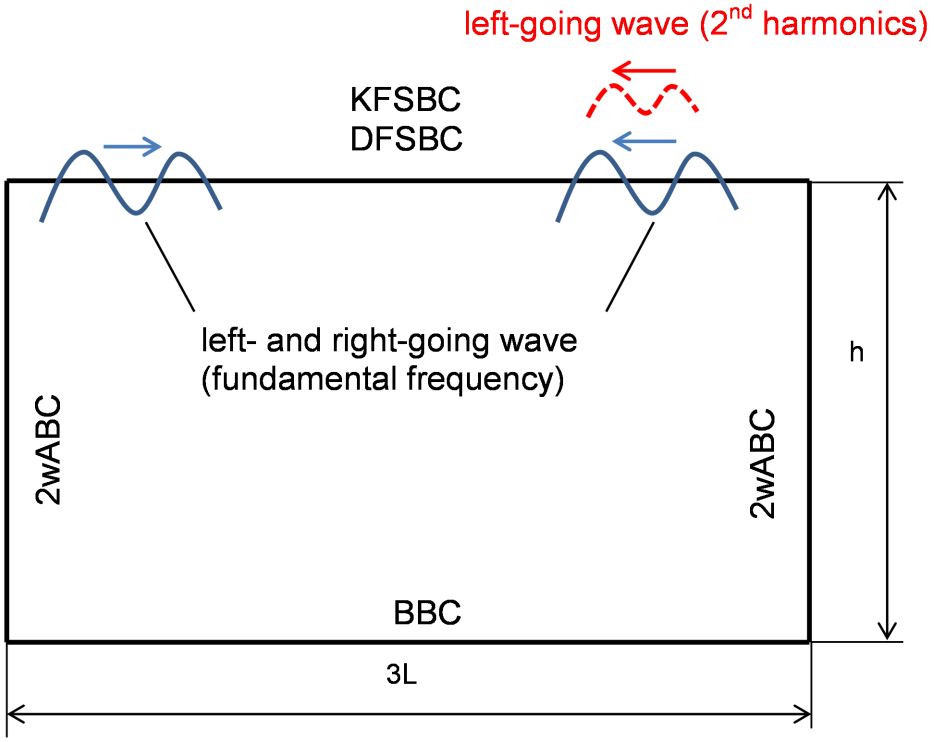

Figure 4.5. Numerical BVP setup: wave interference with present second harmonics.

To ensure that the parameters used for the accuracy test here agree with the actual parameters arising in the final model runs (e.g. wave heights of fundamental and second harmonics wave), the here presented RMS errors have been determined after all submerged flat plate model runs had been completed.

To avoid numerous model runs for the maximum error determination, the combination of highest occurring fundamental and highest generated second harmonics wave and the combination of the mean occurring fundamental and mean generated second harmonics wave have been tested. As wave steepness decreases model accuracy, the former combination represents the worst-case scenario and will, therefore, generate maximum errors whereas the latter will yield the error that will most likely not be exceeded in the majority of the computational results.

Table 4.4. RMS errors for BVP: wave interference with second harmonics present.

Relative water depth			Time step	Ratio of 2nd harmonics [%]	Maximum RMS errors			
	h/L_{fund}	$h/L_{2^{nd}}$	$\Delta t/T$	$\eta_{2^{nd}}/\eta_{fund}$ [m]	η [m]	$\Phi_{surface}$ [m^2/s]	$u_{surface}$ [m/s]	$w_{surface}$ [m/s]
deep	0.50	1.99	0.00025	65.11	0.0171	0.0288	0.0006	0.0006
			0.01250	66.05	0.0178	0.0270	0.0304	0.0305
			0.00025	27.88	0.0038	0.0064	0.0005	0.0005
			0.01250	28.29	0.0038	0.0058	0.0250	0.0250
intermediate	0.25	0.92	0.00025	155.76	0.0472	0.0695	0.0009	0.0008
			0.01250	157.16	0.0478	0.0679	0.0424	0.0422
			0.00025	42.21	0.0059	0.0087	0.0003	0.0003
			0.01250	42.57	0.0060	0.0085	0.0147	0.0137

The results of the error evaluation for the setups when second harmonics are present are summarized in Table 4.4: The first two lines of each of the relative water depths display the error for the worst-case scenario, the second two lines the average error values. The maximum RMS errors in deep water model runs are 0.018m in η, 0.029m^2/s in Φ and 0.031m/s in u and w; in intermediate water the maximum RMS error will be 0.048m in η, 0.07m^2/s in Φ and 0.043m/s in u and w. For the majority of test runs however, the RMS errors will be below 0.006m in η, 0.009m^2/s in Φ and 0.025m/s in u and w as can be seen in Table 4.4. These tests do not accurately represent the real situation as the test setup does not contain the submerged flat plate, but they give a good estimation of the to-be-expected errors.

Having set up the water-wave BVP with RBF Collocation Method and tested the performance of the model including the novel 2wABC, the submerged flat plate can be implemented into the numerical model.

4.5. Setup of the Water-wave/Structure BVP with the RBF Collocation Method

Implementing the submerged flat plate introduces four new internal boundaries (5 to 8 - see Figure 4.6) to the wave propagation BVP represented in Figure 4.3.

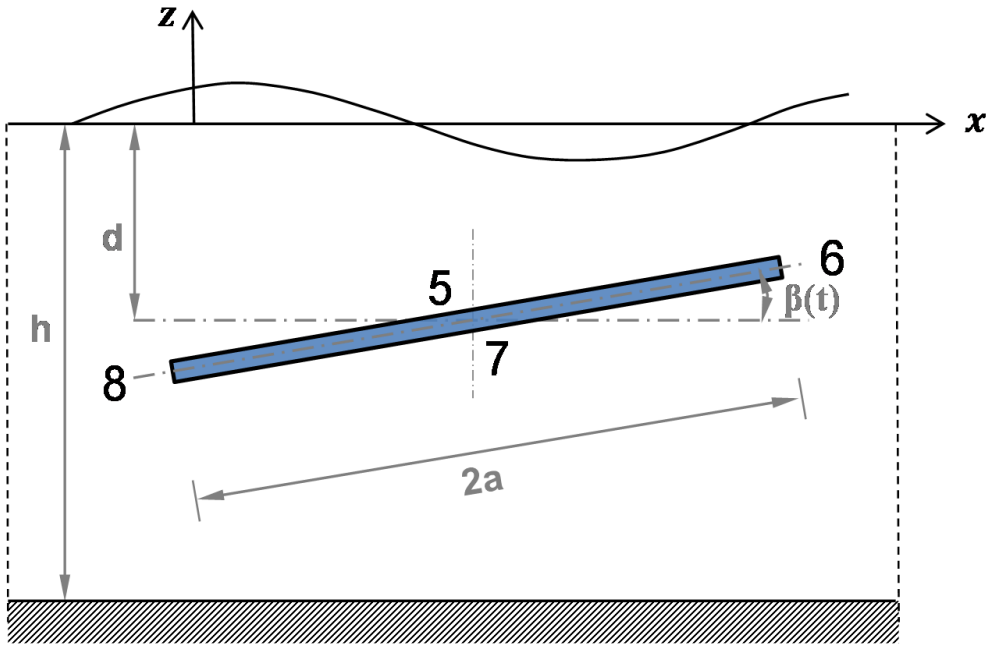

Figure 4.6. Numerical implementation of the plate.

The BCs on these additional boundaries have been derived in Section 2.2; for a stationary plate Equation (2.25) applies, for a moving plate the BC is defined in Equation (2.26).

Using the instantaneous pitching angle $\beta(t)$ as defined in Equation (2.47), dropping the time dependency and using β for convenience, the following numerical boundary conditions apply:

- Flat Plate boundary 5:

$$\begin{aligned} \frac{\partial \Phi}{\partial x}\sin\beta - \frac{\partial \Phi}{\partial z}\cos\beta &= D \\ \underbrace{f_{ij}^{x}\sin\beta - f_{ij}^{z}\cos\beta}_{f_{ij}^{**}}\,\alpha_j &= D \end{aligned} \tag{4.36}$$

- Flat Plate boundary 6:

$$\begin{aligned} -\frac{\partial \Phi}{\partial x}\cos\beta - \frac{\partial \Phi}{\partial z}\sin\beta &= D \\ -\underbrace{\left(f_{ij}^{x}\cos\beta + f_{ij}^{z}\sin\beta\right)}_{f_{ij}^{*}}\,\alpha_j &= D \end{aligned} \tag{4.37}$$

- Flat Plate boundary 7:

$$\begin{aligned} -\frac{\partial \Phi}{\partial x}\sin\beta + \frac{\partial \Phi}{\partial z}\cos\beta &= D \\ \underbrace{-f_{ij}^{x}\sin\beta + f_{ij}^{z}\cos\beta}_{-f_{ij}^{**}}\,\alpha_j &= D \end{aligned} \tag{4.38}$$

- Flat Plate boundary 8:

$$\begin{aligned} +\frac{\partial \Phi}{\partial x}\cos\beta + \frac{\partial \Phi}{\partial z}\sin\beta &= D \\ \underbrace{\left(f_{ij}^{x}\cos\beta + f_{ij}^{z}\sin\beta\right)}_{f_{ij}^{*}}\,\alpha_j &= D \end{aligned} \tag{4.39}$$

In Equations (4.36) - (4.39) $D = 0$ for a stationary plate and $D = V_n$ for a moving plate as derived in Section 2.2.

Substituting α_j in Equations (4.36) - (4.39) using Equation (4.16) and replacing D yields the following expressions for the additional RBF system matrix elements:

- Flat Plate boundary 5:

$$\underbrace{f_{ij}^{**}\ f_{jk}^{-1}}_{m_{ij}^{**}}\ \Phi_k^{(n+1)} = 0 \tag{4.40a}$$

$$\underbrace{f_{ij}^{**(n+1)}\ f_{jk}^{-1(n+1)}}_{m_{ij}^{**(n+1)}}\ \Phi_k^{(n+1)} = V_n^{(n+1)} \tag{4.40b}$$

- Flat Plate boundary 6:

$$\underbrace{-f_{ij}^{*}\ f_{jk}^{-1(n+1)}}_{-n_{ij}^{*}}\ \Phi_k^{(n+1)} = 0 \tag{4.41a}$$

$$\underbrace{-f_{ij}^{*(n+1)}\ f_{jk}^{-1(n+1)}}_{-n_{ij}^{*(n+1)}}\ \Phi_k^{(n+1)} = V_n^{(n+1)} \tag{4.41b}$$

- Flat Plate boundary 7:

$$\underbrace{-f_{ij}^{**}\ f_{jk}^{-1}}_{-m_{ij}^{**}}\ \Phi_k^{(n+1)} = 0 \tag{4.42a}$$

$$\underbrace{-f_{ij}^{**(n+1)}\ f_{jk}^{-1(n+1)}}_{-m_{ij}^{**(n+1)}}\ \Phi_k^{(n+1)} = V_n^{(n+1)} \tag{4.42b}$$

- Flat Plate boundary 8:

$$\underbrace{f_{ij}^{*}\ f_{jk}^{-1(n+1)}}_{n_{ij}^{*}}\ \Phi_k^{(n+1)} = 0 \tag{4.43a}$$

$$\underbrace{f_{ij}^{*(n+1)}\ f_{jk}^{-1(n+1)}}_{n_{ij}^{*(n+1)}}\ \Phi_k^{(n+1)} = V_n^{(n+1)} \tag{4.43b}$$

Equations (4.40a), (4.41a), (4.42a) and (4.43a) have to be applied for the stationary plate and are not time-dependent. In Equations (4.40b), (4.41b), (4.42b) and (4.43b) however, the system matrix elements $m_{ij}^{**(n+1)}$ and $n_{ij}^{*(n+1)}$ are time-dependent due to

the movement of the plate. Thus for a moving plate, the distance, RBF function and the derivative matrices as well as the system matrix have to be updated in each time step whereas for a stationary plate the matrices have to be determined only once as in the water-wave BVP described in Section 4.3.

Using the additional system matrix elements, Equation (4.18) can be extended to include the additional boundaries of the submerged flat plate:

Stationary plate:

$$\underbrace{\begin{bmatrix} 1 & 0 & 0 & 0 & 0 & 0 & 0 & 0 \\ 0 & 1 & 0 & 0 & 0 & 0 & 0 & 0 \\ m^{*}_{31} & m^{*}_{32} & m^{*}_{33} & m^{*}_{34} & m^{*}_{35} & m^{*}_{36} & m^{*}_{37} & m^{*}_{38} \\ 0 & 0 & 0 & 1 & 0 & 0 & 0 & 0 \\ m^{**}_{51} & m^{**}_{52} & m^{**}_{53} & m^{**}_{54} & m^{**}_{55} & m^{**}_{56} & m^{**}_{57} & m^{**}_{58} \\ -n^{*}_{61} & -n^{*}_{62} & -n^{*}_{63} & -n^{*}_{64} & -n^{*}_{65} & -n^{*}_{66} & -n^{*}_{67} & -n^{*}_{68} \\ -m^{**}_{71} & -m^{**}_{72} & -m^{**}_{73} & -m^{**}_{74} & -m^{**}_{75} & -m^{**}_{76} & -m^{**}_{77} & -m^{**}_{78} \\ n^{*}_{81} & n^{*}_{82} & n^{*}_{83} & n^{*}_{84} & n^{*}_{85} & n^{*}_{86} & n^{*}_{87} & n^{*}_{88} \end{bmatrix}}_{\boldsymbol{A}} \times \underbrace{\begin{Bmatrix} \Phi^{(n+1)}_{1\_RBF} \\ \Phi^{(n+1)}_{2\_RBF} \\ \Phi^{(n+1)}_{3\_RBF} \\ \Phi^{(n+1)}_{4\_RBF} \\ \Phi^{(n+1)}_{5\_RBF} \\ \Phi^{(n+1)}_{6\_RBF} \\ \Phi^{(n+1)}_{7\_RBF} \\ \Phi^{(n+1)}_{8\_RBF} \end{Bmatrix}}_{\boldsymbol{\Phi}^{(n+1)}_{RBF}} = \underbrace{\begin{Bmatrix} \Phi^{(n+1)}_{1\_AB4} \\ \Phi^{(n+1)}_{2\_2wABC} \\ 0 \\ \Phi^{(n+1)}_{4\_2wABC} \\ 0 \\ 0 \\ 0 \\ 0 \end{Bmatrix}}_{\boldsymbol{b}^{(n+1)}} \tag{4.44a}$$

Moving plate:

$$\underbrace{\begin{bmatrix} 1 & 0 & 0 & 0 & 0 & 0 & 0 & 0 \\ 0 & 1 & 0 & 0 & 0 & 0 & 0 & 0 \\ m^{*}_{31} & m^{*}_{32} & m^{*}_{33} & m^{*}_{34} & m^{*}_{35} & m^{*}_{36} & m^{*}_{37} & m^{*}_{38} \\ 0 & 0 & 0 & 1 & 0 & 0 & 0 & 0 \\ m^{**}_{51} & m^{**}_{52} & m^{**}_{53} & m^{**}_{54} & m^{**}_{55} & m^{**}_{56} & m^{**}_{57} & m^{**}_{58} \\ -n^{*}_{61} & -n^{*}_{62} & -n^{*}_{63} & -n^{*}_{64} & -n^{*}_{65} & -n^{*}_{66} & -n^{*}_{67} & -n^{*}_{68} \\ -m^{**}_{71} & -m^{**}_{72} & -m^{**}_{73} & -m^{**}_{74} & -m^{**}_{75} & -m^{**}_{76} & -m^{**}_{77} & -m^{**}_{78} \\ n^{*}_{81} & n^{*}_{82} & n^{*}_{83} & n^{*}_{84} & n^{*}_{85} & n^{*}_{86} & n^{*}_{87} & n^{*}_{88} \end{bmatrix}^{(n+1)}}_{\boldsymbol{A}^{(n+1)}} \times \underbrace{\begin{Bmatrix} \Phi^{(n+1)}_{1\_RBF} \\ \Phi^{(n+1)}_{2\_RBF} \\ \Phi^{(n+1)}_{3\_RBF} \\ \Phi^{(n+1)}_{4\_RBF} \\ \Phi^{(n+1)}_{5\_RBF} \\ \Phi^{(n+1)}_{6\_RBF} \\ \Phi^{(n+1)}_{7\_RBF} \\ \Phi^{(n+1)}_{8\_RBF} \end{Bmatrix}}_{\boldsymbol{\Phi}^{(n+1)}_{RBF}} = \underbrace{\begin{Bmatrix} \Phi^{(n+1)}_{1\_AB4} \\ \Phi^{(n+1)}_{2\_2wABC} \\ 0 \\ \Phi^{(n+1)}_{4\_2wABC} \\ V^{(n+1)}_{n\_5} \\ V^{(n+1)}_{n\_6} \\ V^{(n+1)}_{n\_7} \\ V^{(n+1)}_{n\_8} \end{Bmatrix}}_{\boldsymbol{b}^{(n+1)}} \tag{4.44b}$$

The applied time marching scheme described in Section 4.3 applies to the stationary submerged plate BVP too but needs to be adapted for the moving plate BVP due to the continuously changing plate node positions:

Now the initial configuration of collocation points and RBF centres, the initial elements of the RBF matrix $f_{ij}(t = t_0)$ and the initial elements of the derivative matrices $f^{x}_{ij}(t = t_0)$ and $f^{z}_{ij}(t = t_0)$ are computed using Equation (4.2) and (4.3) respectively. Then the initial system matrix $\boldsymbol{A}(t = t_0)$ in Equation (4.18) is generated and the following time marching scheme is applied:

(i) Compute the velocity potential $\Phi_{4\_2wABC}^{(n+1)}$ of the incident wave using the adapted analytical solution - Equation (4.33).

(ii) Integrate the KFSBC to determine $\eta^{(n+1)}$ using Equation (4.7).

(iii) Integrate the DFSBC to determine $\Phi_{1\_AB4}^{(n+1)}$ using Equation (4.8).

(iv) Compute the velocity potential $\Phi_{2\_2wABC}^{(n+1)}$ using Equation (4.27).

(v) Compute the plate velocity normal to the plate boundaries, V_{n_5} - V_{n_8}, utilizing Equations (2.45) for heave and (2.48) for pitch.

(vi) Set up the RBF system with Dirichlet BCs $\Phi_{1\_AB4}^{(n+1)}$ on surface, $\Phi_{2\_2wABC}^{(n+1)}$ on radiation and $\Phi_{4\_2wABC}^{(n+1)}$ on incidence boundaries and determine $\Phi_{3RBF}^{(n+1)}$ on bottom boundary, and $\Phi_{5\_RBF}^{(n+1)}$ - $\Phi_{8\_RBF}^{(n+1)}$ on plate boundaries solving equation (4.44b).

(vii) Determine the partial derivatives of the velocity potential utilizing equations (4.21) and (4.22).

(viii) Update the plate node positions using the prescribed motion (Equations (2.44) for heave and (2.47) for pitch).

(ix) Update r_{ij}, f_{ij}, f_{ij}^{x} and f_{ij}^{z} and generate the new system matrix $\boldsymbol{A}$.

(x) Downshift the solutions and repeat steps 1-10 until the final time has been reached.

The submerged flat plate BVP is here solved in one step by applying the plate boundary condition $\frac{\partial \Phi}{\partial n} = 0$ for a stationary plate and $\frac{\partial \Phi}{\partial n} = V_n$ for a moving plate on the boundaries on a finite thickness plate.

4.6. Preliminary Tests with Stationary Plate

Preliminary test runs done with the model setup described in Section 4.5 were conducted with model time up to $50T$; unfortunately the results were inconclusive and sensitive to small changes in the setup.

The following issues were detected:

(i) Some test runs showed a steady diffracted wave towards incidence and radiation side, others exhibited a pulsating diffracted wave; the pulsating was especially

pronounced towards the incidence side. Plate geometry, number and position of the collocation points and RBF centres for the plate appeared to influence the model behaviour but no conclusive explanation could be found. The author assumed that the plate BC was the reason for the inconclusive results and decided on an adapted BVP setup which will be described in Section 4.7.

(ii) The number of plate nodes has a significant influence on the height of the diffracted wave: by changing only the plate node numbers in the model setup, the wave height of the diffracted wave towards incidence side differed up to 500%, on the radiation side up to 3000%. Similarly, the RBF centre distance from the plate collocation nodes affected the height of the diffracted wave. In order to select the correct plate node number and RBF distance, calibration will be needed. That means that either enough suitable experimental data or an analytical solution is required to calibrate the stationary submerged flat plate model. This issue is further discussed in Section 4.7.2.

(iii) For inclined plates, relative energy flux is not conserved. It is assumed, that with manipulating the RBF centre distance from the plate collocation points (e.g. defining different RBF centre distances for opposite plate side nodes), this problem can be solved because tests indicated this influence. (See Section 5.2)

4.7. Adapted Model Setup and Zero Thickness Plate

4.7.1. Adapted Setup: Solution in 2 BVPs with Superposition

In order to resolve the pulsating problem, a solution in two steps is proposed. The first step is to determine $\eta_{incident}$ on the surface boundary and $\Phi_{incident}$, $\frac{\partial \Phi_{incident}}{\partial x}$ and $\frac{\partial \Phi_{incident}}{\partial z}$ on all boundaries utilizing the analytical solution of the incidence wave (Equations (4.10) - (4.13)) (BVP 1). Then, using $\frac{\partial \Phi_{incident}}{\partial x}$ and $\frac{\partial \Phi_{incident}}{\partial z}$ on the plate nodes, $\frac{\partial \Phi}{\partial n}$ of the incidence wave is computed in dependence on the plate inclination.

Combining Equations (2.25) and (2.27) yields the following relationship between incidence and diffracted wave on the submerged body surface:

$$\frac{\partial \Phi_{diffracted}}{\partial n} = -\frac{\partial \Phi_{incident}}{\partial n} \qquad \text{on} \quad S_B \tag{4.45}$$

With Equation (4.45) $\frac{\partial \Phi_{diffracted}}{\partial n}$ on S_B will be determined and used as wave input for the second step (BVP 2). For the stationary plate case, this is the only wave input for BVP 2; a schematic setup is shown in Figure 4.7.

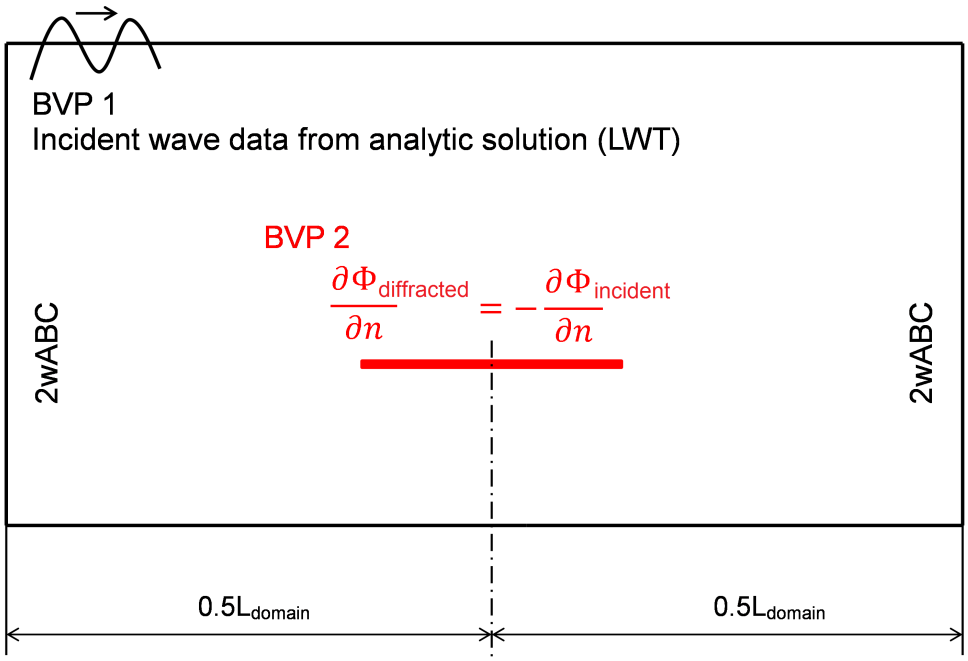

Figure 4.7. Schematic setup of BVP in 2 steps.

If the plate is moving, the prescribed plate velocity normal to the instantaneous plate boundary as defined in Section 2.2.3 is additional wave input for BVP 2.

The superposition of BVP 1 (incident wave) and BVP 2 (radiation and/or diffraction) yields the solution to the complete radiation and/or diffraction problem of a submerged flat plate.

The presence of the plate and - for the moving plate setup - the plate motion are introduced over $5T$ (ramp-up) to avoid numerical oscillations. Preliminary test runs

with the two BVP setup for a stationary plate demonstrated that now the diffracted wave does not pulsate but reaches a steady-state condition after the ramp-up time. The sensitivity to plate node number and RBF centre distance is still present.

4.7.2. Zero Thickness Plate

Due to the fact that plate node number and RBF centre distance affect the height of the diffracted wave, model calibration is required as explained in Section 4.6.

Using experimental data available from a number of researchers (Dattatri *et al.*, 1978; Kojima *et al.*, 1990; Neelamani and Reddy, 1992; Murakami *et al.*, 1994; Patarapanich and Cheong, 1989; Bayram, 2000; Brossard and Chagdali, 2001; Neelamani and Gayathri, 2006; Brossard *et al.*, 2009; Liu *et al.*, 2009; Rao *et al.*, 2009 and Rao *et al.*, 2009) proved to be infeasible as data cover only restricted parameters h/L, d/h, β_0 and Ka.

Although a number of researchers published analytical and/or numerical data, its applicability for calibrating the model was not given due to the restriction in parameters (Patarapanich and Cheong, 1989; Cheong *et al.*, 1996 and Cho and Kim, 2008), due to different geometric model setup for solvability (horizontal plate in front of vertical wall - Cho and Kim, 2008 and Hu and Wang, 2005) and due to the assumption of infinite water depth (Parsons and Martin, 1992).

The only researcher who covered wave diffraction over submerged horizontal and inclined flat plates in finite water depths was Richard Porter (2002) and (2015) using hypersingular integral equation. He agreed to supply analytical data for specified geometric setups. As his analytical solution assumes a zero-thickness plate, the model setup had to be adapted. Figure 4.8 illustrates an example of the node positioning for the zero-thickness plate case.

Additional preliminary test runs showed that the RBF model is able to model a zero-thickness submerged flat plate with collocation points and RBF centres positioned

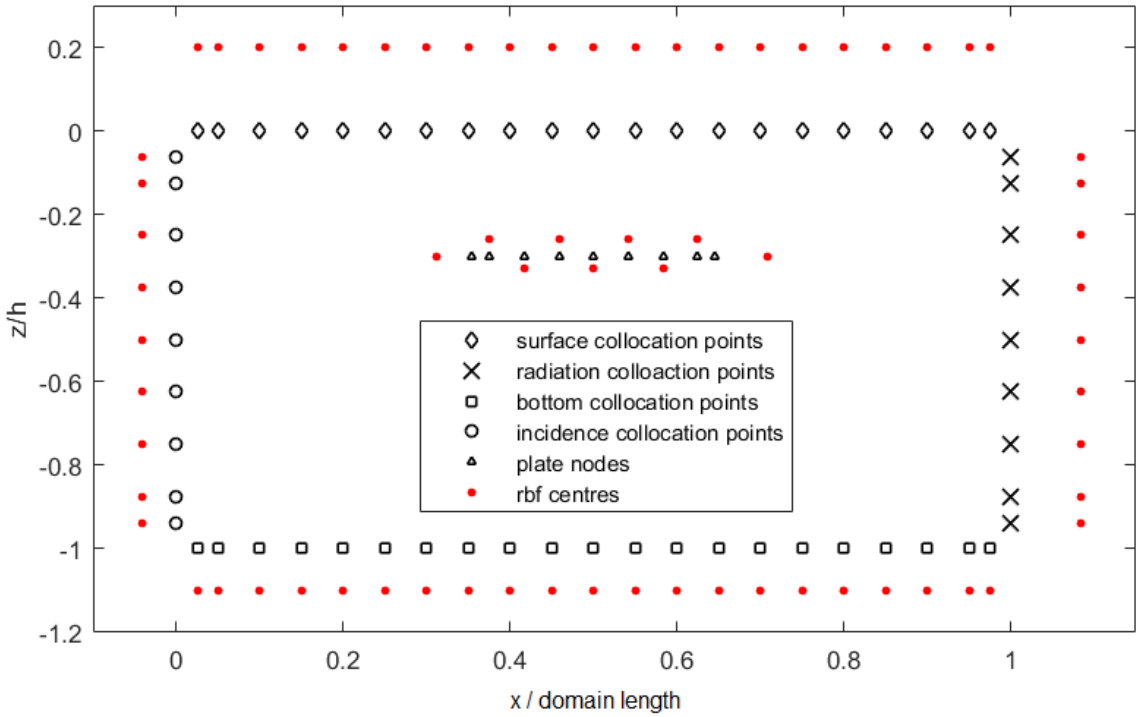

Figure 4.8. Alignment of boundary collocation points and RBF centres in setup of numerical model with zero-thickness plate.

as shown in Figure 4.8. The sensitivity to plate node number and RBF centre distance is still present in the model configuration with a zero-thickness plate and calibration with analytical data is therefore required.

The model setup with zero-thickness plate is utilized for the numerical modelling of a submerged heaving and pitching flat plate in this thesis. The Fortran code can be found in APPENDIX D.

5. MODEL CALIBRATION

As a result of the sensitivity of the numerical model to plate collocation point number and plate RBF centre distances, analytical data were needed to calibrate the model which were available for the zero-thickness stationary submerged flat plate only as explained in Section 4.7.2.

After determining the distances between plate collocation points and RBF centres through calibration test runs for stationary plate setups, these were utilised for the subsequent model runs with a moving plate (heaving, pitching and combined heaving and pitching as described in Sections 2.2.2, 2.2.3 and 4.5).

5.1. Model Parameter Configuration

5.1.1. Physical Model Parameter

For a stationary plate the following parameters affect the performance of a submerged flat plate (see Sections 1.1 and 1.2):

- relative water depth h/L
- relative plate width $Ka \quad (K = \frac{\omega^2}{g})$
- relative submergence d/h
- plate inclination β_0

In order to restrict the required analytical data, relative water depth, relative submergence and inclination were limited to two values so that eight analytical data sets had to be generated. Figure 5.1 displays the selected parameters.

Deep and intermediate water are covered as they represent the range of use of a submerged flat plate breakwater. Relative submergence depths of 1/2 and 1/3 allow for enough freeboard for plate motion and $0 \leq Ka \leq 2.2$ covers plate widths feasible

from engineering perspective for wave periods up to $5s$.

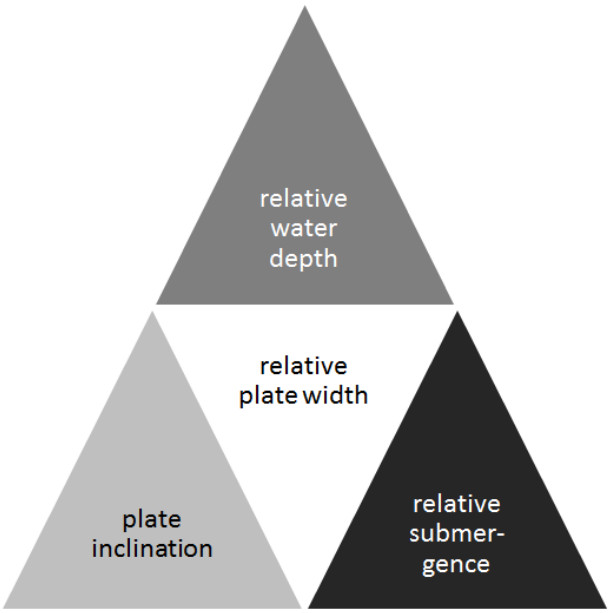

Horizontal and inclined (β_0=5°) plate			
Parameters		$\frac{d}{h}$	
		$\frac{1}{3}$	$\frac{1}{2}$
$\frac{h}{L}$	$\frac{1}{4}$	$0 \leq Ka \leq 2.2$	
	$\frac{1}{2}$		

Figure 5.1. Model configuration parameters for a stationary plate.

For a moving plate, for each of the available DoF two more parameters have to be considered: the motion amplitude and the phase angle between motion and incidence wave. Figure 5.2 depicts the configuration parameters for a moving plate. The phase angle has to cover $0 \leq \theta_{motion} < 2\pi$; the motion amplitude is restricted due to nonlinearity considerations discussed in Section 2.4.2.

With Equations (2.79), (2.80) and (2.81) three conditions were derived that had to be satisfied in order to apply linear approximation to the body-nonlinear wave problem. For convenience the conditions are repeated here and called nonlinearity coefficients:

$$\text{Coefficient 1} \qquad \frac{a_{heave}a + a_{inc}L}{Ld}\frac{a}{L} \ll 1 \tag{5.1}$$

$$\text{Coefficient 2} \qquad \frac{a}{L}\frac{4a_{heave}}{d} \ll 1 \tag{5.2}$$

$$\text{Coefficient 3} \qquad \frac{(a_{heave}a + a_{inc}L)^2}{4a_{heave}L^2d} \ll 1 \tag{5.3}$$

The nonlinearity coefficients have been determined for the selected parameters h/L, d/h and Ka using Equations (5.1) (5.2) and (5.3) for an incidence wave height of $H_0 = 1m$ and have been summarised in Table 5.1; they have been considered sufficiently small when they are $\leq$0.1.

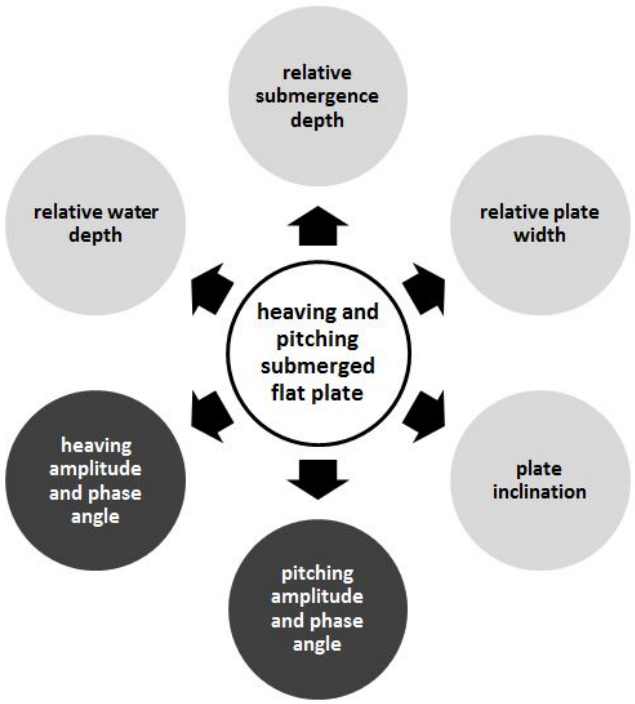

Figure 5.2. Model configuration parameters for a moving plate.

From the displayed data in Table 5.1 and Equations (5.1) - (5.3) it can be seen that the nonlinearity coefficients grow with increasing Ka and decreasing submergence and are bigger in intermediate water than in deep water. Data marked with an asterix indicate that the nonlinearity coefficients are too big. The data for intermediate water show that decreasing the motion amplitude alone does not yield small enough nonlinearity coefficients; here the incidence wave height needs to be decreased too.

In order to ensure equal wave and motion parameters for test runs of equal h/L and d/h, the smallest required wave height and motion amplitude is applied to the

Table 5.1. Restrictions for the heaving amplitude and incidence wave height due to nonlinearity considerations.

H_0=1m			a_{heave}=0.5m			a_{heave}=0.25m		
h/L	d/h	Ka	coefficient			coefficient		
			1	2	3	1	2	3
1/2	1/3	0.5	0.010	0.039	0.035	0.010	0.019	0.065
		1.0	0.022	0.077	0.041	0.021	0.039	0.070
		1.5	0.036	0.116*	0.046	0.032	0.058	0.076
		2.0	0.051	0.154*	0.052	0.045	0.077	0.081
		2.2	0.057	0.169*	0.055	0.050	0.085	0.083
	1/2	0.5	0.007	0.026	0.023	0.007	0.013	0.043
		1.0	0.015	0.051	0.027	0.014	0.026	0.047
		1.5	0.024	0.077	0.031	0.022	0.039	0.050
		2.0	0.034	0.103*	0.035	0.030	0.051	0.054
		2.2	0.038	0.113*	0.037	0.033	0.056	0.056
1/4	1/3	0.5	0.025	0.091	0.077	0.024	0.045	0.143*
		1.0	0.053	0.182*	0.090	0.049	0.091	0.155*
		1.5	0.086	0.273*	0.104*	0.077	0.136*	0.167*
		2.0	0.122*	0.364*	0.119*	0.107*	0.182*	0.180*
		2.2	0.138*	0.400*	0.125*	0.119*	0.200*	0.186*
	1/2	0.5	0.016	0.061	0.052	0.016	0.030	0.095
		1.0	0.036	0.121*	0.060	0.033	0.061	0.103*
		1.5	0.057	0.182*	0.069	0.051	0.091	0.111*
		2.0	0.082	0.242*	0.079	0.071	0.121*	0.120*
		2.2	0.092	0.267*	0.083	0.079	0.133*	0.124*

whole range of Ka as recorded in Table 5.2. When halving the plate motion amplitude, the incident wave height is halved as well to make the transmission and reflection coefficients of different relative water depths h/L.

Table 5.2. Applied heaving amplitude and incidence wave height due to nonlinearity considerations.

(a) Deep Water

H_0=0.5m			a_{heave}=0.25m		
h/L	d/h	Ka	coefficient		
			1	2	3
1/2	1/3	0.5	0.005	0.019	0.180
		1.0	0.011	0.039	0.020
		1.5	0.018	0.058	0.023
		2.0	0.025	0.077	0.026
		2.2	0.029	0.085	0.028
	1/2	0.5	0.003	0.013	0.012
		1.0	0.007	0.026	0.014
		1.5	0.012	0.039	0.015
		2.0	0.017	0.051	0.017
		2.2	0.019	0.056	0.018

(b) Intermediate Water

H_0=0.25m			a_{heave}=0.125m		
h/L	d/h	Ka	coefficient		
			1	2	3
1/4	1/3	0.5	0.006	0.023	0.019
		1.0	0.013	0.045	0.023
		1.5	0.021	0.068	0.026
		2.0	0.031	0.091	0.030
		2.2	0.035	0.100	0.031
	1/2	0.5	0.004	0.015	0.013
		1.0	0.009	0.030	0.015
		1.5	0.014	0.045	0.017
		2.0	0.020	0.061	0.020
		2.2	0.023	0.067	0.021

The deep water setup will be modelled using a deep water wave height and a heave amplitude of $H_0 = 0.5m$ and $a_{heave} = 0.25m$ respectively, the intermediate water setup with $H_0 = 0.25m$ and $a_{heave} = 0.125m$; these values ensure that the nonlinearity coefficients are ≤ 0.1.

The pitching amplitude is defined using the criterion of equal water volume displacement for heaving and pitching motion of a plate with equal Ka. This gives pitching angles of $7.2 \geq \beta_{pitch} \geq 1.6$ for intermediate water and $14.4 \geq \beta_{pitch} \geq 3.3$ for deep water in dependence on Ka.

5.1.2. Final Parameters of Numerical Model

After defining the physical parameters of the model in Section 5.1 (relative plate width Ka, relative submergence h/d, relative water depth h/L, the wave height H_0 and the motion amplitudes a_{heave} and β_{pitch}), now the numerical parameters of the model had to be defined. These include:

- domain size
- node numbers
- time step size
- modelling time and
- RBF centre positioning.

First test runs with the relative time step of $\Delta t/T = 0.00025$ used in runs with the stationary plate revealed that due to the matrix inversion required in every time step the run time of the model increases significantly. Modelling a domain length of $3L$ would have taken up to 47 hours.

Experimenting with the time step in the stationary plate setup showed that test results agree well up to a relative time step of $\Delta t/T = 0.0125$. In order to further reduce the computing time for test runs up to $50T$, the originally planned domain length of $10L$ was reduced to $5L$.

With a relative time step of $\Delta t/T = 0.0125$ and modelling in a domain of of $5L$, the model run time was $1.25 - 2$ hours depending on h/L and Ka.

The RBF model is set up with 51 nodes per wave length in order to yield smooth water surface graphs as in Börekçi (2014); five collocation points per metre depth are arranged on the lateral sides of the domain. The horizontal node distance on the plate was predefined to be $0.5m$ and was automatically adapted to the actual plate width; one vertical plate node was placed on each of the plate edges of the zero-thickness plate.

This arrangement resulted in a maximum of 708 nodes for deep water ($h/L = 1/2$) and $Ka = 2.2$ and a minimum of 586 nodes for $h/L = 1/4$ and $Ka = 0.5$.

All test runs were conducted with a modelling time of $50T$; a number of test runs were repeated with a modelling time of $100T$. The error in k_T, determined with $k_T(t = 100T) - k_T(t = 50T)$ was maximum 0.1%. This shows that the numerical results are stable and do not change with longer modelling time.

5.2. Calibration with Analytical Solution

The numerical model was calibrated with analytical transmission and reflection coefficients (k_T and k_R respectively as defined in Equations (2.58) and (2.59)) provided by Porter (2015a).

For good wave attenuation the transmission coefficient has to be small; the total incoming wave is reflected from the obstacle back towards the wave incidence side when $k_R = 1$, and thus for a stationary plate $k_T = 0$. On the other hand, if $k_T = 1$, the total incident wave is transmitted (zero wave attenuation) and no wave is diffracted towards the incidence side.

5.2.1. Calibration of the Plate RBF Distances

Using the data provided by Porter (2015a) for the parameters summarized in Figure 5.1, the distances between plate collocation points and RBF centres were calibrated so that the numerical transmission and reflection coefficients for the stationary plate agree with the provided analytical data computed using hypersingular integral equation as described in Porter (2002) and Porter (2015).

In addition to generally applied relative plate widths $Ka = \{0.5, 1.0, 1.5, 2.0, 2.2\}$, setup-specific Ka's have been selected to capture the behaviour near the maximum and minimum reflection coefficients.

For the intermediate water cases with relative submergence d/h=1/3, nine calibration runs, for all other cases six calibration runs have been performed. In total 54 configurations have been calibrated and used to determine the influence of plate motion on transmission and reflection coefficients.

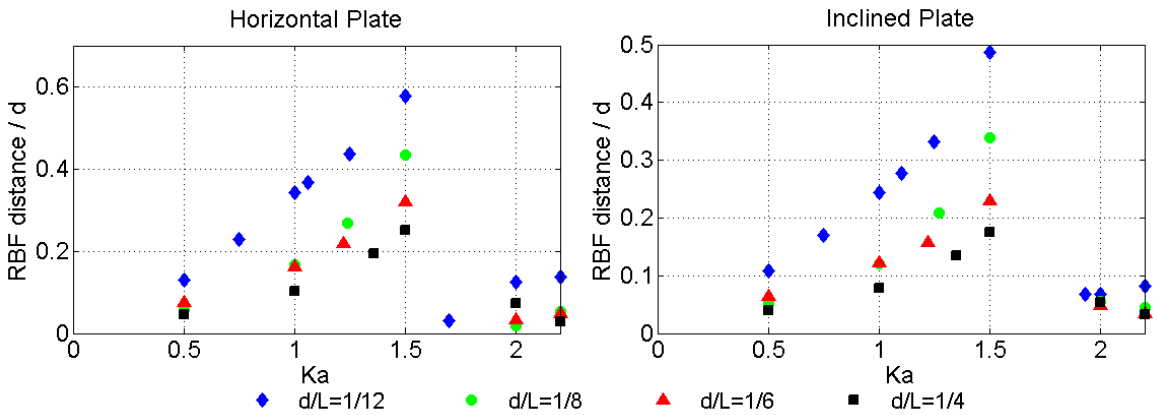

Figure 5.3. Relative RBF distances for shore-side plate edge node.

Figure 5.3 summarizes the calibrated relative distances between shore-side plate edge collocation point and RBF centre. As it can be seen, the RBF distances vary in dependence on h/L, d/h, Ka as well as plate inclination.

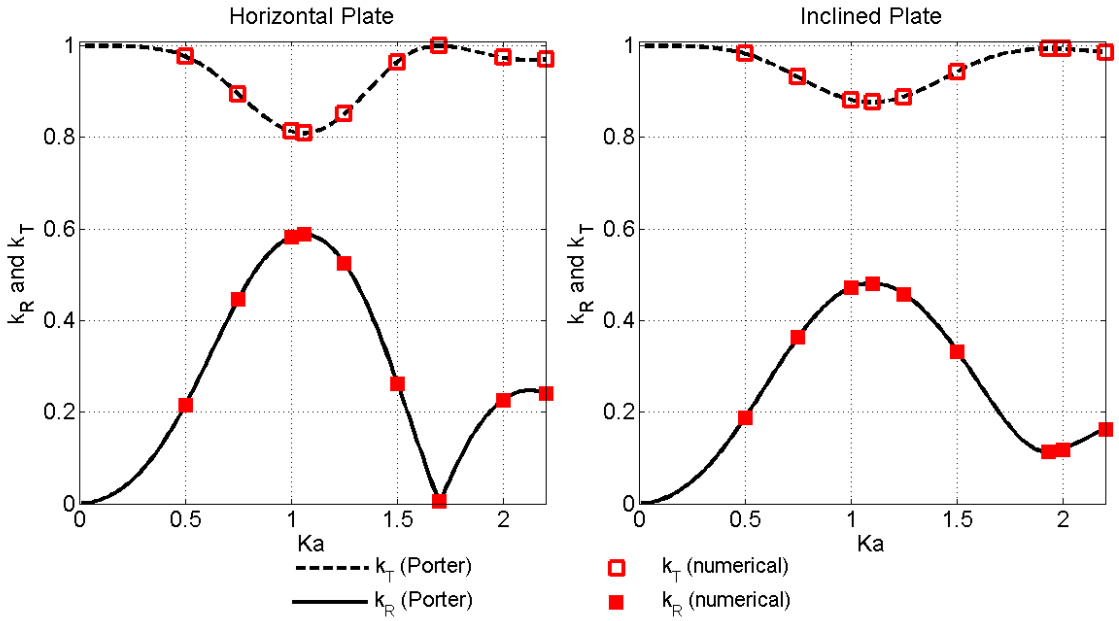

Figure 5.4. Model calibration stationary plate: transmission and reflection coefficient for h/L=1/4 and d/h=1/3.

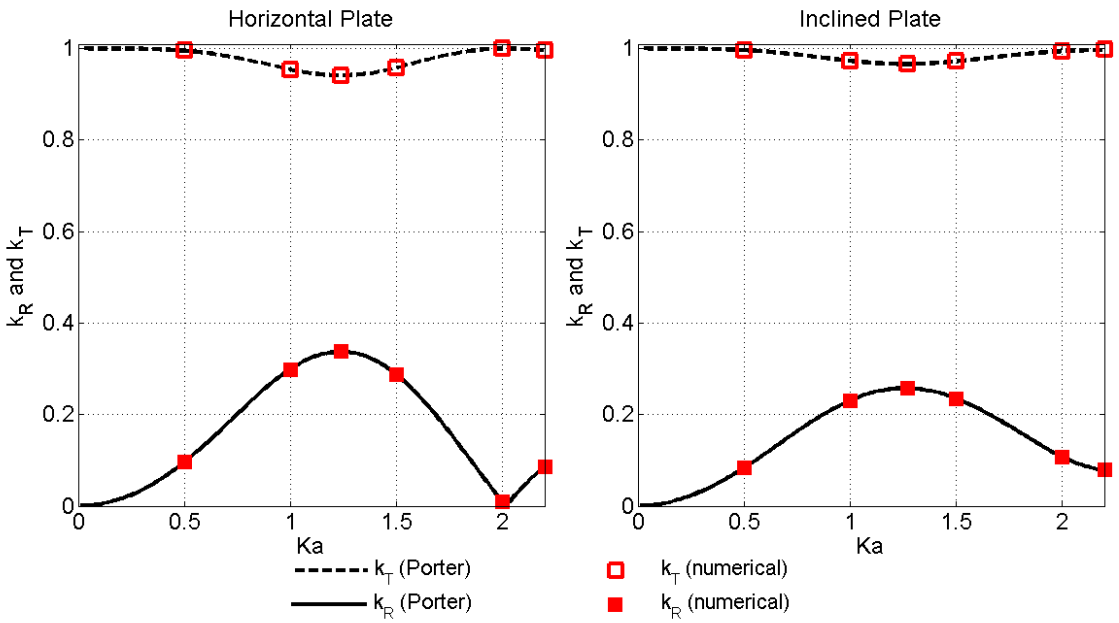

Figure 5.5. Model calibration stationary plate: transmission and reflection coefficient for h/L=1/4 and d/h=1/2.

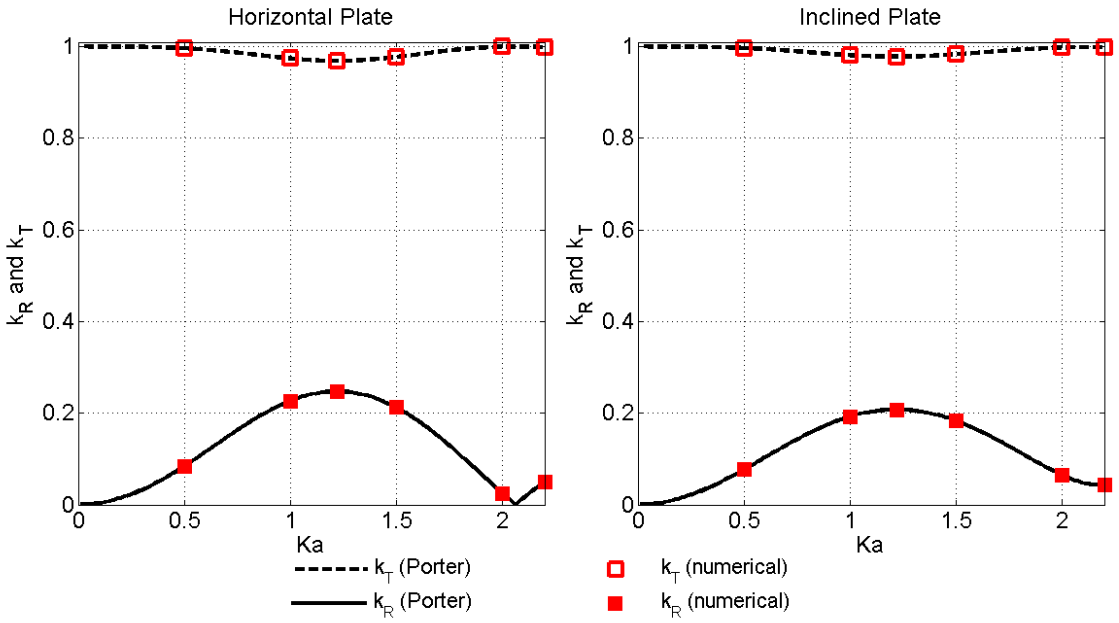

Figure 5.6. Model calibration stationary plate: transmission and reflection coefficient for h/L=1/2 and d/h=1/3.

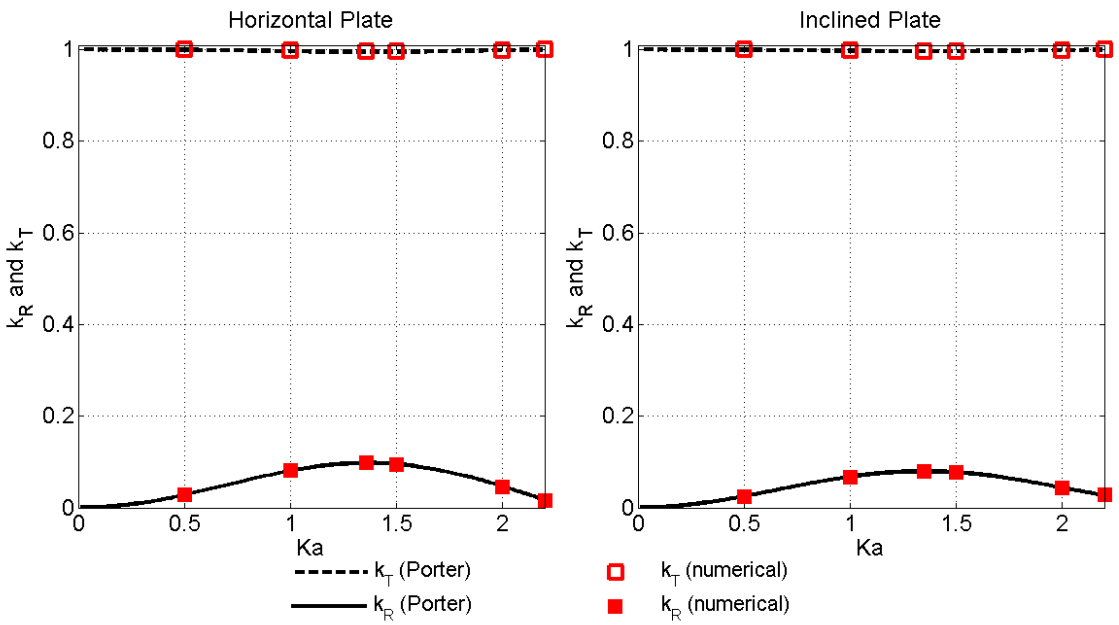

Figure 5.7. Model calibration stationary plate: transmission and reflection coefficient for h/L=1/2 and d/h=1/2.

Figures 5.4 to 5.7 show the excellent agreement between analytical and numerical transmission and reflection coefficients for all setups after calibration. Conservation of relative energy flux is ensured for horizontal and inclined plate test runs owing to the correct choice of plate RBF centre distances from the plate collocation points.

5.2.2. Model Sensitivity to Plate RBF Distances

Systematic tests with varying plate RBF distances have been run for the maximum reflection coefficient setups for a horizontal plate to determine the error introduced when RBF distances deviate from the calibrated value and results are displayed in Figures 5.8 and 5.9.

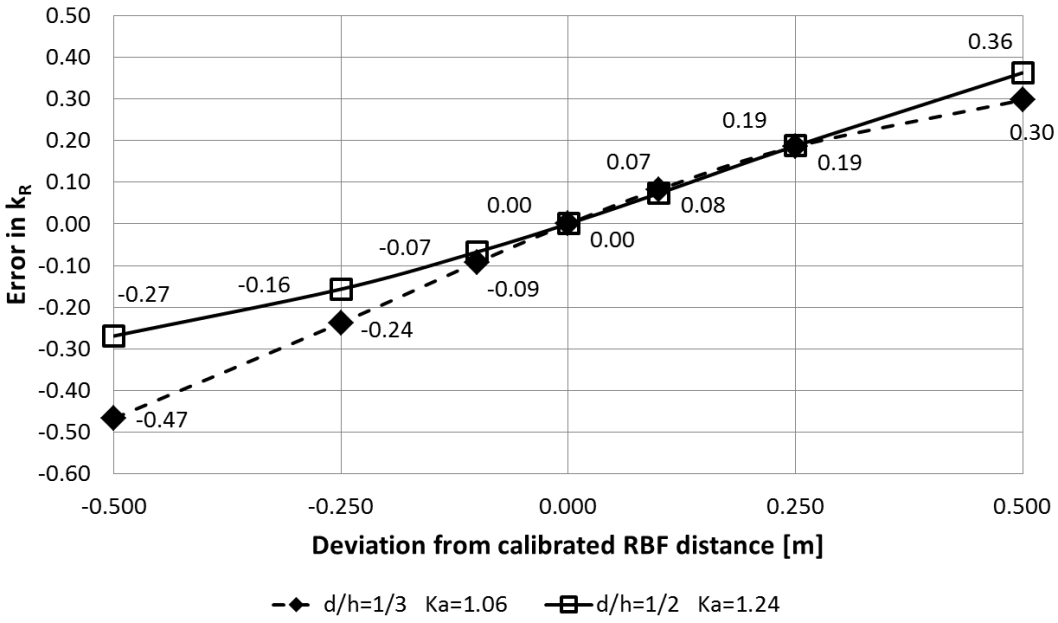

Figure 5.8. Error due to deviation from calibration RBF distance horizontal plate h/L=1/4.

As Figures 5.8 and 5.9 for the submerged horizontal plate case show, the errors in the transmission coefficient k_T are up to 47% for $h/L = 1/4$ and up to 21% for $h/L = 1/2$ when the plate edge RBF distances deviate by 0.5m from the calibrated value. Deviation of $0.1m$ causes errors in k_T of up to 9% in intermediate water. This clearly shows the importance and necessity of model calibration.

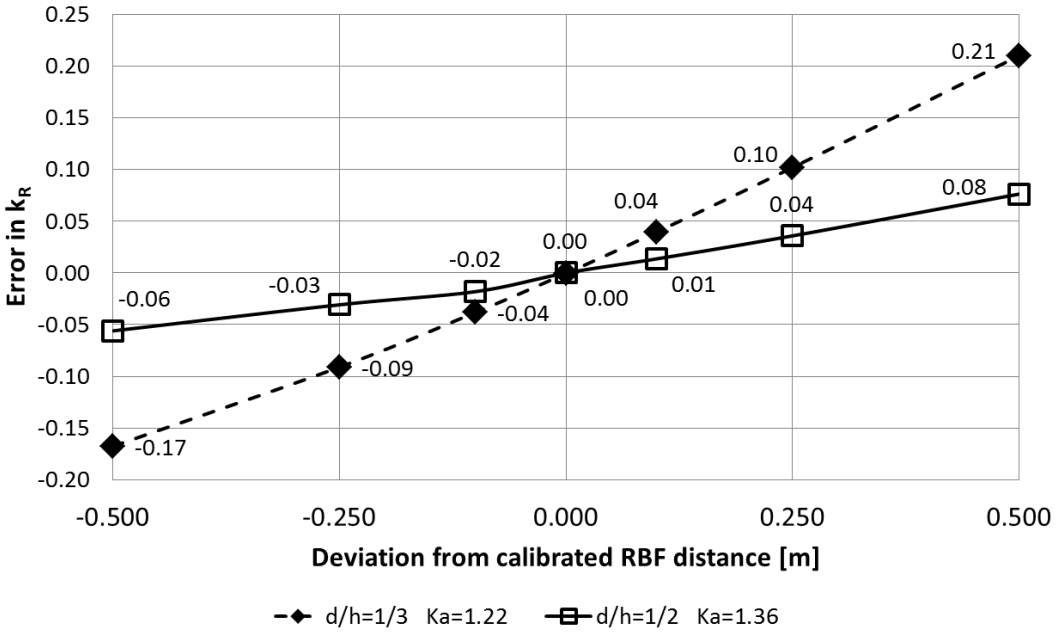

Figure 5.9. Error due to deviation from calibration RBF distance horizontal plate h/L=1/2.

6. RESULT PRESENTATION

In the following Sections 6.1 to 6.11 the results of the numerical research are presented; they will be discussed in detail in Chapter 7.

First, the influence of various parameters on the transmission and reflection coefficients of the submerged heaving and/or pitching plate is examined. Then the relative energy flux of the modelled system and influencing parameters are investigated; this is followed by a presentation of diffracted and radiated waves and factors that affect their magnitude and phase angle. The section closes with an overview of the generation of higher harmonics.

In Table 6.1 the applied parameter settings are summarised. As stated in Section 5.1, the configurations with $h/L = 1/2$ are modelled using a deep water wave height of $H_0 = 0.5m$ and a heave amplitude of $a_{heave} = 0.25m$, the setups with $h/L = 0.25$ are modelled using $H_0 = 0.25m$ and $a_{heave} = 0.125m$. The pitching amplitude is determined based on the criterion of equal water displacement when compared with the equivalent heaving plate setup and therefore varies with Ka.

For the determination of the transmission and reflection coefficients the RMS values of diffracted, radiated and total wave have been utilized. To eliminate errors introduced by the ramping-up of the presence and motion of the plate and to allow for reaching the steady-state condition, only data of the last 50% of the run time ($25T$) have been used. To avoid errors due to plate proximity, only surface displacement data of the first and last $1.5L$ of the domain have been employed; the data of $1L$ left and right of the plate have been discarded for the determination of k_T and k_R.

After determining the maximum and minimum surface displacement values of the last $25T$ on all utilized surface collocation points, the following formula was applied to determine the RMS value of the wave heights of diffracted wave $H_{diffracted}$, radiated

Table 6.1. Summary of Test Parameters.

Parameter		Tested Settings
Relative water depth	$\frac{h}{L}$	$\frac{1}{4}$ $\frac{1}{2}$
Relative submergence	$\frac{d}{h}$	$\frac{1}{3}$ $\frac{1}{2}$
Relative plate width	Ka	$0.5 \ldots 2.2$
Plate inclination	β_0	0° 5°
Heave amplitude	a_{heave}	0.125m 0.25m
Pitch amplitude	a_{pitch}	$1.6^\circ \ldots 14.4^\circ$
Motion phase angle	θ_{motion}	$0 \ldots 2\pi$

wave $H_{radiated}$, transmitted wave H_T and reflected wave H_{Rfl}:

$$H_{RMS} = 2\sqrt{\frac{\sum_{i=1}^{n} \eta_{max}^2(i) + \eta_{min}^2(i)}{2n}} \tag{6.1}$$

If not stated otherwise for all described results below, the radiated wave is tuned to be ≈180° out-of-phase with the wave scattered towards the transmission side in order to yield the biggest wave attenuation.

With this out-of-phase tuning, in deep water ($h/L = 1/2$) transmission coefficients of 0.74 and 0.83 can be achieved with pitching motion for $d/h = 1/3$ and $d/h = 1/2$ respectively (see Figures 6.1 and 6.2). The best transmission coefficients for a stationary plate in deep water are 0.97 and 0.995 respectively.

In intermediate water ($h/L = 1/4$), transmission coefficients of 0.58 and 0.62 can be achieved with pitching motion when $Ka \geq 2.0$ for $d/h = 1/3$ and $d/h = 1/2$ respectively (see Figure 6.3 and 6.4). With heaving motion transmission coefficients of 0.7 can be achieved for $Ka = 1.25$ and inclined plate. The lowest transmission coefficients for a stationary plate are 0.81 and 0.94 respectively. This shows that there is appreciable wave attenuation achievable by introducing plate motion.

6.1. Influence of Plate Width

In deep water, plate motion (heave and pitch) has only little effect on the transmission coefficient for small relative plate widths; introducing plate motion appreciably decreases k_T from approximately $Ka \geq 1.25$ for $d/h = 1/3$ and $Ka \geq 1.36$ for $d/h = 1/2$ as can be seen in Figures 6.1 and 6.2. A moving plate does not exhibit zero reflection like a fixed submerged flat plate. For a pitching plate, k_T decreases with increasing Ka. Heaving submerged plates show minimum transmission at $Ka = 2.0$ for the horizontal setup and at $Ka = 1.5(2.0)$ for the inclined setup ($\beta_0 = 5°$) for $d/h = 1/3$ and $d/h = 1/2$ respectively; increasing Ka (either wider plate or smaller wave period) does not decrease k_T further.

In intermediate water, the plate motion has already for small Ka visible effects on the transmission coefficient. Heaving motion appreciably decreases k_T from approximately $Ka \geq 1.0$ for $d/h = 1/3$ and $d/h = 1/2$ as can be seen in Figures 6.3 and 6.4; minimum k_T is yielded when $1 \leq Ka \leq 1.5$ in dependence on submergence and inclination. Pitching motion affects k_T to a minor degree for $Ka < 1.75$ but for $Ka \geq 1.75$ pitching yields considerably smaller transmission coefficients than heaving. In intermediate water too, zero reflection is not present.

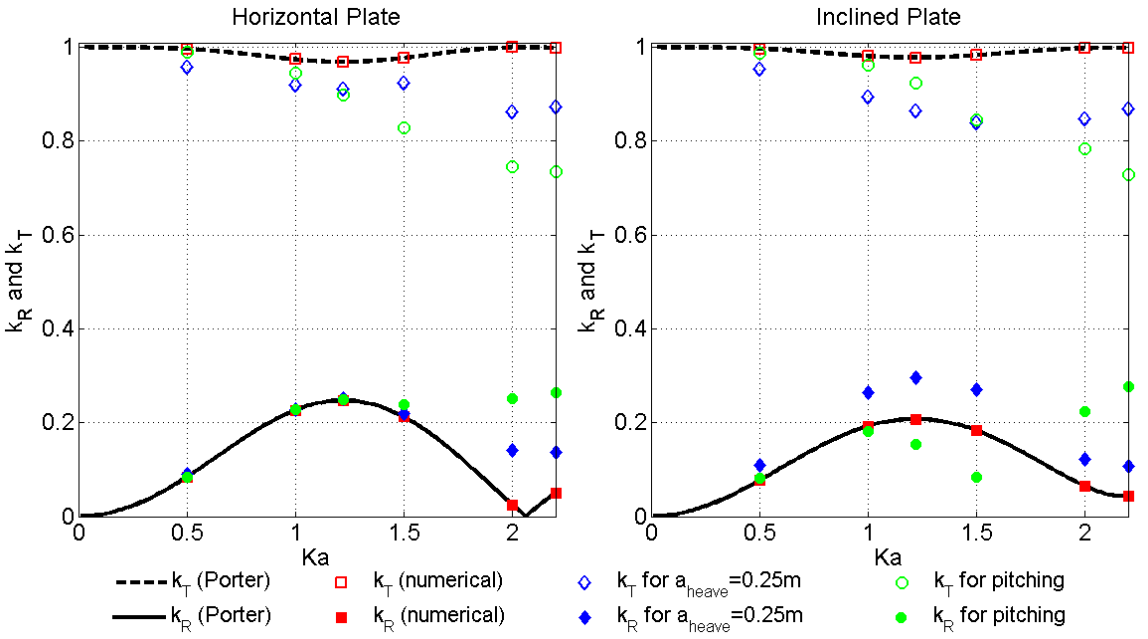

Figure 6.1. Reflection and transmission coefficients for $h/L = 1/2$, $d/h = 1/3$ $(H_0 = 0.5m)$.

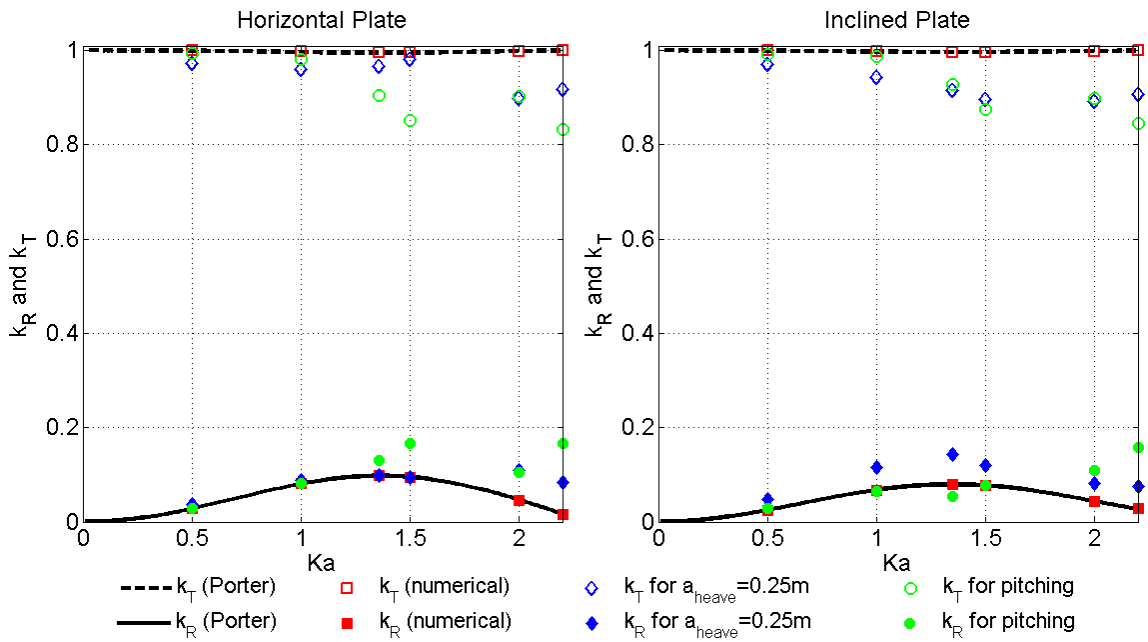

Figure 6.2. Reflection and transmission coefficients for $h/L = 1/2$, $d/h = 1/2$ $(H_0 = 0.5m)$.

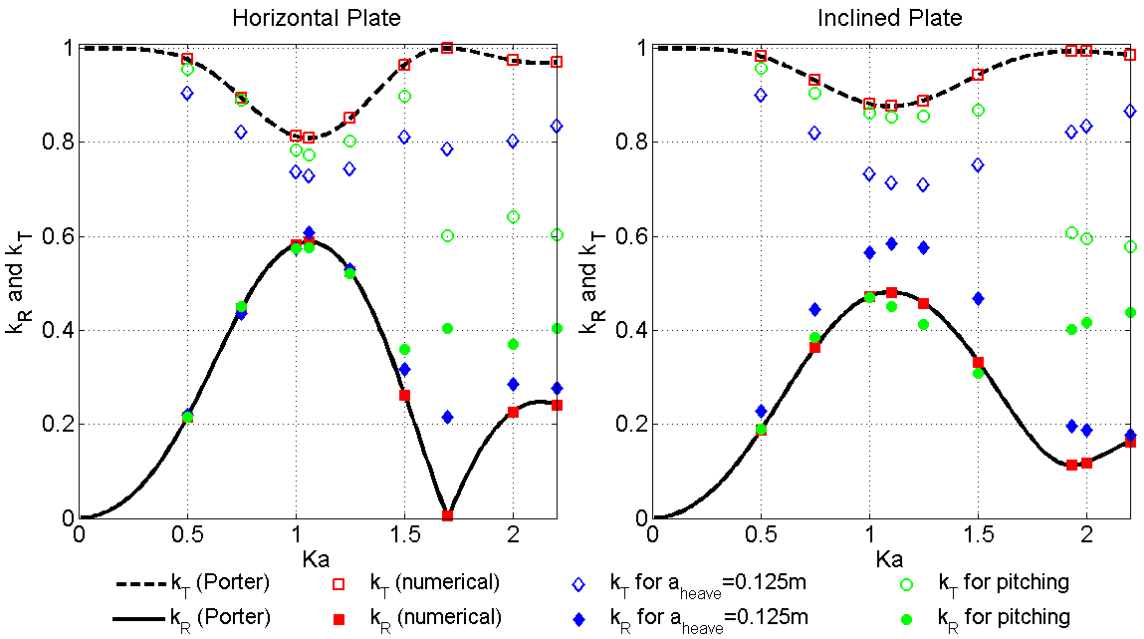

Figure 6.3. Reflection and transmission coefficients for $h/L = 1/4$, $d/h = 1/3$ ($H_0 = 0.25m$).

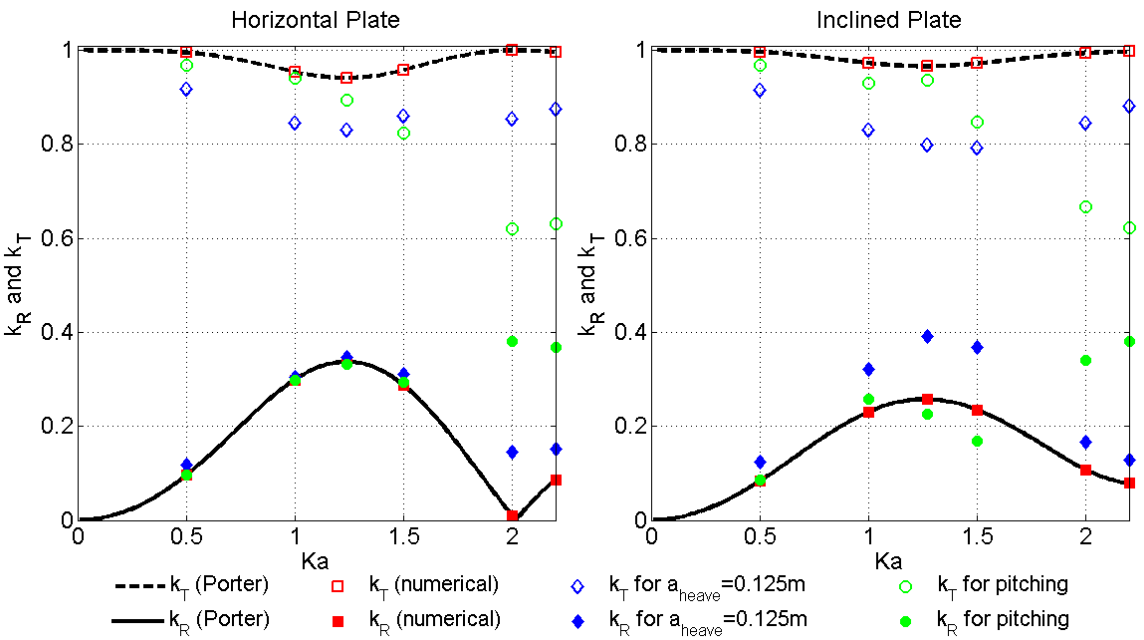

Figure 6.4. Reflection and transmission coefficients for $h/L = 1/4$, $d/h = 1/2$ ($H_0 = 0.25m$).

6.2. Influence of Relative Water Depth

The performance of a submerged moving plate as wave attenuator depends on the relative water depth. Figure 6.5 shows this dependency for pure heave and pitch motion. In intermediate water ($h/L = 1/4$) heaving motion yields smaller k_T than in deep water for all submergence depths and inclinations; the same applies to pitching motion with a relative plate submergence of $d/h = 1/2$. For a plate submergence of $d/h = 1/3$, pitching motion of a plate with relative width of $Ka = 1.5$ yields smaller k_T in deep water than in intermediate water for horizontal and inclined plate configurations.

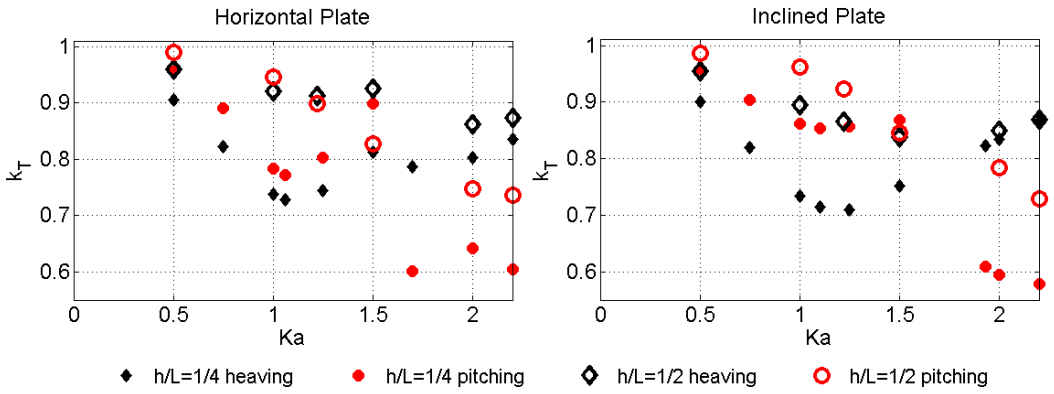

(a) Plate Submergence d/h=1/3.

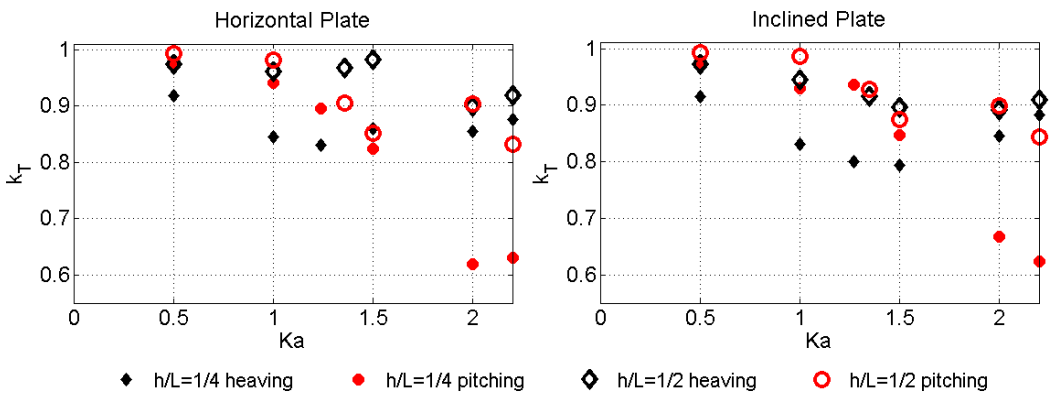

(b) Plate Submergence d/h=1/2.

Figure 6.5. Transmission coefficient in dependence on relative water depth.

6.3. Influence of Submergence Depth

In deep water the plate configurations with the smaller plate submergence of $d/h = 1/3$ result - as expected - in smaller transmission coefficients (Figure 6.6); the differences in k_T in dependence on the submergence depth are consistent throughout the tested relative plate widths Ka for heaving motion whereas for pitching motion the differences in k_T are fluctuating in dependence on Ka.

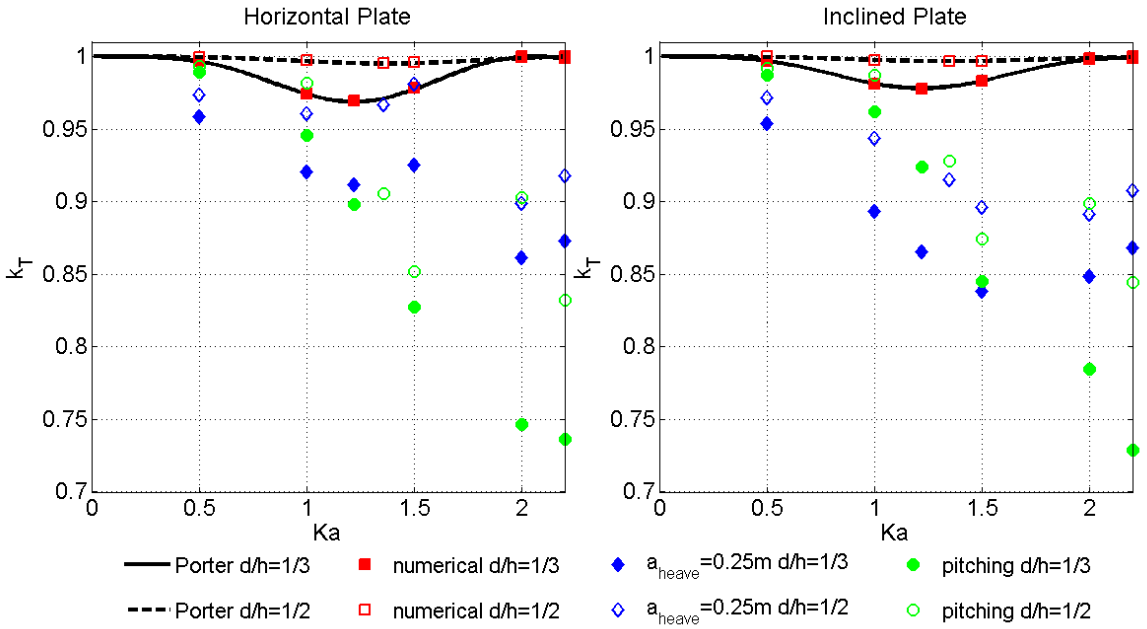

Figure 6.6. Influence of plate submergence on transmission coefficient for h/L=1/2 ($H_0 = 0.5m$).

In intermediate water, the heaving plate with the smaller submergence yields smaller k_T; the difference in k_T varies in dependence on Ka - see Figure 6.7. For pitching motion, several configurations exist where deeper submergence yields smaller k_T: for the horizontal plate deeper submergence results in smaller transmission for $Ka = 1.5$ and 2 and for the inclined plate for $Ka = 1.5$; the differences in k_T fluctuate in dependence of Ka as in deep water.

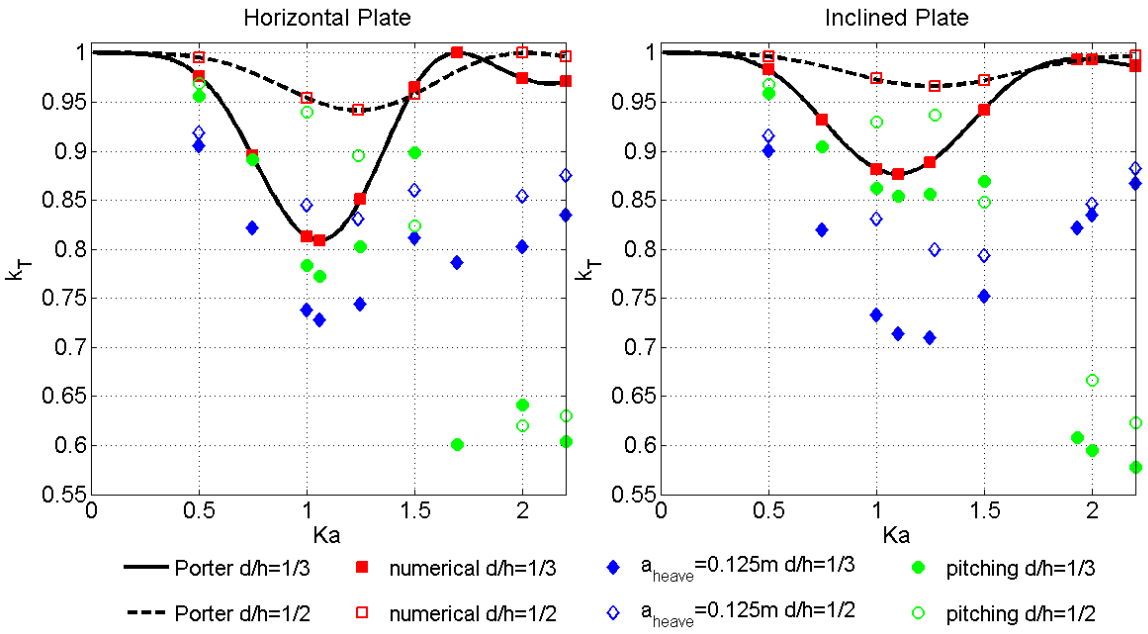

Figure 6.7. Influence of plate submergence on transmission coefficient for h/L=1/4 ($H_0 = 0.25m$).

6.4. Influence of Inclination

In deep water, the inclined heaving plate yields smaller k_T than the horizontal heaving plate for all tested submergence depths and relative plate widths Ka, see Figure 6.8.

The horizontal pitching plate performs better than the inclined pitching plate for all tested submergence depths and relative plate widths; exceptions are for $Ka = 0.5$, for $Ka = 2.2$ $(d/h = 1/3)$ and $Ka = 2.0$ $(d/h = 1/2)$.

In intermediate water, the inclined heaving plate performs better than the horizontal heaving plate for $Ka \leq 1.5$ $(d/h = 1/3)$ and $Ka \leq 2.0$ $(d/h = 1/2)$. Transmission coefficients are displayed in Figure 6.9.

The horizontal pitching plate performs in general better than the inclined pitching plate in intermediate water for $d/h = 1/2$, exceptions are for $Ka = 1.0$ and 2.2; for the

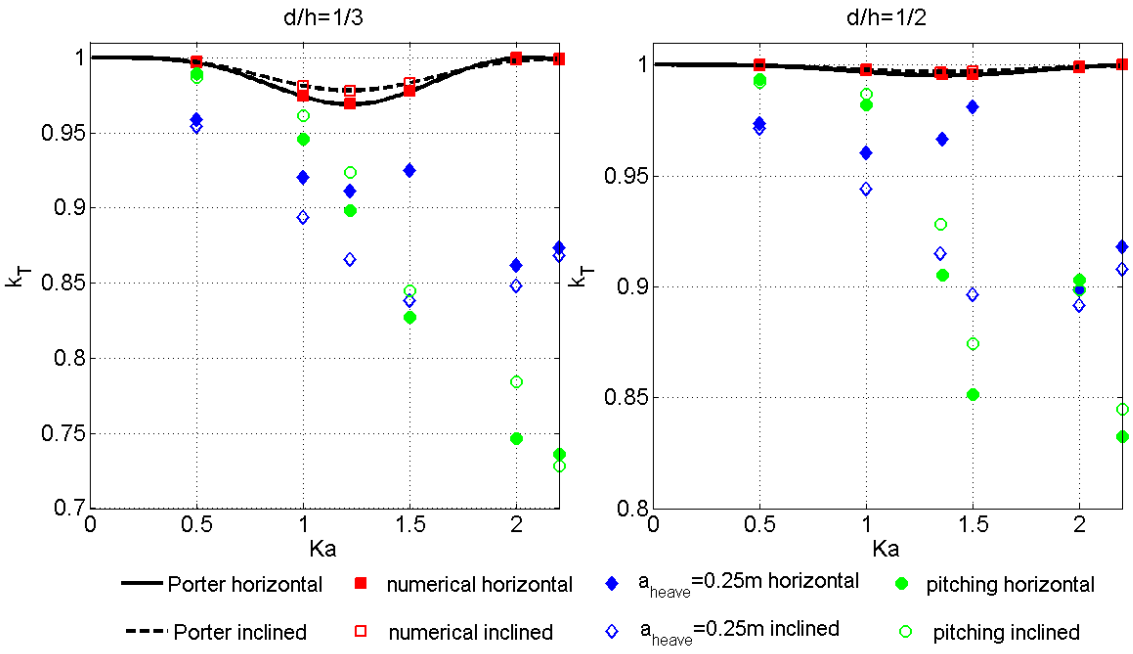

Figure 6.8. Transmission coefficients in dependence on plate inclination for h/L=1/2 ($H_0 = 0.5m$).

smaller plate submergence $d/h = 1/3$, the horizontal pitching plate yields smaller k_T if $Ka \leq 1.25$; for bigger Ka the inclined plate performs better.

Table 6.2 displays the configurations when the inclined plate yields smaller transmission coefficients than the horizontal submerged flat plate.

6.5. Influence of Motion Type

The plate motions - heaving or pitching - exhibit differing behaviour in dependence on submergence depth, inclination and plate width. This can already be seen in Figures 6.1 - 6.9. Combined heaving and pitching motion with respectively 50% of the pure heaving and pitching amplitude yields transmission coefficient values between the k_T values of pure heaving and pitching when radiated wave of both motion types is in-phase on the transmission side. This is shown in Figure 6.10 for $h/L = 1/4$ and $d/h = 1/3$ and applies to the horizontal as well as inclined plate case.

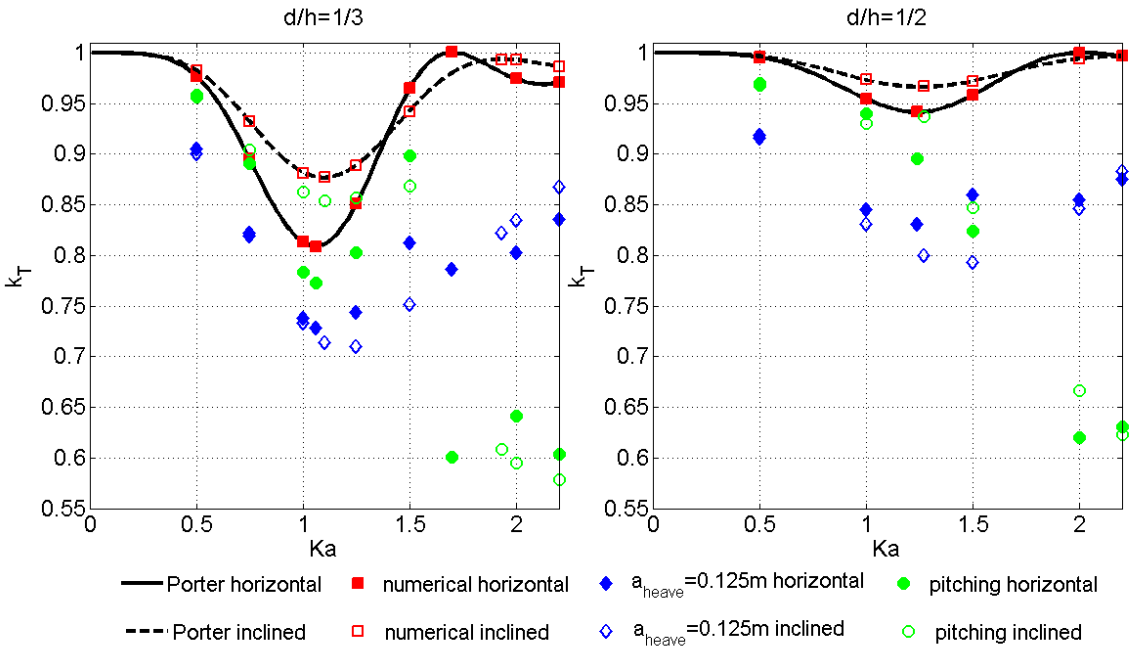

Figure 6.9. Transmission coefficients in dependence on plate inclination for h/L=1/4 ($H_0 = 0.25m$).

Table 6.2. Overview of setups with superior performance of inclined plate.

h/L	d/h	Heave	Pitch	Combined Motion
		Inclined Plate Setup yields better k_T for $Ka =$		
1/4	1/3	0.5 ... 1.5	≥1.5	1.25 ... 1.5
	1/2	0.5 ... 2.0	1.0, 2.2	not available
1/2	1/3	0.5 ... 2.2	0.5, 2.2	not available
	1/2	0.5 ... 2.2	2.0	not available

Figure 6.11 presents k_T data for different submergence depths; here too combined heaving and pitching results in transmission coefficients that lie between the ones achieved with pure heaving and pitching motion.

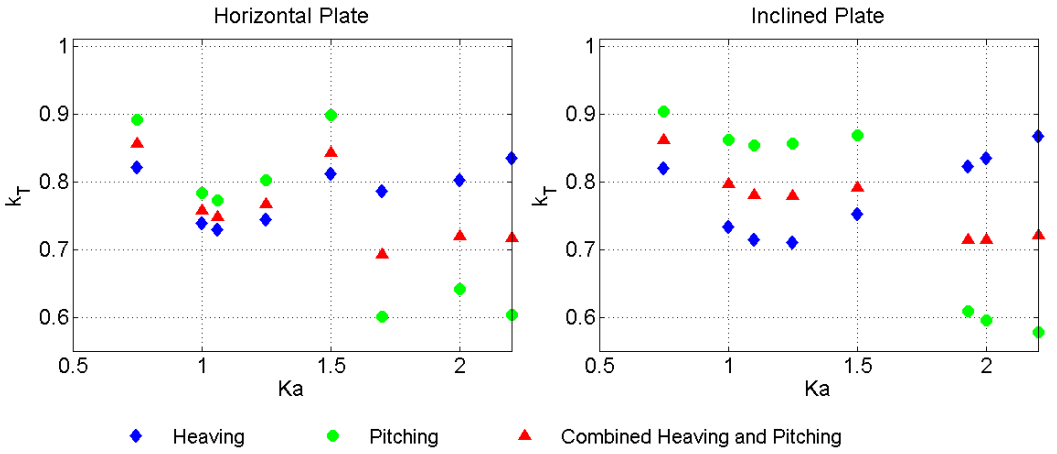

Figure 6.10. Transmission coefficients in dependence on plate motion for h/L=1/4 and d/h=1/3 ($H_0 = 0.25m$).

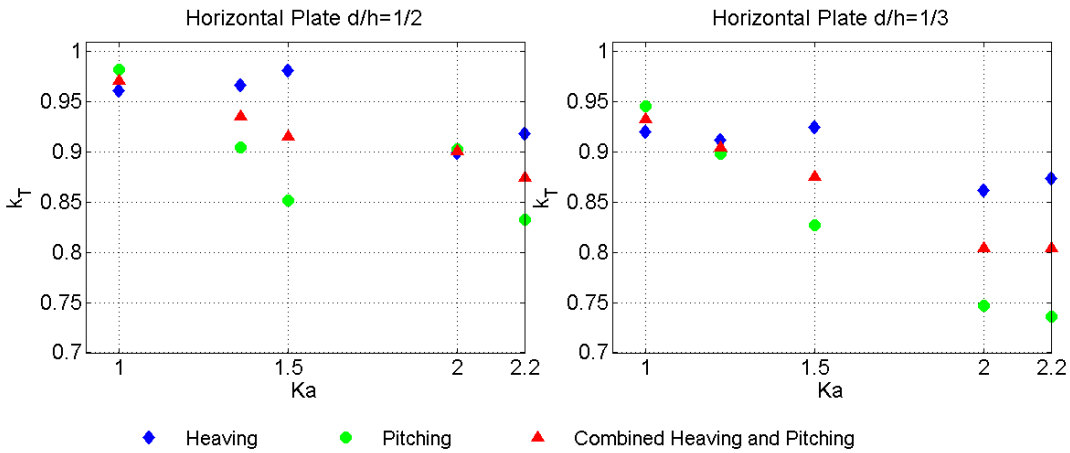

Figure 6.11. Transmission coefficients in dependence on plate motion for horizontal plate with h/L=1/2 ($H_0 = 0.25m$).

6.6. Influence of Phase Angle between Plate Motion and Incident Wave

As discussed in Section 1.2, motion amplitude and the phase angle between radiated and scattered wave define the degree of wave attenuation that can be achieved through plate motion. To investigate the effect of the phase angle, for selected setups phase angles $\theta_{motion} = \{0, \pi/2, \pi, 3\pi/2\}$ have been tested. As this is not a dense coverage of the possible phase angles $0 \leq \theta_{motion} < 2\pi$, it is possible that the optimum

phase angle to achieve minimum wave transmission differs from the here shown data.

In Figure 6.12 the influence of the phase angle between incident wave and plate heave motion for $h/L = 1/2$ and $d/h = 1/2$ is displayed. Here the smallest k_T is achieved for all shown Ka when the plate motion is approximately $\pi/2$ ahead of the incident wave. For this phase angle between plate motion and incident wave, the radiated wave is 180° out-of-phase with the wave scattered towards the transmission side and therefore wave attenuation is maximum.

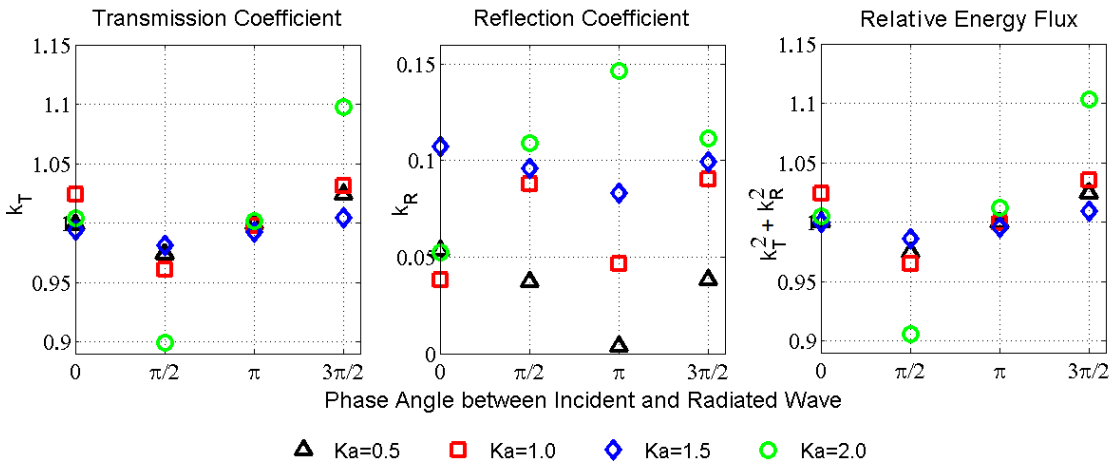

Figure 6.12. Influence of phase angle on relative energy flux for heaving horizontal plate with h/L=1/2 and d/h=1/2.

Figure 6.13 shows the phase angle influence for $h/L = 1/4$, $d/h = 1/3$ and $Ka = 2.0$ for heaving and pitching motion of horizontal and inclined plates. The transmission coefficient is minimum when the plate motion is approximately $\pi/2$ ahead of the incident wave.

The optimum phase angle between incident wave and plate motion for $h/L = 1/4$ and $d/h = 1/2$ is displayed in Figure 6.14. Note that here finer phase angle tuning was attempted through visual estimation and that's why the optimum phase angle values show a bigger variety. It can be seen that the optimum phase angle between incident wave and plate motion depends on the plate width, inclination as well as the plate

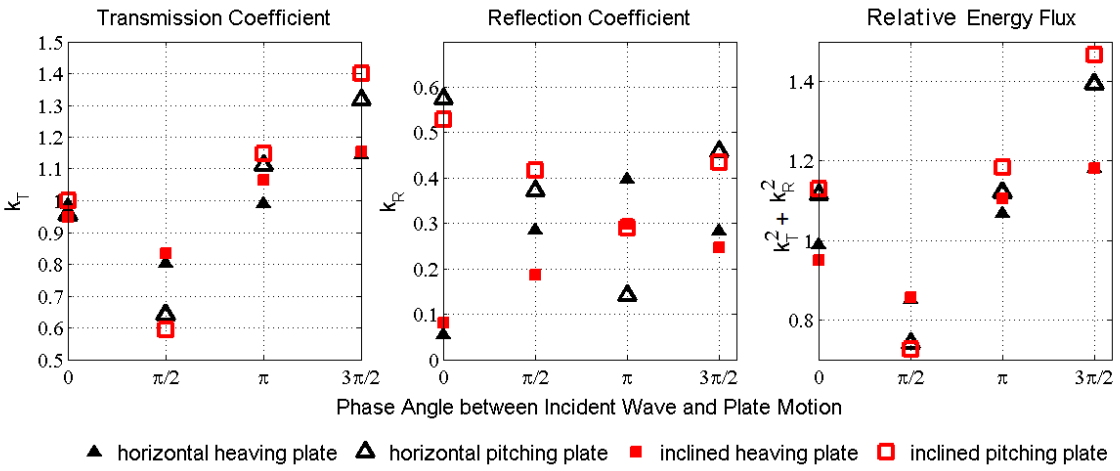

Figure 6.13. Influence of phase angle on transmission and reflection coefficient and relative energy flux for h/L=1/4, d/h=1/3 and Ka=2.0.

motion. Although not shown here, the submergence depth of the plate has also got an influence on the optimum phase angle.

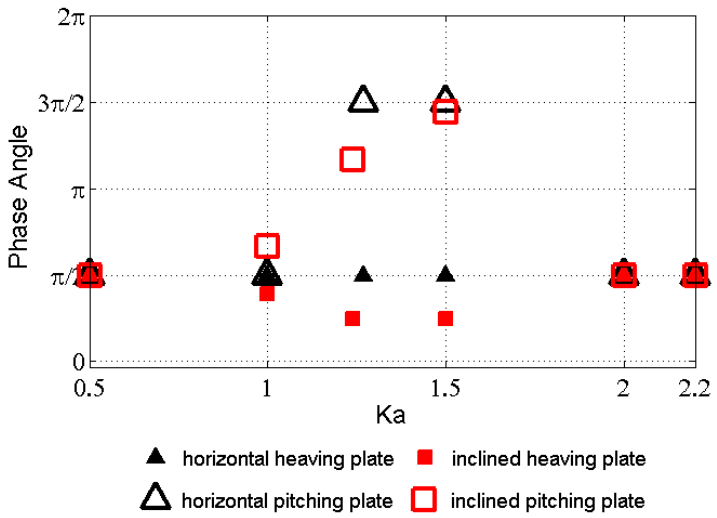

Figure 6.14. Optimum phase angle between incident wave and plate motion for h/L=1/4 and d/h=1/2.

6.7. Influence of Motion Amplitude

Doubling the plate motion amplitude results in a radiated wave with double amplitude. Tests have been performed for heaving, pitching and combined motion; results are displayed in Figure 6.15 and clearly underpin this linear relationship.

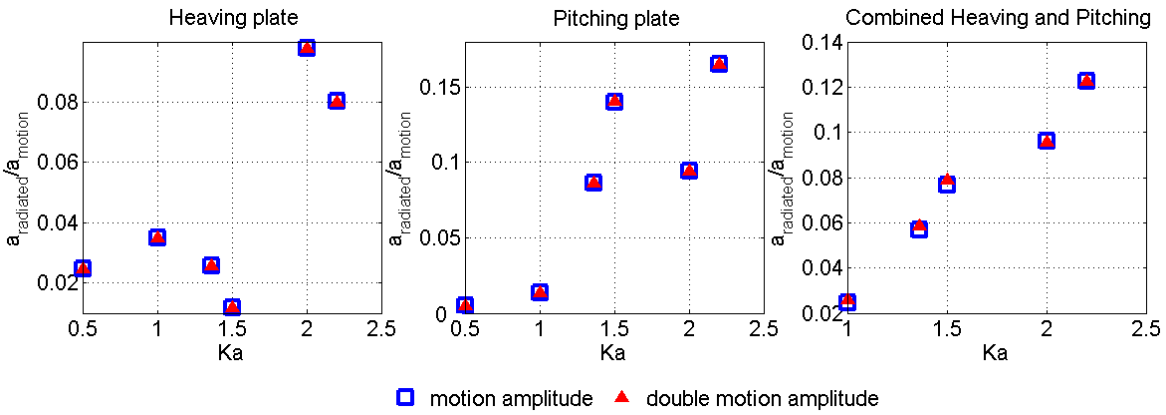

Figure 6.15. Influence of motion amplitude on amplitude of radiated wave for h/L=1/2 and d/h=1/2.

6.8. Energy Flux and Influencing Parameters

As described in Section 2.3, by modelling the moving plate with prescribed plate forcing, energy is added or taken away from the system. Whether energy has to be put into the system or can be taken out depends on the phase angle between plate motion and incidence wave only. Figure 6.12 shows this dependence for different relative plate widths for $h/L = 1/2$ and $d/h = 1/2$, and Figure 6.13 displays this relation for different inclinations and plate motions for $Ka = 2.0$, $h/L = 1/4$ and $d/h = 1/3$. It can be seen that the phase angle required for yielding small transmission coefficients also results in energy loss of the system.

The magnitude of energy gain or loss depends on all other parameters: h/L, d/h, Ka, β_0, motion type and motion amplitude (a_{heave}, β_{pitch} or a combination of both). In Figure 6.12 the influence of the relative plate width is clearly visible: the biggest

energy loss and gain is for $Ka = 2.0$ when $\theta_{motion} = \pi/2$ and $3\pi/2$ respectively; a relative plate width of $Ka = 1.0$ results in bigger energy loss and gain than $Ka = 1.5$.

The influence of inclination and motion type for $Ka = 2.0$, $h/L = 1/4$ and $d/h = 1/3$ is presented in Figure 6.13; here pitching motion leads to bigger magnitudes of energy loss and gain than heaving; the influence of inclination changes in dependence on the phase angle between plate motion and incidence wave - for $\theta_{motion} = 3\pi/2$ the inclined pitching plate setup leads to bigger energy gain than the horizontal pitching plate setup, for $\theta_{motion} = 0$ both setups lead to almost the same energy gain.

Figure 6.16 shows that Ka affects whether pitching or heaving motion yields higher energy losses; in general energy losses are bigger for the motion type that yields the smaller transmission coefficient.

The minimum transmission coefficient achievable with combined plate motion lies always between k_T attainable with pure heave or pure pitch (see Figure 6.10 and 6.11) and is therefore never the best option for attenuation of waves of a single wavelength. However, combined motion can result in maximum energy loss of the system as can be seen in Figure 6.16 for $Ka = 1.06$ and 1.7 for a horizontal plate and for $Ka = 1.5$ and 1.93 for an inclined plate and can, therefore, be favourable for energy harvesting.

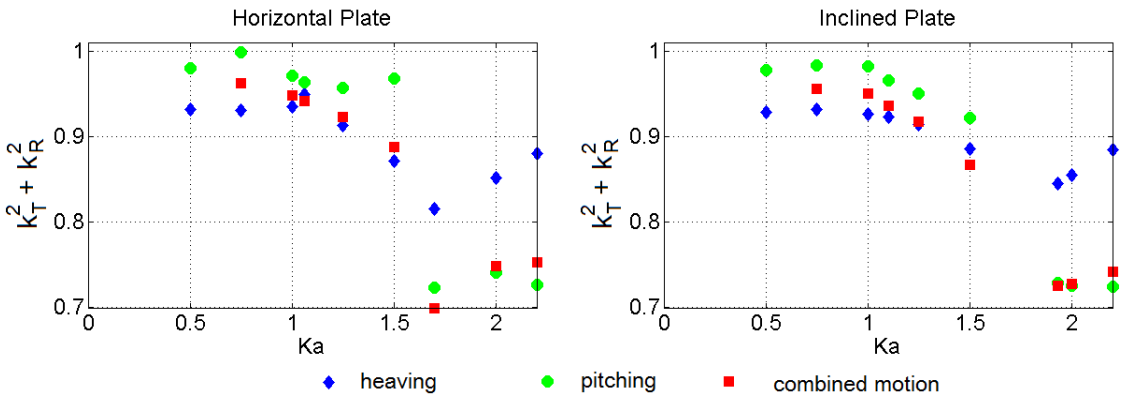

Figure 6.16. Influence of motion type on relative energy flux for h/L=1/4 and d/h=1/3.

Figure 6.17 shows the influence of the plate submergence on the relative energy flux when the phase angle between incidence wave and plate motion is optimized to yield minimum transmission coefficient. Although the heaving motion yields smaller k_T for shallower plate submergence in all intermediate water test runs (see Figure 6.7), the energy loss for $Ka < 1.5$ is bigger for the deeper plate submergence setup. For pitching motion, the relative energy flux for both plate submergence depths is similar apart for $Ka = 1.5$ where for horizontal and inclined plate the deeper plate submergence results in bigger energy loss.

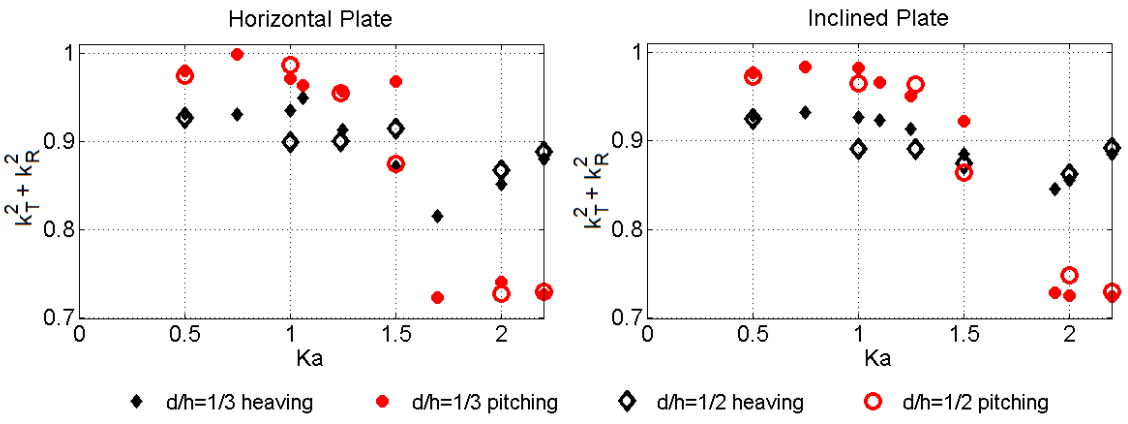

Figure 6.17. Influence of plate submergence on relative energy flux for h/L=1/4.

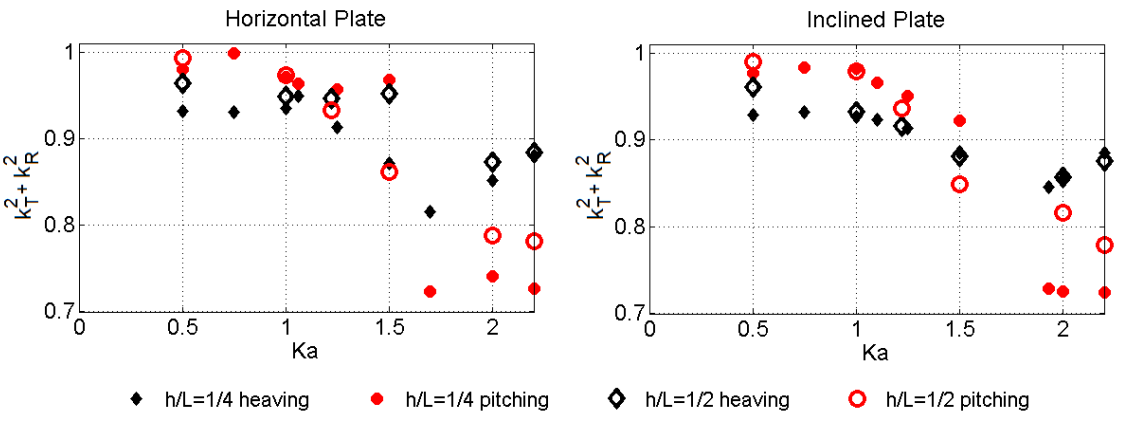

Figure 6.18. Influence of relative water depth on relative energy flux for d/h=1/3.

The influence of relative water depth is displayed in Figure 6.18; heaving motion of a horizontal plate in intermediate water results in energy loss bigger than or equal to the loss in deep water; this also applies to the inclined plate setup with one exception

for $Ka = 2.2$, here the deeper submergence leads to slightly bigger energy loss of the system. Pitching motion in intermediate water also leads to more energy loss than in deep water with exceptions for $Ka \approx 1.24$ and $Ka = 1.5$ for horizontal and inclined plate setups.

As stated in Section 6.7, the wave height of the radiated wave is doubled (halved) when the motion amplitude of the plate is doubled (halved) (see Figure 6.15). In dependence on the phase angle between plate motion and incidence wave, the increased (decreased) wave height of the radiated wave results in either increased (decreased) energy gain or loss of the system.

In Table 6.3 the influence of halving the motion amplitude on the transmission and reflection coefficient and the relative energy flux of the system is shown for pure heaving, pure pitching, and combined motion. Please note that the phase angles between motion and incidence wave are optimized to yield minimum transmission. Halving the motion amplitude results in a radiated wave with half the original wave height and therefore k_T increases while k_R decreases; energy loss of the system decreases.

6.9. Radiated Wave

In the following section the results for the radiated waves are presented separately; in order to have a common basis for heave and pitch motion, the relative motion amplitude $a_{radiated}/a_{motion}$ with a_{motion} being the heave amplitude is utilised for presenting the results. As a reminder, the pitching amplitude has been determined on the basis of equal water volume displacement with the heaving motion.

The magnitude and to a smaller extent the phase angle between plate motion and radiated wave are influenced by the relative water depth. In intermediate water, the wave height of the generated radiated wave is in general bigger than the radiated wave height in deep water; this applies to the horizontal and inclined SFP (see Figure 6.19). Only for pitching motion for $Ka = 1.25$ and 1.5, the deep water setup yields

Table 6.3. Comparison of relative energy flux in dependence on motion amplitude.

h/L	d/h	Ka	Heave Parameters		Pitch Parameters		k_T	k_R	$k_T^2+k_R^2$
			a_{heave} [m]	θ_{heave}	β_{pitch} [°]	θ_{pitch}			
1/2	1/2	2.0	0.25	$\pi/2$	-	-	0.899	0.109	0.905
			0.125	$\pi/2$	-	-	0.948	0.067	0.951
1/2	1/3	2.0	0.25	$\pi/2$	-	-	0.862	0.140	0.873
			0.125	$\pi/2$	-	-	0.930	0.074	0.933
1/2	1/2	2.2	-	-	3.28	$\pi/2$	0.833	0.167	0.849
			-	-	1.64	$\pi/2$	0.916	0.084	0.920
1/2	1/3	2.2	-	-	3.28	$\pi/2$	0.736	0.264	0.782
			-	-	1.64	$\pi/2$	0.867	0.137	0.878
1/2	1/2	2.2	0.125	$\pi/2$	1.64	$\pi/2$	0.875	0.045	0.876
			0.0625	$\pi/2$	0.82	$\pi/2$	0.937	0.027	0.937
1/4	1/2	1.5	0.0625	$\pi/2$	1.2	$3\pi/2$	0.840	0.270	0.882
			0.03125	$\pi/2$	0.6	$3\pi/2$	0.898	0.277	0.940
1/4	1/3	1.7	0.0625	$\pi/2$	1.06	$\pi/2$	0.693	0.094	0.700
			0.03125	$\pi/2$	0.53	$\pi/2$	0.846	0.047	0.847

bigger radiated wave heights than the intermediate water setup.

Smaller plate submergence results in bigger radiated waves; all deep water cases show this behaviour. In intermediate water some exceptions exist (see Figure 6.20): heaving horizontal plate with $Ka = 1.0$, pitching horizontal plate with $Ka = 1.5$ and 2.0 and and inclined pitching plate with $Ka = 1.0$. The plate submergence has also an effect on the phase angle between plate motion and radiated wave.

Inclined heaving plates generate bigger radiated waves towards the transmission side than horizontal heaving plates for all investigated water depths and plate submergences (see Figure 6.21). Whether inclined or horizontal pitching plates generate bigger radiated waves towards the transmission side, depends on Ka as can be seen in

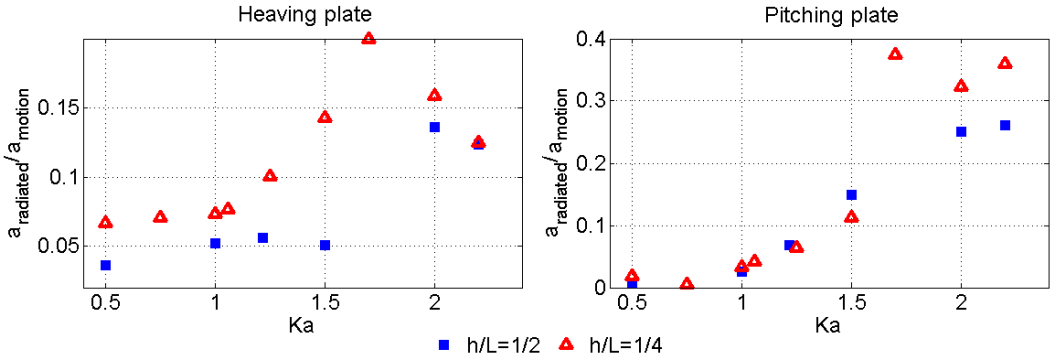

(a) Horizontal plate.

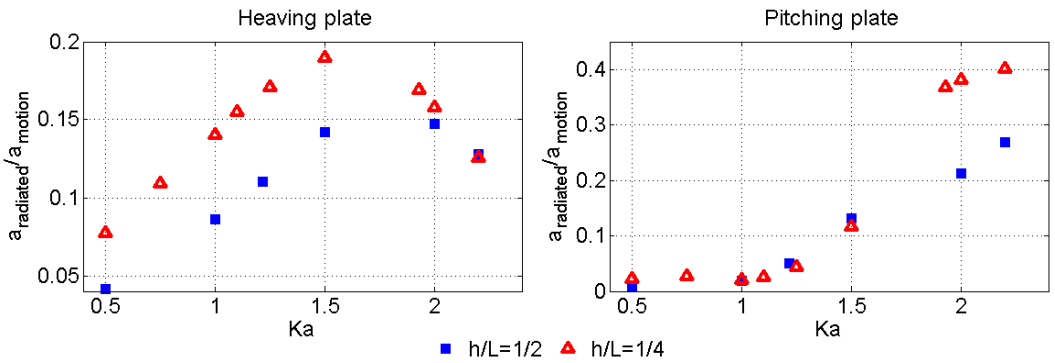

(b) Inclined plate.

Figure 6.19. Radiated wave towards transmission side in dependence on relative water depth for $d/h = 1/3$.

Figure 6.21. The plate inclination also affects the phase angle between plate motion and radiated wave.

The influence of relative plate width on the radiated wave is also twofold: it affects the magnitude of the radiated wave and the phase angle between plate motion and radiated wave.

Figure 6.22 shows both influences for an inclined plate with $h/L = 1/4$ and $d/h = 1/3$. For both configurations the plate motion phase angle is equal, only the relative plate width differs. It can be seen, that the wave height of the radiated waves differs and that additionally, the radiated waves are almost 180° out of phase.

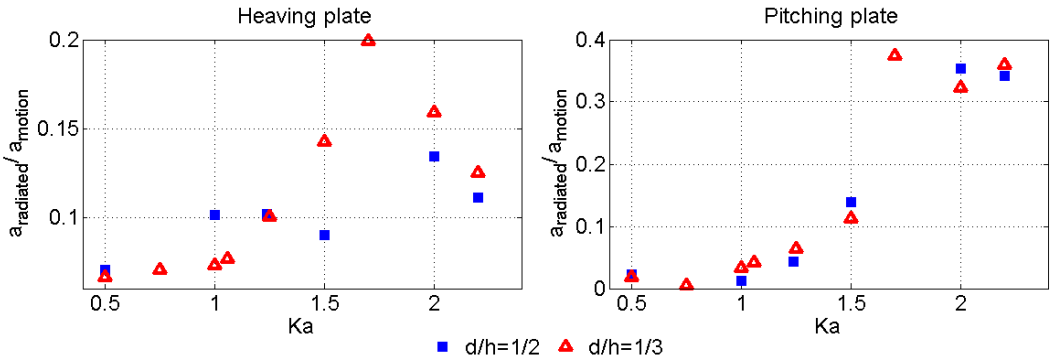

(a) Horizontal plate.

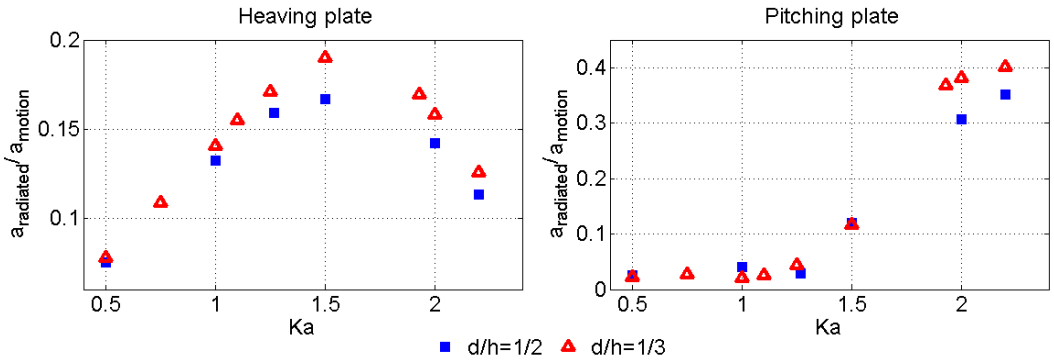

(b) Inclined plate.

Figure 6.20. Radiated wave towards transmission side in dependence on plate submergence for $h/L = 1/4$.

Different relative plate widths, therefore, require new tuning of the phase angle between plate motion and incidence wave to ensure destructive interference between radiated and scattered wave on the transmission side.

Figures 6.19 - 6.21 show that in general radiated waves generated by heaving motion obtain maximum wave heights for $1.0 \leq Ka \leq 1.5$ whereas with pitching motion maximum wave heights are reached when $Ka \geq 2.0$. As shown in Figure 6.15, doubling the motion amplitude results in the double height of the radiated wave. This applies to pure heave, pure pitch, and combined heave and pitch.

The heights of the waves radiated towards incidence and transmission side are equal for pure heaving and pitching motions of a horizontal SFP; combined heaving

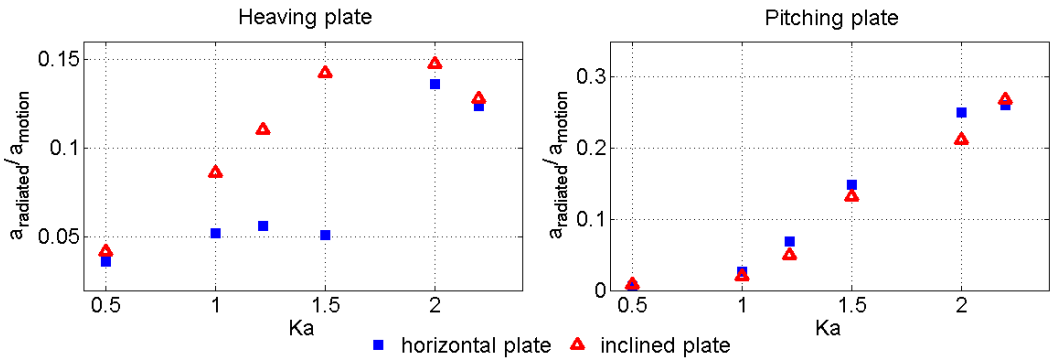

(a) d/h=1/3.

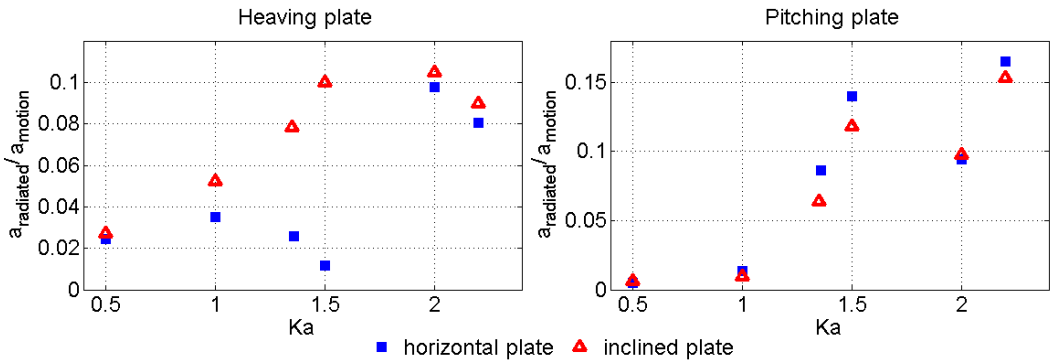

(b) d/h=1/2.

Figure 6.21. Radiated wave towards transmission side in dependence on inclination for $h/L = 1/2$.

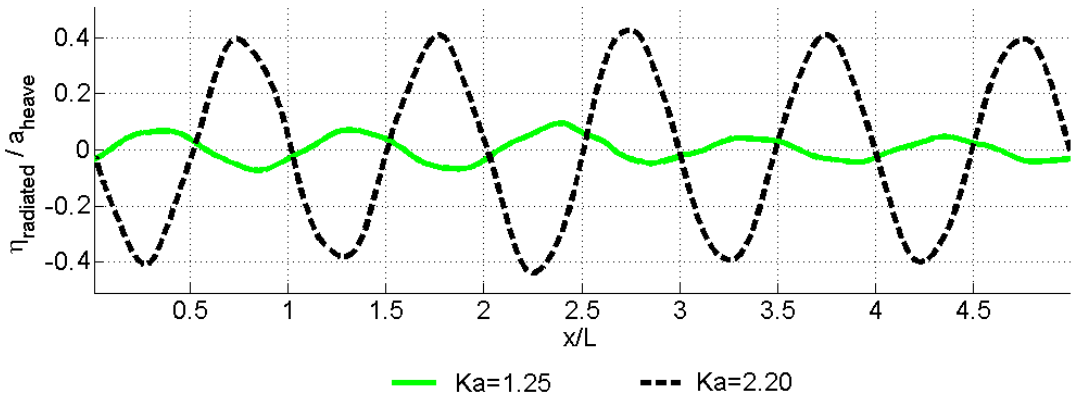

Figure 6.22. Influence of Ka on radiated wave for h/L=1/4 d/h=1/3 inclined plate.

and pitching yields different heights for the waves radiated towards transmission and incidence side (Figure 6.23(a)). As the phase angle between incident wave and plate

motion is tuned for minimizing k_T, the wave radiated towards transmission side generated by combined motion has wave height values that lie between the ones yielded by pure heaving and pitching. This applies to horizontal and inclined plate configurations (see Figure 6.23).

For inclined submerged plates, the heights of the waves radiated towards incidence and transmission side always differ regardless of motion type. Albeit the small plate inclination here, differences in the magnitudes of the waves radiated towards incidence and transmission side are clearly visible (Figure 6.23(b)).

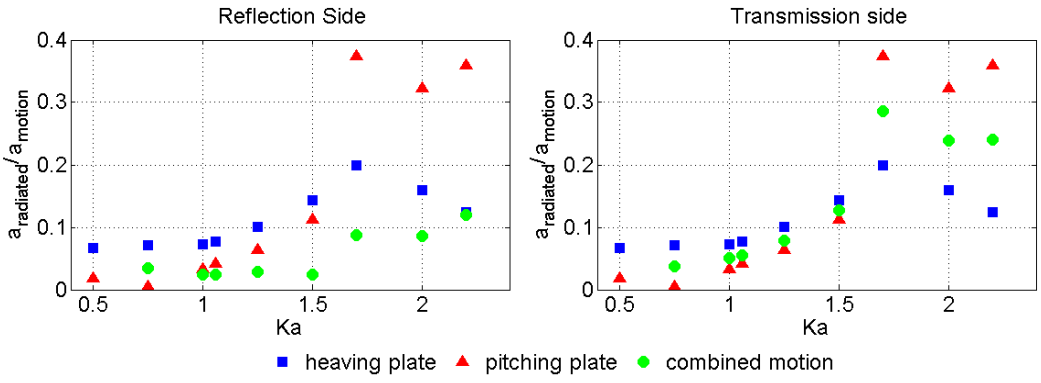

(a) Horizontal plate.

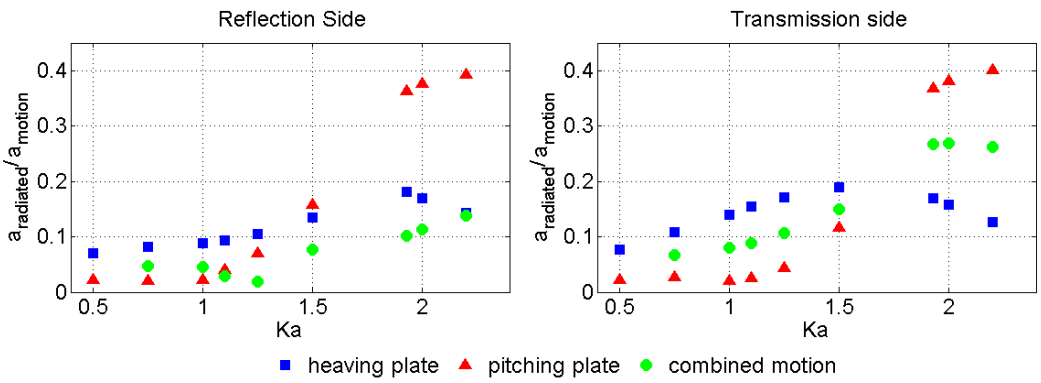

(b) Inclined plate.

Figure 6.23. Radiated wave in dependence on motion type for $h/L = 1/4$ and $d/h = 1/3$.

The wave radiated by a heaving plate is symmetric (see Figure 6.24(a)), the wave radiated by a pitching plate is antisymmetric (see Figure 6.24(b)). When combining

both motion modes, it is possible to manipulate the radiated wave. When the waves radiated by both motions towards the transmission side are in phase, the wave radiated towards the transmission side is maximum and the magnitude depends on the ratio of the motion types. Figure 6.24(c) displays the maximum radiated wave towards transmission for equal share of motion amplitude.

If the waves radiated by both motions towards the incidence side are 180° out-of-phase and additionally the amplitudes of the radiated waves generated by heaving and pitching are equal, then there will be no wave radiation towards wave incidence side (see Figure 6.24(d)).

Similarly, by tuning the radiated waves of heaving and pitching to be 180° out-of-phase towards the transmission side and ensuring that the amplitudes of the radiated waves generated by heaving and pitching are equal, the radiated wave towards transmission side would be zero which would result in zero wave attenuation.

6.10. Influence of Plate Motion on the Diffracted Wave

In addition to the generation of a radiated wave, plate motion also alters the diffracted wave by changing the position of the plate surfaces from which the incident wave is reflected. In this section the research results for the diffracted wave only are presented.

In Figures 6.25 and 6.26 the amplitude of the diffracted wave of stationary plates is compared with the diffracted wave amplitude of moving plates for $h/L = 1/2$ with $d/h = 1/2$ and $h/L = 1/4$ with $d/h = 1/3$ respectively. In the present test runs, the magnitude of the diffracted wave changes in general only to a minor degree when plate motion is present owing to the small incidence wave height and small plate motion required by the applicability conditions of linear approximation (see Section 2.4.2).

It can be expected that with increasing motion amplitude and/or increased incident wave height the influence of the plate motion on the diffracted wave will grow;

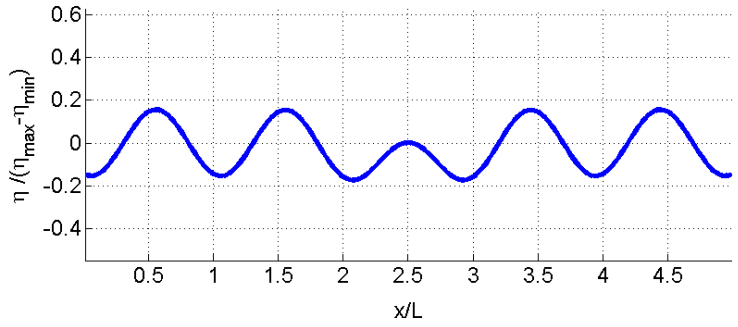

(a) Heaving motion.

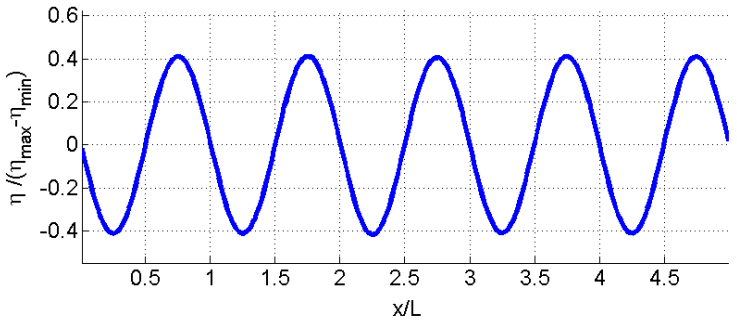

(b) Pitching motion.

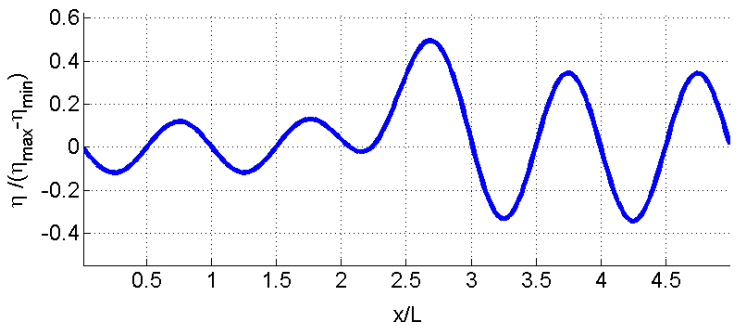

(c) Combined heaving and pitching (Maximum wave towards radiation).

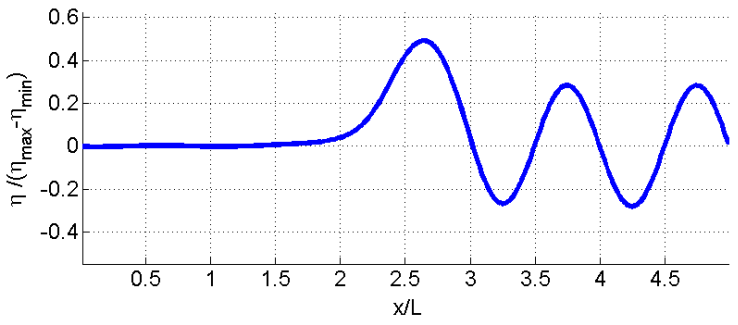

(d) Combined heaving and pitching (Zero wave towards incidence).

Figure 6.24. Radiated wave in dependence on motion type and phase angle for horizontal plate with $h/L = 1/2$, $d/h = 1/2$ and $Ka = 2.2$ at time $t = 50T$.

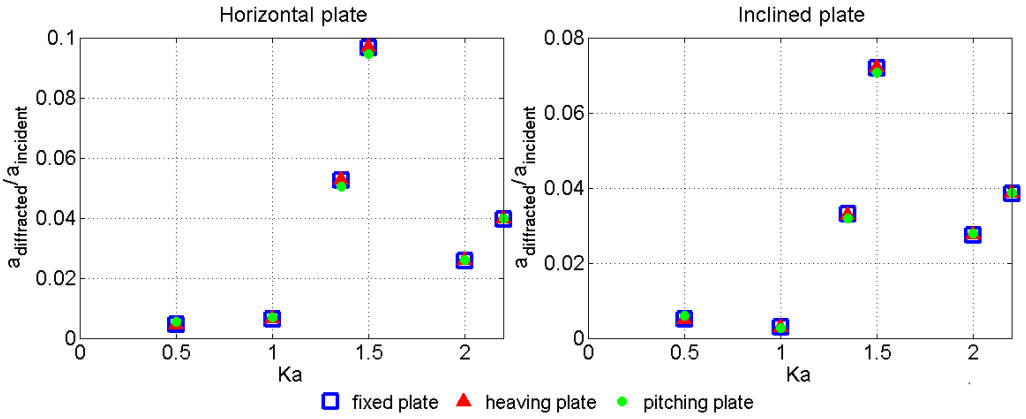

(a) Diffracted wave towards transmission side.

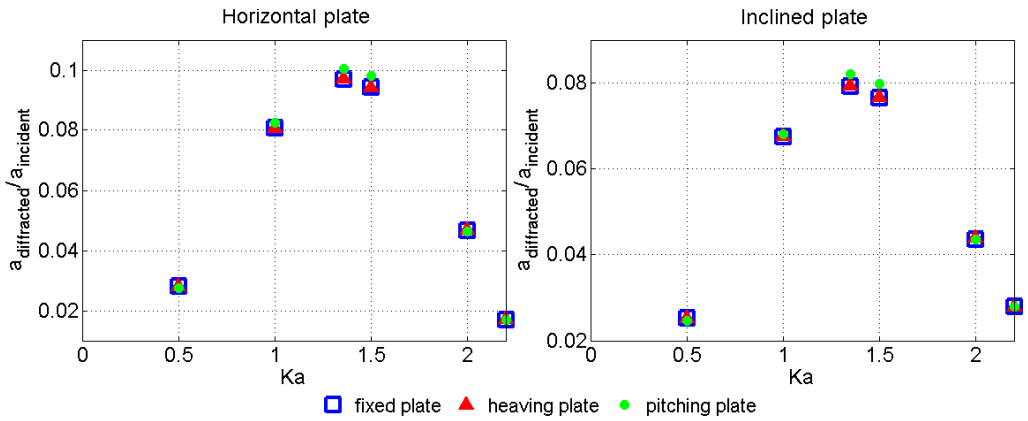

(b) Diffracted wave towards reflection side.

Figure 6.25. Comparison of diffracted waves in dependence on motion for h/L=1/2 and d/h=1/2.

already within the restrictions for applicability of linear approximation of the body-nonlinear wave problem (as derived in Section 2.4.2), small changes could be detected with double pitching amplitude and double incidence wave height for $h/L = 1/2$ and $d/h = 1/2$. Data are displayed in Figure 6.27.

For horizontal and inclined plates changes in the diffracted wave are more pronounced in intermediate water and for smaller plate submergence. Pitching motion leads to bigger differences in the amplitude of the diffracted wave than heaving motion. It appears that the magnitude differences between the diffracted waves of fixed and moving plates are higher for relative plate widths of $1.0 \leq Ka \leq 1.5$.

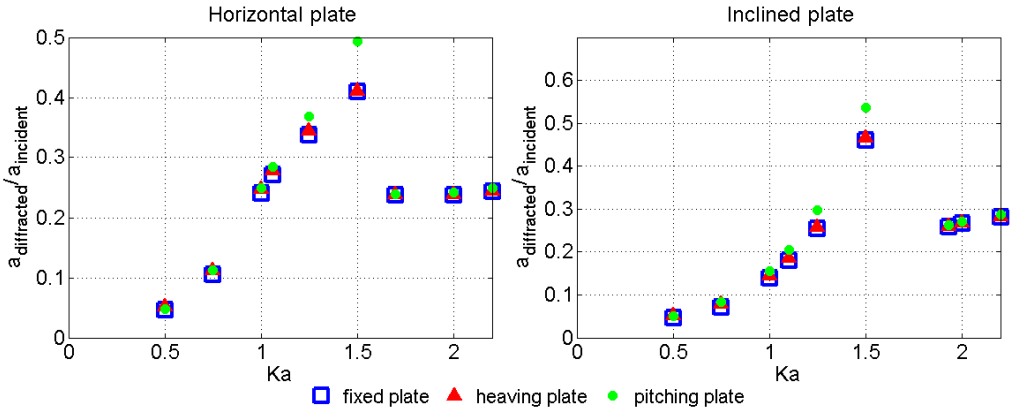

(a) Diffracted wave towards transmission side.

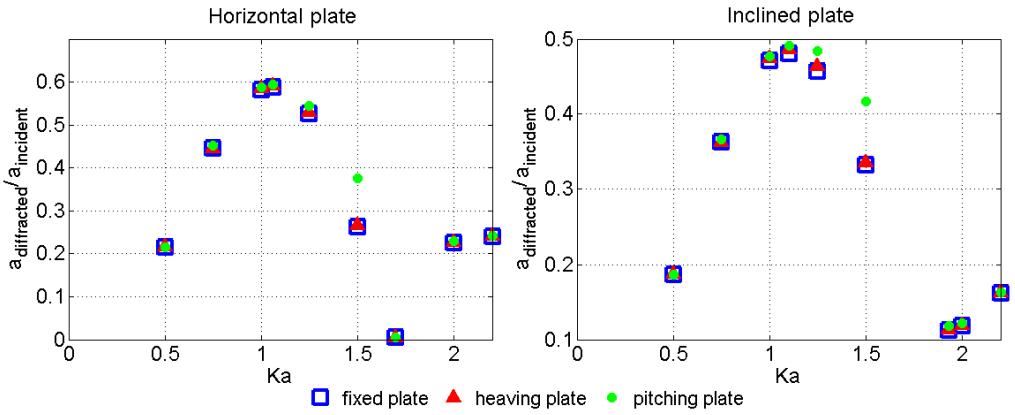

(b) Diffracted wave towards reflection side.

Figure 6.26. Comparison of diffracted waves in dependence on motion for h/L=1/4 and d/h=1/3.

Figures 6.25(a) and 6.26(a) show that the biggest amplitude of the wave diffracted towards transmission side is always at $Ka = 1.5$ regardless of relative water depth, relative submergence, inclination, and whether the plate is stationary or moving. That this configuration never yields the best transmission coefficient for the stationary plate case is due to the fact that the wave attenuation effectiveness of the amplitude of the diffracted wave also depends on the phase angle between diffracted and incidence wave which is influenced by h/L, d/h, Ka and the plate inclination.

On the reflection side, the amplitude of the diffracted wave (for fixed and moving plates) agrees with the trend of the reflection coefficient of the stationary plate; biggest

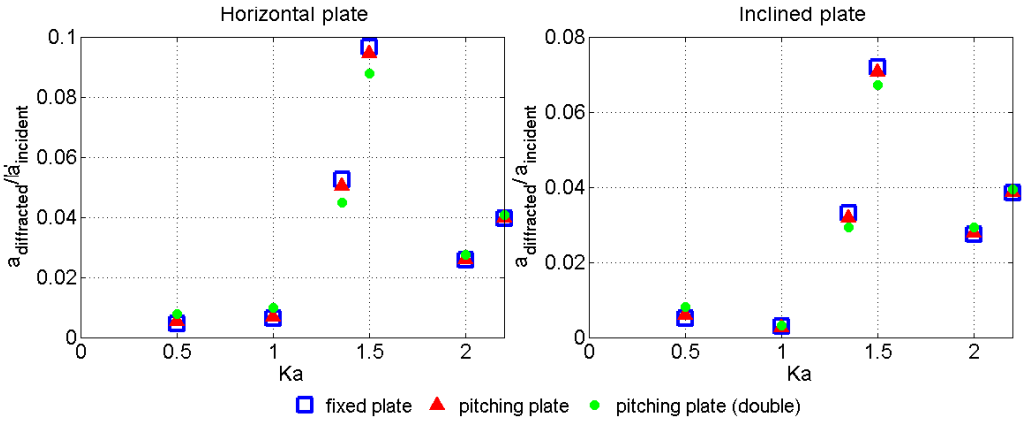

(a) Diffracted wave towards transmission side.

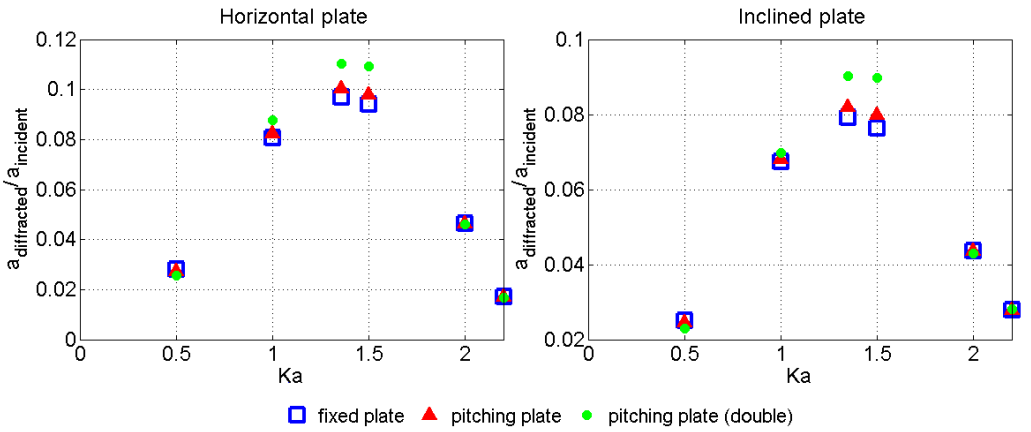

(b) Diffracted wave towards reflection side.

Figure 6.27. Comparison of diffracted waves in dependence on motion and incidence amplitude for h/L=1/2 and d/h=1/2.

amplitudes of diffracted wave towards reflection side are present for $1.0 \leq Ka \leq 1.5$ depending on h/L, d/h and inclination (see Figures 6.25(b) and 6.26(b)). Here the phase angle between motion and incidence wave has no effect as reflected and incident wave move in opposite directions.

Plate motion does not change the phase angle between diffracted and incidence wave as can be seen in Figures 6.28, 6.29, 6.30 and 6.31, where the diffracted wave of a stationary plate is compared with the diffracted wave of a moving plate at time $t = 50T$, but generates small deviations from the sinusoidal diffracted wave of a stationary plate.

When the amplitude ratio of second harmonics to fundamental wave is small ($< 5\%$), the deviations between the diffracted wave of a stationary plate and the diffracted wave of a moving plate are negligibly small. This is the case for the diffracted wave towards incidence side in Figure 6.28 where only 3.4% second harmonics are present.

Figure 6.30 (pitching motion and $h/L = 1/4$, $d/h = 1/3$ and $Ka = 0.75$) clearly demonstrates that higher harmonics are introduced through the body-nonlinear modelling of the plate motion (as analytically derived in Section 2.4.1); this nonlinearity is visible as small deviations in η on the transmission side. In Figure 6.31 the presence of second harmonics is readily identifiable due to amplitude ratios of second harmonics to fundamental wave of 90% on the incidence side and 60% on the transmission side. In the next section the influencing parameters on the generation of higher harmonics are investigated.

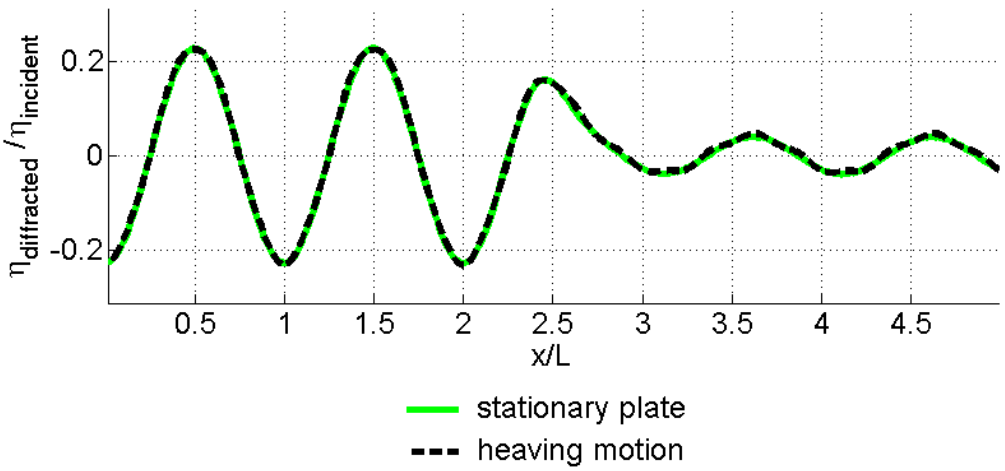

Figure 6.28. Influence of heave motion on diffracted wave for horizontal plate with h/L=1/2, d/h=1/3 and Ka=1.0 (t=50T).

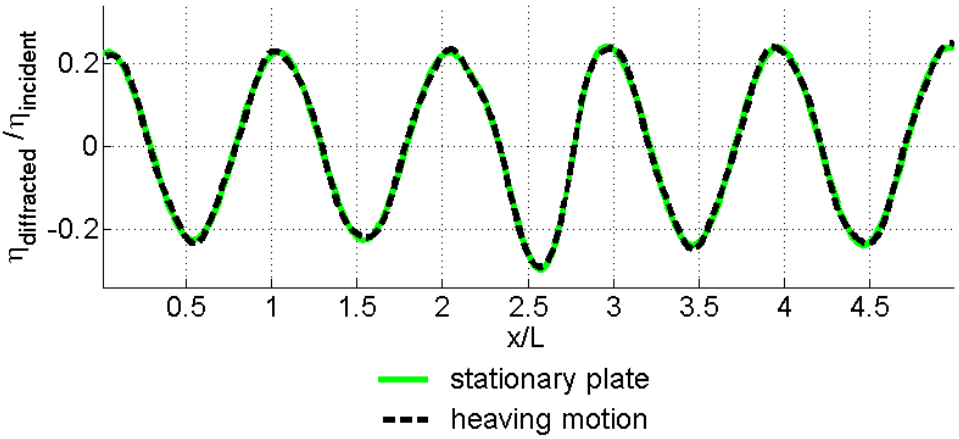

Figure 6.29. Influence of heave motion on diffracted wave for horizontal plate with h/L=1/4, d/h=1/3 and Ka=2.0 (t=50T).

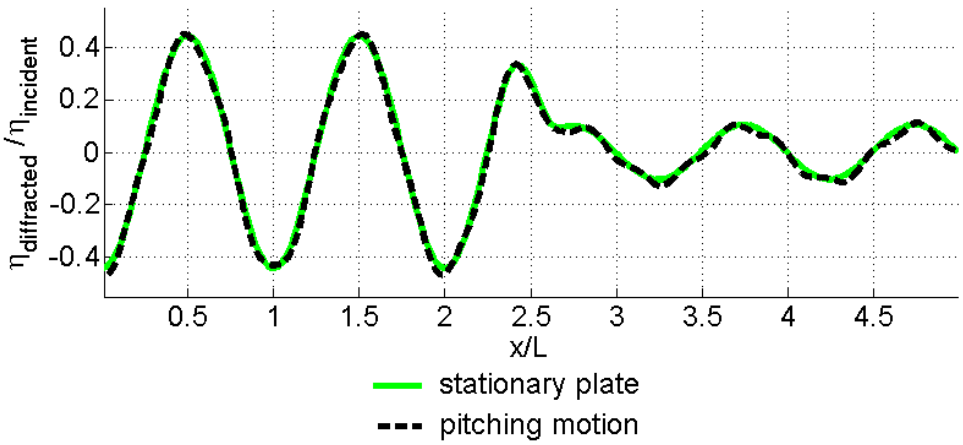

Figure 6.30. Influence of pitch motion on diffracted wave for horizontal plate with h/L=1/4, d/h=1/3 and Ka=0.75 (t=50T).

6.11. Generation of Higher Harmonics

The application of the body-nonlinear method leads to the generation of higher harmonics in the diffracted and the radiated wave. Figures 6.32(a) and 6.32(b) show the magnitudes of the Fourier spectrum of $\eta(f)$ of the diffracted and radiated wave over the relative frequency fT with T being the wave period of the incidence wave. In both figures, peaks in the Fourier spectrum of $\eta(f)$ at $fT = 1$ and $fT = 2$ exist representing the fundamental wave and the second harmonic wave.

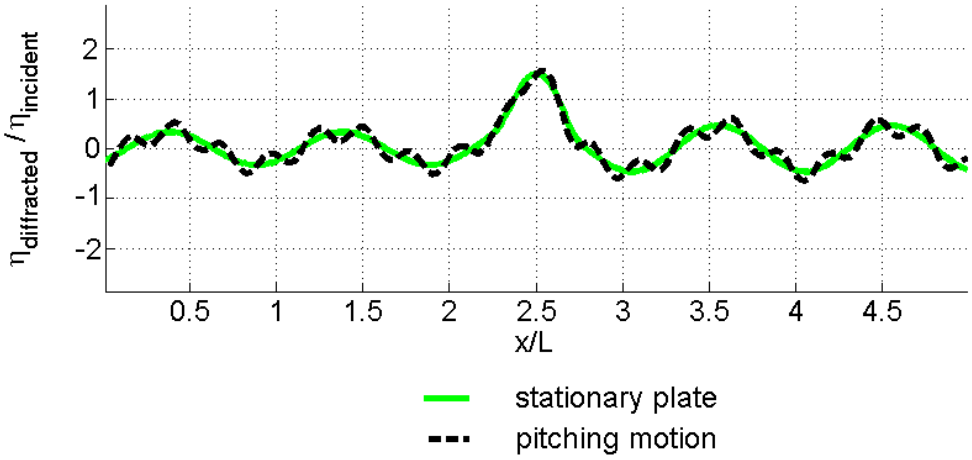

Figure 6.31. Influence of pitch motion on diffracted wave for inclined plate with h/L=1/4, d/h=1/3 and Ka=1.5 (t=50T).

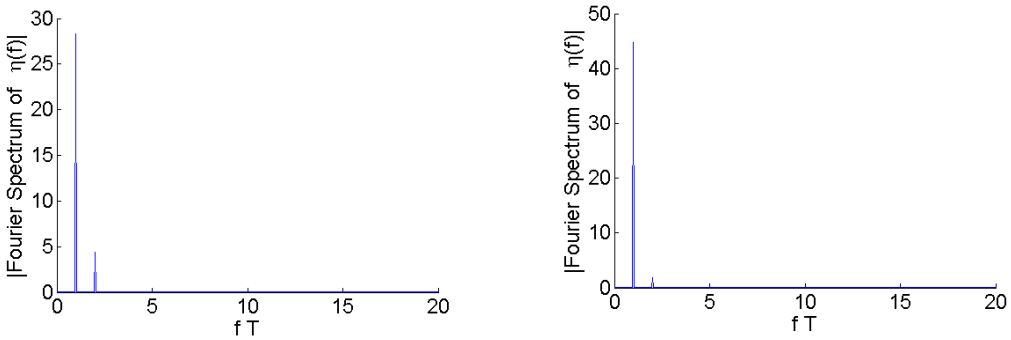

(a) Diffracted wave.

(b) Radiated wave.

Figure 6.32. Higher harmonics on transmission side for h/L=1/4, d/h=1/3 and Ka=2.0.

Higher harmonics in the diffracted wave are more pronounced in intermediate water than in deep water which will be mainly due to the smaller absolute submergence in intermediate water and increase with decreasing submergence depth. Plate inclination affects the magnitude of the generation of higher harmonics; its influence varies in dependence on h/L, d/h and Ka but no general rule could be established.

The magnitudes of the higher harmonics are in general bigger for pitching motion and differ on transmission and incidence side (see Figure 6.33). On the transmission side

heaving generates a higher percentage of harmonics for $Ka \leq 1$ whereas for pitching the higher percentage can be found for $0.75 \leq Ka \leq 1.5$. On the incidence side both motion types generate the highest percentage of harmonics for $Ka > 1.0$.

Increasing the motion amplitude and/or the incidence wave height leads to a higher percentage of second and third harmonics in the diffracted wave. There is no evidence that the phase angle between incidence wave and plate motion has an effect on the magnitude of the generated higher harmonics in the diffracted wave. The data shown in Figure 6.33 represent the highest values of harmonics present; deep water and smaller submergence setups result in smaller percentages of higher harmonics in the diffracted wave.

Referring back to Figure 6.30, a pitching plate with $h/L = 1/4$, $d/h = 1/3$ and $Ka = 0.75$ generates second harmonics of 37% of the wave height of the fundamental diffracted wave on the transmission side.

Generated higher harmonics in the radiated wave are also more prominent in intermediate water than in deep water, although as for the diffracted wave this results primarily from the smaller absolute submergence depth in intermediate water, and their ratio in the radiated wave grows when reducing the plate submergence; pitching motion leads to bigger amplitudes of higher harmonics in the radiated wave (see Figure 6.34).

The horizontal plate configuration generates a bigger ratio of second harmonic for $Ka < 1.5$, for $Ka \leq 1.5$ in general the motion of an inclined plate results in a bigger percentage of second harmonics.

Relative plate widths between $0.5 \leq K \leq 1.5$ generate the highest ratios of second harmonics in the radiated wave; further increase in plate width leads to smaller ratios of second harmonics in the radiated wave.

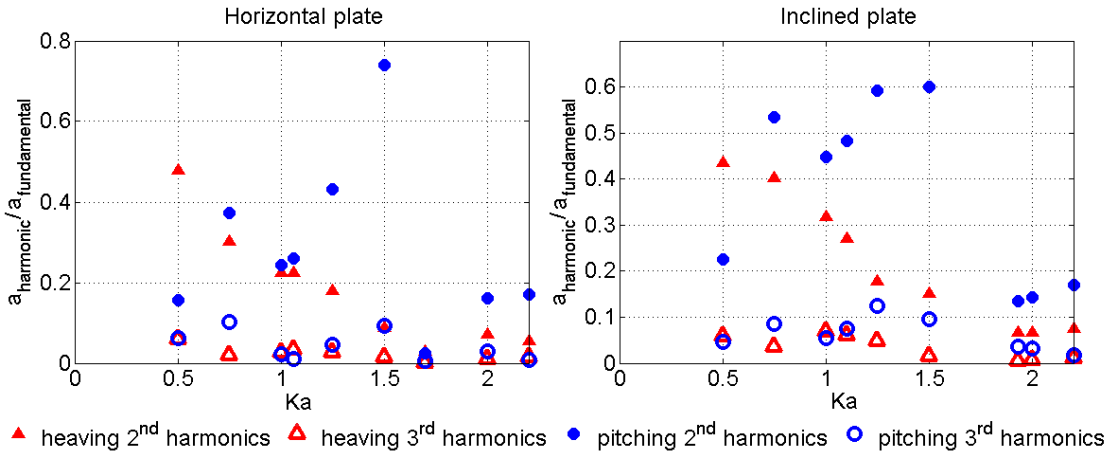

(a) Transmission side.

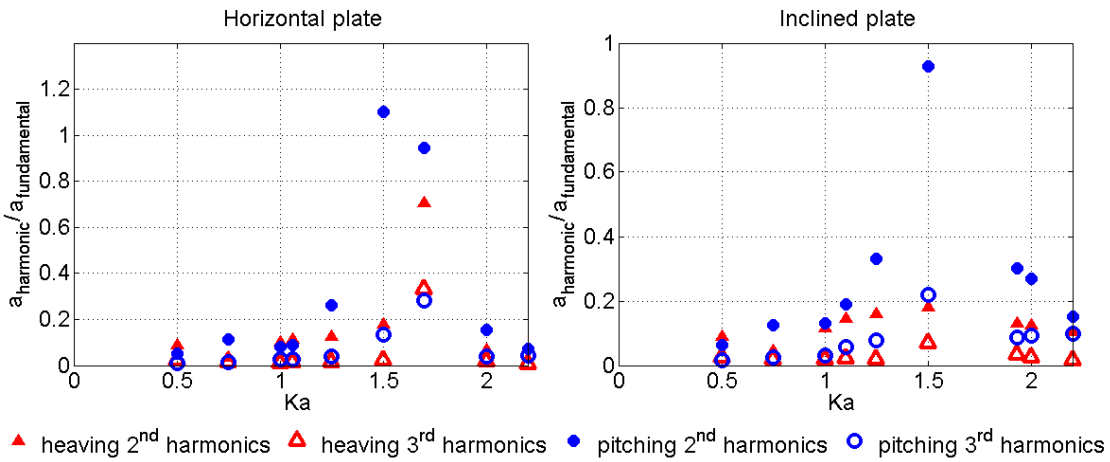

(b) Incidence side.

Figure 6.33. Higher harmonics of diffracted wave for h/L=1/4 and d/h=1/3.

Figure 6.35 shows the effect of the motion type on the generation of second harmonics in the radiated wave; the combined heaving and pitching motion appears to generate in general a smaller ratio of second harmonics than pure heaving and pitching.

A moving horizontal plate generates the same ratio of higher harmonics in the radiated wave towards transmission and incidence side; for an inclined moving plate the higher harmonics towards transmission and incidence side differ. Increasing the motion amplitude and/or the incidence wave height results in a bigger percentage of second and third harmonics in the radiated wave. The phase angle between incidence wave

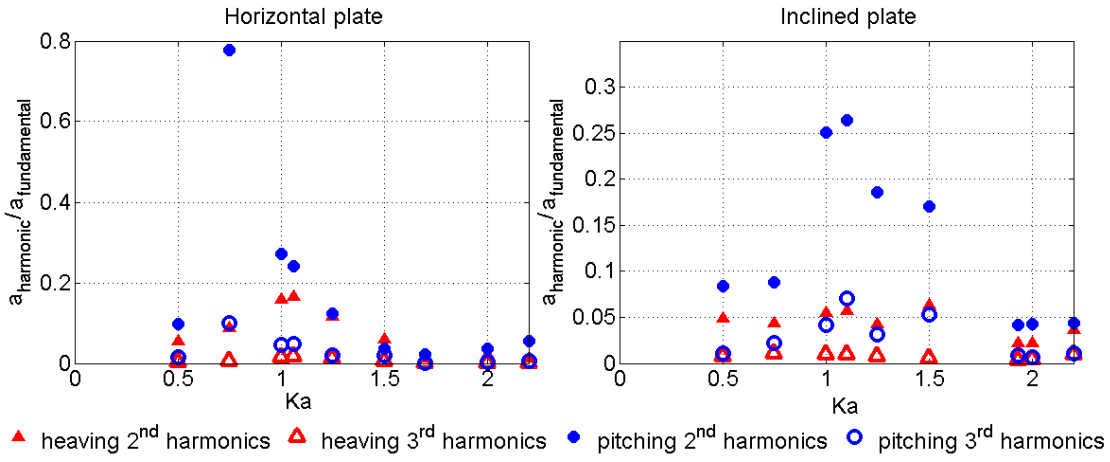

(a) h/L=1/4.

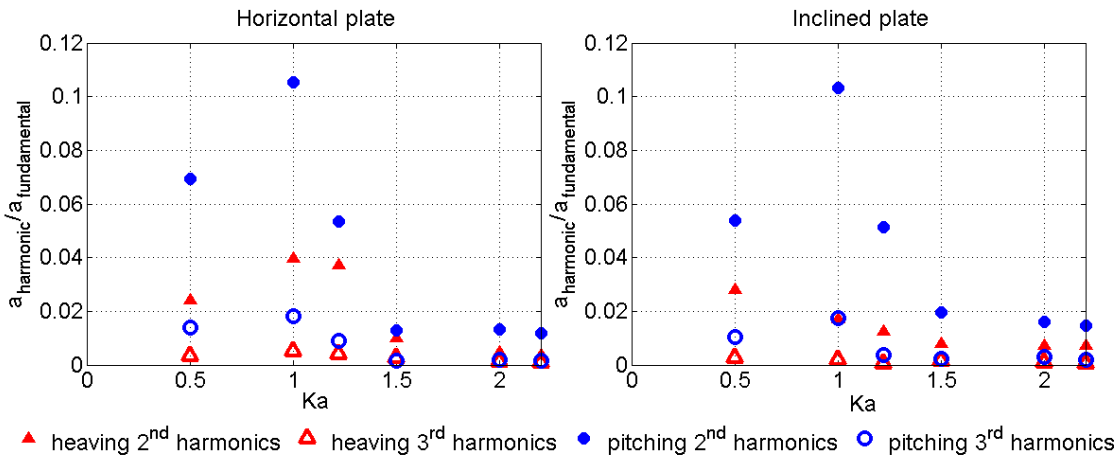

(b) h/L=1/2.

Figure 6.34. Higher harmonics of radiated wave towards transmission side for d/h=1/3.

and plate motion has no influence on the magnitude of the generated higher harmonics in the radiated wave which implies that the numerical treatment of the plate motion is efficient.

In intermediate water, maximum ratios $a_{2^{nd}}/a_{fundamental}$ of 71% for heaving motion and 110% for pitching motion are present in the diffracted wave, 17% and 88% respectively in the radiated wave. The maximum ratio $a_{3^{rd}}/a_{fundamental}$ in the diffracted wave is 33% for heaving and 28% for pitching and in the radiated wave 3% for heaving

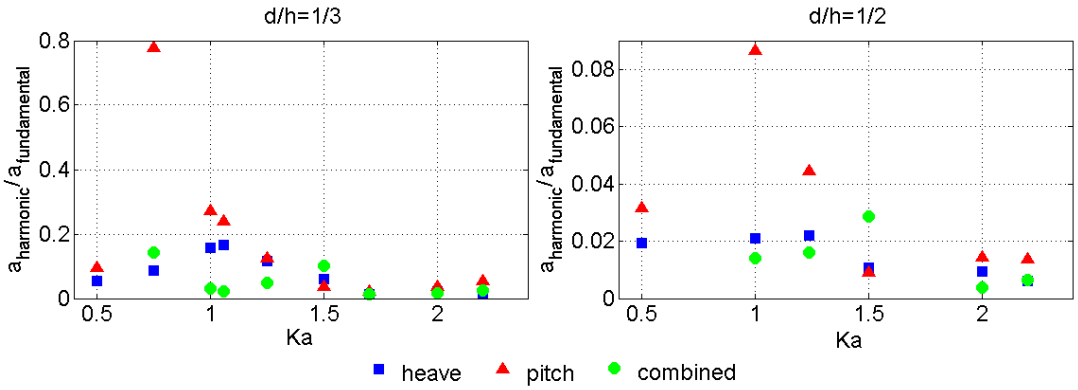

Figure 6.35. Influence of motion type on second harmonics in radiated wave for horizontal plate and h/L=1/4.

and 10% for pitching.

In deep water, maximum ratios $a_{2^{nd}}/a_{fundamental}$ of 29% for heaving motion and 46% for pitching motion are present in the diffracted wave, 4% and 11% respectively in the radiated wave. The maximum ratio $a_{3^{rd}}/a_{fundamental}$ in the diffracted wave is 5% for heaving and 6% for pitching and in the radiated wave 1% for heaving and 2% for pitching.

Analysis showed that through the numerical procedure already in the stationary plate configurations second harmonics of maximum 0.64% and third harmonics of maximum 0.36% are present in the diffracted wave; it is assumed that the ramp-up of the plate presence is responsible for the generation of higher harmonics.

7. DISCUSSION AND ERROR EVALUATION

The arrangement of this chapter follows the arrangement of the result presentation; first the yielded transmission coefficients are evaluated, then the changes in the relative energy flux are analysed, this is followed by a discussion of the influences of motion parameters on the radiated wave and examination of the effect of plate motion on the behaviour of the diffracted wave. Thereafter the generation of higher harmonics and their influence on the research results are discussed and finally error evaluation is conducted.

7.1. Transmission Coefficient

For a stationary plate only the amplitude of the diffracted wave determines the reflection coefficient and the amplitude of the diffracted wave and the phase angle between diffracted and incidence wave determine the magnitude of the transmission coefficient; amplitude and phase angle depend on plate parameters (Ka, d/h and inclination) and cannot be manipulated after plate installation.

For a moving plate, two additional parameters are introduced through the motion: the amplitude of the radiated wave and the phase angle between radiated and scattered wave. Both can be manipulated when prescribing forced plate motion; in order to yield minimum transmission, the radiated wave towards transmission side has to be tuned to be 180° out-of-phase with the scattered wave; increasing the motion amplitude will result in a bigger amplitude of the radiated wave so that the transmitted wave height is further reduced.

The phase angle tuning is crucial for achieving wave attenuation: if radiated wave and scattered wave towards transmission side are in-phase, then the height of the transmitted wave will be the sum of both wave heights (constructive interference) and waves with heights bigger than the incidence wave will move shorewards. The highest transmission coefficient yielded in this study was 1.41 for an inclined pitching plate

with ($h/L = 1/4$), $d/h = 1/3$ and $Ka = 2.2$ when the plate motion is $\theta_{motion} = \pi/2$ behind the incident wave. Instead of an attenuated wave, a wave with almost 1.5 times the wave height of the incident wave would be transmitted. To avoid this problem, continuous monitoring of the period of the incident wave and control of plate motion and position are required.

In this thesis destructive interference between radiated and scattered wave towards transmission side has been attempted through rough visual estimation only; the achieved results may not necessarily be the minimum possible transmission coefficients but are a good indication of the potential wave attenuation through introduction of plate motion.

Due to the requirements of linear wave theory, the freeboard of the plate had to be kept big enough and the plate motion small to allow for sufficient submergence during all motion cycles and avoid violation of the necessary conditions for applicability of linear approximation of body-nonlinear wave problem (see Section 2.4.2).

Consequently, the smallest transmission coefficients for a stationary plate achieved in deep ($h/L = 1/2$) and intermediate ($h/L = 1/4$) water are a disappointing 0.97 and 0.7 respectively for a plate submergence of $d/h = 1/3$ and are almost consistently 1 in deep water with a plate submergence of $d/h = 1/2$.

Through introduction of plate motion these values can be considerably improved as shown in Figures 6.1 - 6.4. Pitching motion yields smallest transmission coefficients for $Ka \geq 2.0$; they can reach 0.74 and 0.83 in deep water for $d/h = 1/3$ and $d/h = 1/2$ respectively and 0.58 and 0.62 respectively in intermediate water.

Heaving motion yields appreciable wave attenuation in deep water with $Ka \geq 1.5$; the minimum transmission coefficient is 0.86 and 0.9 for $d/h = 1/3$ and $d/h = 1/2$ respectively. In intermediate water, minimum transmission coefficients are yielded when $1.0 \leq Ka \leq 1.5$; values of 0.71 and 0.79 are possible for the inclined plate setup with $d/h = 1/3$ and $d/h = 1/2$ respectively. As a reminder, pitching and heaving

amplitude are related through equal water displacement for equal Ka as explained in Section 5.1.

In Tables 7.1 to 7.4 overviews of the configurations that yield the smallest achievable transmission coefficient in dependence on Ka, h/L and d/h are given. Figure 7.1 displays the best-performance graphs of the SFP for $0.5 \leq Ka \leq 2.2$ in dependence on relative water depth and relative plate submergence.

From Figure 7.1 can be seen that for $h/L = 1/4$ with a relative plate submergence of $d/h = 1/3$, transmission coefficients $k_T \leq 0.75$ can be achieved for a wave frequency bandwidth $1.0 \leq Ka \leq 2.2$; transmission coefficients $k_T \leq 0.6$ can be achieved for a wave frequency bandwidth $1.75 \leq Ka \leq 2.2$; this is clearly a wider bandwidth of good wave attenuation performance than achievable with a stationary plate displayed in Figure 5.4. The performance curve of the SFP with deeper submergence follows this trend and especially the values of k_T for $Ka \geq 2$ are almost as good as the ones for the smaller submergence. In deep water, the performance of the SFP deteriorates due to the big actual submergence depths of the plate which can be seen in Table 7.7.

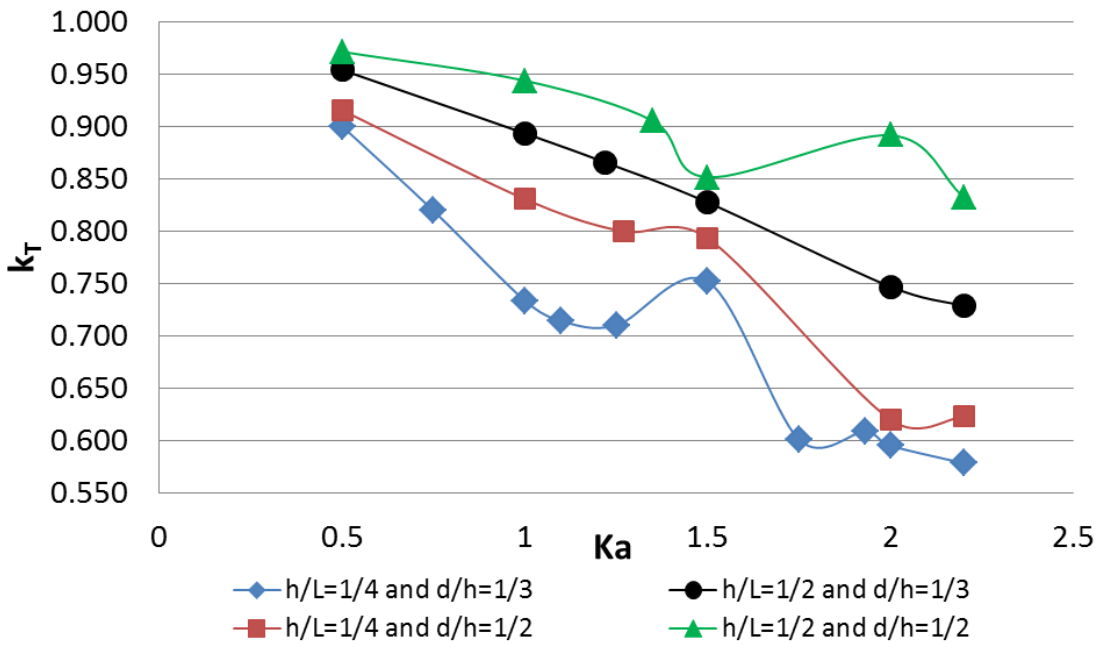

Figure 7.1. Minimum transmission coefficients for optimised plate configurations.

Table 7.1. Optimum wave attenuation configurations of SFP for h/L=1/4 and d/h=1/3.

optimum wave attenuation		Ka									
		0.5	0.75	1	1.1	1.25	1.5	1.75	1.93	2	2.2
d/h=1/3	minimum k_T	0.900	0.819	0.734	0.714	0.710	0.752	0.601	0.609	0.595	0.578
	motion type	heave	heave	heave	heave	heave	heave	pitch	pitch	pitch	pitch
	inclination	inclined	inclined	inclined	inclined	inclined	inclined	horizontal	inclined	inclined	inclined

Table 7.2. Optimum wave attenuation configurations of SFP for h/L=1/4 and d/h=1/2.

optimum wave attenuation		Ka					
		0.5	1	1.27	1.5	2	2.2
d/h=1/2	minimum k_T	0.916	0.831	0.800	0.793	0.620	0.623
	motion type	heave	heave	heave	heave	pitch	pitch
	inclination	inclined	inclined	inclined	inclined	horizontal	inclined

Table 7.3. Optimum wave attenuation configurations of SFP for h/L=1/2 and d/h=1/3.

optimum wave attenuation		Ka					
		0.5	1	1.22	1.5	2	2.2
d/h=1/3	minimum k_T	0.954	0.894	0.866	0.828	0.747	0.729
	motion type	heave	heave	heave	pitch	pitch	pitch
	inclination	inclined	inclined	inclined	horizontal	horizontal	inclined

Table 7.4. Optimum wave attenuation configurations of SFP for h/L=1/2 and d/h=1/2.

optimum wave attenuation		Ka					
		0.5	1	1.35	1.5	2	2.2
d/h=1/2	minimum k_T	0.972	0.944	0.905	0.852	0.892	0.833
	motion type	heave	heave	pitch	pitch	heave	pitch
	inclination	inclined	inclined	horizontal	horizontal	inclined	horizontal

In order to operate the moving plate successfully, the relative plate width Ka should be kept over 1.0. As the actual plate width cannot be changed after the installation, it is important to determine the design width correctly. In dependence on the predominant wave period(s), it should be aimed for covering it (them) in the range of $1.75 \leq Ka \leq 2.2$; this will ensure the best wave attenuation with pitching motion for these prevailing wave periods and also allows for still appreciable wave attenuation with heaving or pitching up to $Ka > 1.0$ which in the case of fixed plate width means waves with bigger wave periods.

Table 7.5 displays plate widths in dependence on the wave period for various values of Ka. Wave periods up to $6.5s$ represent the conditions where FBW and SFP application is feasible from an engineering point of view. Actual plate widths of 20-25m cover Ka values up to 1.0, 1.5, 1.75, 2, 2.2 and more than 2.2 for wave periods of 6.5, 6, 5.5, 5, 4.5 and 4 seconds respectively. Additionally, in Tables 7.6 and 7.7 the values for water depth h, wavelength L and plate submergence depth d covered by the developed numerical model assuming the above stated wave periods up to $6.5s$ are summarised.

Table 7.5. Width of SFP in metres in dependence on design wave period.

Ka	T [s]								
	1	2	3	4	4.5	5	5.5	6	6.5
0.5	0.248	0.994	2.236	3.976	5.032	6.212	7.517	8.946	10.499
0.75	0.373	1.491	3.355	5.964	7.548	9.318	11.275	13.418	15.748
1.0	0.497	1.988	4.473	7.952	10.064	12.425	15.034	17.891	20.997
1.5	0.745	2.982	6.709	11.928	15.096	18.637	22.550	26.837	31.496
1.75	0.870	3.479	7.827	13.915	17.612	21.743	26.309	31.310	36.745
2	0.994	3.976	8.946	15.903	20.128	24.849	30.067	35.783	41.995
2.2	1.093	4.373	9.840	17.494	22.140	27.334	33.074	39.361	46.194

Table 7.6. Covered water depths, wavelengths and plate submergence depths for intermediate water ($h/L = 1/4$).

relative water depth h/L=1/4		wave period T [s]								
		1	2	3	4	4.5	5	5.5	6	6.5
wavelength L [m]		1.43	5.73	12.89	22.91	29.00	35.79	43.31	51.55	60.50
water depth h [m]		0.36	1.43	3.23	5.73	7.25	8.95	10.83	12.89	15.13
plate submer-	$\frac{d}{h} = \frac{1}{3}$	0.12	0.48	1.08	1.91	2.42	2.98	3.61	4.30	5.04
gence d [m] for	$\frac{d}{h} = \frac{1}{4}$	0.18	0.72	1.61	2.86	3.62	4.47	5.41	6.44	7.56

Table 7.7. Covered water depths, wavelengths and plate submergence depths for deep water ($h/L = 1/2$).

relative water depth h/L=1/2		wave period T [s]								
		1	2	3	4	4.5	5	5.5	6	6.5
wavelength L [m]		1.56	6.22	14.00	24.89	31.50	38.89	47.05	56.00	65.72
water depth h [m]		0.78	3.11	7.00	12.44	15.75	19.44	23.53	28.00	32.86
plate submer-	$\frac{d}{h} = \frac{1}{3}$	0.26	1.04	2.33	4.15	5.25	6.48	7.84	9.33	10.95
gence d [m] for	$\frac{d}{h} = \frac{1}{4}$	0.39	1.56	3.50	6.22	7.88	9.72	11.76	14.00	16.43

For a fixed plate width, waves of smaller wave periods will lead to bigger Ka values; in this thesis, the results up to $Ka = 2.2$ indicate that for pitching motion the wave attenuation increases or remains at a high level up to this relative plate width. Further research is required to study the behaviour of a moving SFP for $Ka > 2.2$ so that the wave attenuation for waves with smaller wave periods than the design wave can be predicted. If a considerable part of the wave energy is transported with wave periods smaller than the design wave period, the design width should be determined with $Ka = 0.75$ to allow for good wave attenuation for the smaller wave periods.

If the local wave climate shows two wave energy density peaks for two different wave periods, the installation of two SFP wave attenuators with differing design wave periods could be a feasible solution; the seaward plate would attenuate the wave with the bigger wave period and the shoreward plate would be tuned to the smaller design wave period.

This, of course, would lead to interaction between the two submerged flat plates because the shoreward plate would radiate waves towards the seaward plate; this can generate undesirable wave patterns (partial standing wave) and deteriorate the wave attenuation performance of the seaward plate. In order to avoid this, the shoreward plate could work with combined heaving and pitching and be tuned to zero radiation towards the seaside as explained in Section 6.9.

Even though combined heaving and pitching does not yield the best possible wave attenuation when only a single wave period is present, performance might be advantageous when an incidence wave consisting of a number of wave periods (as it will be in reality) has to be attenuated. Due to the fact that heaving and pitching show the best performance for different Ka values, combined motion might attenuate an incidence wave superposed of different wave periods better than pure pitching or pure heaving because the included heave motion would attenuate the wave with bigger T better and the included pitch the wave with the smaller T simultaneously.

Additionally with regard to a wave-driven SFP, allowing for combined motion widens the periods of forced motion through the incidence wave because the pure pitching and pure heaving condition are mutually exclusive (see Figure 2.4); therefore combined plate motion might decrease the transmission coefficient for a wave-driven SFP and/or increase energy harvesting potential.

As the wave attenuation of a moving plate is in general better in intermediate water than in deep water (see Figure 6.5), installation of the SFP should be in the smallest feasible water depth. As can be seen from Tables 7.6 and 7.7, especially for wave periods $T > 4s$ relative water depths $h/L < 1/4$ are feasible as the real water depths allows for plate installation.

Smaller plate submergence results generally in smaller transmission coefficients; this is due to an increased diffracted wave and/or a bigger radiated wave; exceptions are discussed separately in Sections 7.3 and 7.4.

It can be expected that reducing the plate submergence further without allowing for surface piercing will improve wave attenuation; several experimental, analytical and numerical studies underpin this relation for a stationary plate (Patarapanich and Cheong, 1989; Cheong and Patarapanich, 1992; Neelamani and Reddy, 1992; Parsons and Martin, 1992 and Porter, 2015b). Yip (1997) investigated analytically the influence of plate submergence on the transmission coefficient of a pitching plate and stated that the maximum amplitude of the radiated wave is achieved with a relative plate submergence $d/h = 0.175$. Patarapanich and Cheong (1989) and Neelamani and Reddy (1992) observed that for a stationary plate the transmission coefficient was minimum when $d/h = 0.05 - 0.15$ (regular and random waves) due to induced wave breaking.

The smallest submergence in this thesis is $d/h = 1/3$; from the real plate submergence depths displayed in Tables 7.6 and 7.7 can be concluded that in deep water ($h/L = 1/2$ for $T > 3s$ and in intermediate water $h/L = 1/4$ for $T \geq 4s$ smaller submergence depths than tested are possible without surface piercing of the moving plate, and thereby diffracted and radiated wave heights will increase. This will result

in smaller transmission coefficients.

In addition, modelling with linear wave theory yields conservative results; in reality, the transmission coefficient will be lower because turbulences and wave breaking will convert mechanical energy to thermal energy and therefore decrease the wave height of the transmitted wave.

In order to restrict the number of test runs, only horizontal plate and plate inclined by 5° (see Figure 2.5) configurations have been tested. The heaving inclined plate yields smaller transmission coefficients than the horizontal plate for most of the configurations. This is mainly due to the increased wave radiated towards transmission side and will be discussed in Section 7.3 For pitching, in general, the horizontal plate setup results in smaller k_T.

More inclinations have to be tested in order to reliably predict how the plate inclination affects the transmission coefficient; but from experimental results from Murakami *et al.* (1994) and Rao *et al.* (2009) and analytical data provided by Parsons and Martin (1992) and Porter (2015) it can be deduced that by increasing the plate inclination, wave attenuation is improved.

Increasing the motion amplitude results in an increased radiated wave; provided that the radiated wave and the wave scattered towards the transmission side are 180° out-of-phase, the increased motion amplitude will result in a lower transmission coefficient.

Decreasing the plate submergence restricts the motion amplitude of the plate in order to avoid surface piercing. Here an optimisation is required: the improvement in wave attenuation due to smaller submergence depths versus decrease in wave attenuation owing to motion amplitude restriction.

7.2. Energy Flux

In this thesis plate motion is modelled with prescribed forcing; through this method, energy is either put into the system or taken out of it. As described in Section 6.8, whether energy loss or gain of the system is present only depends on the phase angle between plate motion and incidence wave.

For all the test runs done here, the plate forcing that yields minimum transmission coefficients is also the configuration that results in energy loss of the system. This can be explained as follows: With introducing motion, waves are radiated towards the incidence and towards the transmission side. The phase angle between the radiated wave towards incidence side and transmission side depends on the motion type: heave is a symmetric motion, the phase angle between wave radiated towards transmission and towards is zero; pitch is an antisymmetric motion, the phase angle between wave radiated towards transmission and towards incidence side is π.

The sum of radiated wave and diffracted wave towards incidence side defines the complex reflection coefficient. Phase angle and wave amplitude of diffracted wave are functions of h/L, d/h, Ka and β_0 only. Phase angle and wave amplitude of radiated wave affect the change in k_R: if the radiated wave and diffracted wave are in phase, k_R increases; if radiated wave and diffracted wave are 180° out-of-phase, k_R decreases (under the assumption that $2a_{radiated} < a_{diffracted}$ towards incidence side). If radiated wave and diffracted wave are 180° out-of-phase and $a_{radiated} = a_{diffracted}$, k_R will be zero.

The sum of radiated wave and scattered wave towards transmission side determines the complex transmission coefficient. Phase angle and wave amplitude of radiated wave have an influence on the change in k_T: if the radiated wave and scattered wave are in phase, k_T increases; if radiated wave and scattered wave are 180° out-of-phase, k_T will be minimum.

As obtaining minimum transmission was the aim of this research, out-of-phase tuning on the transmission side was applied and it was achieved that the transmission coefficient of a moving plate is smaller than that of a statinary plate. The phase angle between radiated wave and diffracted wave towards incidence side was then automatically defined through the transmission side tuning and only depended on the motion type applied but the likelihood to be in-phase is very small and it was never the case in the test runs conducted here. This results in a bigger decrease in transmitted wave height (because intentionally induced) than increase in reflected wave height and therefore results in an energy loss.

When combining heaving and pitching motion, the phase angle between radiated wave and diffracted wave towards incidence side, that was not manipulable for pure heaving and pure pitching, can be influenced by changing the ratio of heave and pitch amplitude of the plate motion. This will of course not only change the sum of radiated wave and diffracted wave towards incidence side but also the sum of radiated wave and scattered wave towards transmission side and although not yielding the smallest k_T, can result in maximum energy loss for the system as can be seen in Figure 6.16 for $Ka = 1.06$ and 1.7 for a horizontal plate and for $Ka = 1.5$ and 1.93 for an inclined plate.

The energy losses in intermediate water are - except for a small number of setups - bigger than in deep water; exceptions are due to either an increased radiated wave for deeper submergence (see first two lines in Table 7.8 - this will be discussed in Section 7.3) or due to changes in k_R which are caused by different wave angles between radiated wave and diffracted wave towards incidence side (all other entries in Table 7.8).

The influence of plate submergence, plate width and inclination on the relative energy flux is very complex due to the fact that varying the structural parameters d/h, Ka and β_0 (and aiming for minimum transmission coefficient for each setup) always changes the phase shift and the magnitude of the radiated wave towards incidence side as well. As in this thesis the transmission coefficient minimisation and not energy

Table 7.8. Configurations with more energy loss in deep water for d/h=1/3.

motion	incli-nation	h/L	Ka	Stationary Plate			Moving Plate		
				k_T	k_R	$k_T^2+k_R^2$	k_T	k_R	$k_T^2+k_R^2$
pitch	0°	1/2	1.5	0.977	0.212	1.000	0.828	0.238	0.861
		1/4	1.5	0.965	0.263	1.000	0.898	0.360	0.968
pitch	5°	1/2	1.5	0.983	0.183	1.000	0.845	0.085	0.849
		1/4	1.5	0.943	0.333	1.000	0.869	0.308	0.922
heave	5°	1/2	1.5	0.983	0.183	1.000	0.838	0.270	0.881
		1/4	1.5	0.943	0.333	1.000	0.752	0.467	0.885
pitch	0°	1/2	1.22	0.969	0.247	1.000	0.898	0.250	0.933
		1/4	1.25	0.851	0.526	1.000	0.802	0.521	0.957
pitch	5°	1/2	1.22	0.978	0.208	1.000	0.924	0.155	0.937
		1/4	1.25	0.889	0.458	1.000	0.857	0.413	0.951

loss maximisation was the foremost aim, the changes on the incidence side were only secondary and no consistent rule regarding the influence of d/h, Ka and β_0 could be found.

Increasing the motion amplitude while the phase angles between motion and incidence wave are optimised to yield minimum transmission, will decrease the transmission coefficient and increase the energy loss of the system. Experimental tests are required to show what motion amplitudes are feasible; modelling with forced plate motion will not show where the limitations are as added mass and radiation damping of the SFP are not incorporated and considered.

The most important outcome with regard to the relative energy flux of the system is, that by tuning the motion of the SFP to minimise the transmission coefficient, the system loses energy. This energy can be extracted and used to power the required structural adaptations and to control the plate motion to ensure out-of-phase tuning

for minimum wave transmission.

The maximum energy loss in intermediate water ($h/L = 1/4$) is 27.6% for the horizontal plate with $d/h = 1/3$, $Ka = 1.7$ and pitch motion. In deep water (for $h/L = 1/2$) the maximum energy loss is 22.1% for the inclined plate with $d/h = 1/3$, $Ka = 2.2$ and pitch motion.

Applying the following equations to determine the *total energy* per unit crest width per wave (see McCormick (1981) and Dean and Dalrymple (1991))

$$E_L = \frac{\rho g H^2}{8} L \tag{7.1}$$

and the *energy flux* or more commonly used *wave power* per unit crest width

$$P_L = \frac{\rho g H^2}{8} c_g \quad \text{with} \quad c_g = \frac{c}{2}\left\{1 + \frac{2kh}{\sinh 2kh}\right\} \tag{7.2}$$

and assuming a wave height of $H = 1m$ for a $4s$ wave, yields $E_L = 31.43kJ$ and $P_L = 4.02kW$ in deep and $E_L = 28.94kJ$ and $P_L = 4.60kW$ in intermediate water per unit crest width.

Therefore with a pitching SFP a maximum of 0.89 kJ wave energy can be extracted per second and crest width in deep water with $H = 1m$ and $T = 4s$ while decreasing the wave height on the transmission side to 0.73m; in intermediate water a maximum of 1.27 kJ wave energy can be extracted per second and crest width while decreasing the wave height on the transmission side to 0.6m.

This clearly shows that an installation in intermediate water is advantageous from energy harvesting and wave attenuation perspective.

7.3. Radiated Wave

The magnitude of the radiated wave in intermediate water ($h/L = 1/4$) is for most of the configurations bigger than in deep water ($h/L = 1/2$); this is mainly due to the fact that the actual submergence depth of the plate is bigger in deep water than in intermediate water. Additional tests are necessary to eliminate this influence and investigate the pure influence of the water depth. But it is not expected that the water depth has a major effect on the wave height of the radiated wave which is supported by the research of Evans and Porter (1996).

The amplitude of the radiated wave increases when reducing the submergence depth; the deeper a plate is submerged the smaller are the heights of the surface waves generated by its motion. As explained in APPENDIX A, in the equation of motion the transport of kinetic energy towards infinity in the form of surface waves is implemented via radiation damping coefficients; these damping coefficients decrease with increasing submergence depth as a study by Rahman (2001) for a heaving (surging) submerged sphere shows.

The same study also shows that the radiation damping coefficients for heave motion increase up to $Ka = 1.0$ (here a being the radius of the sphere) and then decrease for higher Ka values. Results yielded in the present thesis indicate a similar behaviour for a submerged heaving plate: the inclined submerged plate shows a maximum radiated wave for $1.5 \leq Ka \leq 2.0$ for all tested submergence and water depths whereas the horizontal plate configuration displays two maxima in radiated wave heights in the tested relative plate width range $0.5 \leq Ka \leq 2.2$.

The pitching motion exhibits a different behaviour: for the tested relative plate width range, the wave height of the radiated wave increases with Ka. Comparing these data with the studies of Yip (1997) and Yip and Chwang (1997) proved to be difficult as the authors displayed the transmission coefficients yielded with constant phase angle between pitching motion and incidence wave only (Figure 8 in Yip and Chwang (1997)) whereas in this thesis the phase angle differs to yield minimum transmission.

For the setup $h/L = 1/4$, $d/h = 1/3$ and $\beta_0 = 5°$ data for three Ka values were available for $\theta_{pitch} = 0$ to compare with data from Yip and Chwang (1997) for $h/L = 1/4$, $d/h = 0.3$ and horizontal plate with the complex pitching parameter $P_g = 0.5$. These data are displayed in Table 7.9; data from Yip and Chwang (1997) Figure 8 are digitised. Although the absolute values are not comparable, the present transmission coefficient data k_T for $\theta_{pitch} = 0$ agree with the declining trend of the data from Yip and Chwang (1997) despite increasing amplitudes of radiated wave.

Table 7.9. Transmission coefficient comparison with Yip and Chwang (1997) for h/L=1/4 and d/h=1/3.

Ka	Data (present thesis)			Yip and Chwang (1997)
	$a_{radiated}/\ a_{motion}$	k_T for optimised θ_{pitch}	k_T for $\theta_{pitch} = 0°$	k_T for $\theta_{pitch} = 0°$
1.5	0.116	0.862	1.019	1.18
2.0	0.382	0.595	0.999	1.05
2.2	0.401	0.578	0.977	0.96

Results displayed in Table 7.9 again underpin the importance of plate motion tuning because the radiated wave towards the transmission side needs to be 180° out-of-phase with the scattered wave to ensure wave attenuation.

The influence of inclination is distinctive for the heaving motion; for all presently tested configurations the inclined plate generates radiated waves with higher amplitudes towards transmission side than the horizontal plate. When comparing the radiated waves towards transmission and incidence side, another influencing factor emerges: the relative plate width Ka, as can be seen in Figure 7.2.

For $0.5 \leq Ka \leq 1.5$ the radiated wave towards the transmission side has a bigger amplitude than the one radiated towards the incidence side; for $Ka > 1.5$ this reverses, implying that for $Ka > 1.5$ an inclined plate with $\beta_0 = -5°$ would generate a radiated wave towards transmission with a bigger wave amplitude and therefore decrease the

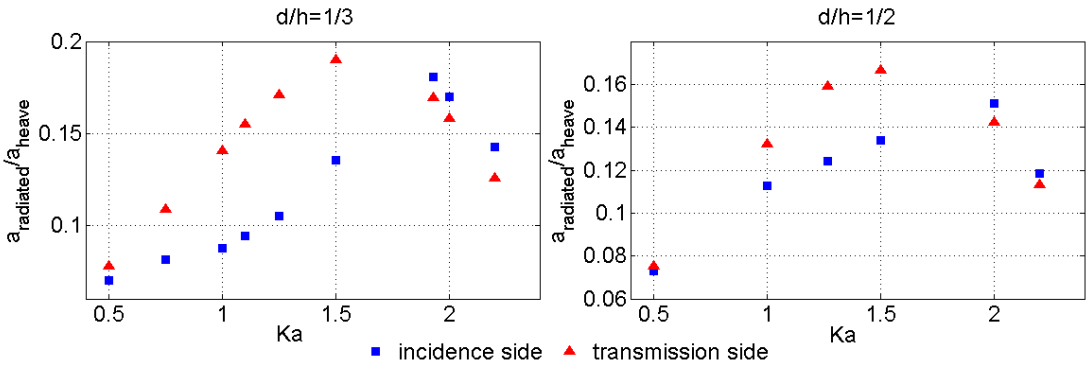

Figure 7.2. Comparison of radiated wave towards transmission and incidence side for h/L=1/4 inclined heaving plate.

transmission coefficient even further.

For pitching motion the effect of an inclination of $\beta_0 = 5°$ is not that prominent and varies with Ka as can be seen in Figure 6.21. The differences in the amplitudes of the radiated wave towards transmission and incidence side are not as pronounced as for the heaving motion but an inclination of $\beta_0 = -5°$ would generate bigger radiated waves towards transmission for a pitching plate with $1 > Ka \leq 1.5$ in intermediate water as can be seen in Figure 7.3.

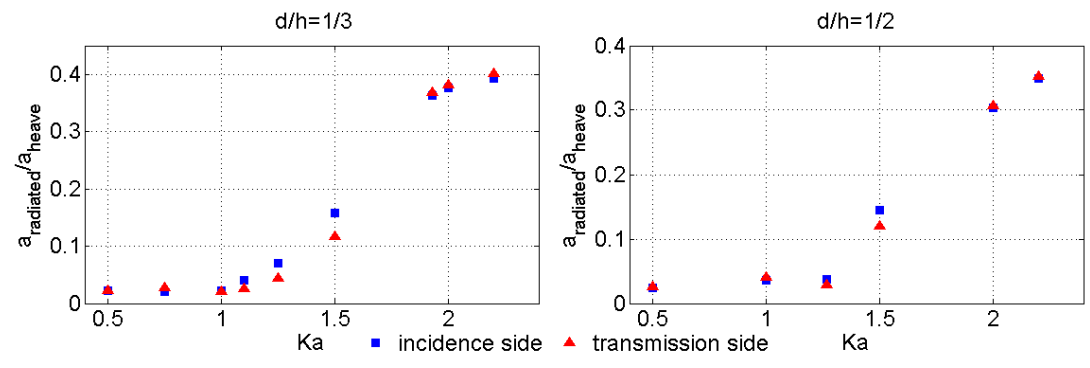

Figure 7.3. Comparison of radiated wave towards transmission and incidence side for h/L=1/4 inclined pitching plate.

The reasons for the behaviour differences between heaving and pitching motion lie in the working mechanism. The two major differences in the working mechanism are that firstly in heaving motion every fluid particle along a surface of the plate has the same magnitude in velocity and experiences the same acceleration whereas the magnitudes of velocity and acceleration of a fluid particle on the surface of a pitching plate are zero on the pitching axis and increase with distance from the axis; additionally, the direction of fluid particle velocity and acceleration on the surface of a pitching plate is different either side of the pitching axis while there is no change in velocity and acceleration direction along the surface of a heaving plate.

The changes in the radiated wave along the relative plate width are contributed by another influence. Evans and Porter (1996), Rahman (2001), Evans and Porter (2007) and Porter (2015) established that the radiation damping coefficients of a system can become zero for a particular oscillation frequency - which results in wave-free oscillations - and reach a maximum when resonance occurs (see APPENDIX A for more information). Although in the present test runs no wave-free oscillations or resonance setups were found, jumps in the amplitude of the radiated wave along the Ka axis (see Figures 6.19(a) - 6.21) can be explained by approaching or skipping these frequencies.

Although Porter (2015) only presents damping coefficients for one particular relative plate submergence, it is assumed that plate submergence also influences the resonance frequency of the system; this could be the reason why in a number of setups the motion of a plate with deeper submergence yielded radiated waves with higher amplitude (see Section 7.2 and Table 7.8).

Combining heaving and pitching motion allows for manipulation of the radiated wave because heaving generates a symmetric and pitching an antisymmetric wave. By changing the phase angle between both motions and varying the amplitude ratio, the pitching axis can be shifted. This provides the possibility of directional pitching amplitude control and can be applied to avoid radiation towards the incidence side when two or more plates are installed as explained in Section 6.9.

All of the above-discussed parameters (h/L, d/h, β_0 and Ka) have an influence on the phase angle of radiated wave which is not important when discussing pure radiation but in the combined diffraction/radiation BVP it is important to consider this effect too, as the phase angle between plate motion and incidence wave has to be adjusted for tuning the motion to minimum transmission.

7.4. Influence of Plate Motion on Diffracted Wave

By varying the location of the plate surfaces in time, plate motion alters the diffracted wave through the generation of higher harmonics. Plate submergence, relative plate width, inclination, incidence wave height, motion type and motion amplitude affect the magnitude of the deviations from the diffracted wave of a stationary plate.

Smaller plate submergence and increased incidence wave height result in an increased generation of higher harmonics in the diffracted wave owing to the higher water particle velocities. Pitching motion generates a higher ratio of higher harmonics than heaving motion because for pitching motion the plate velocity and the plate submergence along a plate surface vary whereas plate velocity and plate submergence along the plate surface are constant at any particular time for heaving motion.

The relative plate width affects the ratio of generated higher harmonics; the maximum ratio $a_{2^{nd}}/a_{fundamental}$ for heaving motion can be found for $Ka \leq 1$ on the transmission side and for $Ka > 1.0$ on the incidence side. For pitching motion the highest percentage of harmonics for $0.75 \leq Ka \leq 1.7$ on the transmission side and for $Ka > 1.0$ on the incidence side. The influence of the plate inclination on the generation of higher harmonics depends on h/L, d/h and Ka but no general rule could be established.

The changes in the surface profiles of the diffracted wave are more pronounced in intermediate water test runs; it is assumed that this is primarily caused by the smaller actual plate submergence in intermediate water. In order to investigate the pure effect of water depth on the diffracted wave, additionally, test runs with fixed

plate submergence in different water depths are required.

Plate motion has no visible effect on the phase angle between diffracted and incidence wave. There is no evidence that the phase angle between plate motion and incidence wave has an influence on the magnitude of the generated higher harmonics in the diffracted wave.

It can be expected that increasing the plate motion amplitude further and allowing for higher incidence waves will intensify the nonlinearities in the diffracted wave. In order to predict the impact of increased nonlinearities in the diffracted wave on the transmission coefficient accurately, fully nonlinear modelling is required.

7.5. Higher Harmonics in Radiated Wave

Submergence depth, plate width and motion amplitude proved to be the parameters that have the biggest effect on the ratio of higher harmonics in the radiated wave as already expected from the derivation of the necessary conditions for applicability of linear approximation of body-nonlinear wave problem (Section 2.4.2).

Smaller plate submergence and increased incidence wave height increase the generation of higher harmonics in the radiated wave because of the higher water particle velocities. A bigger motion amplitude leads to higher plate velocities and accelerations which result in an increase in nonlinearities (see Section 2.4.2). Pitching motion generates more higher harmonics than heaving motion because the plate velocity and acceleration along a plate surface vary whereas plate velocity and acceleration everywhere on a heaving plate are constant at any particular time for heaving motion.

The influence of the inclination on the generation of higher harmonics depends on the relative plate width; for $Ka < 1.5$ the motion of the horizontal plate results in a higher ratio of second harmonics than the motion of the plate inclined by 5°, for bigger Ka this reverses. It can be expected that increasing the plate inclination leads to higher ratios of second and third harmonics due to the fact that through the

inclination the plate submergence of one edge of the plate decreases.

The highest ratios of second harmonics in the radiated wave have been found for $0.5 \leq K \leq 1.5$, this is primarily due to the small amplitude of the generated fundamental radiated wave in this region. The absolute values of radiated second harmonics are maximum 3mm throughout the tested configurations.

Higher harmonics ratios in the radiated wave are more pronounced in intermediate water test runs; this is primarily caused by the smaller actual plate submergence in intermediate water. In order to investigate the unbiased effect of water depth on the radiated wave, additionally, test runs with fixed plate submergence in different water depths are required.

The nonlinearities in the radiated wave will grow when further decreasing the plate submergence depth and/or increasing the plate motion amplitude and will eventually violate the linearity conditions so that superposition will become invalid. Then the body-nonlinear method is not applicable anymore and a fully nonlinear model has to be applied.

7.6. Error Evaluation

The here applied RBF collocation boundary-only model in conjunction with the novel 2wABC is able to accurately model wave propagation and interference boundary value problems. The maximum RMS errors when compared with the analytical solution were for the wave propagation over horizontal bottom setup 0.12% in η, 0.73% in Φ and 0.14% in $\frac{\partial \Phi}{\partial x}$ and 0.13% in $\frac{\partial \Phi}{\partial z}$ for Δt/T=0.00025 (see Table 4.1).

For the partial standing wave over horizontal bottom the maximum RMS errors were 0.02% in η_{max}, 0.42% in η_{min}, 0.07% in Φ, 4.13% in $\frac{\partial \Phi}{\partial x}$ and 3.64% $\frac{\partial \Phi}{\partial z}$ for Δt/T=0.0125 (see Table 4.2) and for a standing wave over horizontal bottom, the following maximum RMS error were detected: 0.02% in η_{max}, 0.68% in η_{min}, 0.1% in Φ, 4.85% in $\frac{\partial \Phi}{\partial x}$ and 4.28% $\frac{\partial \Phi}{\partial z}$ for Δt/T=0.0125 (see Table 4.3).

As the wave steepness in the actual wave-structure BVP was smaller than in the error test runs (H/L=0.02 in deep water and H/L=0.01 in intermediate water), the RMS errors due to the numerical setup in the water wave/structure BVP are expected to be smaller.

Through the application of the body-nonlinear method, higher harmonics are introduced. By Fourier transform, second and third harmonics could be detected in the diffracted as well as in the radiated wave. For all deep water test runs, the amplitude of the present third harmonics (in radiated and diffracted wave) was below 1mm. In intermediated water, the amplitude of the present third harmonics in the radiated wave was maximum 1mm; the maximum amplitude of the third harmonics present in the diffracted wave was 3mm with one exception for the configuration pitching plate with $h/L = 1/4$, $d/h = 1/3$ and $Ka = 1.5$ where its amplitude was 9mm for the inclined plate case and 5mm for the horizontal plate case.

On the basis of these data the evaluation of the performance of the 2wABC in the presence of higher harmonics was limited to the presence of second harmonics only as described in Section 4.4.5 The numerical error introduced through the presence of second harmonics is expected to be below 0.6% in η, 0.9% in Φ and 2.5% in u and w for the majority of test runs as shown in Table 4.4.

Besides the presence of higher harmonics, two other error sources have to be evaluated. Firstly, currently the plate RBF centre distances are determined using analytical data from Porter (2002) and Porter (2015) for diffraction from a stationary plate as explained in Section 5.2 The RBF centre distance from the plate collocation points depends on h/L, d/h, Ka and plate inclination β_0 (see Section 5.2.1 and Figure 5.3).

By introducing plate motion, the relative submergence depth d/h changes continuously for heave motion and the plate inclination β varies continuously for pitch motion. This requires adjustment of the plate RBF centre distances in dependence on the instantaneous plate position. In order to determine the corresponding RBF

centre distances, analytical data for all spanned submergence depths and inclination angles are required. Getting and implementing these data would be an immense and disproportional effort.

A crude estimation of the error in the diffracted wave amplitude that might be introduced by the unchanged plate RBF centre distances for heaving motion has been attempted: The biggest error can be expected in intermediate water due to bigger differences in the RBF centre distance for smaller submergence depth change (see Figure 5.3) and bigger changes in k_T with changing Ka. There the submergence difference between $d/h = 1.3$ and $d/h = 1.2$ is approximately 1m and the maximum change in plate RBF centre distances between these two submergence depths is 0.2m for $Ka = 2.0$. As the heave amplitude is only 0.125m and assuming a linear relation between change in submergence depth and plate RBF centre distance, the RBF centre distance will deviate from its calibration value by less than 0.03m. The deviation from the correct reflection coefficient k_R will then be below 0.03 (see Figure 5.8).

The same crude error estimation for pitching is more difficult because the pitching amplitude changes with Ka to guarantee equal water volume displacement when compared with heave motion. The biggest change in plate RBF centre distance between horizontal plate and plate inclined by 5° is at $Ka = 1.5$ with 0.25m; the maximum pitching amplitude for $Ka = 1.5$ is 2.4°, that gives a deviation from the calibrated plate RBF centre distance of 0.12m (assuming linear dependency between change in plate inclination and plate RBF centre distance) which can lead to a difference in k_R of 0.1 (see Figure 5.8).

But as the plate motion is a periodic up-and-down motion, it might also be possible that the introduced errors (if present) counterbalance over a full plate motion cycle.

When comparing the diffracted waves of stationary and moving plates, for all configurations with small ratios of higher harmonics (¡ 5%), the existent deviations are negligibly small (see diffracted wave towards incidence side in Figure 6.28). If the plate

velocity had been introduced on the plate equilibrium position, the diffracted wave of the moving plate would automatically coincide with the diffracted wave of stationary plate. This is seen as an indication that the error introduced through unchanged RBF distances on a moving plate are negligibly small.

Secondly, the plate RBF distance determined through calibration with analytical data for a stationary plate is utilised for the radiation BVP. Although result trends yielded with this configuration appear to agree with experimental and theoretical findings established by other researchers (e.g. influence of h/L, d/h, Ka, plate inclination, motion amplitude and phase), it is not clear whether the relation between plate motion amplitude and amplitude of the radiated wave is modelled correctly. This can only be checked experimentally; if agreement is not satisfactory, model calibration for the radiation problem is required.

8. SUMMARY, CONCLUSIONS AND FUTURE WORK

In this thesis, active wave attenuation through introduction and control of forced heaving and pitching motion of a submerged flat plate has been investigated. For wave periods up to $6.5s$ - which represent the conditions where the application of an submerged flat plate is feasible from an engineering perspective - the here executed numerical test runs cover water depths from $0.4m - 32.9m$, wavelengths from $1.4m - 65.7m$, and plate submergence depths from $0.1m - 16m$. In intermediate water, the utilized deep-water wave height is $H_0 = 0.25m$; in the deep-water test runs a deep-water wave height of $H_0 = 0.5m$, and for the double-motion-amplitude test runs $H_0 = 1.0m$ is used. Motion amplitudes of $a_{motion} = 0.125m, 0.25m, 0.5m$ have been applied for test runs in intermediate, deep water and deep water with double motion amplitude respectively.

In this section the main research results are summarised, conclusions that can be drawn from the findings are presented and areas for future work suggested.

8.1. Summary and Conclusions

(i) Development of RBF collocation model to numerically solve the wave/structure BVP for a moving submerged flat plate:

In this thesis an RBF collocation model was developed to numerically solve the wave/structure BVP for a submerged horizontal and inclined, heaving and pitching flat plate. By using the fundamental solution of the Laplace equation as radial basis function, the BVP could be solved as boundary-only model so that computation time and computational storage requirements are kept small. The numerical model was set up utilizing LWT; small nonlinearities have been introduced through body-nonlinear method. The research was restricted to monochromatic waves only.

A novel 2wABC has been developed to allow for wave incidence and radiation boundary condition on the same boundary. The 2wABC has been tested as pure

radiation and combined incidence and radiation boundary condition and is also transparent for outgoing waves when second harmonics are present.

The solution of the wave/structure BVP is accomplished in two steps with superposition: 1. analytical wave incidence on plate and 2. numerical diffraction and radiation problem. The plate RBF distances have to be calibrated using analytical data; for the here investigated parameters analytical data have been supplied by Porter (2015a). Plate motion is introduced via prescribed forcing; the plate velocity is applied on the instantaneous plate boundary (body-nonlinear method).

Test results show that the applied RBF collocation method is able to model the wave/structure BVP for horizontal and inclined, heaving and pitching submerged flat plate configurations. Results are stable and model time up to $100T$ is possible without result deterioration. The model is capable to handle the introduced small nonlinearities well.

Although the model is set up for a horizontal sea bottom, piecewise-horizontal bottom could also be modelled when analytical data of the wave reflected seawards from the inclined bottom on the shoreside of the SFP are provided and used as wave incidence data on the leeside domain boundary in addition to the current wave incidence on the seaside.

(ii) Investigation of the wave attenuation performance of an inclined and horizontal SFP that is allowed (forced) to move in heave and pitch:

The introduction of plate motion in conjunction with motion control to ensure that radiated and scattered wave towards transmission side are 180° out-of-phase widens the bandwidth of appreciable wave attenuation and improves the plate performance as wave attenuator. Performance in intermediate water appears to be better than in deep water.

The magnitude of the radiated wave depends on plate parameters such as submergence, width and inclination and on motion parameters like motion amplitude and motion type. The most important findings regarding radiated wave of pure heaving and pitching and combined motion as presented and discussed in Chapters 6 and 7 respectively are summarised here:

- Decreasing the plate submergence without surface piercing and increasing the motion amplitude results in bigger amplitudes of the radiated wave. Smaller plate submergence restricts the permitted motion amplitude in order to avoid surface piercing; optimisation is required to find the configuration with the best wave attenuating performance.
- The effect of the relative plate width depends on the motion mode: for pitch the height of the radiated wave increases with relative plate width up to $Ka = 2.2$, for heave there exists an optimum Ka and further increase in Ka does not lead to bigger amplitudes of the radiated wave.
- Plate inclination of 5° improves the wave attenuating performance of heaving plates; the influence of a plate inclination angle of 5° for pitching plate is not significant. As here only one inclined configuration was tested, it is not possible to reliably describe the inclination influence; more numerical test runs are needed.
- The isolated influence of relative water depth was not investigated; although it appears as if wave attenuation is better in intermediate than in deep water, this might be mainly due to the smaller absolute submergence depth.
- Combined heaving and pitching allows for manipulation of the radiated wave; different amplitudes towards incidence side and transmission side and manipulation of the phase shift are possible. Through separate amplitude and phase control for pitch and heave, zero radiation towards the seaside can be achieved. This might be advantageous for multi-plate wave attenuators.
- Forced combined heaving and pitching never yields better wave attenuation than either pure heaving or pitching. Combined motion might result in better performance of wave-driven plate as pure heaving and pitching condition under wave incidence are mutually exclusive and therefore combined motion increases the forcing periods.

Phase control of plate motion to ensure that the radiated wave towards transmission side is out-of-phase with the scattered wave is of paramount importance as constructive interference between scattered and radiated wave toward transmission side will result in increased wave transmission.

Introducing plate motion and applying the plate velocity on the instantaneous plate position alters the diffracted wave mainly through the introduction of higher harmonics; there is no phase shift change due to plate motion present. The magnitude of generated higher harmonics in radiated and diffracted wave depends on plate parameters such as submergence, inclination and width; there are indications that the relative water depth affects the generation of higher harmonics, but the presence of a bigger ratio of higher harmonics in intermediated water might be mainly due to the smaller actual plate submergence depths.

(iii) Energy Flux:

Through prescribed forcing, energy is added or taken away from the modelled system; forcing with a motion phase shift that yields best wave attenuation is also the configuration with energy loss of the system. That means that while decreasing the transmitted wave height, energy can be extracted and used for forcing the plate motion, performing structural adaptations such as changing inclination and/or submergence depth in dependence on incidence wave climate or can be converted into usable electric energy.

Energy loss of the system increases with decreased plate submergence and increased plate motion amplitude and varies with plate width. In order to harvest most of this energy, energy loss through wave breaking and turbulences has to be kept small. This will lead to an optimum plate submergence depth and a maximum motion amplitude in dependence on the plate width.

Energy losses appear to be bigger in intermediate water than in deep water but this might also be mainly due to the smaller actual submergence depth. Additional test runs are necessary to underpin the findings.

Combined forced heaving and pitching can yield a higher energy loss than pure heaving or pitching and might be a good option when energy harvesting is the main focus of SFP installation.

8.2. Future Work

While deriving the water-wave/structure BVP, developing the numerical model, implementing the body-nonlinear method, calibrating the model with analytical data and analysing and discussing the test run results, automatically the gained knowledge about the model method and wave attenuation with a moving SFP increased. And even though the initial objectives of this research study have been met, through the improved insight and understanding of the water-wave/structure BVP and the applied numerical model, further areas of research have been detected and new problems that need to be investigated have been found.

Future investigations should cover the following tasks:

(i) In order to validate the results obtained with the developed numerical model, experimental research of a heaving and pitching SFP are required. This research should focus on the generation of radiated waves through prescribed plate motion in order to investigate the influence of structural parameters such as submergence depth, inclination and plate width as well as wave parameters such as wave height and relative water depth and motion amplitude and type. The experimental data can then be used to validate the radiation model results.

Furthermore, the influence of plate motion (motion type and amplitude) on the generated diffracted wave can be investigated and compared with the numerical data of this research. The influence of motion phase control on the wave attenuation performance and energy flux of the system established in this thesis can be verified by experimental data.

(ii) Utilise the gained insight into the numerical method to work on solving the wave/structure BVP in one step. This one-step solution will not require superposition and is thus prerequisite for the transition to nonlinear waves.

(iii) Future numerical studies should cover more structural and wave parameters h/L, d/h, β_0, Ka and ensure that the isolated influence of relative water depth h/L is investigated by applying a fixed plate submergence depth.

This will provide a broad data selection as base for result discussion so that con-

clusions drawn are more reliable and general. This, of course, requires additional analytical data to calibrate the numerical model.

(iv) Use these additional calibrated-plate-RBF-centre-distance data to generate empirical formulae to compute the plate RBF distances for not-yet calibrated parameter setups. Establishing such empirical formulae has already been attempted with the available data from this research but due to the sparse parameters (only six or nine Ka data, two h/L, d/h and β_0 configurations) data proved to be insufficient to yield reliable empirical formulae.

(v) The final aim should be to develop a fully nonlinear numerical model and thus avoiding the limitations of the LWT; this would allow for smaller plate submergence, bigger plate motion amplitudes and bigger incidence wave steepness.

Fully nonlinear modelling requires the surface boundary conditions to be applied on the actual surface which is not known in advance and is, therefore, part of the solution.

First steps of solving the nonlinear water wave BVP have been undertaken and the author was able to model one model setup fully nonlinear. In the successful nonlinear setup, the novel 2wABC worked as pure radiation boundary, no sponge layer or perfectly matched layer was required; time integration up to $50T$ was possible.

REFERENCES

Abarbanel, S., and D. Gottlieb. 1997. "A Mathematical Analysis of the PML Method". *Journal of Computational Physics* 134:357–363.

Abarbanel, S., H. Qasimov, and S. Tsynkov. 2009. "Long-Time Performance of Unsplit PMLs with Explicit Second Order Schemes". *Journal of Scientific Computing* 41:1–12.

Abul-Azm, A.G., and M.R. Gesraha. 2000. "Approximation to the hydrodynamics of floating pontoons under oblique waves". *Ocean Engineering* 27:365–384.

Aghili, M., P. Ghadimi, Y. F. Maghrebi, and H. Nowruzi. 2014. "Simulating the interaction of solitary wave and submerged horizontal plate using SPH method". *International Journal of Physical Research* 2 (2): 16–26.

An, S., and O. M. Faltinsen. 2012. "Linear free-surface effects on a horizontally submerged and perforated 2D thin plate in finite and infinite water depths". *Applied Ocean Research* 37:220–230.

— . 2013. "An experimental and numerical study of heave added mass and damping of horizontally submerged and perforated rectangular plates". *Journal of Fluids and Structures* 39:87–101.

Arnold, A. 2007. *Open boundary conditions for wave propagation problems on unbounded domains*. http://www.asc.tuwien.ac.at/ arnold/pdf/graz/graz.pdf, accessed at August 2014.

Bai, K.J. 1975. "Diffraction of oblique waves by an infinite cylinder". *Journal of Fluid Mechanics* 68:513–535.

Bayram, A. 2000. "Experimental study of a sloping float breakwater". *Ocean Engineering* 27:445–453.

Berenger, J.-P. 1994. "A perfectly matched layer for the absorption of electromagnetic waves". *Journal of Computational Physics* 114:185–200.

Bettess, P., and O. C Zienkiewicz. 1977. "Diffraction and Refraction of Surface Wave Using Finite and Infinite Elements". *International Journal for Numerical Methods in Engineering* 11 (8): 1271–1290.

Bird, H. W. K., and R. Sheperd. 1984. "On The Interaction of Surface Waves with Immersed Structures". *International Journal for Numerical Methods in Fluids* 4:765–780.

Black, J. L., C. C Mei, and M. C. G. Bray. 1971. "Radiation and scattering of water waves by rigid bodies". *Journal of Fluid Mechanics* 46 (1): 151–164.

Börekçi, O.S. 2014. *A Solution of the Linear Wave Theory BVP Using the RBFCM: The Linwaves Algorithm*. Personal Communication.

Broeze, J., and J.E. Romate. 1992. "Absorbing Boundary Conditions for Free Surface Wave Simulations with a Panel Method". *Journal of Computational Physics* 99:146–158.

Brossard, J., and M. Chagdali. 2001. "Experimental investigation of the harmonic generation by waves over a submerged plate". *Coastal Engineering* 42:277–290.

Brossard, J., G. Perret, L. Blonce, and A. Diedhiou. 2009. "Higher harmonics induced by a submerged horizontal plate and a submerged rectangular step in a wave flume". *Coastal Engineering* 56:11–22.

Burke, J.E. 1964. "Scattering of Surface Waves on an Infinitely Deep Fluid". *Journal of Mathematical Physics 5, 805 (1964);* 5 (6): 805–819.

Cao, Y., R. E Beck, and W. W. Schultz. 1993. "An absorbing beach for numerical simulations of nonlinear waves in a wave tank". In *Proceedings of the Eighth International Workshop Water Waves and Floating Bodies*, 17–20. IWWWFB.

Cheong, H.F., and M. Patarapanich. 1992. "Reflection and transmission of random waves by a horizontal double-plate breakwater". *Coastal Engineering* 18 (1-2): 63–82.

Cheong, H.F., N.J. Shankar, and S. Nallayarasu. 1996. "Analysis of Submerged Platform Breakwater by Eigenfunction Expansion Method". *Ocean Engineering* 23 (8): 649–666.

Cho, I.H, and M.H. Kim. 1998. "Interactions of a horizontal flexible membrane with oblique incident waves". *Journal of Fluid Mechanics* 367:139–161.

— . 2008. “Wave absorbing system using inclined perforated plates”. *Journal of Fluid Mechanics* 608:1–20.

Cho, I.H., and M.H. Kim. 2013. “Transmission of oblique incident waves by a submerged horizontal porous plate”. *Ocean Engineering* 61:56–65.

Chwang, A.T., and T. Wu. 1994. “Wave Scattering By Submerged Porous Disk”. *Journal of Engineering Mechanics* 120 (12): 2575–2587.

Danmeier, D. 1998. *Multiple-body simulations using a higher-order panel code*. Conference Paper.

Dattatri, J., H. Raman, and N.J. Shankar. 1978. “Performance Characteristics of Submerged Breakwaters”, 2153–2171. Sixteenth Conference on Coastal Engineering.

Dean, Robert G., and Robert A. Dalrymple. 1991. *Water Wave Mechanics for Engineers and Scientists*. Singapore: World Scientific Publishing Co.Ptc.Ltd.

Dgaygui, K., and P. Joly. 1994. “Absorbing Boundary Conditions for Linear Gravity Waves”. *SIAM Journal on Applied Mathematics* 54 (1): 93–131.

Dingemans, M.W. 1997. *Water Wave Propagation Over Uneven Bottoms*. Singapore, Singapore: World Scientific.

Dmitriev, V.I. 2011. *Wiener-Hopf Method. Encyclopedia of Mathematics*. https://www.encyclopediaofmath.org//index.php?title=Wiener-Hopf_ method& oldid=16599, accessed at November 2013.

Engquist, B., and A. Majda. 1977. “Absorbing boundary conditions for the numerical simulation of waves”. *Mathematics of Computation* 31 (139): 629–651.

Espinoza, H., R. Codina, and S. A Badia. 2014. “Sommerfeld non-reflecting boundary condition for the wave equation in mixed form”. *Computer Methods in Applied Mechanics and Engineering* 276:122–148.

Evans, D. V., and R. Porter. 1996. “Hydrodynamic characteristics of a thin rolling plate in finite depth of water”. *Applied Ocean Research* 18:215–228.

— . 1997. “Complementary Methods for Scattering by Thin Barriers”. Chap. 1 in *Mathematical Techniques for Water Waves*, ed. by B. N. Mandal, 1–44. Southampton: Computational Mechanics Publications.

— . 2007. “Wave-free motions of isolated bodies and the existence of motion-trapped modes”. *Journal of Fluid Mechanics* 584:225–234.

Evans, D.V. 1976. “A theory for wave-power absorption by oscillating bodies”. *Journal of Fluid Mechanics* 77 (1): 1–25.

— . 2004. “Mathematical Techniques for Linear Wave-Structure Interactions”. In *19th international workshop on water waves and floating bodies*. IWWWFB.

Evans, D.V., and C.M. Linton. 1989. “Active devices for the reduction of wave intensity”. *Applied Ocean Research* 11 (1): 26–32.

— . 1991. “Submerged Floating Breakwaters”. *Journal of Offshore Mechanics and Arctic Engineering* 113 (3): 205–210.

Evans, D.V., and M.A. Peter. 2011. “Asymptotic reflection of linear water waves by submerged horizontal porous plate”. *Journal of Engineering Mathematics* 69 (2-3): 135–154.

Falcão, A.F. 2007. “Modelling and control of oscillating-body wave energy converters with hydraulic power take-off and gas accumulator”. *Ocean Engineering* 34 (16): 2021–2032.

— . 2008. “Phase control through load control of oscillating-body wave energy converters with hydraulic PTO system”. *Ocean Engineering* 35 (3-4): 358–366.

— . 2010. “Wave energy utilization: A review of the technologies”. *Renewable and Sustainable Energy Reviews* 14:899–918.

Falnes, J. 2002. *Ocean Waves and Oscillating Systems Linear Interaction Including Wave-Energy Extraction*. Cambridge: Cambridge University Press.

Farina, L. 2010. “Water wave radiation by a heaving submerged horizontal disk very near the free surface”. *Physics of Fluids* 22:1–10.

Farina, L., R. L. da Gama, S. Korotov, and J.S. Ziebell. 2015. “Radiation of water waves by a submerged nearly circular plate”. *Journal of Computational and Applied Mathematics* in Press, corrected proof.

Farina, L., and P.A. Martin. 1998. “Scattering of water waves by a submerged disc using a hypersingular integral equation”. *Applied Ocean Research* 20:121–134.

Fibich, G., and S. Tsynkov. 2001. “High-Order Two-Way Artificial Boundary Conditions for Nonlinear Wave Propagation with Backscattering”. *Journal of Computational Physics* 171:632–677.

Försterling, K., and H.-O. Wüster. 1951. “Über die Entstehung von Oberwellen in der Ionosphäre”. *Journal of Atmospheric and Terrestrial Physics* 2 (1): 22–31.

Garrison, C.J. 1969. “On the interaction of an infinite shallow draft cylinder oscillating at the free surface with a train of oblique waves.” *Journal of Fluid Mechanics* 39:227–255.

Givoli, D. 2004. “High-order local non-reflecting boundary conditions: a review”. *Wave Motion* 39:319–326.

Givoli, D., and D. Cohen. 1995. “Nonreflecting boundary conditions based on Kirchhoff-type formulae”. *Journal of Computational Physics* 117 (1): 102–113.

Haas, P.C.A. de. 1997. *Numerical Simulation of Nonlinear Water Waves Using a Panel Method; Domain Decomposition and Applications*. PhD Thesis. Twente University.

Hall, K.R., and M.P. Fischer. 1998. “Performance of Submerged Active Breakwaters in a Hydraulic Model”. American Sciety of Civil Engineers.

Hamilton, J. A., and R.W. Yeung. 2000. “Nonlinear Motion of a Submerged Body in Waves”. In *International Workshop on Water Waves and Floating Bodies*. IWWWFB15.

Hammack, J. L. 1973. “A note on tsunamis: their generation and propagation in an ocean of uniform depth”. *Journal of Fluid Mechanics* 60 (4): 769–799.

Haren, P., and C.C. Mei. 1981. “Head-sea diffraction by a slender raft with application to wave-power absorption”. *Journal of Fluid Mechanics* 104:505–626.

Heins, A.E. 1948. “Water Waves Over a Channel of Finite Depth with a Dock”. *American Journal of Mathematics* 70 (4): 730–748.

— . 1950. “Water Waves over a channel of Finite depth with a submerged plane barrier”. *Canadian Journal of Mathematics* 2:210–222.

Hesthaven, J.S. 1997. *The Analysis and Construction of Perfectly Matched Layers for the Linearized Euler Equations*. Report. NASA.

Holmes, S., S. Bhat, P. Beynet, A. Sablok, and I. Prislon. 2001. "Heave Plate Design With Computational Fluid Dynamics". *Journal of Offshore Mechanics and Arctic Engineering* 123 (February): 22–28.

Hsu, H.-H., and Y.-C. Wu. 1999. "Scattering of water wave by a submerged horizontal plate and a submerged permeable breakwater". *Ocean Engineering* 26 (4): 325–341.

Hu, F.G., X.D. Li, and D.K. Lin. 2008. "Absorbing boundary conditions for nonlinear Euler and Navier-Stokes equations based on the perfectly matched layer technique". *Journal of Computational Physics* 227:4398–4424.

Hu, H.H., and K.H. Wang. 2005. "Damping Effect on Waves Propagating Past a Submerged Horizontal Plate and a Vertical Porous Wall". *Journal of Engineering Mechanics* 131:427–437.

Ijima, T., S. Ozaki, Y. Eguchi, and A. Kobayashi. 1970. "Breakwater and quay wall by horizontal plates". In *12th Coastal Engineering Conference*, 1537–1556. ASCE.

Isaacson, M., and O.U. Nwogu. 1987. "Wave loads and motions of long structures in directional seas". *Jornal of Offshore Mechanics and Arctic Engineering* 109:126–132.

Isichenko, M. B., and V. V. Yan'kov. 1984. "Generation of high harmonics of laser radiation in plasma during electron wavebreaking". *Soviet Physics - Journal of Experimental and Theoretical Physic* 60 (6): 1101–1107.

Kanoria, M., and B.N. Mandal. 2001. "Water Wave Scattering by Inclined Barrier Submerged in Finite Depth Water". IWWWFB.

Kansa, E.J. 1990. "Multiquadrics-A scattered data approximation scheme with applications to computational fluid-dynamics-II solutions to parabolic, hyperbolic and elliptic partial differential equations". *Computers and Mathematics With Applications* 19 (8-9): 147–161.

Keller, J.B., and D. Givoli. 1989. "A finite element method for large domains". *Computer Methods in Applied Mechanics and Engineering* 76 (1): 41–66.

Kojima, H., T. Ijima, and A. Yoshida. 1990. “Decomposition and interception of long waves by a submerged horizontal plate”. In *22nd International Confonference on Coastal Engineering*, vol. 2. ASCE.

Lee, C.H., and J.N. Newman. 2005. “Computation of wave effects using the panel method”. In *Numerical Models in Fluid-Structure Interaction*, ed. by S.K. Chakrabarti, 211–251. Cambridge: MIT Press.

Leppington, F.G. 1972. “On the radiation and scattering of short surface waves. Part 1”. *Journal of Fluid Mechanics* 56 (1): 101–119.

Levine, H. 1965. “Scattering of surface waves by a submerged circular cylinder”. *Journal of Mathematical Physics* 6 (8): 1231–1243.

Li, M. 2012. *Three-Dimensional Wave-Structure Interaction Modelling Using the Scaled Boundary Finite Element Method*. PhD Thesis. Griffith University.

Linton, C. M. 1997. “The use of multipoles in channel problems”. In *Mathematical Techniques for Water Waves*, ed. by B. N. Mandal, 45–78. Southampton: Computational Mechanics Publications.

— . 2002. “The Finite Dock Problem”. Chap. 5 in *IUTAM Symposium on Diffraction and Scattering in Fluid Mechanics and Elasticity*, ed. by I. D. Abrahams, P.A. Martin, and M.J. Simon, 45–51. Dordrecht: Springer-Science+Business Media, B.V.

Linton, C.M. 2000. *The finite dock problem*. https://dspace.lboro.ac.uk/dspace-jspui/bitstream/2134/739/1/00-03.pdf, accessed at July 2013.

Linton, C.M., and P. McIver. 2001. *Handbook of Mathematical Techniques for Wave-Structure Interactions*. Boca Raton, Florida: CRC Press LLC.

Liu, C., Z. Huang, and S.K. Tan. 2009. “Nonlinear scattering of non-breaking waves by a submerged horizontal plate: Experiments and simulations”. *Ocean Engineering* 36:1332–1345.

Liu, P.L.F., and M. Abbaspour. 1982a. “An integral equation method for the diffraction of oblique waves by an infinite cylinder”. *International Journal for Numerical Methods in Engineering* 18:1497–1504.

— . 1982b. “Wave Scattering by a Rigid Thin Barrier”. *Journal of the Waterway Port Coastal and Ocean Division* 108 (4): 479–491.

Liu, P.L.-F., and M. Iskandarani. 1991. “Scattering of Short-Wave Groups by Submerged Horizontal Plate”. *Journal of Waterway, Port, Coastal and Ocean Engineering* 117:235–246.

Liu, Y., and Y.C. Li. 2011. “An alternative analytical solution for water-wave motion over a submerged horizontal porous plate”. *Journal of Engineering Mathematics* 69 (4): 385–400.

Liu, Y., Y.C. Li, B. Teng, and S. Dong. 2008. “Wave motion over a submerged breakwater with an upper horizontal porous plate and a lower horizontal solid plate”. *Ocean Engineering* 35 (16): 1588–1596.

Loeffler-Lenz, F. 1994. *Floating dynamic breakwater*. http://www.freepatent sonline.com/5304005.pdf. Patent.

Mandal, B. N., and S. De. 2015. *Water Wave Scattering*. Boca Raton, Florida: CRC Press.

Martin, P.A., and L. Farina. 1997. “Radiation of water waves by a heaving submerged horizontal disc”. *Journal of Fluid Mechanics* 337:365–379.

McCormick, M.E. 1981. *Ocean Wave Energy Conversion*. Mineola, New York: Dover Publications, Inc.

McIver, M. 1985. *Diffraction of Water Waves by a Moored, Horizontal, Flat Plate*. http://www.iwwwfb.org/Abstracts/iwwwfb01/iwwwfb01_19.pdf, accessed at January 2013.

— . 1996. “Global relationships between two-dimensional water wave potentials”. *Journal of Fluid Mechanics* 312:299–309.

— . 2000. “Trapped modes supported by submerged obstacles”. *Proceedings of the Royal Society of London Series A* 456:1851–1860.

McIver, P., and M. McIver. 1997. “Trapped modes in an axisymmetric water wave problem”. *Quarterly Journal of Mechanics and Applied Mathematics* 50 (2): 165–178.

McKee, S., M. F. Tome, V. G. Ferreira, J.A. Cuminato, A. Castelo, F. S. Sousa, and N. Mangiavacchi. 2008. "The MAC method". *Computers and Fluids* 37:907–930.

Mei, C.C. 1978. "Numerical Methods in Water-Wave Diffraction and Radiation". *Annual Review of Fluid Mechanics* 10:393–416.

— . 1989. *The Applied Dynamics of Ocean Surface Waves*. Singapore: World Scientific Publishing Co. Pte. Ltd.

Mei, C.C., and J.L. Black. 1969. "Scattering of surface waves by rectangular obstacles in waters of finite depth". *Journal of Fluid Mechanics* 38 (3): 499–511.

Milgram, J.H. 1970. "Active water-wave absorbers". *Journal of Fluid Mechanics* 43 (4): 846–859.

Mousavizadegan, S.H., and M. Rahman. 2005. "Numerical Method in Wave Body Interactions". *Journal of Applied Mathematics and Computing* 17 (1-2): 73–91.

Murakami, H., S. Itoh, Y. Hosoi, and Y. Sawamura. 1994. "Wave Induced Flow around Submerged Sloping Plates". In *24th International Conference on Coastal Engineering*. ASCE.

Nataf, F. 2013. "Absorbing boundary conditions and perfectly matched layers in wave propagation problems". *Direct and Inverse problems in Wave Propagation and Applications*: 219–231.

Neelamani, S., and T. Gayathri. 2006. "Wave interaction with twin plate wave barrier". *Ocean Engineering* 33 (3-4): 495–516.

Neelamani, S., and M.S. Reddy. 1992. "Wave transmission and reflection characteristics of a rigid surface and submerged horizontal plate". *Ocean Engineering* 19 (4): 327–341.

Neves, M.de G., I.J. Losada, and M.A. Losada. 2000. "Short-Wave and Wave Group Scattering by Submerged Porous Plate". *Journal of Engineering Mechanics* 126 (10): 1048–1056.

Newman, J.N. 2008. "Trapping of water waves by moored bodies". *Journal of Engineering Mathematics* 62:303–314.

Noble, B. 1958. *Methods Based on the Wiener-Hopf Technique for the Solution of Partial Differential Equations*. New York: Pergamon Press.

Parsons, N.F., and P.A. Martin. 1992. "Scattering of water waves by submerged plates using hypersingular integral equations". *Applied Ocean Research* 14 (5): 313–321.

— . 1994. "Scattering of water waves by submerged curved plates and by surface-piercing flat plates". *Applied Ocean Research* 16:129–139.

— . 1995. "Trapping of water waves by submerged plates using hypersingular integral equations". *Journal of Fluid Mechanics* 284:359–375.

Patarapanich, M. 1984a. "Forces and moment on a horizontal plate due to wave scattering". *Coastal Engineering* 8 (3): 279–301.

— . 1984b. "Maximum and zero reflection from submerged plate". *Journal of Waterway, Port, Coastal, and Ocean Engineering* 110 (2): 171–181.

Patarapanich, M., and H.-F. Cheong. 1989. "Reflection and transmission characteristics of regular and random waves from a submerged horizontal plate". *Coastal Engineering* 13 (2): 161–182.

Polinder, H., M.A. Mueller, M. Scuotto, and M. Goden de Sousa Prado. 2007. "Linear generator systems for wave energy conversion". European Wave / Tidal Energy Conference.

Porter, R. 2002. "Surface wave scattering by submerged cylinders of arbitrary cross-section". *Proceedings of the Royal Society A: Mathematical, Physical & Engineering Sciences* 458:581–606.

— . 2015a. Personal Communication.

— . 2015b. "Linearised water wave problems involving submerged horizontal plates". *Applied Ocean Research* 50:91–109.

Qiu, W., and H. Peng. 2007. *Numerical Solution of Body-Exact Problem in the Time Domain with a Panel-Free Method*. Conference Paper. Plitvice, Croatia.

Qiu, W., H. Peng, and J.M. Chuang. 2006. "Computation of Wave-Body Interactions Using the Panel-Free Method and Exact Geometry". *Journal of Offshore Mechanics and Arctic Engineering* 128:31–38.

Rahman, M. 2001. "Effects of diffraction and radiation on a submerged sphere". *International Journal of Mathematics and Mathematical Sciences* 28 (9): 499–515.

Rao, S., K.G. Shirlal, R.V. Varghese, and K.R. Govindaraja. 2009. "Physical model studies on wave transmission of a submerged inclined plate breakwater". *Ocean Engineering* 36:1199–1207.

Rao, S., K.G. Shirlal, R.V. Varghese, and S. Prashanth. 2009. "Experimental Investigation of Hydraulic Performance of a Horizontal Plate Breakwater". *International Journal of Earth Sciences and Engineering* 2 (5): 424–432.

Romate, J.E. 1992. "Absorbing Boundary Conditions for Free Surface Waves". *Journal of Computational Physics* 99:135–145.

Sannasiraj, S. A., V. Sundar, and R. Sundaravadivelu. 1995. "The hydrodynamic behaviour of long floating structures in directional seas". *Applied Ocean Research* 17:233–243.

— . 1998. "Mooring Forces and Motion Response of Pontoon-Type Floating Breakwaters". *Ocean Engineering* 25 (1): 27–48.

Schot, S.H. 1992. "Eighty Years of Sommerfeld's Radiation Condition". *Historia Mathematica* 19:385–401.

Shankar, N.J., H.F. Cheong, and S. Nallayarasu. 1996. *Coastal Protection by Submerged Plate Breakwater*. http:// www.eng.nus.edu.sg/EResnews/9602/feb96p8a.html, accessed at June 2012.

Shankar, P.N. 2005. "Eigenfunction expansions on arbitrary domains". *Proceedings of the Royal Society A* 461:2121–2133.

Siew, P.F., and D.G. Hurley. 1977. "Long surface waves incident on a submerged horizontal plate". *Journal of Fluid Mechanics* 83 (1): 141–151.

Takaki, M. 2001. "Hydrodynamic Forces on a Submerged Plate". Eleventh International Offshore / Polar Engineering Conference.

Takaki, M., Y. Imai, and S.-M. Lee. 2002. "Reduction Effect of a Submerged-Plate toward Wave Exciting Forces Acting on a Very Large Floating Structure". Twelfth International Offshore / Polar Engineering Conference.

Takaki, M., and S.M. Lee. 2003. "Hydrodynamic Forces on Submerged-Plate Heaving near a Free Surface". Thirteenth International Offshore / Polar Engineering Conference.

Ting, L., and M.J. Miksis. 1986. "Exact boundary conditions for scattering problems". *Journal of the Acoustical Society of America* 80:1825–1827.

Tsynkov, S.V. 1998. "Numerical solution of problems on unbounded domains. A review". *Applied Numerical Mathematics* 24:465–532.

Usha, R., and T. Gayathri. 2005. "Wave motion over a twin-plate breakwater". *Ocean Engineering* 32:1054–1072.

Vay, J.-L. 2002. "Asymmetric Perfectly Matched Layer for the Absorption of Waves". *Journal of Computational Physics* 183:367–399.

Wang, K., Z.Q. Zhang, and Z. Chen. 2012. "Flow Field Analysis of Submerged Horizontal Plate Type Breakwater". *World Academy of Science, Engineering and Technology* 68:75–83.

Wang, K.H., and Q. Shen. 1999. "Wave motion over a group of submerged horizontal plates". *International Journal of Engineering Science* 37:703–715.

Williams, A.N., and W.G. McDougal. 1996. "A Dynamic Submerged Breakwater". *Journal of Waterway, Port, Coastal and Ocean Engineering* 122:288–296.

Wu, C. S., D. L. Young, and C. L. Chiu. 2013. "Simulation of wave-structure interaction by hybrid Cartesian/immersed boundary and arbitrary Lagrangian-Eulerian finite-element method". *Journal of Computational Physics* 254:155–183.

Wu, J., Z. Wan, and Y. Fang. 1998. "Wave reflection by a vertical wall with a horizontal submerged porous plate". *Ocean Engineering* 25 (9): 767–779.

Wu, N. J., T. K. Tsay, and D. L. Young. 2006. "Meshless numerical simulation for fully nonlinear water waves". *International Journal for Numerical Methods in Fluids* 50:219–234.

— . 2008. "Computation of Nonlinear Free-Surface Flows by a Meshless Numerical Method". *Journal of Waterway, Port, Coastal and Ocean Engineering* 134 (2): 97–103.

Yip, T.L. 1997. *Active water-wave control by a submerged pitching plate*. PhD Thesis. University of Hong Kong.

Yip, T.L., and A.T. Chwang. 1997. "Water Wave Control by Pitching Plate". *Journal of Engineering Mechanics* 123:800–807.

— . 1998. "Water Wave Control by Submerged Pitching Porous Plate". *Journal of Engineering Mechanics* 124:428–434.

Yu, X. 2002. "Functional Performance of a Submerged and Essentially Horizontal Plate for Offshore Wave Control: A Review". *Coastal Engineering Journal* 44 (2): 127–147.

Yu, X., and A.T. Chwang. 1994. "Water Waves above Submerged Porous Plate". *Journal of Engineering Mechanics* 120:1270–1282.

Yu, X., M. Isobe, and A. Watanabe. 1995. "Wave Breaking Over Submerged Horizontal Plate". *Journal of Waterway, Port, Coastal, and Ocean Engineering* 121 (2): 105–113.

Zhang, S., and A. N. Williams. 1996. "Wave scattering by submerged elliptical disk". *Journal of Waterway, Port, Coastal and Ocean Engineering* 122:38–45.

Zheng, Y.H., Y.M. Shen, and J. Tang. 2007. "Radiation and diffraction of linear water waves by an infinitely long submerged rectangular structure parallel to a vertical wall". *Ocean Engineering* 34:69–82.

Zheng, Y.H., Y.M. Shen, Y.G. You, B.J. Wu, and D.S. Jie. 2006. "Wave radiation by a floating rectangular structure in oblique seas". *Ocean Engineering* 33 (1): 59–81.

Zheng, Y.H., Y.M. Shen, Y.G. You, B.J. Wua, and D.S. Jie. 2004. "On the radiation and diffraction ofwater waves by a rectangular structure with a sidewall". *Ocean Engineering* 31:2087–2104.

Zhou, B.-Z., D.-Z. Ning, B. Teng, and M. Zhao. 2014. "Fully nonlinear modeling of radiated waves generated by floating flared structures". *Acta Mechanica Sinica* 30 (5): 667–680.

Ziebell, J.S., and L. Farina. 2012. "Water wave radiation by a submerged rough disc". *Wave Motion* 49:34–49.

APPENDIX A: STRUCTURE MOTION RESPONSE

In Appendix A the process of determining the motion response of the structure and implementing control via damping is briefly decribed. It includes the computation of the forces and moments induced onto the submerged plate by the incidence wave, the determination of added mass and radiation damping coefficient of the system for each of the motion modes and solving the equations of motion for every time step as well as the implementation of motion control via linear spring and damper.

The force and the moment on a structure submerged in water are determined by integrating the pressure over the structure surface. Following the approach of Linton and McIver (2001) the pressure can be determined from the Bernoulli equation (2.4). After linearization and referencing to atmospheric pressure, the pressure is defined as:

$$p = - \underbrace{\rho \frac{\partial \Phi}{\partial t}}_{\text{hydrodynamic}} - \underbrace{\rho g z}_{\text{hydrostatic}} \tag{A.1}$$

The hydrodynamic force component m on the structure due to the fluid motion is found by integrating the hydrodynamic pressure multiplied by the unit normal vector n^m over the surface of the structure

$$\mathcal{F}^{(m)}(t) = -\rho \iint_{S_B} \frac{\partial \Phi}{\partial t} n^{(m)} \, dS_B \tag{A.2}$$

where $\{n^m; m = 1, 2, 3\}$ are the x, y, z components of the inward unit normal to the body defined by the directional cosines given in Equation (2.37) and $\{n^m; m = 4, 5, 6\}$ represent the components due to rotation about the x, y and z axis. For a point (x, y, z) on S_B rotating about the equilibrium position of the centre of rotation (x', y', z'), $n^{(4)}$, $n^{(5)}$ and $n^{(6)}$ are defined in Equation (2.38).

The hydrodynamic force component m for m=1,2,3 represents the hydrodynamic force on the structure in x, y, z direction respectively whereas the components $\mathcal{F}^{(4)}$, $\mathcal{F}^{(5)}$, $\mathcal{F}^{(6)}$ represent the moments about the x, y, z axis respectively.

Separating the time dependency of the harmonic motion of angular frequency ω yields:

$$\mathcal{F}^{(m)}(t) = \mathrm{Re}\left\{F^{(m)}e^{-i\omega t}\right\} \tag{A.3}$$

With $\Phi = \mathrm{Re}\left\{\phi e^{-i\omega t}\right\}$ and (A.3), Equation (A.2) gives:

$$F^{(m)} = i\omega\rho \iint\limits_{S_B} \phi n^{(m)}\, dS_B \tag{A.4}$$

As derived in Section 2.2.2, the total velocity potential of a wave - structure interaction BVP can be divided into the scattered velocity potential $\phi_{Sc} = \phi_I + \phi_D$ (Equation (2.27)) and radiated velocity potential $\phi_R = \sum_{m=1}^{6} \phi_R^{(m)}$ (Equation (2.33)).

The total hydrodynamic force on the submerged plate due to diffracted, incident and radiated wave can also be divided into these components and Equation (A.4) becomes:

$$F^{(m)} = F_{exc}^{(m)} + \sum_{n=1}^{6} \hat{\xi}^{(n)} f^{(nm)} \tag{A.5}$$

Here $\hat{\xi}^{(n)}$ is the complex motion amplitude as defined in Equation (2.34), the vector $\mathbf{F_{exc}} = \left[F_{exc}^{(m)}\right]$ with

$$F_{exc}^{(m)} = i\omega\rho \iint\limits_{S_B} (\phi_I + \phi_D) n^{(m)}\, dS_B \tag{A.6}$$

represents the exciting force on the stationary structure due to the scattered wave field while the matrix $\mathbf{f} = \left[f^{nm}\right]$ with

$$f^{nm} = i\omega\rho \iint\limits_{S_B} \phi_R^{(n)} n^{(m)}\, dS_B \tag{A.7}$$

is called the restoring force matrix (see Mei (1989)) and f^{nm} represents the hydrodynamic reaction in direction m arising from structure oscillations in mode n.

Separating the real and imaginary parts of f^{nm} results in:

$$f^{(nm)} = i\omega\Big(a^{(nm)} + \frac{ib^{(nm)}}{\omega}\Big) \tag{A.8}$$

where

$$a^{(nm)} = \frac{1}{\omega}\,\mathrm{Im}\left(f^{(nm)}\right) \tag{A.9}$$

represents the added mass coefficient in direction m due to structure oscillation in mode n and

$$b^{(nm)} = -\,\mathrm{Re}\left(f^{(nm)}\right) \tag{A.10}$$

represents the radiation damping coefficient in direction m due to structure oscillation in mode n.

The added mass term represents an augmentation of the mass or inertia of the submerged body to account for the presence of the fluid and the opposing force (moment) the body experiences when moving in the fluid (see Evans and Porter (2007)). This opposing force (moment) is 180° out-of-phase with the acceleration in mode n.

The radation damping coefficient takes account of the surface disturbances generated by the body motion - this part of the force is in phase with the velocity in mode

n (as described in Evans and Porter (2007) and Linton and McIver (2001)).

Both coefficients are frequency-depending. The added mass terms can become negative for small submergences; this occurs when the potential energy of the fluid is greater than its kinetic energy. The damping coefficients are always non-negative due to the fact that the radiated waves travel away from the body towards infinity as stated in Evans and Porter (2007).

At resonance, the damping coefficients are maximum and a jump in the added mass or added inertia occurs. Evans and Porter (1996), Rahman (2001), Evans and Porter (2007) and Porter (2015) also explain that the damping coefficient can decrease to zero at a particular frequency which means that there are no waves radiated away from the body albeit a local wave field close to the body still exists.

Using general identities for the diffraction and radiation of simple harmonic waves and applying them to two radiation problems under consideration of the radiation condition, Mei (1989) (p.302/303) derived that the restoring force, the added mass coefficient and the radiation damping coefficient matrix must be symmetric irrespective of structure symmetry:

$$f^{(nm)} = f^{(nm)}, \qquad a^{(nm)} = a^{(nm)}, \qquad b^{(nm)} = b^{(nm)} \tag{A.11}$$

Combining Equations (A.7) and (A.8) yields the following expression:

$$\rho \iint_{S_B} \phi_R^{(n)} n^{(m)} \, dS_B = \left(a^{(nm)} + \frac{i b^{(nm)}}{\omega} \right) \tag{A.12}$$

Splitting the expression into real and imaginary parts gives the following expressions for the computation of the added mass and radiation damping coefficients:

$$a^{(nm)} = a^{(nm)} = \rho \iint\limits_{S_B} \mathrm{Re}\left\{\phi_R^{(n)}\right\} n^{(m)}\, dS_B = \mathrm{Re}\left\{f^{(nm)}\right\} \tag{A.13}$$

$$b^{(nm)} = b^{(nm)} = \rho\omega \iint\limits_{S_B} \mathrm{Im}\left\{\phi_R^{(n)}\right\} n^{(m)}\, dS_B = \mathrm{Im}\left\{\omega f^{(nm)}\right\} \tag{A.14}$$

With known incident, diffracted and radiated velocity potentials, the hydrodynamic forces and moments $F^{(m)}$ on the structure can be computed. It is important to note that the forces are frequency-dependent through the factor $\omega = 2\pi/T = 2\pi f$; that implies that the forces have to be computed for the range of frequencies the submerged structure is used for.

For the 2DV wave/structure BVP investigated in this thesis, the submerged flat plate is restrained in surge (see Section 2.2.2); that leaves only two possible motions: heave and pitch and Equation (A.5) under consideration of Equations (A.6) and (A.7) becomes:

$$\begin{aligned} F^{(m)} =& i\omega\rho\Bigg[\iint\limits_{S_B} (\phi_I + \phi_D) n^{(m)}\, dS_B \\ &+ \hat{\xi}^{(3)} \iint\limits_{S_B} \phi_R^{(3)} n^{(m)}\, dS_B + \hat{\xi}^{(5)} \iint\limits_{S_B} \phi_R^{(5)} n^{(m)}\, dS_B\Bigg] \end{aligned} \tag{A.15}$$

To obtain the dynamic response of the SFP to the exciting forces due to wave motion $\mathbf{F_{exc}(t)}$ and to implement control via damping and/or restricting the heave and pitch motion, the equations of motion have to be solved.

In three dimensions every structure has six DoF as explained in Section 2.2.2; therefore six equations of motions are required to describe the dynamic response of a submerged structure. If linear wave theory is applied and small structure motions are assumed, the dynamic response of the structure can be modelled by a linear mass-spring-dashpot system where the fluid resistance to the structure motion has to be considered by implementing an added mass term:

$$\mathbf{m}\ddot{\mathbf{x}}(t) + \mathbf{b}\dot{\mathbf{x}}(t) + \mathbf{k}\mathbf{x}(t) = \mathbf{F_{exc}}(t) - \mathbf{a}\ddot{\mathbf{x}}(t) \tag{A.16}$$

Here $\mathbf{m}$ represents the mass matrix of the structure, $\mathbf{a}$ the added mass coefficients, $\mathbf{b}$ the radiation damping coefficients, $\mathbf{k}$ are the spring coefficients due to buoyancy and $\mathbf{x}$ represents the coordinates of the six DoF (as explained in Section 2.2.2) with: $\mathbf{x} = (x, y, z, \Xi, \Upsilon, \Psi)^T$.

Reordering the terms of Equation (A.16) and dropping the time-dependency for convenience yields:

$$(\mathbf{m} + \mathbf{a})\ddot{\mathbf{x}} + \mathbf{b}\dot{\mathbf{x}} + \mathbf{k}\mathbf{x} = \mathbf{F_{exc}} \tag{A.17}$$

In order to control the motion of the structure, additional damping terms consisting of linear spring coefficients ($\mathbf{k_c}$) and damper coefficients ($\mathbf{c_c}$) are implemented as $\mathbf{f_{control}} = \mathbf{k_c}\mathbf{x} + \mathbf{c_c}\mathbf{x}$:

$$(\mathbf{m} + \mathbf{a})\ddot{\mathbf{x}} + \mathbf{b}\dot{\mathbf{x}} + \mathbf{k}\mathbf{x} = \mathbf{F_{exc}} + \mathbf{f_{control}} \tag{A.18}$$

Substituting the individual term for $\mathbf{f_{control}}$ and reordering the equation terms gives:

$$(\mathbf{m} + \mathbf{a})\ddot{\mathbf{x}} + (\mathbf{b} - \mathbf{c_c})\dot{\mathbf{x}} + (\mathbf{k} - \mathbf{k_c})\mathbf{x} = \mathbf{F_{exc}} \tag{A.19}$$

For the 2DV heaving and pitching SFP case, the DoF and therefore the number of equations of motion reduce to three: surge (x-direction (1)), heave (z-direction (3)) and pitch (about y-axis (5)). The symmetry of the flat plate in z-direction allows for simplification in the **m** and **k** matrices. For a fully submerged structure the buoyancy is always the same and therefore it does not affect the dynamic equilibrium. This results in simplifications in the spring coefficient matrix **k**. An in-detail derivation can be found in Mei (1989).

In matrix form the general coupled 2DV SFP system can be written as:

$$\begin{aligned}
&\left[\begin{pmatrix} m & 0 & m(z_c - z_r) \\ 0 & m & -m(x_c - x_r) \\ m(z_c - z_r) & -m(x_c - x_r) & I_{xx} + I_{zz} \end{pmatrix} + \begin{pmatrix} a_{11} & a_{13} & a_{15} \\ a_{31} & a_{33} & a_{35} \\ a_{51} & a_{53} & a_{55} \end{pmatrix}\right] \begin{pmatrix} \ddot{X} \\ \ddot{Z} \\ \ddot{\Xi} \end{pmatrix} \\
&\qquad + \left[\begin{pmatrix} b_{11} & b_{13} & b_{15} \\ b_{31} & b_{33} & b_{35} \\ b_{51} & b_{53} & b_{55} \end{pmatrix} - \begin{pmatrix} c^{(11)} & 0 & 0 \\ 0 & c_c^{(33)} & 0 \\ 0 & 0 & c_c^{(55)} \end{pmatrix}\right] \begin{pmatrix} \dot{X} \\ \dot{Z} \\ \dot{\Xi} \end{pmatrix} \\
&\quad + \left[\begin{pmatrix} 0 & 0 & 0 \\ 0 & 0 & 0 \\ 0 & 0 & k_{55} \end{pmatrix} - \begin{pmatrix} k^{(11)} & 0 & 0 \\ 0 & k_c^{(33)} & 0 \\ 0 & 0 & k_c^{(55)} \end{pmatrix}\right] \begin{pmatrix} X \\ Z \\ \Xi \end{pmatrix} + \begin{pmatrix} 0 \\ 0 \\ 0 \end{pmatrix} = \begin{pmatrix} F_{exc}^{(1)} \\ F_{exc}^{(3)} \\ F_{exc}^{(5)} \end{pmatrix}
\end{aligned} \tag{A.20}$$

Here x_c and z_c represent the coordinates of the centre of mass of the plate, x_r and z_r are the coordinates of the axis of rotation, a^{mn} are the added mass coefficients, b^{mn} represent the radiation damping coefficients, $k_c^{(mn)}$ and $c_c^{(mn)}$ are the spring and damper coefficients of the motion control.

As the here proposed SFP is restrained in surge ($x, \dot{x}, \ddot{x} = 0$), motion control for heave and pitch only is applicable; that means that:

$$\mathbf{k_c} = \begin{pmatrix} 0 & 0 & 0 \\ 0 & k_c^{(33)} & 0 \\ 0 & 0 & k_c^{(55)} \end{pmatrix} \qquad \text{and} \qquad \mathbf{c_c} = \begin{pmatrix} 0 & 0 & 0 \\ 0 & c_c^{(33)} & 0 \\ 0 & 0 & c_c^{(55)} \end{pmatrix} \tag{A.21}$$

and a horizontal supporting force $F_s^{(1)}$ is required to balance the horizontal wave force and prevent plate movement in x-direction.

For the surge-restrained SFP the equations of motion reduce to:

$$\begin{aligned}
&\left[\begin{pmatrix} m & 0 & m(z_c-z_r) \\ 0 & m & -m(x_c-x_r) \\ m(z_c-z_r) & -m(x_c-x_r) & I_{xx}+I_{zz} \end{pmatrix} + \begin{pmatrix} 0 & 0 & 0 \\ 0 & a_{33} & a_{35} \\ 0 & a_{53} & a_{55} \end{pmatrix}\right] \begin{pmatrix} 0 \\ \ddot{Z} \\ \ddot{\Xi} \end{pmatrix} \\
&\qquad + \left[\begin{pmatrix} 0 & 0 & 0 \\ 0 & b_{33} & b_{35} \\ 0 & b_{53} & b_{55} \end{pmatrix} - \begin{pmatrix} 0 & 0 & 0 \\ 0 & c_c^{(33)} & 0 \\ 0 & 0 & c_c^{(55)} \end{pmatrix}\right] \begin{pmatrix} 0 \\ \dot{Z} \\ \dot{\Xi} \end{pmatrix} \\
&\quad + \left[\begin{pmatrix} 0 & 0 & 0 \\ 0 & 0 & 0 \\ 0 & 0 & k_{55} \end{pmatrix} - \begin{pmatrix} 0 & 0 & 0 \\ 0 & k_c^{(33)} & 0 \\ 0 & 0 & k_c^{(55)} \end{pmatrix}\right] \begin{pmatrix} 0 \\ Z \\ \Xi \end{pmatrix} + \begin{pmatrix} F_s^{(1)} \\ 0 \\ 0 \end{pmatrix} = \begin{pmatrix} F_{exc}^{(1)} \\ F_{exc}^{(3)} \\ F_{exc}^{(5)} \end{pmatrix}
\end{aligned} \tag{A.22}$$

Note that in Equations (A.20) and (A.22) coupling between heave and pitch motions is allowed for in the mass matrices to accommodate the proposed shift in the pitching axis which annihilates the symmetry in x-direction.

The influence of control by linear spring and damper on amplitude and phase of the waves radiated by the structure can now be investigated by introducing the coefficients $c_c^{(33)}$, $c_c^{(55)}$, $k_c^{(33)}$ and $k_c^{(55)}$ isolatedly.

The heaving motion of a structure forced by waves can be described by:

$$\mathbf{x} = \mathbf{x_a} \cos(\omega t + \epsilon) \tag{A.23}$$

where $\mathbf{x_a}$ represents the vector of the amplitude of the harmonic motion and ϵ the phase lag vector between excitations and radiation responses. Then the time derivatives of x

are:

$$\dot{\mathbf{x}} = -\omega \mathbf{x_a} \sin(\omega t + \epsilon) \tag{A.24}$$

$$\ddot{\mathbf{x}} = -\omega^2 \mathbf{x_a} \cos(\omega t + \epsilon). \tag{A.25}$$

This shows that $\mathbf{x}$ and $\dot{\mathbf{x}}$ are out of phase by 90° and $\mathbf{x}$ and $\ddot{\mathbf{x}}$ are out of phase by 180° (destructive interference). Applying this knowledge to consider the effects of introducing control spring and damping coefficients allows the deduction that the influence of the control by spring ($\mathbf{x}$) has to be compensated by the change of added mass ($\ddot{\mathbf{x}}$) of the system and the radiation damping of the system ($\dot{\mathbf{x}}$) will adapt to balance the effect of the control damping ($\dot{\mathbf{x}}$).

After determining the adapted added mass and radiation damping coefficients, Equation (A.8) can be used to determine the adapted restoring forces $f^{(nm)}$. By applying Equation (A.7) the velocity potential of the modified radiated waves can be computed and the far-field behaviour can be evaluated to determine the altered transmission and reflection coefficients.

By computing the altered transmission (k_T) and reflection (k_R) coefficients for a range of control spring and control damping values, performance matrices can be generated as shown in Table A.1. Here m, p= 3, 5 for heave and pitch motion control.

As the added mass and radiation damping coefficients are all frequency-dependent, these matrices apply only to one frequency and it is necessary to perform the computations for all frequencies under consideration.

With the computed transmission coefficient matrices it is now possible to determine the optimum control configuration/configurations to achieve minimum transmis-

Table A.1. Transmission coefficient matrix for linear spring and damper control implementation.

$k_c^{(m)}$ \ $c_c^{(p)}$	0	$c_{c1}^{(p)}$	$c_{c2}^{(p)}$	$\dots$	$c_{cn}^{(p)}$
0	k_{T_00}	k_{T_01}	k_{T_02}	$\dots$	k_{T_0n}
$k_{c1}^{(m)}$	k_{T_10}	k_{T_11}	k_{T_12}	$\dots$	k_{T_1n}
$k_{c2}^{(m)}$	k_{T_20}	k_{T_21}	k_{T_22}	$\dots$	k_{T_2n}
$\vdots$	$\vdots$	$\vdots$	$\vdots$	$\ddots$	$\vdots$
$k_{cn}^{(m)}$	k_{T_n0}	k_{T_n1}	k_{T_n2}	$\dots$	k_{T_nn}

sion for each wave period/frequency.

Transmission and reflection coefficients are important parameters to evaluate the performance of FBWs as they indicate how much energy is reflected by the structure or transmitted past the structure. They are complex numbers with the magnitude stating the ratios of the heights of the transmitted and reflected wave respectively to the height of the incident wave and the arguments corresponding to the phase shift between transmitted and reflected wave respectively and incident wave and have to be determined from the far-field behaviour of the velocity potentials or water elevations.

As LWT is employed, energy conservation is assumed; therefore the Equation (2.60) has to be satisfied and is here rewritten for convenience:

$$k_T^2 + k_R^2 = 1 \tag{A.26}$$

with k_T being the magnitude of the complex transmission coefficient and k_R being the magnitude of the complex reflection coefficient as defined in Equations (2.58) and (2.59).

Defining $T_{stationary}$ and $R_{stationary}$ as the complex transmission and reflection coefficients for waves incident on a stationary plate, and $\hat{\eta}^{(3)}$ and $\hat{\eta}^{(5)}$ as the complex wave amplitude due to radiation by heaving and rolling motion of the plate respectively, the water elevation in the far-field is defined as:

$$\begin{aligned} \eta(x) &\sim e^{-ikx} + \left(R_{stationary} + \hat{\eta}^{(3)} + \hat{\eta}^{(5)}\right)e^{ikx} \qquad \text{as} \qquad x \to -\infty \\ \eta(x) &\sim \left(T_{stationary} - \hat{\eta}^{(3)} - \hat{\eta}^{(5)}\right)e^{-ikx} \qquad \text{as} \qquad x \to \infty \end{aligned} \tag{A.27}$$

The complex total transmission and reflection coefficients T_{total} and R_{total} are given as (see Evans and Linton (1991)):

$$\begin{aligned} T_{total} &= T_{stationary} - \hat{\eta}^{(3)} - \hat{\eta}^{(5)} \\ R_{total} &= R_{stationary} + \hat{\eta}^{(3)} + \hat{\eta}^{(5)} \end{aligned} \tag{A.28}$$

APPENDIX B: OVERVIEW RESEARCH METHODS

Appendix B contains an overview of the theoretical research methods applied to submerged and floating obstacles in the context of linear wave theory during the last 68 years. It is not an exhaustive list but rather intended to give an idea of the different approaches used to solve the water-wave/structure BVP.

Not many of these researchers have solved the radiation problem; the main focus of most of the studies was the diffraction problem.

Table B.1. Summary of past researches regarding methodology.

Researcher	**Water Depth**	**Obstacle Type**	**Applied Solution Method**
Heins (1948)	finite	surface plate of zero thickness	Exponential technique (Wiener-Hopf integral equation)
Heins (1950)	finite	submerged plate of zero thickness	Exponential technique (Wiener-Hopf integral equation)
Burke (1964)	infinite	submerged & surface plate of finite width	Wiener-Hopf technique
Levine (1965)	infinite	submerged rigid circular cylinder	BVP is reduced to integral equation by use of Green's function
Garrison (1969)	finite	floating zero draft cylinder of infinite length	integral equation of second kind
Mei and Black (1969)	finite	submerged & floating rectangular obstacle; zero and finite thickness	variational formulation approach
Ijima *et al.* (1970)	finite	surface plate of zero thickness	Eigenfunction expansion
Black *et al.* (1971)	finite	infinitely long surface or bottom plate	Schwinger's variational formulation
Leppington (1972)	infinite and finite	zero thickness plate with finite width	matched asymptotic expansions

Table B.1. Summary of past researches regarding methodology (cont.)

Researcher	**Water Depth**	**Obstacle Type**	**Applied Solution Method**
Bai (1975)	finite and infinite	vertical flat plate, floating horizontal flat plate	Finite-element techniques based on variational principle
Siew and Hurley (1977)	shallow water	zero thickness submerged plate	method of matched asymptotic expansions
Bettess and Zienkiewicz (1977)	variable	cylindrical shape, parabolic shoal, rectangular harbour	Finite and Infinite Element Method
Haren and Mei (1981)	deep water	slender body with draft¡¡width	method of matched asymptotic expansions
Liu and Abbaspour (1982)	finite and uniform outside auxiliary boundaries	floating infinite uniform cylinder	Matched Eigenfunction Expansion (MEE) in combination with boundary integral equation
Liu and Abbaspour (1982)	finite	inclined, surface piercing plate	Matched Eigenfunction Expansion (MEE) in combination with boundary integral equation
Bird and Sheperd (1984)	finite	fixed submerged object of arbitrary cross-section and infinite length	boundary element method
Patarapanich (1984)	shallow water	submerged horizontal plate of zero thickness	Matched Eigenfunction Expansion (MEE) in combination with Finite Element Method

Table B.1. Summary of past researches regarding methodology (cont.)

Researcher	**Water Depth**	**Obstacle Type**	**Applied Solution Method**
McIver (1985)	finite	moored, submerged, horizontal plate	matched eigenfunction expansion method
Isaacson and Nwogu (1987)	finite and variable	an infinitely long, semi-immersed floating cylinder of arbitrary shape	Boundary Element Method
Evans and Linton (1989)	finite and constant	infinitely long, submerged cylinder	Multipole Method
Liu and Iskandarani (1991)	finite and constant	submerged horizontal plate of finite thickness	eigenfunction expansion method
Parsons and Martin (1992)	infinite	submerged inclined plate	hypersingular integral equation
Chwang and Wu (1994)	finite and constant	submerged porous circular disk with zero thickness	eigenfunction expansion method
Parsons and Martin (1994)	infinite	submerged inclined plate	hypersingular integral equation
Yu and Chwang (1994)	finite and constant	submerged horizontal porous plate of zero thickness	boundary element method
Parsons and Martin (1995)	infinite	submerged inclined plate	hypersingular integral equation

Table B.1. Summary of past researches regarding methodology (cont.)

Researcher	**Water Depth**	**Obstacle Type**	**Applied Solution Method**
Sannasiraj *et al.* (1995)	finite depth	rigid pontoon type floating body	2D finite element model
Zhang and Williams (1996)	finite and constant	submerged elliptical disk	Eigenfunction Expansion Method (with Mathieu functions)
Cheong *et al.* (1996)	finite	submerged horizontal plate	Eigenfunction Expansion Method
Williams and McDougal (1996)	finite	submerged or surface-piercing rectangular body	eigenfunction expansion technique
Martin and Farina (1997)	deep water	submerged heaving thin rigid plate/disc	hypersingular boundary integral equation (solvable numerically with BEM or for flat plate with expansion collocation method)
Yip and Chwang (1997)	finite and constant	submerged pitching plate of zero thickness	method of matched eigenfunction expansions
Yip (1997)	finite and constant	submerged porous pitching plate of zero thickness	method of matched eigenfunction expansions
Yip and Chwang (1998)	finite and constant	submerged pitching plate of zero thickness	method of matched eigenfunction expansions

Table B.1. Summary of past researches regarding methodology (cont.)

Researcher	**Water Depth**	**Obstacle Type**	**Applied Solution Method**
Wu *et al.* (1998)	constant and finite	vertical wall with a horizontal submerged porous plate of zero thickness	eigenfunction expansion method
Cho and Kim (1998)	finite	submerged horizontal flexible membrane	eigenfunction expansion method and multi-domain boundary element method (BEM)
Farina and Martin (1998)	deep water	thin rigid horizontal circular plate	expansion-collocation method for solving the hypersingular integral equation
Sannasiraj *et al.* (1998)	finite depth	rigid pontoon type floating body	2D finite element model
Danmeier (1998)	finite depth	circular cylinders (one free to move in surge)	Higher-order panel method; body-nonlinear method
Hsu and Wu (1999)	finite depth	fixed, submerged, horizontal, impermeable plate and a submerged permeable breakwater	boundary element method (BEM)
Wang and Shen (1999)	finite	group of submerged horizontal plates	method of eigenfunction expansions

Table B.1. Summary of past researches regarding methodology (cont.)

Researcher	**Water Depth**	**Obstacle Type**	**Applied Solution Method**
Linton (2000)	finite depth	finite dock (horizontal floating rigid plate)	combination of matched eigenfunction expansions and residue calculus theory
Hamilton and Yeung (2000)	finite depth	submerged bodies	shell function method (hybrid integral equation method) body-nonlinear method
Neves *et al.* (2000)	uniform water depth	horizontal porous plate of finite thickness	eigenfunction expansion method and multiple-scale perturbation method
Takaki (2001), Takaki *et al.* (2002)	finite	submerged horizontal and inclined plate	numerical simulation using the Marker and Cell method (MAC method)
Kanoria and Mandal (2001)	finite	submerged inclined thin barrier of arbitrary shape	hypersingular integral equation
Holmes *et al.* (2001)	finite	heaving plate	CFD and commercial Navier-Stokes flow solver
Porter (2002)	finite or infinite	submerged cylinder of arbitrary cross-section and thin submerged plates	hypersingular integral equation
Zheng *et al.* (2004)	finite	rectangular floating structure with leeward wall boundary	Eigenfunction expansion method in combination with separation of variables

Table B.1. Summary of past researches regarding methodology (cont.)

Researcher	**Water Depth**	**Obstacle Type**	**Applied Solution Method**
Mousavizadegan and Rahman (2005)	finite	submerged or floating sphere or semi-ellipsoids	Boundary Integral Equation method BIEM (or BEM)
Usha and Gayathri (2005)	uniform finite depth	twin plate system consisting of one surface and one submerged plate	Eigenfunction expansion method
Lee and Newman (2005)	infinite or finite, constant depth	surface or submerged impermeable body (spar)	boundary integral equation method (BIEM) (WAMIT and TiMIT); time-domain impulse-response function
Zheng *et al.* (2006)	finite and constant depth	floating rectangular structure	eigenfunction expansion matching method
Qiu *et al.* (2006)	finite and infinite depth	floating hemisphere, a vertically floating axisymmetric cylinder	panel-free method
Zheng *et al.* (2007)	finite depth	submerged rectangular structure in front of vertical wall	eigenfunction expansion matching method
Qiu and Peng (2007)	not specified	submerged sphere, vertical cylinder (heave)	de-singularized integral equations; body-nonlinear method

Table B.1. Summary of past researches regarding methodology (cont.)

Researcher	**Water Depth**	**Obstacle Type**	**Applied Solution Method**
Cho and Kim (2008)	finite and constant	thin horizontal submerged porous plate / thin inclined submerged porous plate in front of vertical wall	matched eigenfunction expansion /multi-domain Boundary Element Method
Liu *et al.* (2008)	finite and constant	submerged two layer horizontal plate of zero thickness	matched eigenfunction expansion method
Liu *et al.* (2009)	finite and constant	submerged two layer horizontal plate of non-zero thickness	matched eigenfunction expansion method
Farina (2010)	deep water	heaving horizontal disk of zero thickness	generalized Love's integral equation
Liu and Li (2011)	finite and constant	submerged horizontal porous-plate	matched-eigenfunction-expansions method
An and Faltinsen (2012)	finite and infinite water depths	thin submerged horizontal plate (solid or perforated)	semi-analytical approach
Wang *et al.* (2012)	infinite	thin submerged horizontal plate	boundary element method
Ziebell and Farina (2012)	infinite	thin circular non-planar body	boundary perturbation method for solving the hypersingular integral equation
Cho and Kim (2013)	finite and constant	thin submerged horizontal porous plate	matched eigenfunction expansion method

Table B.1. Summary of past researches regarding methodology (cont.)

Researcher	**Water Depth**	**Obstacle Type**	**Applied Solution Method**
Wu *et al.* (2013)	finite	complex submerged body in viscous fluid	hybrid Cartesian/immersed boundary and arbitrary Lagrangian-Eulerian finite-element method
An and Faltinsen (2013)	finite	heaving thin submerged horizontal perforated plate	MEE with inner BEM
Aghili *et al.* (2014)	finite and constant	floating, semi-submerged and submerged horizontal plate	computational fluid dynamic simulation (CFD)
Zhou *et al.* (2014)	finite and constant	truncated cylinder (heave and pitch; radiation problem only)	higher-order boundary element method; body-nonlinear method
Mandal and De (2015)	deep water	two symmetric thin inclined submerged plates	hypersingular integral equations
Porter (2015)	finite and infinite	heaving and pitching submerged horizontal plate	hypersingular integral equations
Farina *et al.* (2015)	deep water	heaving submerged thin nearly circular plate	hypersingular integral equations

APPENDIX C: AVAILABLE SOLUTION METHODS FOR BVP

Appendix C contains a summary of the advantages and disadvantages of the analytical and numerical methods applicable to the solution of wave/structure boundary value problems. A description of the solution methods is given in Chapter 3.

Table C.1. Advantages and shortcomings of solution methods for wave structure boundary value problems.

Method	**Advantages**	**Shortcomings**
Eigenfunction Expansion Technique & Matched Eigenfunction Expansion	Simple and accurate solution of the BVP (Linton and McIver, 2001) Powerful tool for simple geometries admitting complete sets of eigenfunctions (Shankar, 2005) Evanescent waves are easily implemented	Method requires regions of constant finite depth (Linton and McIver, 2001) Boundaries of regions have to coincide with coordinate lines or surfaces (Linton and McIver, 2001), (Porter, 2002)
Multipole Expansion Method	High speed of convergence for simple geometries (Evans and Linton, 1989) Uncomplicated evaluation of the hydrodynamic forces (Linton and McIver, 2001) Applicable to array configurations of cylindrical or spherical bodies (Linton, 1997) p.51 Method is well suited to model the phenomenon of trapped modes in wave-structure problems. (McIver, 2000), (McIver and McIver, 1997) and (Newman, 2008)	In order to apply the body boundary condition, the body has to coincide with a coordinate surface. This condition limits the number of geometries to which this method can be applied. (Linton, 1997) and (Linton and McIver, 2001)

Table C.1. Advantages and shortcomings of solution methods for wave structure boundary value problems (cont.)

Method	**Advantages**	**Shortcomings**
Wiener-Hopf Technique	Powerful method to obtain explicit analytic solution for certain boundary value problems (uniform strip or half-plane domain with different boundary conditions on one boundary) (Linton and McIver, 2001) and (Evans, 2004) Method can also be used to obtain approximate solutions to more complex problems. (Noble, 1958) Singularity of the fluid velocity at the edge of the submerged plate is automatically satisfied.	Limited applicability: • Semi-infinite plate width (Evans and Peter, 2011) • For infinite depth the limit for normally incident waves cannot be determined (Linton and McIver, 2001) Factorization into $L_+(\lambda)$ and $L_-(\lambda)$ may prove difficult or impossible (Noble, 1958)

Table C.1. Advantages and shortcomings of solution methods for wave structure boundary value problems (cont.)

Method	**Advantages**	**Shortcomings**
Combination of Matched Eigenfunction Expansions and Residue Calculus Theory	Powerful method to obtain explicit analytic solution to problems involving semi-infinite boundaries which can be expressed as eigenfunction expansions (Linton and McIver, 2001) and (Evans, 2004) Method can be easily modified to obtain numerically efficient solutions for finite structures. (Linton and McIver, 2001) Fluid velocity singularity at the edge of the submerged plate is automatically satisfied. (Evans and Peter, 2011)	For the finite plate case this technique is only valid if the plate width compared to the wavelength is big enough (Linton and McIver, 2001) and (Linton, 2002). Results for normal wave incidence have to be determined by taking the limit; error will be maximum for normal incidence (Linton and McIver, 2001).

Table C.1. Advantages and shortcomings of solution methods for wave structure boundary value problems (cont.)

Method	**Advantages**	**Shortcomings**
Hypersingular Integral Equation	By appropriate selection of the fundamental solution the radiation condition is satisfied automatically. (Parsons and Martin, 1992), (Martin and Farina, 1997) and (Porter, 2002) The singular behaviour of the velocity potential at the edges of a plate can be easily enforced. (Parsons and Martin, 1992), (Martin and Farina, 1997) and (Porter, 2002) The method can be applied to a wide class of geometries. (Parsons and Martin, 1992), (Martin and Farina, 1997) and (Porter, 2002) Radiation by forced motion can be modelled using this method (Porter, 2015b).	Only in a few cases singular and hypersingular integral equations can be solved exactly; mostly these equations have to be solved numerically using Boundary Element Method or expansion-collocation method. (Mei, 1978) For varying depth the computation cost increases and restricts the applicability of this method. (Mei, 1978)

Table C.1. Advantages and shortcomings of solution methods for wave structure boundary value problems (cont.)

Method	**Advantages**	**Shortcomings**
Finite Element Method (FEM)	System matrix is symmetric and banded. (Sannasiraj *et al.*, 1998) Bai (1975) states that the main advantage of FEM is that complex boundary geometry can be easily accommodated.	Treatment of unbounded domains is difficult; damping at radiation boundary can lead to big computational domain size. (Li, 2012) In general, re-meshing is required for moving obstacles in water domain. (Li, 2012)
Boundary Element Method (BEM)	With BEM the radiation condition at infinity is satisfied with correct choice of fundamental solution. (Li, 2012) Method shows good convergence and accuracy. Computational costs are kept small as only domain boundaries are discretised. (Li, 2012)	Evaluation of singular integrals can be difficult. (Li, 2012) Matrices are nonsymmetric and dense. (Li, 2012)

APPENDIX D: FORTRAN CODE

Appendix D contains the Fortran code that has been developed and used to model the diffraction and/or radiation BVP for a submerged flat plate.

```
program HeavingPlateLWT
! Time integrator Adam-Bashforth O(4)
! two way ABC on incidence side and on radiation side implemented
! incidence Eta and Phi are determined using the analytical solution to save time (code lines for numerical determination are
left in but not complete as BVP has to be set up without plate nodes)
implicit none
real*8::g, T, H0R, d, dhdx, L0, Omega, pi, k, HR, L, kd, ks, C, t0, noperiods, factor, factorm
real*8::lambda, dx, dz, dt, ds, r, r2, dtprint, dl, meanPhidiffract, meanPhirad
real*8::wp,tp,zp,xp,beta, betarad, deltaxp, deltazp, zpinitial, inclinitial
real*8::drbf1, drbf2, drbf3, drbf4,drbf5, drbf7, drbf6, drbf8
real*8::Thetah, nplate, nedge, vheave, aheave
real*8::Thetap, vpitchang, apitch, pitchrad, dummy
integer::nv, nperL, nh, nwave, n, marker
integer::i,j,it,index1, ii, ip, nprint, finaltime
integer::nfsb, nfse, nrsb, nrse, nbsb, nbse, nisb, nise, nfs, nrs, nbs, nis
integer::npub, npue, nprb, npre, npbb, npbe, nplb, nple, npu, npr, npb, npl
integer::nvp,nhp, ndiffx1
real*8, allocatable::xc(:), zc(:), xrbf(:), zrbf(:), diffx1(:),xpc(:), zpc(:), intxc(:,:), intzc(:,:), intxrbf(:,:), intzrbf(:,:)
real*8, allocatable::xcpinitial(:),zcpinitial(:), xrbfpinitial(:), zrbfpinitial(:), vpitch(:), xcp(:),zcp(:), xrbfp(:), zrbfp(:)
```

Figure D.1. Fortran code.

```
real*8, allocatable::xileft(:), zileft(:), xiright(:), ziright(:)
real*8, allocatable::f(:,:), fx(:,:), fz(:,:), finv(:,:)
real*8, allocatable::Phiinneranalyticleft(:), Phiinneranalyticright(:)
real*8, allocatable::Finnerleft(:,:), Finnerright(:,:), Phiinnerleftinc(:), Phiinnerleftdiffract(:), phiinnerrightrad(:)
real*8, allocatable::Phiinnerrightinc(:), Phiinnerrightdiffract(:), phiinnerleftrad(:)
real*8, allocatable::phidiffleftdiffract(:), phidiffrightdiffract(:), phidiffleftrad(:), phidiffrightrad(:),alphadiffract(:), alphainc(:),
alpharad(:)
real*8, allocatable::fxfinv(:,:), fzfinv(:,:), m1star(:,:), m2star(:,:), nstar(:,:)
real*8, allocatable::Ident(:,:), Adiffract(:,:), Adiffractinv(:,:), b(:), bdiffract(:), binc(:)
real*8, allocatable::Arad(:,:), Aradinv(:,:), brad(:), intpitchrad(:)
real*8, allocatable::etanewanalyticinc(:)
real*8, allocatable::etadiffract(:), etanewdiffract(:), etaold1diffract(:), etaold2diffract(:), etaold3diffract(:)
real*8, allocatable::etainc(:), etanewinc(:), etaold1inc(:), etaold2inc(:), etaold3inc(:)
real*8, allocatable::etarad(:), etanewrad(:), etaold1rad(:), etaold2rad(:), etaold3rad(:)
real*8, allocatable::phinewadapdiffract(:), phinewadapinc(:), phinewadaprad(:)
real*8, allocatable::phiold1inc(:), phiinc(:), phinewanalyticinc(:), phinewinc(:)
real*8, allocatable::phiold1diffract(:), phidiffract(:), phinewdiffract(:)
real*8, allocatable::phiold1rad(:), phirad(:), phinewrad(:)
real*8, allocatable::dphidxold1inc(:), dphidxold2inc(:), dphidxold3inc(:)
```

Figure D.1. Fortran code (cont.)

```
real*8, allocatable::dphidxold1diffract(:), dphidxold2diffract(:), dphidxold3diffract(:)
real*8, allocatable::dphidxinc(:),dphidxdiffract(:), dphidxnewinc(:), dphidxnewdiffract(:)
real*8, allocatable::dphidzold1inc(:), dphidzold2inc(:), dphidzold3inc(:)
real*8, allocatable::dphidzold1diffract(:), dphidzold2diffract(:), dphidzold3diffract(:)
real*8, allocatable::dphidxold1rad(:), dphidxold2rad(:), dphidxold3rad(:), dphidxrad(:), dphidxnewrad(:)
real*8, allocatable::dphidzold1rad(:), dphidzold2rad(:), dphidzold3rad(:), dphidzrad(:), dphidznewrad(:)
real*8, allocatable::intetainc(:,:), intphidiffdiffract(:,:), intmeanphidiffract(:), intmeanphirad(:)
real*8, allocatable::dphidzinc(:), dphidzdiffract(:), dphidznewinc(:), dphidznewdiffract(:)
real*8, allocatable::intetadiffract(:,:), intdphidxdiffract(:,:), intdphidzdiffract(:,:), intphidiffract(:,:), intphiinc(:,:),
intdphidxinc(:,:), intdphidzinc(:,:)
real*8, allocatable::intetarad(:,:), intphirad(:,:), intdphidxrad(:,:), intdphidzrad(:,:), intphidiffrad(:,:)
real*8, allocatable::cotran(:,:), xcstar(:), zcstar(:), xrbfstar(:), zrbfstar(:)
integer, allocatable::itype(:), reftime(:)
open(10,file='wavedata.dat')
read(10,*)T
read(10,*)H0R
read(10,*)d
read(10,*)g
open(11,file='nodedata.dat', status='unknown')
```

Figure D.1. Fortran code (cont.)

```
read(11,*)nv
read(11,*)nperL
read(11,*)nwave
read(11,*)nh
read(11,*)drbf5
read(11,*)drbf6
read(11,*)drbf7
read(11,*)drbf8
open (12, file='rundata.dat', status='unknown')
read(12,*)noperiods
read(12,*)dt
read(12,*)dtprint
open (13,file='nodepositioning.dat', status='unknown')
open (130,file='nodepositioninner.dat', status='unknown')
open(14,file='datasummary.dat', status='unknown')
open(15,file='initialdata.dat', status='unknown')
open (16, file='finaleta.dat', status='unknown')
open (17, file='finalphi.dat', status='unknown')
open (18, file='finalanalytical.dat', status='unknown')
```

Figure D.1. Fortran code (cont.)

```
open (19, file='flatplategeometry.dat', status='unknown')
open (190, file='heavingparameter.dat', status='unknown')
open (191, file='pitchingparameter.dat', status='unknown')
open (20, file='platenodes.dat', status='unknown')
open (24, file='platecorner.dat', status='unknown',action='write')
open (26, file='intermediateetaan.csv', status='unknown',action='write')
open (21, file='intermediateetadiffract.csv', status='unknown',action='write')
open (36, file='intermediateetarad.csv', status='unknown',action='write')
open (30, file='intermediatedphidxa.csv', status='unknown',action='write')
open (31, file='intermediatedphidza.csv', status='unknown',action='write')
open (22, file='intermediatedphidxdiffract.csv', status='unknown',action='write')
open (23, file='intermediatedphidzdiffract.csv', status='unknown',action='write')
open (37, file='intermediatedphidxrad.csv', status='unknown',action='write')
open (38, file='intermediatedphidzrad.csv', status='unknown',action='write')
open (25, file='intermediatephidiffdiffract.csv', status='unknown',action='write')
open (39, file='intermediatephidiffrad.csv', status='unknown',action='write')
open (29, file='intermediatephia.csv', status='unknown',action='write')
open (27, file='intermediatephidiffract.csv', status='unknown',action='write')
open (40, file='intermediatephirad.csv', status='unknown',action='write')
```

Figure D.1. Fortran code (cont.)

```
open (28, file='meanintermediatephidiffracted.dat', status='unknown', action='write')
open (41, file='meanintermediatephirad.dat', status='unknown',action='write')
open (32, file='intermediateplatexc.csv', status='unknown',action='write')
open (33, file='intermediateplatexrbf.csv', status='unknown',action='write')
open (34, file='intermediateplatezc.csv', status='unknown',action='write')
open (35, file='intermediateplatezrbf.csv', status='unknown',action='write')
open (42, file='intermediatepitchrad.dat', status='unknown',action='write')
open (100, file='errormessages.dat', status='unknown',action='write')
read(19,*)wp
read(19,*)tp
read(19,*)zp
read(19,*)beta
read(190,*)Thetah
read(190,*)aheave
read(191,*)Thetap
read(191,*)apitch
pi=4*datan(1.d0)
dhdx=0
!=================================================
```

Figure D.1. Fortran code (cont.)

```
! Incidence Wave Data
!=====================================================
Omega=2*pi/T
lambda=d*Omega**2/g ! variable that is used to compute the wavenumber in the subroutine
call DispersionSolver(lambda, kd) ! computing wavenumber*water depth in dependence on water depth
k=kd/d
ks=dsqrt((2*dcosh(kd)**2)/(2*kd+dsinh(2*kd))) ! shoaling coefficient
HR=H0R*ks ! wave height at given depth
if (HR/d>=0.78) then
write(6,*) "Wave is broken"
stop
end if
if (kd/(2*pi)>0.5) write(14,'(/2x,"Deep Water Wave")')
if (kd/(2*pi)<0.05) write(14,'(/2x,"Shallow Water Wave")')
if(kd/(2*pi)<=0.5.and.kd/(2*pi)>=0.05) write(14,'(/2x,"Intermediate Water Wave")')
L = ((g * T**2)/(2*pi))*dtanh(kd)
c = L/T
!generating data summary
write(14,"(T2,'omega',T15,f8.4)")Omega
```

Figure D.1. Fortran code (cont.)

```
write(14,"(T2,'d/L',T15,f8.4)")kd/(2*pi)
write(14,"(T2,'kd',T15,f8.4)")kd
write(14,"(T2,'k',T15,f8.4)")k
write(14,"(T2,'Ks',T15,f8.4)")Ks
write(14,"(T2,'HR/L',T15,f8.4)")HR/L
write(14,"(T2,'T',T15,f8.4)")T
write(14,"(T2,'d',T15,f8.4)")d
write(14,"(T2,'L',T15,f8.4)")L
write(14,"(T2,'HR',T15,f8.4)")HR
write(14,"(T2,'H0R',T15,f8.4)")H0R
write(14,"(T2,'c',T15,f8.4)")c
! preliminary checks to make sure that model is applicable
if (HR/2.ge.abs(zp-tp/2))then
write(100,'(/2x,"Wave Amplitude bigger than Freeboard")')
stop
else
write(100,'(/2x,"Setup is okay")')
end if
!=============================================
```

Figure D.1. Fortran code (cont.)

```
! Geometry With Plate
!================================================
! Number of nodes in the horizontal BVP without plate (no corner nodes)
nh = nwave*nperL
! Free Surface Node placement
dx = (nwave * L)/(nh - 1)
dz = d/(nv-1)
! location of plate centre
xp=0.5*nwave*L
! nodes at flat plate
!!!!!!!!!!!!!!!!!!!!!!!!!!!!!!!!!!!!!!!!!!!!!!!!!!!!!!!!!!!!!!!!!!!!!!!!!!!!!!!!!!!!!!!!!!!!!!
! determining number of nodes on plate
deltaxp=0.5 ! predetermined horizontal node distance on plate
deltazp=0.25 ! predetermined vertical node distance on plate
if (beta.eq.90) then
deltaxp=0.25
deltazp=0.5
end if
nhp=floor(wp/deltaxp)+1
```

Figure D.1. Fortran code (cont.)

```
if (nhp.lt.2) then
nhp=2
deltaxp=wp
end if
nvp=floor(tp/deltazp)+1
if (nvp.lt.2) then
nvp=2
deltazp=tp
end if
deltaxp=wp/(nhp-1)
deltazp=tp/(nvp-1)
if (tp.eq.0) then
nvp=1
!if (beta.eq.90) then
! nvp=0
!end if
deltazp=0
end if
write(20,"(T2,'nhp',T15,i4)")nhp
```

Figure D.1. Fortran code (cont.)

```
write(20,"(T2,'nvp',T15,i4)")nvp
!!!!!!!!!!!!!!!!!!!!!!!!!!!!!!!!!!!!!!!!!!!!!!!!!!!!!!!!!!!!!!!!!!!!!!!!!!!!!!!!
! total number of nodes in BVP
n=2*(nh+nv+nhp+nvp)
print *, nwave*L
write(14,"(T3,'dx',T15,e14.7)")dx
write(14,"(T3,'dz',T15,e14.7)")dz
ndiffx1=int((xp-wp/2)/dx+3)
allocate(xc(n),zc(n),xrbf(n),zrbf(n),itype(n), diffx1(ndiffx1)) ! itype describes the location of nodes 1=surface, 2=radiation,
3=bottom, 4=incidence
allocate(xcpinitial(2*(nhp+nvp)), zcpinitial(2*(nhp+nvp)), xrbfpinitial(2*(nhp+nvp)), zrbfpinitial(2*(nhp+nvp)),
vpitch(2*(nhp+nvp)))
allocate(xcp(2*(nhp+nvp)), zcp(2*(nhp+nvp)), xrbfp(2*(nhp+nvp)), zrbfp(2*(nhp+nvp)))
!==========================================
! Input of rbf centre distance from collocation points
!==========================================
drbf1=2*HR ! free surface
if (HR.lt.0.5) then
drbf1=2! for test runs with smaller HR
```

Figure D.1. Fortran code (cont.)

```
end if
if (HR.eq.0) then
drbf1=2!*aheave
end if
drbf2=0.4 ! radiation boundary
drbf3=1.05 ! bottom - should be optimized
drbf4=0.4 ! wave incidence side
marker =0
if (nvp.eq.0) then
ds=0
else
ds=0.25 ! first and last plate nodes are moved in by ds*delatxp(deltazp)
end if
if ((nvp.eq.1).AND.(wp.gt.0.5)) then
ds=0.5
end if
!================================================
! Outer boundary nodes
!================================================
```

Figure D.1. Fortran code (cont.)

```
do i = 1,nh
itype(i) = 1
xc(i) = (i-1)*dx
zc(i) = 0
xrbf(i) = xc(i)
zrbf(i) = zc(i) + drbf1
end do
! Move first and last node in by dx/2
xc(1) = xc(1) + dx/2
xrbf(1) = xc(1)
xc(nh) = xc(nh) - dx/2
xrbf(nh) = xc(nh)
! First and last node on fs
nfsb = 1
nfse = nh
nfs = abs(nfse-nfsb) + 1
! Radiation Boundary Node placement
j = nh
do i = 1,nv
```

Figure D.1. Fortran code (cont.)

```
j = j + 1
itype(j) = 2 ! radiation boundary
xc(j) = L * nwave
zc(j) = 0 - (i-1)*dz
xrbf(j) = xc(j) + drbf2
zrbf(j) = zc(j)
end do
! Move first and last node in by ds
zc(nh+1) = zc(nh+1) - dz/2
zrbf(nh+1) = zc(nh+1)
zc(nh+nv) = zc(nh+nv) + dz/2
zrbf(nh+nv) = zc(nh+nv)
! First and last node on radiation boundary
nrsb = nfse + 1
nrse = nrsb + nv - 1
nrs = abs(nrse-nrsb) + 1
! Bottom node placement (flat bottom)
j = nh + nv
do i = 1,nh
```

Figure D.1. Fortran code (cont.)

```
j = j+1
itype(j) = 3 ! bottom boundary
xc(j) = nwave * L - (i-1)*dx
zc(j) = -d
xrbf(j) = xc(j)
zrbf(j) = zc(j) - drbf3
end do
! Move first and last node in by dx/2
xc(nh+nv+1) = xc(nh+nv+1) - dx/2
xrbf(nh+nv+1) = xc(nh+nv+1)
xc(nh+nv+nh) = xc(nh+nv+nh) + dx/2
xrbf(nh+nv+nh) = xc(nh+nv+nh)
! First and last node on bottom boundary
nbsb = nrse + 1
nbse = nbsb + nh - 1
nbs = abs(nbse-nbsb) + 1
! Wave Incidence Boundary node placement
j = nh+nv+nh
do i = 1,nv
```

Figure D.1. Fortran code (cont.)

```
j = j + 1
itype(j) = 4 ! wave incidence boundary
xc(j) = 0
zc(j) = -d + (i-1)*dz
xrbf(j) = xc(j) - drbf4
zrbf(j) = zc(j)
end do
! Move first and last node in by dz/2
zc(nh+nv+nh+1) = zc(nh+nv+nh+1) + dz/2
zrbf(nh+nv+nh+1) = zc(nh+nv+nh+1)
zc(nh+nv+nh+nv) = zc(nh+nv+nh+nv) - dz/2
zrbf(nh+nv+nh+nv) = zc(nh+nv+nh+nv)
! First and last node on wave incidence boundary
nisb = nbse + 1
nise = nisb + nv - 1
nis = abs(nise-nisb) + 1
!!!!!!!!!!!!!!!!!!!!!!!!!!!!!!!!!!!!!!!!!!!!!!!!!!!!!!!!!!!!!!!!!!!!!!!!!!!!!!!!!!!!!!!!!!!!!!!!!!!!
! Include flat plate nodes
! start with horizontal setup and perform coodinate transformation according to plate inclination angle afterwards
```

Figure D.1. Fortran code (cont.)

```
! in order to implement phase shift between incidence wave and heaving motion, the initial submergence is manipulated
! according to the intended phase shift as motion has to be about zp
!!!!!!!!!!!!!!!!!!!!!!!!!!!!!!!!!!!!!!!!!!!!!!!!!!!!!!!!!!!!!!!!!!!!!!!!!!!!!!!!!!!!!!!!!!!!!!!!!!!!!!!!!!!!!!!!!!!!!!!!!!!!!!!!!!!
nprb=0 ! this is for the case of no edge nodes
npre=0
npr=0
nplb=0
nple=0
npl=0
!**************************************************************************************
! Preparation for Heaving and Pitching Implementation
!**************************************************************************************
! determine the initial plate normals for heaving and pitching implementation
! if phase shift in pitching is present initial angle is beta + initial pitching angle
t0=0
betarad=beta*pi/180 ! originally prescribed inclination without additional inclination due to phase shift in pitching
apitch=apitch*pi/180
if (Thetap.ne.0) then
nplate=dcos(betarad+apitch*dsin(Omega*t0+Thetap-pi/2))
```

Figure D.1. Fortran code (cont.)

```
nedge=dsin(betarad+apitch*dsin(Omega*t0+Thetap-pi/2))
else
nplate=dcos(betarad)
nedge=dsin(betarad)
end if
!**************************************************************************
! determine zpinitial in dependence on phase shift of heave motion; for no phase shift between incidence and heave zpinitial=zp
zpinitial=-zp+aheave*dsin(Omega*t0+Thetah)
! determine initial plate inclination in dependence on phase shift of pitch motion; for no phase shift between incidence and
heave inclinitial=beta
inclinitial=betarad+apitch*dsin(Omega*t0+Thetap-pi/2) ! actual initial inclination - includes inclination due to shift in pitching
!**************************************************************************
!**************************************************************************
! flat plate upper side
j = nh+nv+nh+nv
j = j+1
itype(j) = 5 ! flat plate upper side
xc(j) = xp-wp/2+(i-1)*deltaxp
zc(j) = zpinitial+0.5*tp
```

Figure D.1. Fortran code (cont.)

```
xrbf(j) = xc(j)
zrbf(j) = zc(j) - drbf5
end do
! Move first and last node in by deltaxp*ds
if (nvp.ne.0) then
xc(2*(nh+nv)+1) = xc(2*(nh+nv)+1) + deltaxp*ds
xrbf(2*(nh+nv)+1) = xc(2*(nh+nv)+1)
xc(2*(nh+nv)+nhp) = xc(2*(nh+nv)+nhp) - deltaxp*ds
xrbf(2*(nh+nv)+nhp) = xc(2*(nh+nv)+nhp)
else
xc(2*(nh+nv)+nhp) = xc(2*(nh+nv)+nhp) - 0.02
xrbf(2*(nh+nv)+nhp) = xc(2*(nh+nv)+nhp)
end if
! First and last node on plate upper boundary
npub = nise + 1
npue = npub + nhp - 1
npu = abs(npue-npub) + 1
! flat plate vertical side towards Radiation Boundary
if (nvp.ne.0) then
```

Figure D.1. Fortran code (cont.)

```
j = nh+nv+nh+nv+nhp
do i = 1,nvp
j = j + 1
itype(j) = 6 ! flat plate towards radiation boundary
xc(j) = xp+wp/2
zc(j) = zpinitial+tp/2 - (i-1)*deltazp
xrbf(j) = xc(j) - drbf6
zrbf(j) = zc(j)
end do
! Move first and last node in by deltazp*ds
zc(2*(nh+nv)+nhp+1) = zc(2*(nh+nv)+nhp+1) - deltazp*ds
zrbf(2*(nh+nv)+nhp+1) = zc(2*(nh+nv)+nhp+1)
zc(2*(nh+nv)+nhp+nvp) = zc(2*(nh+nv)+nhp+nvp) + deltazp*ds
zrbf(2*(nh+nv)+nhp+nvp) = zc(2*(nh+nv)+nhp+nvp)
! First and last node on plate right boundary
nprb = npue + 1
npre = nprb + nvp - 1
npr = abs(npre-nprb) + 1
end if
```

Figure D.1. Fortran code (cont.)

```
! Flat Plate Bottom node placement
if ((nvp.eq.1).OR.(nvp.eq.0)) then
j = 2*(nh+nv)+nhp+nvp
do i = 1,nhp
j = j+1
itype(j) = 7 ! flat plate bottom boundary
xc(j) = xc(2*(nh+nv)+nhp+1-i)+0.02
zc(j) = zpinitial-0.5*tp
xrbf(j) = xc(j)
zrbf(j) = zc(j) + drbf7
end do
else
do i = 1,nhp
j = j+1
itype(j) = 7 ! flat plate bottom boundary
xc(j) = xp+wp/2-(i-1)*deltaxp
zc(j) = zpinitial-0.5*tp
xrbf(j) = xc(j)
zrbf(j) = zc(j) + drbf7
```

Figure D.1. Fortran code (cont.)

```
end do
! Move first and last node in by deltaxp*ds
xc(2*(nh+nv)+nhp+nvp+1) = xc(2*(nh+nv)+nhp+nvp+1) - deltaxp*ds
xrbf(2*(nh+nv)+nhp+nvp+1) = xc(2*(nh+nv)+nhp+nvp+1)
xc(2*(nh+nv)+nhp+nvp+nhp) = xc(2*(nh+nv)+nhp+nvp+nhp) + deltaxp*ds
xrbf(2*(nh+nv)+nhp+nvp+nhp) = xc(2*(nh+nv)+nhp+nvp+nhp)
end if
! First and last node on plate bottom boundary
if (nvp.ne.0) then
npbb = npre + 1
npbe = npbb + nhp - 1
npb = abs(npbe-npbb) + 1
else
npbb = npue + 1
npbe = npbb + nhp - 1
npb = abs(npbe-npbb) + 1
end if
! Flat Plate vertical side towards Wave Incidence Boundary
if (nvp.ne.0) then
```

Figure D.1. Fortran code (cont.)

```
j = (2*(nh+nv)+nhp+nvp+nhp)
do i = 1,nvp
j = j + 1
itype(j) = 8 ! flat plate towards wave incidence boundary
xc(j) = xp-wp/2
zc(j) = zpinitial-tp/2 + (i-1)*deltazp
xrbf(j) = xc(j) + drbf8
zrbf(j) = zc(j)
end do
! Move first and last node in by deltazp*ds
zc(2*(nh+nv)+nhp+nvp+nhp+1) = zc(2*(nh+nv)+nhp+nvp+nhp+1) + deltazp*ds
zrbf(2*(nh+nv)+nhp+nvp+nhp+1) = zc(2*(nh+nv)+nhp+nvp+nhp+1)
zc(2*(nh+nv+nhp+nvp)) = zc(2*(nh+nv+nhp+nvp)) - deltazp*ds
zrbf(2*(nh+nv+nhp+nvp)) = zc(2*(nh+nv+nhp+nvp))
! First and last node on plate left boundary
nplb = npbe + 1
nple = nplb + nvp - 1
npl = abs(nple-nplb) + 1
end if
```

Figure D.1. Fortran code (cont.)

```
! test whether plate rbf centres are too close together; if yes give error message and stop
do i = npub, n-1
do j = i+1, n
r = dsqrt((xrbf(i)-xrbf(j))**2 + (zrbf(i)-zrbf(j))**2)
if (r.lt.0.005) then
marker=1
end if
end do
end do
if ((marker.ne.0).AND.(nvp.ne.0)) then
drbf6=drbf6+0.01
!drbf8=drbf6
! flat plate vertical side towards Radiation Boundary
j = nh+nv+nh+nv+nhp
do i = 1,nvp
j = j + 1
itype(j) = 6 ! flat plate towards radiation boundary
xc(j) = xp+wp/2
zc(j) = zpinitial+tp/2 - (i-1)*deltazp
```

Figure D.1. Fortran code (cont.)

```
xrbf(j) = xc(j) - drbf6
zrbf(j) = zc(j)
end do
! Move first and last node in by deltazp*ds
zc(2*(nh+nv)+nhp+1) = zc(2*(nh+nv)+nhp+1) - deltazp*ds
zrbf(2*(nh+nv)+nhp+1) = zc(2*(nh+nv)+nhp+1)
zc(2*(nh+nv)+nhp+nvp) = zc(2*(nh+nv)+nhp+nvp) + deltazp*ds
zrbf(2*(nh+nv)+nhp+nvp) = zc(2*(nh+nv)+nhp+nvp)
! Flat Plate vertical side towards Wave Incidence Boundary
j = (2*(nh+nv)+nhp+nvp+nhp)
do i = 1,nvp
j = j + 1
itype(j) = 8 ! flat plate towards wave incidence boundary
xc(j) = xp-wp/2
zc(j) = zpinitial-tp/2 + (i-1)*deltazp
xrbf(j) = xc(j) + drbf8
zrbf(j) = zc(j)
end do
! Move first and last node in by deltazp*ds
```

Figure D.1. Fortran code (cont.)

```
zc(2*(nh+nv)+nhp+nvp+nhp+1) = zc(2*(nh+nv)+nhp+nvp+nhp+1) + deltazp*ds
zrbf(2*(nh+nv)+nhp+nvp+nhp+1) = zc(2*(nh+nv)+nhp+nvp+nhp+1)
zc(2*(nh+nv+nhp+nvp)) = zc(2*(nh+nv+nhp+nvp)) - deltazp*ds
zrbf(2*(nh+nv+nhp+nvp)) = zc(2*(nh+nv+nhp+nvp))
end if
!**********************************************************************
! perform coordinate transformation if plate is inclined
!**********************************************************************
do i=2*(nh+nv)+1,2*(nh+nv+nhp+nvp)
xcpinitial(i-2*(nh+nv))=xc(i)
xrbfpinitial(i-2*(nh+nv))=xrbf(i)
zcpinitial(i-2*(nh+nv))=zc(i)
zrbfpinitial(i-2*(nh+nv))=zrbf(i)
end do
if (inclinitial.ne.0) then
call coordtransf(nhp,nvp,inclinitial,xp,zp,xcpinitial,zcpinitial,xrbfpinitial,zrbfpinitial)
do i=2*(nh+nv)+1,2*(nh+nv+nhp+nvp)
xc(i)=xcpinitial(i-2*(nh+nv))
xrbf(i)=xrbfpinitial(i-2*(nh+nv))
```

Figure D.1. Fortran code (cont.)

```
zc(i)=zcpinitial(i-2*(nh+nv))
zrbf(i)=zrbfpinitial(i-2*(nh+nv))
end do
end if
! record the initial plate position as reference for plate motion implementation for the horizontal case
if (inclinitial.eq.0) then
do i=2*(nh+nv)+1,2*(nh+nv+nhp+nvp)
xcpinitial(i-2*(nh+nv))=xc(i)
xrbfpinitial(i-2*(nh+nv))=xrbf(i)
zcpinitial(i-2*(nh+nv))=zc(i)
zrbfpinitial(i-2*(nh+nv))=zrbf(i)
end do
end if
!*********************************************************************
! determine positions of plate corners
!*********************************************************************
if (nvp.eq.1) then
allocate (xpc(2), zpc(2))
xpc(1)=xc(2*(nh+nv)+nhp+1)
```

Figure D.1. Fortran code (cont.)

```
xpc(2)=xc(2*(nh+nv)+2*nhp+2)
zpc(1)=zc(2*(nh+nv)+nhp+1)
zpc(2)=zc(2*(nh+nv)+2*nhp+2)
! record position of plate corners
write(24,"(/T3,'no.',T10,'xpc',T26,'zpc'/)")
do i = 1,2
write(24,'(1x,i4,2(2x,e14.7))')i,xpc(i),zpc(i)
end do
! check whether highest plate edge allow for enough submergence
do i = 1,2
if ((-zpc(i)-HR/2).lt. 0.1) then
write (100,'(/2x,"not enough submergence")')
stop
end if
end do
else
allocate (xpc(4), zpc(4))
xpc(1)=xc(2*(nh+nv)+1)-deltaxp*dcos(inclinitial)*ds
xpc(2)=xc(2*(nh+nv)+nhp)+deltaxp*dcos(inclinitial)*ds
```

Figure D.1. Fortran code (cont.)

```
xpc(3)=xc(2*(nh+nv)+nhp+nvp+1)+deltaxp*dcos(inclinitial)*ds
xpc(4)=xc(2*(nh+nv+nhp)+nvp)-deltaxp*dcos(inclinitial)*ds
zpc(1)=zc(2*(nh+nv)+1)-deltaxp*dsin(inclinitial)*ds
zpc(2)=zc(2*(nh+nv)+nhp)+deltaxp*dsin(inclinitial)*ds
zpc(3)=zc(2*(nh+nv)+nhp+nvp+1)+deltaxp*dsin(inclinitial)*ds
zpc(4)=zc(2*(nh+nv+nhp)+nvp)-deltaxp*dsin(inclinitial)*ds
! record position of plate corners
write(24,"(/T3,'no.',T10,'xpc',T26,'zpc'/)")
do i = 1,4
write(24,'(1x,i4,2(2x,e14.7))')i,xpc(i),zpc(i)
end do
! check whether highest plate edge allow for enough submergence
do i = 1,4
if ((-zpc(i)-HR/2).lt. 0.1) then
write (100,'(/2x,"not enough submergence")')
stop
end if
end do
end if
```

Figure D.1. Fortran code (cont.)

```
!*****************************************************************
! record the node positioning
write(13,"(T3,'no.',T10,'xc',T26,'zc',T42,'xrbf',T58,'zrbf',T69,'type'/)")
do i = 1,2*(nh+nv+nhp+nvp)
write(13,'(1x,i4,4(2x,e14.7),2x,i1)')i,xc(i),zc(i),xrbf(i),zrbf(i),itype(i)
end do
! determine the surface node closest to the incidence side of the flat plate
do i=1,ndiffx1
diffx1(i)=abs(xc(i)-(xp-wp/2))
end do
index1=minloc(diffx1,1)-1 ! last surface node left of plate
write(20,"(T2,'index1',T15,i4)")index1
write(20,"(T2,'deltaxp',T15,f14.7)")deltaxp
write(20,"(T2,'deltazp',T15,f14.7)")deltazp
write(20,"(T2,'drbf5',T15,f14.7)")drbf5
write(20,"(T2,'drbf6',T15,f14.7)")drbf6
write(20,"(T2,'drbf7',T15,f14.7)")drbf7
write(20,"(T2,'drbf8',T15,f14.7)")drbf8
write(20,"(T2,'initial_inclination',T25,f14.7)")inclinitial
```

Figure D.1. Fortran code (cont.)

```
! test whether plate rbf centres are again too close together; if yes give error message and stop
! this is done after recording the node positioning to be able to find which rbf centres are too close
do i = npub, n-1
do j = i+1, n
r = dsqrt((xrbf(i)-xrbf(j))**2 + (zrbf(i)-zrbf(j))**2)
if (r.lt.0.005) then
write (100,'(/2x,"plate rbf centres are too close to each other")')
stop
end if
end do
end do
write (100,'(/2x,"plate rbf centres are okay")')
!*****************************************************************
! set up inner nodes close to left/right boundary for left/right boundary condition adaptation
!*****************************************************************
! determining the distance that the wave travels in one dt for correct adaptation of left/right boundary condition
dl=c*dt
allocate(xileft(nv),zileft(nv), finnerleft(nv,n))
allocate(xiright(nv),ziright(nv), finnerright(nv,n))
```

Figure D.1. Fortran code (cont.)

```
j=0
do i = 1,nv
j = j + 1
itype(j) = 10 ! left side inner nodes
xileft(j) = dl ! 1*dl right of left incidence side nodes
zileft(j) = zc(nisb+j-1) ! same z as incidence side nodes
end do
j=0
do i = 1,nv
j = j + 1
itype(j) = 30 ! right side inner nodes
xiright(j) = L * nwave-dl ! 1*dl left of right incidence side nodes
ziright(j) = zc(nrsb+j-1) ! same z as incidence side nodes
end do
! setting up the ln(r) matrices for inner nodes
do i = 1,nv
do j = 1,n
r = dsqrt((xileft(i)-xrbf(j))**2 + (zileft(i)-zrbf(j))**2)
finnerleft(i,j) = dlog(r)
```

Figure D.1. Fortran code (cont.)

```
end do
end do
do i = 1,nv
do j = 1,n
r = dsqrt((xiright(i)-xrbf(j))**2 + (ziright(i)-zrbf(j))**2)
finnerright(i,j) = dlog(r)
end do
end do
!*****************************************************************
! record the inner node positioning
write(130,"(T3,'no.',T10,'xi',T26,'zi'T42,'type'/)")
do i = 1,nv
write(130,'(1x,i4,2(2x,e14.7),2x,i2)')i,xileft(i),zileft(i),10
end do
do i = 1,nv
write(130,'(1x,i4,2(2x,e14.7),2x,i2)')i+nv,xiright(i),ziright(i),30
end do
!*****************************************************************
! Setting Up the BVP System Equations
```

Figure D.1. Fortran code (cont.)

```
!*************************************************************
allocate (etanewanalyticinc(nfs))
allocate (etaold1diffract(nfs), etaold2diffract(nfs), etaold3diffract(nfs), etadiffract(nfs), etanewdiffract(nfs))
allocate (etaold1inc(nfs), etaold2inc(nfs), etaold3inc(nfs), etainc(nfs), etanewinc(nfs))
allocate (etarad(nfs), etanewrad(nfs), etaold1rad(nfs), etaold2rad(nfs), etaold3rad(nfs))
allocate (phiold1inc(n), phiold1diffract(n), phiold1rad(n))
allocate (phiinc(n), phidiffract(n), phirad(n), phinewadapdiffract(n), phinewadapinc(n), phinewadaprad(n))
allocate (phinewdiffract(n), phinewinc(n), phinewrad(n))
allocate (phinewanalyticinc(n))
allocate (dphidxold1inc(n), dphidxold2inc(n), dphidxold3inc(n), dphidxinc(n), dphidxnewinc(n))
allocate (dphidxold1diffract(n), dphidxold2diffract(n), dphidxold3diffract(n), dphidxdiffract(n), dphidxnewdiffract(n))
allocate (dphidxold1rad(n), dphidxold2rad(n), dphidxold3rad(n), dphidxrad(n), dphidxnewrad(n))
allocate (dphidzold1inc(n), dphidzold2inc(n), dphidzold3inc(n), dphidzinc(n), dphidznewinc(n))
allocate (dphidzold1diffract(n), dphidzold2diffract(n), dphidzold3diffract(n), dphidzdiffract(n), dphidznewdiffract(n))
allocate (dphidzold1rad(n), dphidzold2rad(n), dphidzold3rad(n), dphidzrad(n), dphidznewrad(n))
allocate (f(n,n), fx(n,n), fz(n,n), finv(n,n), fxfinv(n,n), fzfinv(n,n))
allocate (Ident(n,n), Adiffract(n,n), Adiffractinv(n,n), b(n), bdiffract(n), binc(n), m1star(n,n), m2star(n,n), nstar(n,n))
allocate (Arad(n,n), Aradinv(n,n), brad(n))
allocate (Phiinnerleftinc(nv), Phiinnerleftdiffract(nv), phiinnerleftrad(nv))
```

Figure D.1. Fortran code (cont.)

```
allocate (alphadiffract(n), alphainc(n), alpharad(n))
allocate (phidiffleftdiffract(nv), phidiffrightdiffract(nv), phidiffleftrad(nv), phidiffrightrad(nv))
allocate (Phiinnerrightinc(nv), Phiinnerrightdiffract(nv), phiinnerrightrad(nv))
allocate (Phiinneranalyticleft(nv), Phiinneranalyticright(nv))
! generate identity matrix
Ident=0
do i=1,n
Ident(i,i)=1
end do
!!!!!!!!!!!!!!!!!!!!!!!!!!!!!!!!!!!!!!!!!!!!!!!!!!!!!!!!!!!!!!!!!!!!!!!!!!!!!!!!!!!!!!!!!!!!!
! LWT everywhere as initial conditions
! generate the initial conditions for t=0,-1,-2,-3 using the analytic solution
do i=1,nh
etaold1inc(i)=HR/2*dsin(k*xc(i)-Omega*(t0-dt))
etaold1diffract(i)=0
etaold1rad(i)=0
etaold2inc(i)=HR/2*dsin(k*xc(i)-Omega*(t0-2*dt))
etaold2diffract(i)=0
etaold2rad(i)=0
```

Figure D.1. Fortran code (cont.)

```
etaold3inc(i)=HR/2*dsin(k*xc(i)-Omega*(t0-3*dt))
etaold3diffract(i)=0
etaold3rad(i)=0
etainc(i)=HR/2*dsin(k*xc(i)-Omega*t0)
etadiffract(i)=0
etarad(i)=0
end do
do i=1,n
phiinc(i)=-HR/2*g/Omega*dcosh(k*(d+zc(i)))/dcosh(kd)*dcos(k*xc(i)-Omega*t0)
phidiffract(i)= 0
phirad(i)= 0
dphidxinc(i)=HR/2*Omega*dcosh(k*(d+zc(i)))/dsinh(kd)*dsin(k*xc(i)-Omega*t0)
dphidxdiffract(i)= 0
dphidxrad(i)= 0
dphidxold1inc(i)=HR/2*Omega*dcosh(k*(d+zc(i)))/dsinh(kd)*dsin(k*xc(i)-Omega*(t0-dt))
dphidxold1diffract(i)= 0
dphidxold1rad(i)= 0
dphidxold2inc(i)=HR/2*Omega*dcosh(k*(d+zc(i)))/dsinh(kd)*dsin(k*xc(i)-Omega*(t0-2*dt))
dphidxold2diffract(i)= 0
```

Figure D.1. Fortran code (cont.)

```
dphidxold2rad(i)= 0
dphidxold3inc(i)=HR/2*Omega*dcosh(k*(d+zc(i)))/dsinh(kd)*dsin(k*xc(i)-Omega*(t0-3*dt))
dphidxold3diffract(i)= 0
dphidxold3rad(i)= 0
dphidzinc(i)=-HR/2*Omega*dsinh(k*(d+zc(i)))/dsinh(kd)*dcos(k*xc(i)-Omega*t0)
dphidzdiffract(i)= 0
dphidzrad(i)= 0
dphidzold1inc(i)=-HR/2*Omega*dsinh(k*(d+zc(i)))/dsinh(kd)*dcos(k*xc(i)-Omega*(t0-dt))
dphidzold1diffract(i)= 0
dphidzold1rad(i)= 0
dphidzold2inc(i)=-HR/2*Omega*dsinh(k*(d+zc(i)))/dsinh(kd)*dcos(k*xc(i)-Omega*(t0-2*dt))
dphidzold2diffract(i)= 0
dphidzold2rad(i)= 0
dphidzold3inc(i)=-HR/2*Omega*dsinh(k*(d+zc(i)))/dsinh(kd)*dcos(k*xc(i)-Omega*(t0-3*dt))
dphidzold3diffract(i)= 0
dphidzold3rad(i)= 0
end do
!!!!!!!!!!!!!!!!!!!!!!!!!!!!!!!!!!!!!!!!!!!!!!!!!!!!!!!!!!!!!!!!!!!!!!!!!!!!!!!!!!!!!!!!!!!!!!
! record the initial conditions
```

Figure D.1. Fortran code (cont.)

```
write(15,'(/T2,a18)')"Initial conditions"
write(15,'(/T4,a1,T9,a6,T25,a6)')"i","phiinc","etainc"
do i=1,n
if(i.le.nfse)then
write(15,'(i4,T6,f16.7,T23,f11.7)')i,phiinc(i),etainc(i)
else
write(15,'(i4,T6,f16.7)')i,phiinc(i)
end if
end do
if (apitch.eq.0) then
pitchrad=0
end if
! if no heaving and pitching is present, the distance, rbf and system matrices have to be set up only once and only betarad is used
if ((aheave.eq.0).AND.(apitch.eq.0)) then
! generate the initial distance matrix r, the initial f=ln(r) matrix and the initial derivative matrices fx and fz
do i = 1,n
do j = 1,n
r = dsqrt((xc(i)-xrbf(j))**2 + (zc(i)-zrbf(j))**2)
f(i,j) = dlog(r)
```

Figure D.1. Fortran code (cont.)

```
fx(i,j) = (xc(i)-xrbf(j))/(r*r)
fz(i,j) = (zc(i)-zrbf(j))/(r*r)
end do
end do
call invertSVD(n,f,finv)
! Generate the initial derivative operators fxfinv and fzfinv
call dgemm('N','N',n,n,n,1.d0,fx,n,finv,n,0.d0,fxfinv,n)
call dgemm('N','N',n,n,n,1.d0,fz,n,finv,n,0.d0,fzfinv,n)
! generate the initial system matrix elements
nstar=fxfinv*dcos(betarad)+fzfinv*dsin(betarad) ! prepare the elements of A matrix for originally vertical plate boundaries
m2star=-fxfinv*dsin(betarad)+fzfinv*dcos(betarad) ! prepare the elements of A matrix for originally horizontal plate boundaries
m1star=fzfinv ! prepare the elements of A matrix for bottom nodes
! elements of A matrix
Adiffract=0
! at free surface (nodes 1-nh)
do i = nfsb,nfse
Adiffract(i,i) = 1
end do
! at radiation boundary (nodes nh+1 - nh+nv)
```

Figure D.1. Fortran code (cont.)

```
do i = nrsb,nrse
Adiffract(i,i) = 1
end do
! at bottom boundary
do i = nbsb,nbse
do j = 1,n
Adiffract(i,j) = -m1star(i,j)
end do
end do
! at incidence boundary
do i = nisb,nise
Adiffract(i,i) = 1
end do
! at plate boundaries
do i = npub,npue
do j = 1,n
Adiffract(i,j) = m2star(i,j) ! upper plate boundary
end do
end do
```

Figure D.1. Fortran code (cont.)

```
do i = npbb,npbe
do j = 1,n
Adiffract(i,j) = m2star(i,j) ! lower plate boundary
end do
end do
if (nvp.ne.0) then
do i = nprb,npre
do j = 1,n
Adiffract(i,j) = nstar(i,j) ! flat plate boundary towards radiation
end do
end do
do i = nplb,nple
do j = 1,n
Adiffract(i,j) = nstar(i,j) ! flat plate boundary towards incidence
end do
end do
end if
!*****************************************************************
! Invert the initial system matrix
```

Figure D.1. Fortran code (cont.)

```
call invertSVD(n,Adiffract,Adiffractinv)
Arad=Adiffract
Aradinv=Adiffractinv
end if
!**********************************************************************
!**********************************************************************
! condition vector for bottom nodes
!**********************************************************************
! elements of b vector
binc(nbsb:nbse) = 0 ! condition vector on bottom is zero
bdiffract(nbsb:nbse) = 0 ! condition vector on bottom is zero
brad(nbsb:nbse) = 0 ! condition vector on bottom is zero
!**********************************************************************
!**********************************************************************
! set up the time vector for data recording
nprint=T/dtprint*noperiods
allocate (reftime(nprint))
ip=1
do i=1,nprint
```

Figure D.1. Fortran code (cont.)

```
reftime(i)=dtprint/dt*i
end do
!*********************************************************************
!*********************************************************************
! intermediate Etas and Phis
!*********************************************************************
allocate (intetadiffract(nh,nprint), intdphidxdiffract(n,nprint), intdphidzdiffract(n,nprint), intetainc(nh,nprint),
intdphidxinc(n,nprint), intdphidzinc(n,nprint))
allocate (intphidiffract(n,nprint), intphiinc(n,nprint), intphidiffdiffract(nv+nv,nprint), intmeanphidiffract(nprint),
intmeanphirad(nprint))
allocate (intetarad(nh,nprint), intphirad(n,nprint), intdphidxrad(n,nprint), intdphidzrad(n,nprint), intphidiffrad(nv+nv,nprint))
allocate (intxc(2*(nvp+nhp),nprint), intzc(2*(nvp+nhp),nprint), intxrbf(2*(nvp+nhp),nprint), intzrbf(2*(nvp+nhp),nprint))
allocate (intpitchrad(nprint))
! to be able to retrieve the data in the case of aborted test run (e.g. eta and phi values become insensible)
! all intermediate data are set zero at the start, that avoids NaN values when no more data is written
intetainc=0
intphiinc=0
intdphidxinc=0
intdphidzinc=0
```

Figure D.1. Fortran code (cont.)

```
intmeanphidiffract=0
intmeanphirad=0
intetadiffract=0
intphidiffract=0
intdphidxdiffract=0
intdphidzdiffract=0
intphidiffdiffract=0
intetarad=0
intphirad=0
intdphidxrad=0
intdphidzrad=0
intphidiffrad=0
intxc=0
intzc=0
intxrbf=0
intzrbf=0
! determine the difference at inner nodes next to left incidence boundary for initial time
do i = 1,nv
phidiffleftdiffract(i)= 0 ! no initial left-going wave due to reflection
```

Figure D.1. Fortran code (cont.)

```
phidiffleftrad(i)= 0 ! no initial left-going wave due to radiation
end do
! determine the difference at inner nodes next to right incidence boundary for initial time
do i = 1,nv
phidiffrightdiffract(i)=0 ! no initial right-going wave due to reflection
phidiffrightrad(i)=0 ! no initial right-going wave due to radiation
end do
phinewadapinc=0
phinewadapdiffract=0
phinewadaprad=0
phiinnerrightdiffract=0
phiinnerrightinc=0
phiinnerrightrad=0
phiinnerleftdiffract=0
phiinnerleftinc=0
phiinnerleftrad=0
xcp=0
zcp=0
xrbfp=0
```

Figure D.1. Fortran code (cont.)

```
zrbfp=0
!*****************************************************************
! Time Integration Using AB O(4)
!*****************************************************************
do it=1,T/dt*noperiods
write(6,*)it
!*****************************************************************
! (1) Update plate node positions by using the prescribed heave and pitch motion equations
!*****************************************************************
! if heave and pitch are present - heave only for horizontal and inclined but not for vertical plate
! plate motions are introduced over 5T
if (it< 5*T/dt+1) then
factorm=it*dt/(5*T)
end if
!factorm=1
if ((aheave.ne.0).OR.(apitch.ne.0)) then
do i=1,2*(nhp+nvp)
xcp(i)=xcpinitial(i)
zcp(i)=zcpinitial(i)
```

Figure D.1. Fortran code (cont.)

```
xrbfp(i)=xrbfpinitial(i)
zrbfp(i)=zrbfpinitial(i)
end do
! first do coordinate transformation to implement pitching motion from initial plate location
! determine the current pitching angle in relation to initial inclination angle
if (apitch.ne.0) then
pitchrad= (betarad+apitch*dsin(Omega*(t0+it*dt)+Thetap-pi/2)-inclinitial)*factorm
call coordtransf(nhp,nvp,pitchrad,xp,zp,xcp,zcp,xrbfp,zrbfp)
end if
! now add heave motion
do j=npub,npue ! plate top
xc(j) = xcp(j-npub+1)
zc(j) = zcp(j-npub+1) + aheave*(dsin(Omega*(t0+it*dt)+Thetah)-dsin(Omega*t0+Thetah))*factorm
xrbf(j) = xrbfp(j-npub+1)
zrbf(j) = zrbfp(j-npub+1) + aheave*(dsin(Omega*(t0+it*dt)+Thetah)-dsin(Omega*t0+Thetah))*factorm
end do
do j=npbb,npbe ! plate bottom
xc(j) = xcp(j-npub+1)
zc(j) = zcp(j-npub+1) + aheave*(dsin(Omega*(t0+it*dt)+Thetah)-dsin(Omega*t0+Thetah))*factorm
```

Figure D.1. Fortran code (cont.)

```
xrbf(j) = xrbfp(j-npub+1)
zrbf(j) = zrbfp(j-npub+1) + aheave*(dsin(Omega*(t0+it*dt)+Thetah)-dsin(Omega*t0+Thetah))*factorm
end do
if (nvp.ne.0) then
do j=nprb,npre ! plate radiation side
xc(j) = xcp(j-npub+1)
zc(j) = zcp(j-npub+1) + aheave*(dsin(Omega*(t0+it*dt)+Thetah)-dsin(Omega*t0+Thetah))*factorm
xrbf(j) = xrbfp(j-npub+1)
zrbf(j) = zrbfp(j-npub+1) + aheave*(dsin(Omega*(t0+it*dt)+Thetah)-dsin(Omega*t0+Thetah))*factorm
end do
do j=nplb,nple ! plate incidence side
xc(j) = xcp(j-npub+1)
zc(j) = zcp(j-npub+1) + aheave*(dsin(Omega*(t0+it*dt)+Thetah)-dsin(Omega*t0+Thetah))*factorm
xrbf(j) = xrbfp(j-npub+1)
zrbf(j) = zrbfp(j-npub+1) + aheave*(dsin(Omega*(t0+it*dt)+Thetah)-dsin(Omega*t0+Thetah))*factorm
end do
end if
!*************************************************
! (2) Updating f, fx and fz when Heaving and/or Pitching is present
```

Figure D.1. Fortran code (cont.)

```
! generate the new distance matrix r, the new f=ln(r) matrix and the new derivative matrices fx and fz
do i = 1,n
do j = 1,n
r = dsqrt((xc(i)-xrbf(j))**2 + (zc(i)-zrbf(j))**2)
f(i,j) = dlog(r)
fx(i,j) = (xc(i)-xrbf(j))/(r*r)
fz(i,j) = (zc(i)-zrbf(j))/(r*r)
end do
end do
call invertSVD(n,f,finv)
! Generate the new derivative operators fxfinv and fzfinv
call dgemm('N','N',n,n,n,1.d0,fx,n,finv,n,0.d0,fxfinv,n)
call dgemm('N','N',n,n,n,1.d0,fz,n,finv,n,0.d0,fzfinv,n)
!*****************************************************
! generate the new system matrix elements - here the current plate inclination for plate normals are needed!!!
nstar=fxfinv*dcos(inclinitial+pitchrad)+fzfinv*dsin(inclinitial+pitchrad) ! prepare the elements of A matrix for originally
vertical plate boundaries
m2star=-fxfinv*dsin(inclinitial+pitchrad)+fzfinv*dcos(inclinitial+pitchrad) ! prepare the elements of A matrix for originally
horizontal plate boundaries
```

Figure D.1. Fortran code (cont.)

```
m1star=fzfinv ! prepare the elements of A matrix for bottom nodes
! elements of A matrix
Adiffract=0
! at free surface (nodes 1-nh)
do i = nfsb,nfse
Adiffract(i,i) = 1
end do
! at radiation boundary (nodes nh+1 - nh+nv)
do i = nrsb,nrse
Adiffract(i,i) = 1
end do
! at bottom boundary
do i = nbsb,nbse
do j = 1,n
Adiffract(i,j) = -m1star(i,j)
end do
end do
! at incidence boundary
do i = nisb,nise
```

Figure D.1. Fortran code (cont.)

```
Adiffract(i,i) = 1
end do
! at plate boundaries
do i = npub,npue
do j = 1,n
Adiffract(i,j) = m2star(i,j) ! upper plate boundary
end do
end do
do i = npbb,npbe
do j = 1,n
Adiffract(i,j) = m2star(i,j) ! lower plate boundary
end do
end do
if (nvp.ne.0) then
do i = nprb,npre
do j = 1,n
Adiffract(i,j) = nstar(i,j) ! flat plate boundary towards radiation
end do
end do
```

Figure D.1. Fortran code (cont.)

```
do i = nplb,nple
do j = 1,n
Adiffract(i,j) = nstar(i,j) ! flat plate boundary towards incidence
end do
end do
end if
!*********************************************************
! Invert the new system matrix
call invertSVD(n,Adiffract,Adiffractinv)
Arad=Adiffract
Aradinv=Adiffractinv
end if
! (3) Generating new analytical solution for incidence wave
do i = 1,n
phinewanalyticinc(i)=-HR/2*g/Omega*dcosh(k*(d+zc(i)))/dcosh(kd)*dcos(k*xc(i)-Omega*(t0+it*dt))
dphidxnewinc(i)=HR/2*Omega*dcosh(k*(d+zc(i)))/dsinh(kd)*dsin(k*xc(i)-Omega*(t0+it*dt))
dphidznewinc(i)=-HR/2*Omega*dsinh(k*(d+zc(i)))/dsinh(kd)*dcos(k*xc(i)-Omega*(t0+it*dt))
end do
!*********************************************************
```

Figure D.1. Fortran code (cont.)

```
! (4) Adapting the velocity potentials for scattered wave (diffraction and radiation) on lateral boundaries
! adapting the left boundary velocity potential with the inner Phi value
do i=nisb,nise
phinewadapdiffract(i)=phidiffleftdiffract(i-nisb+1) ! represents the left-going wave due to reflection from plate
phinewadaprad(i)=phidiffleftrad(i-nisb+1) ! represents the left-going wave due to radiation from plate
end do
! adapting the right boundary velocity potential with inner Phi value
do i=nrsb,nrse
phinewadapdiffract(i)=phidiffrightdiffract(i-nrsb+1) ! represents the right-going wave due to diffraction from plate
phinewadaprad(i)=phidiffrightrad(i-nrsb+1) ! represents the right-going wave due to radiation from plate
end do
! (5) generating the condition vector b at time step i+1
! ********************************************************
! Update vector b for left domain boundary using 2wABC
do i = nisb,nise
phinewdiffract(i)=phinewadapdiffract(i)
bdiffract(i)=phinewadapdiffract(i)
phinewrad(i)=phinewadaprad(i)
brad(i)=phinewadaprad(i)
```

Figure D.1. Fortran code (cont.)

```
end do
! Update vector b for free surface - computing phi and eta using AB predictor O(4)
do i=nfsb,nfse
etanewdiffract(i)=etadiffract(i)+dt/24*(55*dphidzdiffract(i)-59*dphidzold1diffract(i)+37*dphidzold2diffract(i)
-9*dphidzold3diffract(i))
phinewdiffract(i)=phidiffract(i)-g*dt/24*(55*etadiffract(i)-59*etaold1diffract(i)+37*etaold2diffract(i)-9*etaold3diffract(i))
bdiffract(i)=phinewdiffract(i)
etanewrad(i)=etarad(i)+dt/24*(55*dphidzrad(i)-59*dphidzold1rad(i) +37*dphidzold2rad(i)-9*dphidzold3rad(i))
phinewrad(i)=phirad(i)-g*dt/24*(55*etarad(i)-59*etaold1rad(i)+37*etaold2rad(i)-9*etaold3rad(i))
brad(i)=phinewrad(i)
end do
! Update vector b for right domain boundary using 2wABC
do i=nrsb,nrse
phinewdiffract(i)=phinewadapdiffract(i)
bdiffract(i)=phinewadapdiffract(i)
phinewrad(i)=phinewadaprad(i)
brad(i)=phinewadaprad(i)
end do
! Update vector bdiffract for all plate boundaries using analytical dPhidxnewinc and dPhidznewinc
```

Figure D.1. Fortran code (cont.)

```
! Plate is at position of time step (n)
! Plate is introduced slowly over 5T to avoid oscillations
if (it<5*T/dt+1) then
factor=it*dt/(5*T)
end if
!factor=1
do i=npub,npue ! plate top
bdiffract(i)=(-dphidznewinc(i)*dcos(inclinitial+pitchrad)+dphidxnewinc(i)* dsin(inclinitial+pitchrad))*factor
end do
do i=npbb,npbe ! plate bottom
bdiffract(i)=(-dphidznewinc(i)*dcos(inclinitial+pitchrad)+dphidxnewinc(i)* dsin(inclinitial+pitchrad))*factor
end do
if (nvp.ne.0) then
do i=nprb,npre ! plate radiation side
bdiffract(i)=(-dphidznewinc(i)*dsin(inclinitial+pitchrad)-dphidxnewinc(i)* dcos(inclinitial+pitchrad))*factor
end do
do i=nplb,nple ! plate incidence side
bdiffract(i)=(-dphidznewinc(i)*dsin(inclinitial+pitchrad)-dphidxnewinc(i)* dcos(inclinitial+pitchrad))*factor
end do
```

Figure D.1. Fortran code (cont.)

```
end if
! Update vector brad for all plate boundaries using prescribed plate velocity for heaving and pitching
! vertical velocity due to heaving
vheave= Omega*aheave*dcos(Omega*(t0+it*dt)+Thetah)*factorm
! angular velocity due to pitching
vpitchang=Omega*apitch*dcos(Omega*(t0+it*dt)+Thetap-pi/2)*factorm
do i = 1,2*(nhp+nvp)
dummy=sqrt((xc(2*(nh+nv)+i)-xp)**2)
if (dummy.eq.0) then
dummy=1
end if
vpitch(i)=vpitchang*sqrt((xc(2*(nh+nv)+i)-xp)**2+(zc(2*(nh+nv)+i)+zp)**2)* (xc(2*(nh+nv)+i)-xp)/dummy
end do
do i=1,nvp
vpitch(nhp+i)=0
vpitch(2*nhp+nvp+i)=0 ! normal velocities on edge nodes due to pitching is always zero!!!
end do
! Plate motion is introduced slowly over 5T to avoid oscillations - determining the normal velocity on plate
! as plate pitches, plate normal depends on pitch and initial inclination angle
```

Figure D.1. Fortran code (cont.)

```
do i=npub,npue ! plate top
brad(i)=vheave*dcos(inclinitial+pitchrad)+vpitch(i-npub+1)
end do
do i=npbb,npbe ! plate bottom
brad(i)=vheave*dcos(inclinitial+pitchrad)+vpitch(i-npub+1)
end do
if (nvp.ne.0) then
do i=nprb,npre ! plate radiation side
brad(i)=vheave*dsin(inclinitial+pitchrad)+vpitch(i-npub+1)
end do
do i=nplb,nple ! plate incidence side
brad(i)=vheave*dsin(inclinitial+pitchrad)+vpitch(i-npub+1)
end do
end if
! ****************************************************************
! (6) Compute the new velocity potentials phinew at time step i+1
call dgemv ( 'N', n, n, 1.d0, Adiffractinv, n, bdiffract, 1,0.d0,phinewdiffract, 1 )
call dgemv ( 'N', n, n, 1.d0, Aradinv, n, brad, 1,0.d0,phinewrad, 1 )
! ****************************************************************
```

Figure D.1. Fortran code (cont.)

```
! (7) Restore Dirichlet conditions
phinewdiffract(nfsb:nfse) = bdiffract(nfsb:nfse) ! at free surface use the with time stepping computed potential
phinewdiffract(nisb:nise) = bdiffract(nisb:nise) ! at left incidence boundary adapted analytical solution
phinewdiffract(nrsb:nrse) = bdiffract(nrsb:nrse) ! at radiation boundary with adapted solution
phinewrad(nfsb:nfse) = brad(nfsb:nfse) ! at free surface use the with time stepping computed potential
phinewrad(nisb:nise) = brad(nisb:nise) ! at left incidence boundary adapted analytical solution
phinewrad(nrsb:nrse) = brad(nrsb:nrse) ! at radiation boundary with adapted solution
!=============================================
! Determine the mean of the surface and bottom Phis (for checking whether shift in phi exist)
meanPhidiffract=(sum(phinewdiffract(nfsb:nfse))+sum(phinewdiffract (nbsb:nbse))) /(2*nh)
meanPhirad=(sum(phinewrad(nfsb:nfse))+sum (phinewrad(nbsb:nbse))) /(2*nh)
!=============================================
! (8) Determine derivatives of phinew: dphidxnew and dphidznew
call dgemv ( 'N', n, n, 1.d0, fzfinv, n, phinewdiffract, 1,0.d0,dphidznewdiffract, 1 )
call dgemv ( 'N', n, n, 1.d0, fxfinv, n, phinewdiffract, 1,0.d0,dphidxnewdiffract, 1 )
call dgemv ( 'N', n, n, 1.d0, fzfinv, n, phinewrad, 1,0.d0,dphidznewrad, 1 )
call dgemv ( 'N', n, n, 1.d0, fxfinv, n, phinewrad, 1,0.d0,dphidxnewrad, 1 )
! (9) Restore Neumann Condition on Plate Nodes
! horizontal plate and no pitching, heaving can be present
```

Figure D.1. Fortran code (cont.)

```
if ((beta.eq.0).AND.(apitch.eq.0)) then
dphidznewdiffract(npub:npue)= -dphidznewinc(npub:npue)*factor ! plate top
dphidxnewdiffract(npub:npue)=0
dphidznewdiffract(npbb:npbe)= -dphidznewinc(npbb:npbe)*factor ! plate bottom
dphidxnewdiffract(npbb:npbe)=0
dphidznewrad(npub:npue)=brad(npub:npue) ! prescribed vertical velocity plate top
dphidxnewrad(npub:npue)=0 ! no motion parallel to plate
dphidznewrad(npbb:npbe)=brad(npbb:npbe) ! prescribed vertical velocity plate bottom
dphidxnewrad(npbb:npbe)=0 ! no motion parallel to plate
if (nvp.ne.0) then
dphidxnewdiffract(nprb:npre)= -dphidxnewinc(nprb:npre)*factor ! plate radiation side
dphidznewdiffract(nprb:npre)=0
dphidxnewdiffract(nplb:nple)= -dphidxnewinc(nplb:nple)*factor ! plate incidence side
dphidznewdiffract(nplb:nple)=0
dphidxnewrad(nprb:npre)=brad(nprb:npre) ! prescribed horizontal velocity plate right edge = 0
dphidxnewrad(nplb:nple)=brad(nplb:nple) ! prescribed horizontal velocity plate left edge = 0
end if
end if
! Vertical plate and no pitching
```

Figure D.1. Fortran code (cont.)

```
if ((beta.eq.90).AND.(apitch.eq.0)) then
dphidxnewdiffract(npub:npue)= -dphidxnewinc(npub:npue)*factor ! plate top facing towards incidence side
dphidznewdiffract(npub:npue)=0
dphidxnewdiffract(npbb:npbe)= -dphidxnewinc(npbb:npbe)*factor ! plate bottom facing towards radiation side
dphidznewdiffract(npbb:npbe)=0
dphidxnewrad(npub:npue)=brad(npub:npue) ! prescribed horizontal velocity plate top facing towards incidence side= 0
dphidxnewrad(npbb:npbe)=brad(npbb:npbe) ! prescribed horizontal velocity plate bottom facing towards radiation side= 0
if (nvp.ne.0) then
dphidznewdiffract(nprb:npre)= -dphidznewinc(nprb:npre)*factor ! plate radiation side facing towards surface
dphidxnewdiffract(nprb:npre)=0
dphidznewdiffract(nplb:nple)= -dphidznewinc(nplb:nple)*factor ! plate incidence side facing towards bottom
dphidxnewdiffract(nplb:nple)=0
dphidznewrad(nprb:npre)=brad(nprb:npre) ! prescribed vertical velocity plate top edge
dphidznewrad(nplb:nple)=brad(nplb:nple) ! prescribed vertical velocity plate bottom edge
end if
end if
! inclined flat plate with or without pitching/heaving
if ((beta.ne.0).OR.(apitch.ne.0)) then
dphidznewdiffract(npub:npue)= bdiffract(npub:npue)*dcos(inclinitial+pitchrad) ! plate top
```

Figure D.1. Fortran code (cont.)

```
dphidxnewdiffract(npub:npue)= -bdiffract(npub:npue)*dsin(inclinitial+pitchrad) ! plate top
dphidznewdiffract(npbb:npbe)= bdiffract(npbb:npbe)*dcos(inclinitial+pitchrad) ! plate bottom
dphidxnewdiffract(npbb:npbe)= -bdiffract(npbb:npbe)*dsin(inclinitial+pitchrad) ! plate bottom
dphidznewrad(npub:npue)=brad(npub:npue)*dcos(inclinitial+pitchrad) ! vertical velocity plate top determined from
prescribed normal velocity
dphidznewrad(npbb:npbe)=brad(npbb:npbe)*dcos(inclinitial+pitchrad) ! vertical velocity plate bottom determined from
prescribed normal velocity
dphidxnewrad(npub:npue)=-brad(npub:npue)*dsin(inclinitial+pitchrad) ! horizontal velocity plate top determined from
prescribed normal velocity
dphidxnewrad(npbb:npbe)=-brad(npbb:npbe)*dsin(inclinitial+pitchrad) ! horizontal velocity plate bottom determined from
prescribed normal velocity
if (nvp.ne.0) then
dphidxnewdiffract(nprb:npre)= bdiffract(nprb:npre)*dcos(inclinitial+pitchrad) ! plate radiation side
dphidznewdiffract(nprb:npre)= bdiffract(nprb:npre)*dsin(inclinitial+pitchrad) ! plate radiation side
dphidxnewdiffract(nplb:nple)= bdiffract(nplb:nple)*dcos(inclinitial+pitchrad) ! plate incidence side
dphidznewdiffract(nplb:nple)= bdiffract(nplb:nple)*dsin(inclinitial+pitchrad) ! plate incidence side
dphidznewrad(nprb:npre)=brad(nprb:npre)*dsin(inclinitial+pitchrad) ! vertical velocity plate right edge determined from
prescribed normal velocity
dphidznewrad(nplb:nple)=brad(nplb:nple)*dsin(inclinitial+pitchrad) ! vertical velocity plate left edge determined
```

Figure D.1. Fortran code (cont.)

```
from prescribed normal velocity
dphidxnewrad(nprb:npre)=brad(nprb:npre)*dcos(inclinitial+pitchrad) ! horizontal velocity plate right edge determined from
prescribed normal velocity
dphidxnewrad(nplb:nple)=brad(nplb:nple)*dcos(inclinitial+pitchrad) ! horizontal velocity plate left edge determined from
prescribed normal velocity
end if
end if
! ************************************************************
! correcting the shift in Phirad
phinewrad=phinewrad-meanPhirad
! correcting the shift in Phidiffract for moving plate
if ((aheave.ne.0).OR.(apitch.ne.0)) then
phinewdiffract=phinewdiffract-meanPhidiffract
end if
! ************************************************************
! (10) Computation of inner Phis and adaptation of boundary potentials for 2wABC
! compute the alphas for computation of inner nodes Phi close to left/right boundary - boundary condition adaptation
call dgemv ( 'N', n, n, 1.d0, finv, n, phinewdiffract, 1,0.d0,alphadiffract, 1 )
call dgemv ( 'N', n, n, 1.d0, finv, n, phinewrad, 1,0.d0,alpharad, 1 )
```

Figure D.1. Fortran code (cont.)

```
! compute the inner Phis at nodes close to right boundary
call dgemv ( 'N', nv, n, 1.d0, Finnerright, nv, alphadiffract, 1,0.d0,Phiinnerrightdiffract, 1 )
call dgemv ( 'N', nv, n, 1.d0, Finnerright, nv, alpharad, 1,0.d0,Phiinnerrightrad, 1 )
! compute the inner Phis at nodes close to left boundary
call dgemv ( 'N', nv, n, 1.d0, Finnerleft, nv, alphadiffract, 1,0.d0,Phiinnerleftdiffract, 1 )
call dgemv ( 'N', nv, n, 1.d0, Finnerleft, nv, alpharad, 1,0.d0,Phiinnerleftrad, 1 )
! adapt the incidence boundary phi by using the left inner phi of time step n-1
do i = 1,nv
phidiffleftdiffract(i)=Phiinnerleftdiffract(i) ! represents the left going wave at inner left nodes
phidiffleftrad(i)=Phiinnerleftrad(i) ! represents the left going wave at inner left nodes
end do
! adapt the radiation boundary phi by using the right inner phi of time step n-1
do i = 1,nv
phidiffrightdiffract(i)=Phiinnerrightdiffract(i) ! phidiffrightdiffract represents the right going wave at inner right nodes
phidiffrightrad(i)=Phiinnerrightrad(i) ! phidiffrightrad represents the right going wave at inner right nodes
end do
! (11) Downshift solutions in time
!phiold1inc=phiinc
phiold1diffract=phidiffract
```

Figure D.1. Fortran code (cont.)

```
phiold1rad=phirad
!phiinc=phinewinc
phidiffract=phinewdiffract
phirad=phinewrad
!etaold3inc=etaold2inc
etaold3diffract=etaold2diffract
etaold3rad=etaold2rad
!etaold2inc=etaold1inc
etaold2diffract=etaold1diffract
etaold2rad=etaold1rad
! etaold1inc=etainc
etaold1diffract=etadiffract
etaold1rad=etarad
! etainc=etanewinc
etadiffract=etanewdiffract
etarad=etanewrad
! dphidxold3inc=dphidxold2inc
dphidxold3diffract=dphidxold2diffract
dphidxold3rad=dphidxold2rad
```

Figure D.1. Fortran code (cont.)

```
! dphidxold2inc=dphidxold1inc
dphidxold2diffract=dphidxold1diffract
dphidxold2rad=dphidxold1rad
! dphidxold1inc=dphidxinc
dphidxold1diffract=dphidxdiffract
dphidxold1rad=dphidxrad
! dphidxinc=dphidxnewinc
dphidxdiffract=dphidxnewdiffract
dphidxrad=dphidxnewrad
! dphidzold3inc=dphidzold2inc
dphidzold3diffract=dphidzold2diffract
dphidzold3rad=dphidzold2rad
! dphidzold2inc=dphidzold1inc
dphidzold2diffract=dphidzold1diffract
dphidzold2rad=dphidzold1rad
! dphidzold1inc=dphidzinc
dphidzold1diffract=dphidzdiffract
dphidzold1rad=dphidzrad
! dphidzinc=dphidznewinc
```

Figure D.1. Fortran code (cont.)

```
dphidzdiffract=dphidznewdiffract
dphidzrad=dphidznewrad
!*****************************************************
! record the intermediate values of Eta and Phi at certain time intervals for future reference
! if plate motion is present record plate position
if (it==reftime(ip)) then
! generate intermediate analytic etas for error analysis
do i=1,nh
etanewanalyticinc(i)=HR/2*dsin(k*xc(i)-Omega*(t0+it*dt))
end do
! record the intermdiate data in arrays int...
intetadiffract(:,ip)=etadiffract ! numerical etas
intetainc(:,ip)=etanewanalyticinc ! analytical etas
intetarad(:,ip)=etanewrad ! analytical etas
intphidiffdiffract(1:nv,ip)=phidiffleftdiffract ! difference in phi that is used to modify the left bc
intphidiffdiffract(nv+1:nv+nv,ip)=phidiffrightdiffract ! difference in phi that is used to modify the right bc
intphidiffrad(1:nv,ip)=phidiffleftrad ! difference in phi that is used to modify the left bc
intphidiffrad(nv+1:nv+nv,ip)=phidiffrightrad ! difference in phi that is used to modify the right bc
intphidiffract(:,ip)=phidiffract ! numerical phis
```

Figure D.1. Fortran code (cont.)

```
intphiinc(:,ip)=phinewanalyticinc ! analytical phis (incidence wave)
intphirad(:,ip)=phirad ! radiation phis
intmeanphidiffract(ip)=meanPhidiffract
intmeanphirad(ip)=meanPhirad
! record the intermediate numerical dphidxs and dphidzs in intdphidx and intdphidz
intdphidxdiffract(:,ip)=dphidxnewdiffract
intdphidzdiffract(:,ip)=dphidznewdiffract
intdphidxinc(:,ip)=dphidxnewinc
intdphidzinc(:,ip)=dphidznewinc
intdphidxrad(:,ip)=dphidxnewrad
intdphidzrad(:,ip)=dphidznewrad
! record the intermediate plate position in intxc, intzc, intxrbf and intzrbf
intxc(1:2*(nhp+nvp),ip)=xc(2*(nh+nv)+1:n)
intzc(1:2*(nhp+nvp),ip)=zc(2*(nh+nv)+1:n)
intxrbf(1:2*(nhp+nvp),ip)=xrbf(2*(nh+nv)+1:n)
intzrbf(1:2*(nhp+nvp),ip)=zrbf(2*(nh+nv)+1:n)
intpitchrad(ip)=pitchrad
if (ip<nprint) then
ip=ip+1
```

Figure D.1. Fortran code (cont.)

```
end if
end if
! ************************************************************
! checking the value of eta to avoid unnecessary computations if the data become ridiculously high
! here an eta of more than 3 times the wave height HR + HL is used
if (maxval(etadiffract)>3*HR) exit
if (minval(etadiffract)<-3*HR) exit
end do
!************************************************************
! Time integration finished
!************************************************************
! record the intermediate values of eta, dPhidx and dPhidz at certain time intervals for future reference
write(26,'(/T2,a40, f8.3,a1)')"Intermediate Analytic Eta Values every ", reftime(1)*dt,'s'
write(26,'(a4,< nprint >(3x,f16.8))')"Time",reftime*dt
do i=1,nfse
write(26,'(i4,< nprint >(3x,f16.8))')i,intetainc(i,:)
end do
write(21,'(/T2,a30, f8.3,a1)')"Intermediate Eta Values every ", reftime(1)*dt,'s'
write(21,'(a4,< nprint >(3x,f16.8))')"Time",reftime*dt
```

Figure D.1. Fortran code (cont.)

```
do i=1,nfse
write(21,'(i4,< nprint >(3x,f16.8))')i,intetadiffract(i,:)
end do
write(36,'(/T2,a30, f8.3,a1)')"Intermediate Eta Values every ", reftime(1)*dt,'s'
write(36,'(a4,< nprint >(3x,f16.8))')"Time",reftime*dt
do i=1,nfse
write(36,'(i4,< nprint >(3x,f16.8))')i,intetarad(i,:)
end do
write(30,'(/T2,a50, f8.3,a1)')"Intermediate incidence dPhidx Values every ", reftime(1)*dt,'s'
write(30,'(a4,< nprint >(3x,f16.8))')"Time",reftime*dt
do i=1,n
write(30,'(i4,< nprint >(3x,f16.8))')i,intdphidxinc(i,:)
end do
write(22,'(/T2,a36, f8.3,a1)')"Intermediate dPhidx Values every ", reftime(1)*dt,'s'
write(22,'(a4,< nprint >(3x,f16.8))')"Time",reftime*dt
do i=1,n
write(22,'(i4,< nprint >(3x,f16.8))')i,intdphidxdiffract(i,:)
end do
write(37,'(/T2,a36, f8.3,a1)')"Intermediate dPhidx Values every ", reftime(1)*dt,'s'
```

Figure D.1. Fortran code (cont.)

```
write(37,'(a4,< nprint >(3x,f16.8))')"Time",reftime*dt
do i=1,n
write(37,'(i4,< nprint >(3x,f16.8))')i,intdphidxrad(i,:)
end do
write(31,'(/T2,a50, f8.3,a1)')"Intermediate incidence dPhidz Values every ", reftime(1)*dt,'s'
write(31,'(a4,< nprint >(3x,f16.8))')"Time",reftime*dt
do i=1,n
write(31,'(i4,< nprint >(3x,f16.8))')i,intdphidzinc(i,:)
end do
write(23,'(/T2,a36, f8.3,a1)')"Intermediate dPhidz Values every ", reftime(1)*dt,'s'
write(23,'(a4,< nprint >(3x,f16.8))')"Time",reftime*dt
do i=1,n
write(23,'(i4,< nprint >(3x,f16.8))')i,intdphidzdiffract(i,:)
end do
write(38,'(/T2,a36, f8.3,a1)')"Intermediate dPhidz Values every ", reftime(1)*dt,'s'
write(38,'(a4,< nprint >(3x,f16.8))')"Time",reftime*dt
do i=1,n
write(38,'(i4,< nprint >(3x,f16.8))')i,intdphidzrad(i,:)
end do
```

Figure D.1. Fortran code (cont.)

```
write(29,'(/T2,a40, f8.3,a1)')"Intermediate Analytical Phi every ", reftime(1)*dt,'s'
write(29,'(a4,< nprint >(3x,f16.8))')"Time",reftime*dt
do i=1,n
write(29,'(i4,< nprint >(3x,f16.8))')i,intphiinc(i,:)
end do
write(27,'(/T2,a40, f8.3,a1)')"Intermediate Numerical Phi every ", reftime(1)*dt,'s'
write(27,'(a4,< nprint >(3x,f16.8))')"Time",reftime*dt
do i=1,n
write(27,'(i4,< nprint >(3x,f16.8))')i,intphidiffract(i,:)
end do
write(40,'(/T2,a40, f8.3,a1)')"Intermediate Numerical Phi every ", reftime(1)*dt,'s'
write(40,'(a4,< nprint >(3x,f16.8))')"Time",reftime*dt
do i=1,n
write(40,'(i4,< nprint >(3x,f16.8))')i,intphirad(i,:)
end do
write(25,'(/T2,a40, f8.3,a1)')"Intermediate Difference in Phi every ", reftime(1)*dt,'s'
write(25,'(a4,< nprint >(3x,f16.8))')"Time",reftime*dt
do i=1,2*nv
write(25,'(i4,< nprint >(3x,f16.8))')i,intphidiffdiffract(i,:)
```

Figure D.1. Fortran code (cont.)

```
end do
write(39,'(/T2,a40, f8.3,a1)')"Intermediate Difference in Phi every ", reftime(1)*dt,'s'
write(39,'(a4,< nprint >(3x,f16.8))')"Time",reftime*dt
do i=1,2*nv
write(39,'(i4,< nprint >(3x,f16.8))')i,intphidiffrad(i,:)
end do
! record the intermediate mean phis
write(28,'(/T2,a30)')"Intermediate Mean Phi values"
write(28,'(/T4,a8,T14,a22)')"time [s]","intermediate mean phi"
do i=1,nprint
write(28,'(f5.1,T14,f11.8)')i*dtprint,intmeanphidiffract(i)
end do
write(41,'(/T2,a30)')"Intermediate Mean Phi values"
write(41,'(/T4,a8,T14,a22)')"time [s]","intermediate mean phi"
do i=1,nprint
write(41,'(f5.1,T14,f11.8)')i*dtprint,intmeanphirad(i)
end do
! record intermediate plate positions xc
write(32,'(/T2,a50, f8.3,a1)')"Intermediate Plate Nodes xc every ", reftime(1)*dt,'s'
```

Figure D.1. Fortran code (cont.)

```
write(32,'(a4,< nprint >(3x,f16.8))')"Time",reftime*dt
do i=1,2*(nvp+nhp)
write(32,'(i4,< nprint >(3x,f16.8))')i,intxc(i,:)
end do
! record intermediate plate positions xrbf
write(33,'(/T2,a50, f8.3,a1)')"Intermediate Plate Nodes xrbf every ", reftime(1)*dt,'s'
write(33,'(a4,< nprint >(3x,f16.8))')"Time",reftime*dt
do i=1,2*(nvp+nhp)
write(33,'(i4,< nprint >(3x,f16.8))')i,intxrbf(i,:)
end do
! record intermediate plate positions zc
write(34,'(/T2,a50, f8.3,a1)')"Intermediate Plate Nodes zc every ", reftime(1)*dt,'s'
write(34,'(a4,< nprint >(3x,f16.8))')"Time",reftime*dt
do i=1,2*(nvp+nhp)
write(34,'(i4,< nprint >(3x,f16.8))')i,intzc(i,:)
end do
! record intermediate plate positions zrbf
write(35,'(/T2,a50, f8.3,a1)')"Intermediate Plate Nodes zrbf every ", reftime(1)*dt,'s'
write(35,'(a4,< nprint >(3x,f16.8))')"Time",reftime*dt
```

Figure D.1. Fortran code (cont.)

```
do i=1,2*(nvp+nhp)
write(35,'(i4,< nprint >(3x,f16.8))')i,intzrbf(i,:)
end do
! record intermediate pitching angle (without plate inclination)
write(42,'(/T2,a30)')"Intermediate Pitch Angles"
write(42,'(/T4,a8,T14,a25)')"time [s]","intermediate pitch angle"
do i=1,nprint
write(42,'(f5.1,T14,f11.8)')i*dtprint,intpitchrad(i)
end do
!*************************************************
! record the final numerical etas
write(16,'(/T2,a23)')"Final eta values"
write(16,'(/T4,a1,T9,a20,T30,a20)')"i","etafinaldiffract","etafinaldiffract-dt"
do i=1,nfse
write(16,'(i4,T9,f16.8,T30,f16.8)')i,etadiffract(i),etaold1diffract(i)
end do
! record the final numerical phis
write(17,'(/T2,a23)')"Final Phi values"
write(17,'(/T4,a1,T9,a16,T30,a20)')"i","phifinaldiffract","phifinalold1diffract"
```

Figure D.1. Fortran code (cont.)

```
do i=1,n
write(17,'(i4,T9,f16.8,T30,f16.8)')i,phidiffract(i),phiold1diffract(i)
end do
!*****************************************************
! record the final analytical conditions
write(18,'(/T2,a23)')"Final analytical values"
write(18,'(/T4,a1,T9,a11,T25,a11)')"i","phianalytic","etaanalytic"
do i=1,n
if(i.le.nfse)then
write(18,'(i4,T9,f11.8,T25,f11.8)')i,phinewanalyticinc(i),etanewanalyticinc(i)
else
write(18,'(i4,T9,f11.8)')i,phinewanalyticinc(i)
end if
end do
!*****************************************************
end program HeavingPlateLWT
```

Figure D.1. Fortran code (cont.)